INFORMATION TO USERS

This manuscript has been reproduced from the microfilm master. UMI films the text directly from the original or copy submitted. Thus, some thesis and dissertation copies are in typewriter face, while others may be from any type of computer printer.

The quality of this reproduction is dependent upon the quality of the copy submitted. Broken or indistinct print, colored or poor quality illustrations and photographs, print bleedthrough, substandard margins, and improper alignment can adversely affect reproduction.

In the unlikely event that the author did not send UMI a complete manuscript and there are missing pages, these will be noted. Also, if unauthorized copyright material had to be removed, a note will indicate the deletion.

Oversize materials (e.g., maps, drawings, charts) are reproduced by sectioning the original, beginning at the upper left-hand corner and continuing from left to right in equal sections with small overlaps.

Photographs included in the original manuscript have been reproduced xerographically in this copy. Higher quality 6" x 9" black and white photographic prints are available for any photographs or illustrations appearing in this copy for an additional charge. Contact UMI directly to order.

Bell & Howell Information and Learning
300 North Zeeb Road, Ann Arbor, MI 48106-1346 USA
800-521-0600

UMI®

NANOPARTICLE SIZE CONTROL AND CORONAL STRUCTURE IN BLOCK IONOMER MICELLES

by

Matthew Moffitt

A thesis
submitted to the Faculty of Graduate Studies and Research
in partial fulfillment of the requirements for the degree of

Doctor of Philosophy

Department of Chemistry
McGill University
Montreal, Quebec
Canada
H3A 2K6

September 1997

National Library
of Canada

Acquisitions and
Bibliographic Services

395 Wellington Street
Ottawa ON K1A 0N4
Canada

Bibliothèque nationale
du Canada

Acquisitions et
services bibliographiques

395, rue Wellington
Ottawa ON K1A 0N4
Canada

Your file Votre référence

Our file Notre référence

0-612-44517-8

Canada

Abstract

Quantum-confined semiconductors have been synthesized in ionomer microdomains, demonstrating thermodynamic control of nanoparticle sizes via a priori knowledge of ion aggregation numbers. In block ionomers, cadmium sulfide (CdS) nanoparticle sizes are found to scale with the ionic block length (N_B) as $N_B^{3/5}$. CdS-polymer composites from block ionomers can be suspended in organic solvents as reverse micelles. Micelle stability is improved by reneutralization of acrylic acid blocks surrounding the nanoparticle. Reloading of microreactors and controlled continued growth of nanoparticles is demonstrated. Novel assemblies of CdS-containing reverse micelles are formed by secondary self-assembly in aqueous media. Scaling relations are also determined for microreactors containing different metal ions. For all metal ions investigated, the ionic core size scales as $N_B^{0.58\pm0.03}$, in agreement with starlike models; the proportionality constant is found to depend on the metal ion.

Coronal structure in block ionomers has been investigated by small-angle neutron scattering (SANS), using deuterated labels at various distances from the ionic core. Near the outside of the polymer brush, the scattered intensity scales with the scattering vector (q) as $q^{-5/3}$, suggesting a semidilute environment for the label. Chain conformations are influenced by neighbouring coronae above the micelle overlap concentration. Closer to the ionic core, the chains become more crowded, and the semidilute assumption is not applicable. For labels directly connected to the core, intensity scaling suggests highly extended chains.

Résumé

Des semi-conducteurs de dimensions quantiques sont synthétisés dans des microdomaines ionomèriques, prouvant ainsi le contrôle thermodynamique de la taille des nanoparticules à partir de la connaissance du nombre d'aggrégation de l'ion. Pour des ionomères blocs, la taille des nanoparticules de sulfure de cadmium (CdS) varie en fonction de la longueur du bloc ionique (N_B), typiquement selon $N_B^{3/5}$. Les composites de polymères de CdS obtenus à partir d'ionomères blocs forment une suspension de micelles inversées dans des solvents organiques. La stabilité de telles micelles est améliorée par une nouvelle neutralisation du bloc d'acide acrylique qui entoure la nanoparticule. Il a été démontré que l'on peut remplir à nouveau les microréacteurs et maîtriser la croissance continue des particules. Il est possible de former de nouveaux assemblages de micelles inversées contenant du CdS par auto-assemblage secondaire en milieu aqueux. Des relations géométriques sont aussi déterminées pour des microréacteurs contenant différents ions métalliques. Pour tous les ions étudiés, la taille du coeur ionique est proportionnelle à $N_B^{0.58\pm0.03}$, ce qui correspond au modèle d'une micelle étoile ; il a été prouvé que la constante de proportionnalité dépend de la nature de l'ion métallique.

La structure de la couronne du ionomère bloc a été caractérisée par diffraction de neutrons à faible angle d'incidence, par marcage au Deutérium à différentes distances du coeur ionique. Proche de l'extérieur de la brosse de polymère, l'intensité diffractée varie en fonction du vecteur de diffraction q à la puissance $-5/3$ ($q^{-5/3}$), impliquant que le marqueur se trouve dans un environnement semi-dilué. La conformation des chaînes dépend des couronnes voisines au delà de la concentration de chevauchement des micelles. Plus près du coeur ionique, les chaînes sont plus nombreuses et l'hypothèse de semi-dilution n'est plus valide. En ce qui concerne les marqueurs directement attachés au coeur, la variation de l'intensité montre que les chaînes sont très étendues.

Foreword

In accordance with Thesis Specifications of the "Guidelines for Thesis Preparation" (Faculty of Graduate Studies and Research, McGill University), the following text is cited:

> "Candidates have the option of including, as part of the thesis, the text of one or more papers submitted or to be submitted for publication, or the clearly-duplicated text of one or more published papers. These texts must be bound as an integral part of the thesis.
>
> If this option is chosen, **connecting texts that provide logical bridges between the different papers are mandatory.** The thesis must be written in such a way that it is more than a mere collection of manuscripts; in other words, results of a series of papers must be integrated.
>
> The thesis must still conform to all other requirements of the "Guidelines for Thesis Preparation". The thesis must include: A Table of Contents, an abstract in English and French, an introduction which clearly states the rationale and objectives of the study, a review of the literature, a final conclusion and summary, and a thorough bibliography or reference list.
>
> Additional material must be provided where appropriate (e.g. in appendices) and in sufficient detail to allow clear and precise judgment to be made of the importance and originality of the research reported in the thesis.
>
> In the case of manuscripts co-authored by the candidate and others, **the candidate is required to make an explicit statement in the thesis as to who contributed to such work and to what extent.** Supervisors must attest to the accuracy of such statements at the doctoral oral defense. Since the task of the examiners is made more difficult in these cases, it is in the candidate's interest to make perfectly clear the responsibilities of all the authors of the co-authored papers."

This dissertation consists of seven papers, each of which comprises one chapter, with an introduction and general conclusions provided in the first and final chapters, respectively. Following normal procedures, slightly modified versions of these papers have been published in scientific journals; others have been submitted or are to be submitted for publication. A list of the papers is given below:

Chapter 2: *Acc. Chem. Res.* **1996**, *29*, 95.
Chapter 3: *Chem. Mater.* **1995**, *7*, 1178.
Chapter 4: *Chem. Mater.* **1995**, *7*, 1185.[a]
Chapter 5: *Macromolecules* **1997**, *30*, 4363.[b]
Chapter 6: *Chem. Mater.* (submitted).
Chapter 7: *Polymer* (to be submitted).
Chapter 8: *Macromolecules* (to be submitted).

[a] In chapter 4, Figures 4.6 and 4.7 did not appear in the original manuscript, and have been added for the sake of clarity.

[b] In chapter 5, Table 5.2 and parts of Table 5.7 were published as Supplemental Material with the original manuscript.

All of these papers were co-authored by the research director, Dr. Adi. Eisenberg. The review in chapter 2 also includes Dr. Karine Khougaz, who co-wrote the article. Chapter 4 includes Ms. Lynne McMahon and Ms. Valerie Pessel; both of these co-authors were undergraduate students working under the direct supervision of the author. Chapter 6 includes Dr. H. Vali from the Department of Earth and Planetary Sciences at McGill, in recognition of his assistance with some of the transmission electron microscopy experiments, in particular with the operation of the JEOL FX200 instrument. Chapters 7 and 8 include Dr. Yisong Yu, who synthesized the deuterated samples used for small-angle neutron scattering work, along with Drs. Diep Nguyen and Dieter Schneider, in recognition of their expertise in carrying out the SANS experiments. Mr. Vito Graziano provided assistance in the data reduction process, and is also included as a co-author of chapters 7 and 8. Other than the supervision, advice and direction of Dr. Eisenberg, and the aforementioned contributions to the chapters, all of the work presented in this dissertation was performed by the author.

Acknowledgments

I would like to express my immense gratitude to **Dr. Adi Eisenberg**, for his guidance, advice, and encouragement over the past five years. His scientific insights and boundless enthusiasm are second only to his rare appreciation for puns. Thank you for keeping me "laboriously challenged". ☺

I would also like to specially thank my parents, **Gordon and Mary Moffitt**, my brother, **Steve Moffitt** and my grandparents, **Greta and Willard Moffitt** and **Eva Thorburn**, for their love and support through this and all other endeavours. I can never thank them enough.

In addition, I would like to thank:

- **Joon,** for his friendship, wisdom, and inestimable dependability.
- **Xing Fu,** for teaching me anionic polymerization, and for many useful discussions.
- **Diep,** for being "the boss" and a friend to boot. Thanks also for her invaluable help with small-angle scattering experiments.
- **Ray,** for teaching me the ways of dynamic light scattering, and infusing me with the Fear of Dust.
- **Karine,** for passing on her static light scattering expertise.
- **Lifeng,** for numerous helpful discussions. Thanks also for providing one of the block copolymer samples used in chapter 6.
- **Neil,** for fixing the computer on which most of this thesis was written; also for his reliable "know-how", which extends far beyond an eerie ability to reason with microchips.
- **Carl,** "Computer Guru Too". Thanks for useful discussions regarding inorganic nanoparticles, and for his terrifying knowledge of *Star Wars* trivia.
- **Luc,** pour la traduction (*Merci*).
- **Yisong,** for providing the polymer samples used in chapters 7 and 8.
- **Valerie, Lynne, Joyce, and Muriel,** for their hard work and input into various aspects of the nanoparticle research.
- Thanks also to **Francis, Michelle, Irina, Zhisheng, Sheng, Kui, Hongwei, George, Sabrina, Nishi, Monali, Chris, Ga-er, Christine, Bruce, Diane and Juliet,** for making the lab a pretty nice place to spend so many hours of so many days. ☺
- **Dr. Dieter Schneider, Mr. Vito Graziano**, and other folks at Brookhaven National Labs, for expertise and assistance, and for making me feel "at home" on my visits to BNL.
- **Dr. G. Bazuin** in the Department of Chemistry at Lavel University.
- **Ms. Kathy Hewitt** in the EM center of the Department of Biology.
- **Ms. Jeannie Mui and Ms. Matilda Cheung** in the Anatomy EM center.
- **Dr. H. Vali** in the Department of Earth and Planetary Sciences.
- All of my former professors and teachers in the Department of Chemistry.
- Also in the Department of Chemistry, I would like to thank **Dr. Mark Andrews, Dr. G. Wilczek, Mr. Fred Kluck, Ms. Reneé Charron, and Ms. Paulette Henault.**
- Thanks also to former 180-204/213 students, for making my T.A. experience a positive one. It was a real gas. ☺
- And to anyone I have forgotten to mention, my sincere apologies, and *Thank You!*

Table of Contents

Chapter 1. General Introduction 1

Contents of Tables

List of Figures

For Mum and Dad

and in loving memory of

Howard Joseph Thorburn and Kathleen May Johnston

In all these things we are more than conquerors through Him who loved us.
Romans 8:37

And thus do we of wisdom and of reach,
With windlasses and with assays of bias,
By indirections find directions out.

William Shakespeare

CHAPTER 1

General Introduction

1.1. Introduction

This dissertation consists of two main parts, both concerning "reverse" micelles of ion-containing block copolymers. First, the use of ionic cores of block ionomer micelles as inorganic microreactors of controllable size is discussed, especially in connection with the synthesis of quantum-confined semiconducting nanoparticles. The techniques that are relevant to this discussion include static and dynamic light scattering, small-angle x-ray scattering, transmission electron microscopy, and UV-vis absorption spectroscopy. The second part of the thesis describes an investigation of coronal structure in block ionomers by small-angle neutron scattering, using deuterated labels to probe specific parts of the micelle corona.

The present chapter is divided into seven sections. The remainder of section 1.1 is an introduction to polymers and copolymers, including a discussion of the synthesis and characterization of block copolymers. Section 1.2 concerns the phenomenon of microphase separation of block copolymers in bulk. This is followed in section 1.3 by a discussion of microphase separation of block copolymers in selective solvents to form micelles. In section 1.4, the concept of block ionomers is introduced, including a summary of other work on the characterization of these materials. Section 1.5 provides a brief history of semiconducting nanoparticles; this encompasses a discussion of different strategies of nanoparticle preparation, along with a simplified description of the quantum-confinement effect. In section 1.6, a short description of small-angle neutron scattering is given, in which basic concepts are introduced and critical terms are defined. Finally, the focus and scope of the thesis is described in section 1.7.

1.1.1. Polymers and Copolymers: Some Basic Definitions

A *polymer* is defined as a large molecule, natural or synthetic, made from smaller structural units known as *monomers* that are connected through covalent links.[1] To qualify as a monomer, a molecule must possess at least two bonding sites, though which it can be connected to other monomers in the process of polymerization. If the monomer building blocks are bifunctional (i.e., possess two bonding sites), the resultant polymers resemble linear chains, whereas polyfunctional monomers (i.e., three or more bonding sites) will form branched chains or large three-dimensional networks. Once they have been incorporated into a polymer chain, monomers are often termed "structural units", "repeat units", or simply "units"; the number of repeat units making up the polymer is referred to as the degree of polymerization.

When a polymer consists of only one species of monomer, it is called a *homopolymer.*[1] In some cases, polymers will be made up of two different repeat units, and these are known as a *copolymers*. If two distinct monomers, A and B, are considered, it is obvious that different copolymers can be obtained through variations in the relative amounts of A and B that are copolymerized. As well, the copolymers can be further subdivided into four categories, depending on the arrangement of A and B units within the chain (Figure 1.1). In a *random copolymer*, the distribution of A and B along the linear chain is essentially random, though influenced by the relative reactivities of the two monomers. *Alternating copolymers* are made up of A and B units that are distributed with a regular alternating pattern along the chain. When substantial sequences (or blocks) of A units are covalently linked to substantial blocks of B units in a linear chain, the resulting copolymer is called a *block copolymer*. In a *diblock copolymer*, one A block is linked to one B block, whereas a triblock copolymer consists of a central B block connected to two terminal A blocks (or vice versa); polyblock copolymers are also possible, containing any number of blocks. *Graft copolymers* are formed by grafting blocks of one monomer onto a backbone of the other monomer, much like grafting foreign branches onto the trunk of a tree. In most of the work described in this thesis, the primary materials are diblock copolymers; however, as described later, tetrablock copolymers (four blocks) are used in SANS experiments with perdeuterated-polystyrene labeling.

```
ABAAABBABBBAABAAABA          Random copolymer
ABABABABABABABABABA          Alternating copolymer
AAAAAAAAAAABBBBBBBB          Block copolymer
AAAAAAAAAAAAAAAAAAA          Graft copolymer
   B        B
   B        B
   B        B
   B        B
   B
```

Figure 1.1. Types of copolymers synthesized from monomers A and B.

1.1.2. Synthesis of Block Copolymers: Sequential Anionic Polymerization

Diblock copolymers are typically synthesized by anionic polymerization, in which electronegative monomers are "activated" by a highly electropositive initiator, resulting in the formation and growth of a "living" polycarbanion. The term *living polymer* is attributed to Szwarc,[2] and refers to the fact that the polymerization reaction has no formal termination step; therefore, the chains continue to grow as more monomer is introduced into the system. A termination step is provided by the addition of a small molecule with a labile proton (e.g. methanol), which reacts with the polycarbanion to "kill" the chain.

In the sequential anionic polymerization of an AB diblock copolymer, initiation of monomer A and subsequent propagation of the living chains results in the growth of the first block, followed by the addition of monomer B and growth of the second block.[3-7] Since the degree of polymerization for each block can be controlled by the amount of added monomer, block copolymers of well-defined compositions can be made by this method. As well, block copolymers synthesized by sequential anionic polymerization generally have a low degree of molecular weight polydispersity; this is attributed to the rapid rate of initiation compared with that of propagation, the latter being controlled via the speed of monomer addition.

The synthesis of polystyrene-*b*-poly(*tert*-butylacrylate) is of particular relevance to the present thesis, and will therefore be described in some detail. It is important to note that water and molecular oxygen will both react with polycarbanions to terminate living chains. For this reason, each step of this procedure is carried out under an atmosphere of ultra-pure nitrogen, and with careful drying of all glassware.

In the initiation step, *sec*-butyllithium initiator is added to a solution of α-methylstyrene and LiCl in tetrahydrofuran (THF); α-methylstyrene acts as both an indicator and an end-capping agent, and LiCl is a stabilizer for the polymerization reaction.[3,7] As the solution is titrated with *sec*-butyllithium at room temperature, the initiator first reacts with any impurities in the system, then activates the α-methylstyrene to yield short polycarbanions of a deep red colour. At room temperature, the α-methylstyrene monomer is above its ceiling temperature, and therefore does not polymerize completely.

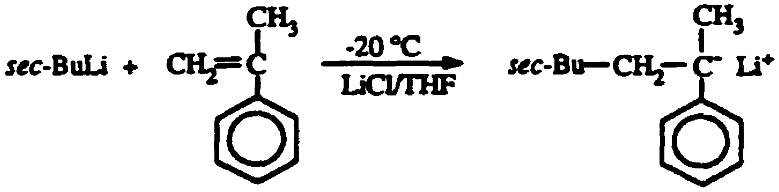

The styrene monomer is then added at low temperature (-78 °C), and the living polycarbanions initiate polymerization of styrene. The colour of the solution changes from deep red to orange-yellow, which is the colour of "activated" styrene. The active centers are regenerated at the chain ends as the polymerization proceeds, and the process continues until all of the styrene monomer is consumed. At that point, the remaining α-methylstyrene reacts with the living chains, and the deep red colour reappears.[3]

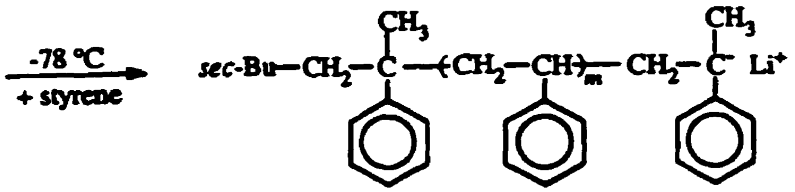

The polymerization resumes when the second monomer, *tert*-butylacrylate, is added to the reaction flask. The initiation of the extremely reactive *tert*-butylacrylate monomer by the living chains is sterically regulated by the presence of α-methylstyrene end-cap. Terminating side reactions or chain transfer reactions are also prevented by the LiCl stabilizer, which associates with the living chain ends, thus lowering their activity. The colour of the solution disappears completely with addition of the second monomer, since activated *tert*-butylacrylate is colourless.

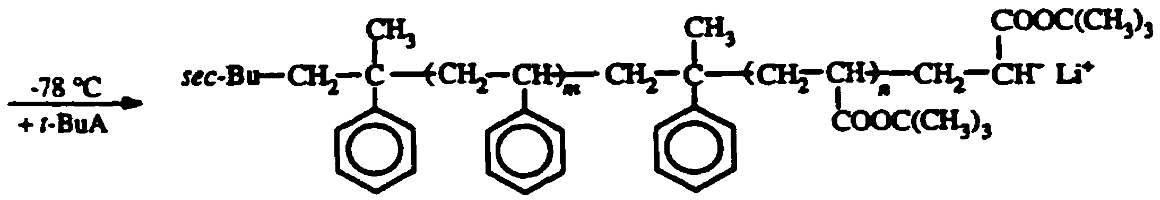

In the final step, the polymerization is terminated by the addition of a small amount of methanol.

1.1.3. Characterization of Block Copolymers

After a block copolymer has been synthesized, certain characteristics of the polymer must be determined in order to proceed with further experiments. The most important of these characteristics are composition, average molecular weight, and polydispersity index; for most purposes, these parameters together define a given AB block copolymer.

Assuming that monomers A and B are known, the composition of the AB block copolymer is defined by the relative lengths of the two blocks. This is usually expressed as a weight or mole fraction of either block, and can be determined quantitatively by techniques such as nuclear magnetic resonance spectroscopy (NMR) or infrared spectroscopy (IR).[7] If either monomer shows a well-defined resonance or absorption mode by one of these methods, and if the appropriate calibration has been obtained, then the concentration of monomer A or B in a solution of the block copolymer can be determined. For solutions in which the concentration of polymer is known, the concentration of monomer is then converted into a relative block length.

One feature that distinguishes synthetic polymers from small molecules is the problem of assigning an unambiguous molecular weight to the former. This is because a sample of synthetic polymer contains a population of different chain lengths, the features of which are determined partly by the statistical nature of the polymerization reaction.[2] A polymer is therefore most suitably characterized by a molecular weight distribution, such as that shown below.[1]

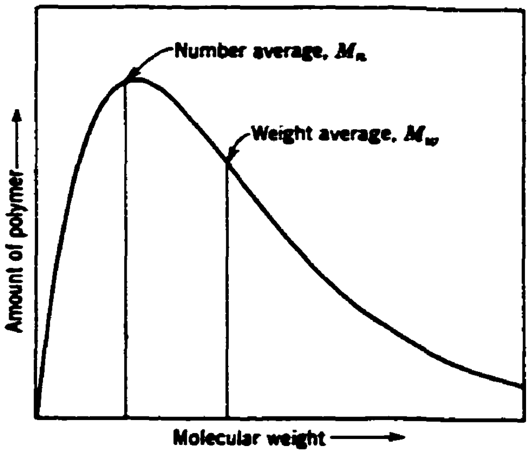

Figure 1.2. An example of a molecular weight distribution for a sample of synthetic polymer.

From Figure 1.2, M_n is the number-average molecular weight, and is defined by

$$M_n = \frac{\sum_i N_i M_i}{\sum_i N_i} = \frac{\sum_i W_i}{\sum_i (W_i / N_i)} \tag{1}$$

where N_i and W_i and M_i are the number, weight, and molecular weight of species i. M_n can be obtained directly by methods that measure colligative properties of a polymer solution (e.g. osmotic pressure). The weight-average molecular weight, M_w, on the other hand, is obtained by methods that are sensitive to the weight, rather than the number, of molecules in solution (e.g. static light scattering). The weight-average molecular weight is defined by

$$M_w = \frac{\sum_i N_i M_i^2}{\sum_i N_i M_i} = \frac{\sum_i W_i M_i}{\sum_i W_i} \qquad (2)$$

Another useful average is the *z*-average molecular weight, M_z, which is obtained by methods such as sedimentation equilibrium:

$$M_w = \frac{\sum_i N_i M_i^3}{\sum_i N_i M_i^2} = \frac{\sum_i W_i M_i^2}{\sum_i W_i M_i} \qquad (3)$$

Along with the above averages, the molecular weight distribution is characterized by the *polydispersity index* (P.I.), which describes the width of the distribution, or the spread of molecular weights. The polydispersity index is defined

$$P.I. = \frac{M_w}{M_n} \qquad (4)$$

The lowest possible value of P.I. is unity, in which case the sample is said to be *monodisperse*. The value of the polydispersity index depends largely on the method of polymerization. For example, it was mentioned earlier that sequential anionic polymerization can be used to obtain block copolymers with relatively low polydispersities; by this method, P.I. values are typically between 1.05 and 1.10.[7]

1.2. Diblock Copolymers in the Solid State

Block copolymers have been shown to have a number of interesting and useful properties, which have been attributed to the unique morphological features of the bulk polymers.[8-10] These features arise from the covalent links between incompatible blocks; due to thermodynamic factors, the immiscible blocks want to separate, but their mutual connectivity prevents them from getting very far from each other. The inherent interest surrounding such competitions between natural forces is aptly described by Helfand and Wasserman:[8]

> *"Like a child contemplating the results of tying the cat's tail to that of a dog, scientists perhaps find a certain mischievous delight in considering the effect of joining two immiscible polymer blocks into one macromolecule."*

As in most competitions between equally assertive opponents, the "result" is, in fact, a compromise; the competing blocks separate into "microphases" or "microdomains", in which they are surrounded by "like" blocks while, at the same time, being spatially close to "unlike" blocks. In effect, phase separation is restricted to dimensions on the order of the polymer dimensions. The size and shape of the microdomains define the *morphology* of the block copolymer; both theorists and experimentalists have investigated block copolymer morphology as a function of numerous variables (e.g., block copolymer composition, temperature, etc.).[8-10] Before looking at some of these morphologies, it is useful to consider the salient aspects of the thermodynamics of block copolymer microphase separation.

1.2.1. Thermodynamic Considerations

The thermodynamic tendency of a physical or chemical process is generally determined by the change in free energy, ΔG, which is calculated from entropic and enthalpic components.[11] For the mixing of two homopolymers, the free energy of mixing, ΔG_{mix}, can be written:

$$\Delta G_{mix} = \Delta H_{mix} - T\Delta S_{mix} \tag{5}$$

where ΔH_{mix} is the enthalpy of mixing, T is the temperature, and ΔS_{mix} is the entropy of mixing.[12] Since the system will tend to minimize its free energy, mixing will take place if ΔG_{mix} is negative; the polymers will then be miscible on a molecular level.

For the mixing of high molecular weight polymers, ΔS_{mix} is known to be very small, such that the free energy is dominated by the enthalpic component.[12] To determine ΔH_{mix}, the enthalpy of transferring a single unit of polymer A from pure A surroundings to pure B surroundings is defined as $\chi_{\mathrm{AB}}kT$, where χ_{AB} is the Flory-Huggins interaction parameter, and k is the Boltzmann constant. For most polymers, χ_{AB} is a positive quantity, making ΔH_{mix} and ΔG_{mix} positive; therefore, the phase separation of polymers is generally more favourable than mixing. In the case of polymer blends, favourable interactions between specific functional groups on the two chains (e.g. ionic interactions, hydrogen bonding) are employed to make χ_{AB} negative, so that dissimilar polymers become miscible.

The phase separation of two homopolymers is macroscopic, as the system is driven to minimize the contact surface area between the two components. The size of the phases which form is limited only by the amount of material.[9] However, when two immiscible polymers are joined by a covalent bond, the phase separation is restricted to microscopic dimensions; block copolymers therefore form microdomains with sizes that are comparable to polymer chain lengths.

The conditions under which block copolymers will form microdomains are governed both by enthalpic and entropic factors.[10] In general, microphase separation becomes enthalpically more favourable as the interaction parameter between the blocks, χ_{AB}, increases. However, the ordering of chains into microdomains is at the expense of the configurational entropy of the system-- a cost which becomes greater as the total number of repeat units in the block copolymer, N, decreases. The product $\chi_{\mathrm{AB}}N$ is thus said to define the conditions, and the extent, of microphase separation. In general, block copolymers are expected to form microdomains above $\chi_{AB}N \sim 10$, below which the system is disordered.[10] Just above this crossover, the system exists in the weak segregation limit (WSL); interfacial boundaries are poorly defined, and the sizes of microdomains scale as $N^{1/2}$. This scaling relation indicates Gaussian chain statistics, which is also expected in the disordered state, suggesting that chain conformations remain largely unperturbed in the weak segregation limit. Under the conditions $\chi_{AB}N \gg 10$, the system exists in the strong segregation limit (SSL). Under these conditions, the interfacial boundaries are well defined, and the "narrow interface approximation" is said to hold. As well, the sizes of microdomains scale as $N^{2/3}$, suggesting marked perturbations in chain dimensions. Khokhlov has also proposed the existence of a superstrong segregation limit;[13] this regime of phase behaviour will be discussed later in the chapter, in connection with block ionomers.

The thermodynamic factors that determine microdomain morphology have been described in the strong segregation limit by Helfand and Wasserman.[8] They identified three main contributions to the free energy of microdomain growth:

1. Interfacial contact enthalphy between microdomains of pure A and pure B polymers.
2. Entropy loss from chain extension within microdomains.
3. Entropy loss from confinement of block copolymer joints at the interface.

The first of these contributions promotes the growth of microdomains, as the system tends to minimize the surface area of interfacial contact. This growth is restricted by the other two contributions, both of which result in a decrease in entropy as the microdomains become larger. It should be noted that the driving force for chain extension within the microdomains is a strong tendency to maintain a constant bulk density of polymer; as the microdomains increase in size, the chains are forced to stretch into the center, in order to fill up space. These three factors are the basis of a mean field model,[8] which has been used to describe the growth of microdomains, along with the conditions which result in morphological transitions between lamellae, cylinders, and spheres.

1.2.2. Block Copolymer Morphologies

In the strong segregation limit ($\chi_{AB}N \gg 10$), block copolymer morphology is found to depend largely on the relative amounts of the two components (A and B), and to be virtually independent of temperature.[8,10] For the system polystyrene-*b*-polyisoprene (PS-*b*-PI), seven equilibrium morphologies have been identified, and these are shown in Figure 1.3 as a function of the polystyrene volume fraction, ϕ_S.[10] For $\phi_S < 0.17$, the system forms PS spheres in a matrix of PI. As ϕ_S increases, the system progresses through PS cylinders, PS ordered bicontinuous double diamonds (OBDD), then to PS/PI lamellae in the neighborhood of $\phi_S \sim 0.50$. The block copolymers become PS-rich as ϕ_S continues to increase above 0.50, and the system "inverts" to form PI microdomains in a PS matrix. All of these observed morphologies were predicted by the mean field theory of Helfand and Wasserman for the strong segregation regime, with the exceptions of the OBDD phase; this was subsequently discovered by Aggarwal in star-block copolymers[14a] and then observed by Hasegawa in linear block copolymers.[14b] More recent theories have called into question the existence of an equilibrium OBDD phase in the SSL,[15a] and certain workers have claimed that the OBDD is a metastable manifestation.[15b] Continued experimental work in this area has shown that the phase boundaries described in Figure 1.3 are not rigourously defined; as well, certain "nonclassical" phases, such as hexagonally perforated layers (HPL) have been observed.[15b]

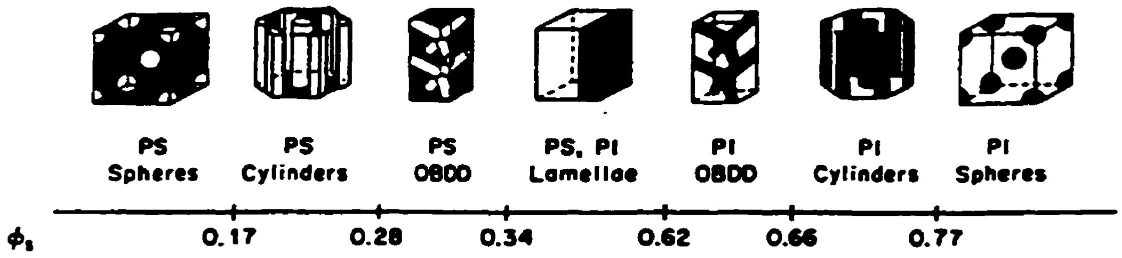

Figure 1.3. Morphologies of PS-*b*-PI diblock copolymers in the strong segregation limit.

In the weak segregation limit ($\chi_{AB}N > 10$), morphological transitions in block copolymers were first described by Leibler.[16] The theoretical phase diagram in Figure 1.4 for an arbitrary AB block copolymer in the WSL shows that morphology depends both on the block fraction, *f*, and on the product $\chi_{AB}N$. Since χ_{AB} will change with temperature, the morphological transitions are temperature-dependent in the weak segregation limit. The predicted critical point for microphase separation is $(\chi_{AB}\,N)_c = 10.5$ and $f_c = 0.5$.[16]

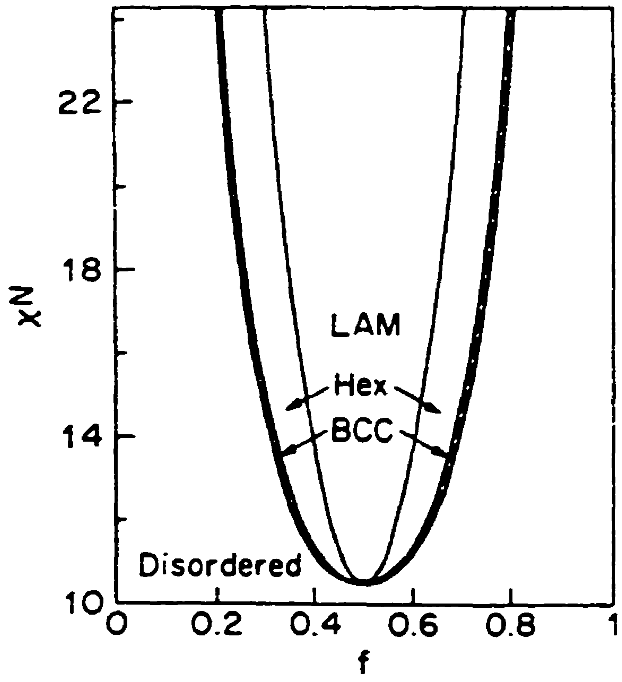

Figure 1.4. Theoretical phase diagram for diblock copolymers in the weak segregation limit. LAM, Hex, and BCC correspond to lamellar, hexagonal (cylindrical morphology), and body-centered-cubic (spherical morphology) symmetries.

1.3. Block Copolymer Micelles

Block copolymers are also known to undergo microphase separation in solution, forming spherical and non-spherical structures that are similar to micelles of small molecule surfactants (e.g. sodium bis(2-ethylhexyl)sulfosuccinate (AOT)) in water or organic solvents.[17-19] The resulting *block copolymer micelles* have been the subject of extensive investigation in recent years, due both to potential applications (e.g. drug delivery, pollutant extraction, viscosity modification, catalysis, nanoparticle synthesis) and similarities to systems of theoretical interest (polymer-stabilized colloids). In this section, some basic principles and terminology pertaining to block copolymer micelles are first defined, followed by a comparison between micelles of block copolymers and those of small molecule surfactants. Some methods of characterization are then described, especially those of particular relevance to this thesis. Finally, the theoretical treatment of block copolymer micelles is considered, and scaling laws relating micelle parameters to block copolymer composition are given.

1.3.1. Micellization of Block Copolymers in Solution

The interesting physico-chemical properties of block copolymer solutions arise from the tendency of block copolymers to undergo microphase separation in selective solvents.[17-19] For an AB block copolymer, a selective solvent is one in which the B block is insoluble and the A block is soluble. Above a certain concentration of the block copolymer, known as the critical micelle concentration (cmc), the insoluble B blocks will self-assemble to minimize contact with the solvent; this results in microdomains of the insoluble material, surrounded and protected by the solubilized A blocks. The driving force for micellization is enthalpic, although the shape and size of the resulting structures are expressions of both enthalpic and entropic factors.

In many cases, block copolymer micelles are spherical in shape. Analogous to their surfactant counterparts, spherical micelles of block copolymers consist of a spherical *core* of insoluble blocks, surrounded by a *corona*, or shell, of the solubilized blocks. Based on the relative lengths of the soluble and insoluble blocks, two categories of spherical micelles can be identified. In *crew-cut micelles*, the insoluble blocks are long compared to the soluble blocks, such that the micelles have large cores and short coronal "hair".[20] *Starlike micelles*, on the other hand, are made up of copolymers with relatively short insoluble blocks; the cores are therefore small and compact, surrounded by coronae of long soluble blocks that extend into the solution.[21] Though starlike micelles bear a vague resemblance to their astronomical cousins, they are certainly more closely related to star polymers, which consist of numerous polymer arms radiating from a fixed chemical link.[21] Representative drawings of starlike and crewcut micelles are shown in Figure 1.5. Along with spherical micelles, other non-spherical morphologies have also been observed in solutions of block copolymers.[22]

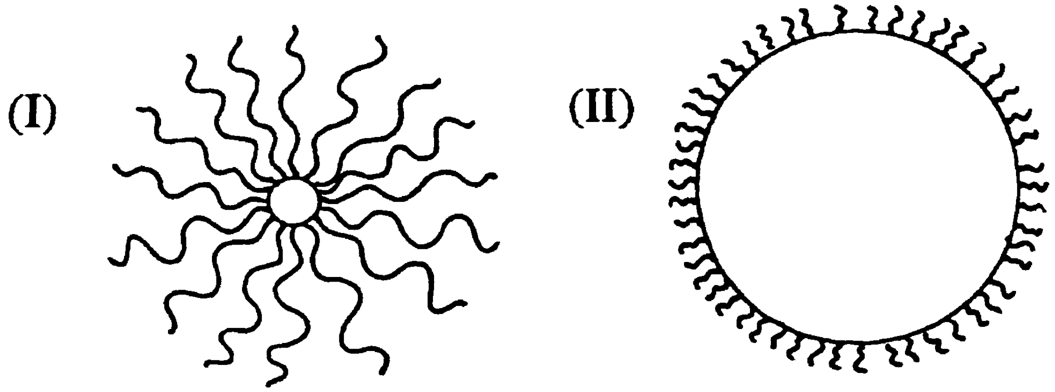

Figure 1.5. Starlike (I) and crew-cut (II) micelles.

The micellization of block copolymers occurs by a mechanism of closed association,[18] meaning that a single equilibrium exists between the micelles (M) and their constituent single chains, or unimers (U):

$$ZU \xleftrightarrow[c>cmc]{} M_Z \qquad (5)$$

where Z is the number of unimers that make up the micelle, and is called the micelle aggregation number, or simply the aggregation number. By contrast, an open association process involves numerous equilibria between aggregates of different sizes:

$$\begin{aligned} &U + U \longleftrightarrow M_2 \\ &M_2 + U \longleftrightarrow M_3 \\ &M_3 + U \longleftrightarrow M_4 \\ &M_N + U \longleftrightarrow M_{N+1} \end{aligned} \tag{6}$$

An open association process has been found to govern the micellization of small molecule surfactants in non-polar solvents.[18] The main consequence of closed association in block copolymer systems is that the micelle sizes tend to have relatively low polydispersities, compared with those of micelles formed from some surfactants. In the following section, some additional features that distinguish block copolymer micelles from their surfactant counterparts are described.

1.3.2. Block Copolymer and Surfactant Micelles: a Comparison of Analogues

Small molecule surfactants such as AOT are generally monodisperse, so that above the cmc all molecules have the same tendency to form micelles; in water, therefore, the cmc is directly related to the length of the alkyl chains. In block copolymer systems, however, the relationship between cmcs and average insoluble block lengths is less clearly defined, an experimental observation that has been attributed to block length polydispersity.[23] As previously stated, polydispersity is an important feature of polymers; every synthetic polymer is a distribution of macromolecules with different molecular weights. In their theoretical treatment of block copolymer micellization, Gao and Eisenberg argue that chains with longer insoluble blocks will tend to undergo microphase separation at lower concentrations than those with shorter insoluble blocks.[23] As well, the authors state that, in block copolymer systems, the insoluble blocks will coil into a ball below the cmc; the free energy of micellization for a single chain therefore scales as $N^{1/3}$ (where N is the number of repeat units in the insoluble block), rather than the N scaling determined for surfactants. The model shows that cmc values for block copolymers are not sharply defined, and that the concentration of single chains continues to increase above the cmc. This is in contrast to monodisperse surfactant systems, in which the concentration of single chains is constant above the cmc (for closed association). As well, a general lowering of the cmc was found in block copolymer systems with increasing polydispersity of chain lengths.

Another important difference between micelles of surfactants and block copolymers is kinetic, rather than thermodynamic, in origin. The exchange between micelles and unimers represented in eq 5 is a rapid process for small molecule surfactants, with unimer residence times on the order of 10^{-5} s.[18] In block copolymers micelles, however, chain entanglements within the core severely retard the entrance and exit of single chains; kinetics are stalled even more drastically when the core-forming blocks are below their glass transition temperature.[24] In the latter case, block copolymer micelles are said to be "frozen" or "dead", as no dynamic equilibrium exits on a reasonable time scale. Such micelles are often formed under equilibrium conditions (for example, in the presence of a core-swelling solvent), and become frozen with further treatment; equilibrium models can often be used successfully to describe these structures, despite a lack of dynamic equilibrium in their final state. It should be noted that the terms "aggregate" and "aggregation" generally refer to non-reversible processes; they are often applied to the micellization of block copolymers, although micelles of this type do often exhibit a dynamic equilibrium, or else are formed under equilibirum conditions. The terms "associate" and "association", on the other hand, imply complete reversibility, and are usually reserved for the micellization of small molecule surfactants.

1.3.3. Characterization of Block Copolymer Micelles

The study of block copolymer micelle solutions has involved the characterization of aggregates in terms of critical micelle concentrations, aggregation numbers, structure, and hydrodynamic behaviour.[17-19] Techniques used to determine these parameters include static and dynamic light scattering, size exclusion chromatography, viscometry, ultracentrifugation, small-angle x-ray scattering, small-angle neutron scattering, nuclear magnetic resonance, fluorescence, and transmission electron microscopy. Further details on these techniques can be found in a review by Tuzar and Kratochvil.[19] Descriptions of techniques that are of particular relevance to this thesis are reserved for subsequent chapters, with the exception of small-angle neutron scattering, the details of which are presented at the end of the present chapter.

1.3.4. Theories of Block Copolymer Micelles: Models and Scaling Relations

Several theoretical studies of block copolymer micelles have focused on the description of important micelle parameters in terms of characteristics of the constituent block copolymers.[21,25-29] In these models, expressions for the total free energy of the micelle, including terms pertaining to the core, the corona, and the core/corona interface, are minimized with respect to such variables as aggregation number and core radius, in order to determine the dependence of these variables on the lengths of insoluble and soluble blocks. It should be noted that, in comparison with the theoretical treatment of block copolymers in bulk, an additional component-- the solvent-- is brought to bear on block copolymer solutions. The enthalpy of micellization is therefore determined by relative contributions from polymer-solvent interaction parameters for the two blocks, χ_{AS} and χ_{BS}.

In their general form, scaling laws for aggregation numbers and core radii of block copolymer micelles can be written

$$\begin{aligned} Z &\sim N_B^{\alpha} N_A^{-\beta} \\ R_{core} &\sim N_B^{\kappa} N_A^{-\gamma} \end{aligned} \tag{7}$$

where N_A and N_B are the number of units in the soluble and insoluble blocks, respectively. This trend, where aggregation numbers and core radii increase with the insoluble block length and decrease with the soluble block length, is predicted by theory and corroborated by experimental evidence in a wide range of systems.[19] The actual exponent values vary from system to system, depending on such factors as the chemical nature of both blocks, the type of solvent, and the relative block lengths; however, in scaling laws of the type shown in eq 7, the N_B dependence is generally found to be stronger than the negative N_A dependence.

Whitmore and Noolandi developed scaling laws using the free energy minimization approach, to describe micellization in block copolymer-homopolymer blends (the homopolymer is regarded as a high-molecular weight "solvent").[25] They determined that exponents for the scaling of the core radius were in the range $0.67 < \kappa < 0.76$ and $0.1 < \gamma < 0$, indicating that the soluble block length dependence is very weak. For micelles in low-molecular weight solvent, specifically polystyrene-*b*-polybutadiene in heptane, Bluhm and Whitmore[26] refined an earlier model of Noolandi and Hong,[27] and obtained $R_{\mathrm{core}} \sim N_{\mathrm{B}}^{0.67} N_{\mathrm{A}}^{-0.01}$.

Nagarajan and Ganesh developed a more general theory that was used to calculate aggregation numbers and core radii for several block copolymer/solvent systems.[28] Scaling laws were determined in terms of the effective number of repeat units, m_{A} and m_{B}:

$$\begin{aligned} m_A &= N_A v_A / v_s \\ m_B &= N_B v_B / v_s \end{aligned} \qquad (8)$$

where v_{A} and v_{B} are the molecular volumes of the soluble and insoluble repeat units, and v_s is the molecular volume of the solvent. For micelles of polystyrene-*b*-polybutadiene in heptane, the theory predicts that the core radius scales as $R_{\mathrm{core}} \sim m_{\mathrm{B}}^{0.70} m_{\mathrm{A}}^{-0.08}$; this shows a stronger soluble block length dependence than that predicted by Bluhm and Whitmore for the same system.[26]

Halperin[21] developed a scaling theory for starlike block copolymer micelles, in which $N_{\mathrm{A}} >> N_{\mathrm{B}}$, and found the following:

$$\begin{aligned} Z &\sim N_B^{0.8} \\ R_{core} &\sim N_B^{0.6} \end{aligned} \qquad (9)$$

The same scaling laws were determined independently by Zhulina and Birshtein,[29] who investigated scaling behaviour in four different regimes of block copolymer composition. The scaling laws in eq 9 reflect a negligible N_{A} dependence when $N_{\mathrm{A}} >> N_{\mathrm{B}}$. Such behaviour was attributed to the high curvature of the cores in starlike micelles, which allows the soluble blocks to occupy a relatively large interfacial area.[21] The perturbations of coronal chains are therefore minimized, such that contributions of the soluble block length to the entropic penalty of micelle growth become insignificant. Most of the block copolymer micelles discussed in this thesis are starlike, so the predicted scaling laws in eq 9 are especially relevant to subsequent chapters.

1.4. Micellization of Diblock Ionomers

The focus of this thesis is the study and application of diblock ionomers, which are a particular group of materials in the larger family of ion-containing block copolymers (or ionic block copolymers). In general, ionic block copolymers consist of hydrophobic blocks covalently linked to blocks containing a significant number of ionic moieties.[24,30-32] A variety of synthetic ionic polymers are available, and some of these, including poly(4-vinylpyridinium alkyl halides), poly(metal acrylates), poly(metal methacrylates), and sulfonated polystyrene, have been introduced into block copolymers. The initial studies on the colloidal behaviour of ion-containing block copolymers were carried out by Selb and Gallot, who have written an excellent review of their early work.[33] In this section, the micellization of ion-containing block copolymers is compared with that of nonionic block copolymers; the two main groups of ionic block copolymers, block polyelectrolytes and block ionomers, are defined. The discussion then focuses on the second group of materials, and a summary of previous work on diblock ionomers is provided.

1.4.1. Ionic Block Copolymers: Block Polyelectrolytes and Block Ionomers

Much of the interest in ion-containing block copolymers arises from the extreme incompatibility between ionic and hydrophobic blocks, which results in stronger driving forces for microphase separation than are found in nonionic block copolymers.[24,30-32] The strong tendency to form micelles in both organic and aqueous solvents gives ionic block copolymers unusually low critical micelle concentrations compared with their nonionic counterparts. As well, aggregates of ionic block copolymers show impressive stability over long periods of time, even at extreme temperatures. This stability, though partially thermodynamic in nature, contains a predominant kinetic component; due to extreme incompatibility between the blocks, the cores of ionic block copolymers in aqueous or organic solutions are generally free of solvent, usually resulting in glassy cores and slow exchange between micelles and single chains.

Along with creating low critical micelle concentrations and high aggregate stability, the large driving force for microphase separation in ionic block copolymers allows micellization to be investigated over an impressively wide range of block copolymer compositions. In organic solvents, the micellization of diblock ionomers has been observed for extremely short ionic block lengths, down to a single ionic unit.[34-37] In aqueous environments, decreasing the length of the ionic block results in a transition from starlike to crew-cut micelles;[38] when the relative length of the ionic block is decreased even further, a wide range of non-spherical morphologies, dependent on the block copolymer composition, become thermodynamically favourable.[22] A varied array of aggregate sizes and shapes can thus be obtained from a single type of material, through changes in the relative lengths of the ionic and nonionic blocks.

It is useful to distinguish between two classes of ionic block copolymers: block polyelectrolytes and block ionomers. The difference between polyelectrolytes and ionomers has been the subject of some debate, and certain workers have suggested a classification based on the ion content of the copolymer. Eisenberg and Rinaudo, however, have classified polyelectrolytes and ionomers according to the effect of the ionic groups on the material properties.[39] According to their definitions, block polyelectrolytes are materials in which the properties are governed by electrostatic interactions over the relatively large distances within the micelle coronae and between the aggregates; conversely, block ionomers are materials in which the properties are governed by strong, short-range electrostatic interactions within ionic microdomains.[24]

It follows from the above definitions that a given ionic block copolymer may be either a block polyelectrolyte or a block ionomer, depending on the nature of the solvent in which self-assembly occurs.[24] In aqueous environments, it is the hydrophobic blocks which form the micelle core, and long-range electrostatic interactions among solvated ionic blocks allow these water-soluble systems to be classified as block polyelectrolytes;

the term "regular micelle" is also applied to the aggregates. In organic solvents, ionic block copolymers are classified as block ionomers, or "reverse micelles", as microphase separation results in compact ionic cores, solubilized by hydrophobic coronae. These materials are also known as block ionomers in the bulk state; in this case, the coronal chains form a matrix phase, in which the ionic cores are evenly dispersed. The discussion now focuses on the micellization of ionic block copolymers in organic solvents, and the characterization of the resulting diblock ionomer aggregates in solution and the solid state.

1.4.2. Other Studies of Diblock Ionomer Micelles

The first study on the colloidal properties of ion-containing block copolymers in organic solvents was published in 1991,[4] and since then a number of investigations on such systems have appeared in the literature. A large number of these studies have focused on polystyrene-based diblock ionomers, with relatively long PS blocks covalently linked to short ionic segments. This composition regime is known to form starlike spherical micelles, with small ionic cores and large PS coronae. The work described in this section involved the following species of ionic blocks: poly(metal acrylates), poly(metal methacrylates), and quaternized poly(4-vinylpyridine) (P4VP). As well, systems such as quaternized P4VP-*b*-PS-*b*-P4VP triblock ionomers[40] and sodium-neutralized poly(*tert*-butylstyrene)-*b*-lightly sulfonated polystyrene[41] in nonpolar solvents have also been investigated.

In the first detailed investigation block ionomer reverse micelles, polystyrene-*b*-poly(sodium methacrylate) (PS-*b*-PMANa) and polystyrene-*b*-poly(cesium methacrylate) (PS-*b*-PMACs) of various compositions were studied in different solvents selectively good for polystyrene.[4] Size-exclusion chromatography (SEC) was used to demonstrate that the resulting micelles were extremely stable, and did not show an appreciable dynamic equilibrium over long periods of time. For a wide range of PS-*b*-PMANa and PS-*b*-PMACs samples, SEC coupled with viscometry was used to determine aggregation numbers and hydrodynamic radii as functions of block ionomer composition. By this method, the micellar molecular weights and aggregation numbers were determined from a universal calibration curve of $\log([\eta]M)$ versus the SEC elution volume, where $[\eta]$ is the intrinsic viscosity and M is the molecular weight of the eluting sample. Hydrodynamic radii were calculated from the following relationship:

$$[\eta]M = (10/3)Z\pi R_h^{\,3} \qquad (10)$$

where Z in the micelle aggregation number and R_h is the hydrodynamic radius. Both aggregation numbers and hydrodynamic radii were found to increase as the number of ionic repeat units was increased for a given PS block length. Aggregation numbers decreased as the length of the soluble PS block increased, suggesting an increase in the solubility of single chains; however, the hydrodynamic radius was found to increase. This finding is not surprising, since the thickness of the corona increases with the length of the PS block, resulting in an overall increase in micelle radius, despite a lowering of the aggregation number. In a subsequent study, hydrodynamic radii from SEC and viscometry were confirmed by dynamic light scattering (DLS).[42]

Information on the internal structure of block ionomer micelles is not available using light scattering techniques (SLS and DLS), due to the limited length scales which can be probed with visible light. In order to probe dimensions smaller than the micelle, therefore (e.g., the radius of the ionic core), radiation with much shorter wavelengths must be used. To this end, small-angle x-ray scattering (SAXS) has been used to determine core sizes in starlike reverse micelles, in systems of polystyrene-*b*-poly(cesium acrylate) (PS-*b*-PACs) and PS-*b*-PMACs in toluene.[43] The interpretation of form factors from SAXS data revealed that ionic core radii scale roughly as $N_B^{3/5}$ (where N_B is the number of repeat units in the ionic block), independent of the PS block length. This is in agreement with the predictions of Halperin's model of starlike block copolymer micelles.[21] The data were fitted to the scaling law and a proportionality constant of 6.5 Å was determined. In further work, core sizes were determined for quaternized PS-*b*-P4VP, and the same fit to the Halperin model was obtained.[44] SAXS data and computer modeling were also used to determine radii polydispersity indexes (RPI), which were between 1.02 and 1.04, suggesting that the populations of ionic cores had very low polydispersities. A comparison of ionic core radii and contour (fully extended) lengths of the core-forming blocks revealed a high degree of chain extension within the cores of block ionomers. High extension of the core-forming blocks was also observed for nonionic cores within an ionic matrix.[45] It was therefore concluded that high degrees of chain extension within the cores of block ionomers is due, not to electrostatic repulsion, but to the minimization of interfacial energy between ionic and nonionic components.

As mentioned earlier, the strong segregation limit of microphase separation is characterized by well-defined interfaces and perturbed chain conformations within the microdomains. The high degrees of chain extension observed in block ionomers (in some cases, greater than 100% of the contour length)[45] imply that these systems are certainly in the SSL, and are, in fact, an extreme example of strong segregation. For such cases, Khokhlov[13] has proposed the existence of a third regime, based on the following physical limits: (1) complete extension of the core-forming blocks, or (2) complete occupation of the microphase interface with AB junctions (i.e., no room for another chain to enter the micelle). When either of these limits are reached, the system is said to enter the superstrong segregation limit (SSSL). Although micelles of block ionomers appear to be excellent candidates for the SSSL, core radii determined in ref. 45 do not completely agree with theoretical scaling laws for superstrong segregation, which predict a linear increase in R_{core} with increasing N (the total degree of polymerization).

Another micellar parameter that has been recently investigated is chain mobility within the PS corona.[46] Using nuclear magnetic resonance spectroscopy (NMR), the coronal chain dynamics can be determined in some detail at the segmental level. This was demonstrated in systems of PS-*b*-PACs in CCl_4, by probing the mobility of ^{2}H-labeled PS "tags" at various distances from the ionic core. A comparative analysis of relaxation times revealed that segmental mobility is considerably restricted close to the ionic core, and approaches that of "free" homopolystyrene at ca. 40 units from the ionic-nonionic junction. Segmental mobility within the corona was also found to become more restricted as the size of the ionic core increased.

It is well established that reverse micelles of surfactants such as AOT are able to solubilize significant amounts of water within their ionic cores, resulting in water pools that can act as "microreactors" for hydrophilic reagents. The applicability of block ionomers for such localized, microscale (or nanoscale) chemistry is dependent on the ability of the ionic cores to solubilize polar species of low molecular weight. The solubilization of water into the cores of block ionomers has been studied by proton NMR, in order to determine the distribution of water between the micelle and the nonpolar solvent.[47,48] In these experiments, a single proton chemical shift was observed; this was a weighted average of the chemical shift of water in the ionic core and in the solvent. The single chemical shift indicated fast exchange of water between the micelle and the solvent, which suggested that the ionic cores are liquid-like in the presence of water.

From an analysis of the chemical shift of water protons in solutions of block ionomers, the equilibrium constants in favour of the reverse micelles were determined for various nonpolar solvents, and were found to occur in the following order: cyclohexane > benzene ~ toluene >> THF ~ DMF.[47] For different ionic moieties, the equilibrium constants in favour of water solubilization were found to decrease as follows: sodium sulfonates > sodium carboxylates >> methyl iodide pyridinium.[48]

1.5. Semiconducting Nanoparticles: Materials of "Neglected Dimensions"

In recent years, a great amount of attention has focused on the synthesis and characterization of metal and *semiconducting nanoparticles*. Such nanoparticles range in size from < 1 nm to almost 10 nm, containing from < 10 to several hundred molecular units.[49] Much of the interest surrounding these "ultrasmall" particles is based on their unusual optical and electronic properties, which are quite different from those of the bulk materials; for this reason, the study of nanoparticles has been said to bridge the "neglected dimensions"[50] between single atoms or molecules and bulk metals or semiconductors.[51] Along with such fundamental interest, the potential applications of nanoparticles to photocatalysis, electro-optical materials, and nonlinear optical devices has been recognized; for such applications, particle stability, size and polydispersity control, along with the dispersion of nanoparticles in a suitable medium, have become critical issues. This section begins with a brief discussion of the quantum-confinement effect in semiconducting nanoparticles, or "quantum dots"; theories of small metal particles are not mentioned here, as they do not pertain directly to this thesis. A summary of different strategies of nanoparticle synthesis will then be given, including the recent application of block copolymer microreactors.

1.5.1. The Quantum-Confinement Effect

The band structure in bulk semiconductors is not a property of the individual "molecules" or ion pairs that make up the solid, but rather arises from the overlap of molecular orbitals from a large number of these ion pairs arranged in a crystal lattice.[52] In effect, the molecular orbitals are delocalized over the entire crystal, and the movement of electrons is restricted only by the relatively small energy gap separating valence and conduction bands. The energy of the first excited state, termed the exciton, is therefore virtually identical to the band gap energy in bulk. It should be noted that in some solids, electrons are "bound" in the exciton state by electrostatic attraction to the holes left behind in the valence band, and can only escape into the conduction band at energies slightly higher than the exciton. In bulk semiconductors, however, the thresholds for exciton absorption and photoconduction are nearly identical.

When the size of a semiconducting particle is comparable to, or smaller than, the exciton in the macrocrystalline material (i.e., the size of the de Broglie wavelength of the electron) the delocalized bands become quantized, and the energy of the exciton increases.[49] This situation has been described by Brus as a particle (the electron) in a spherical box (the nanoparticle), in which the movement of the particle is confined by an infinitely high potential at the interface.[53] Brus determined the exciton energy for the semiconducting nanoparticle by calculating the confinement energy of the electron:

$$E^* \cong E_g + \frac{\hbar^2\pi^2}{2R^2}\left[\frac{1}{m_e} + \frac{1}{m_h}\right] - \frac{1.8e^2}{\varepsilon R} + \ldots \qquad (11)$$

where E^* is the energy of the exciton, E_g is the band gap energy in bulk, m_e and m_h are the masses of electrons and holes in the lattice, R is the radius of the particle, e is the charge of an electron and ε is the permittivity. The band gap energy in bulk is a constant for each semiconductor (e.g., for CdS, $E_g = 2.4$ eV). The second term on the right-hand-side of eq 11 is the quantum-confinement term, which increases as the particle size decreases; the third term arises from Coulombic attraction between electrons and holes, and is much smaller than the confinement term. The "particle-in-a-box" model thus predicts an increase in the energy of the exciton as the particles decrease in size, with E^* asymptotically approaching E_g as particle dimensions extend into the bulk.

The quantum-confinement effect is clearly manifested in the absorption spectra of semiconducting nanoparticles; increases in the exciton energy are observed via "blue shifts" (increases in energy) in the onset of absorption.[54,55] In CdS semiconductors, large particles show an absorption onset of around 515 nm, corresponding to the bulk band gap energy of 2.4 eV. Below a particle diameter of about 60 Å, however, the absorption onset is found to shift to higher energies (lower wavelengths), as shown in Figure 1.6.[49] Also in the Figure 1.6, it will be noted that the spectra exhibit increasing structure as the quantum-confinement effect becomes more pronounced.

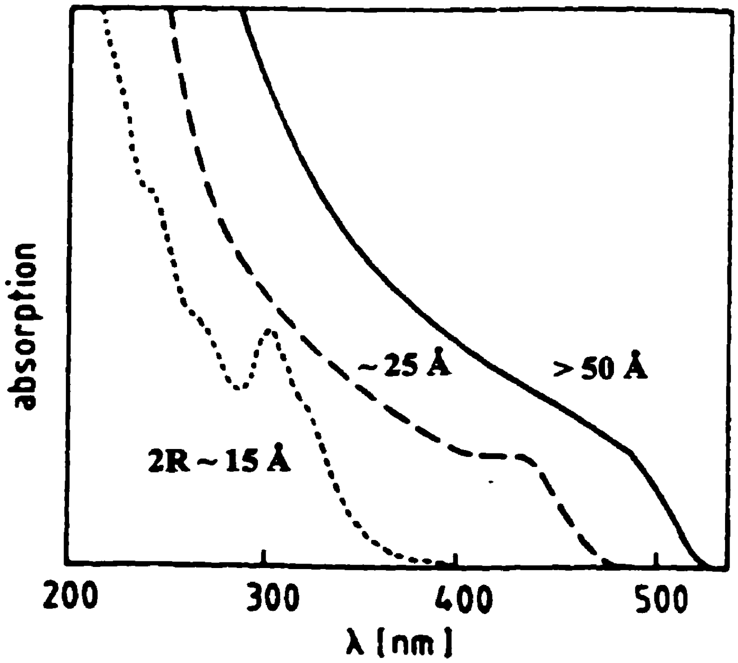

Figure 1.6. UV-vis absorption spectra of CdS nanoparticles with different mean particle sizes.

Using both theoretical and empirical methods, the quantum-confinement effect has been quantified in plots of the absorption threshold versus average particle size. Such plots for PbS, CdS and ZnO are shown in Figure 1.7; the band gap energies of the bulk materials are indicated in parentheses.[49] The curves for PbS and CdS are used in subsequent chapters to determine semiconducting nanoparticle sizes from absorption data.

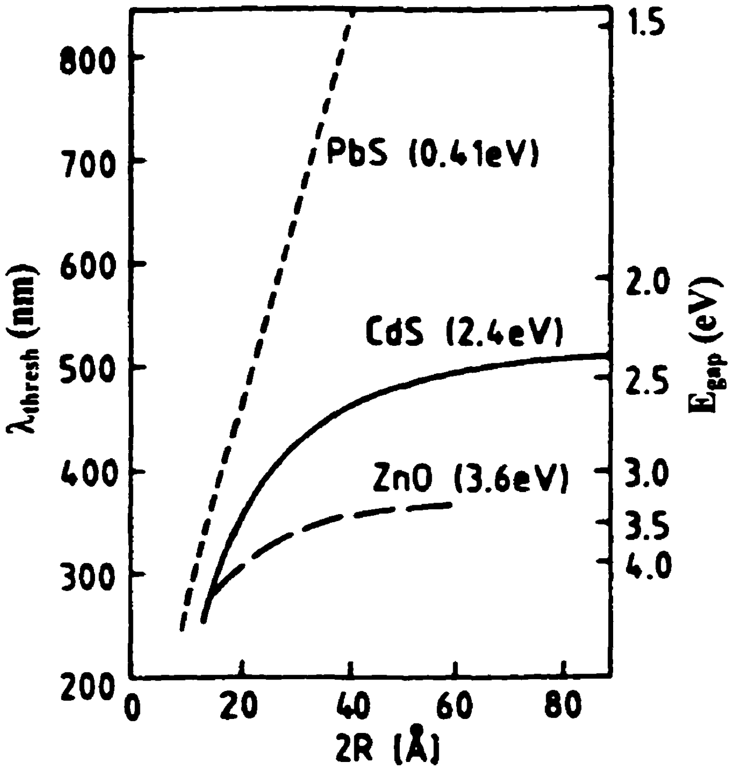

Figure 1.7. Absorption threshold and band gap energy as a function of particle size for CdS, ZnO, and PbS.

1.5.2. Strategies of Nanoparticle Synthesis

A common goal behind many methods of semiconducting nanoparticle synthesis is the arrested precipitation of ions into a crystal lattice, such that the particle is unable to grow to bulk dimensions. Earlier methods involved the simple kinetic strategy of controlling the rate of crystal growth with respect to the rate of nucleation. This was first accomplished by rapid stirring of the constituent ions in dilute solutions; size control was exerted to some extent through variations in the temperature, with colder temperatures giving smaller colloidal particles.[56] Kinetic control has also been accomplished in surfactant-stabilized systems such as reverse micelles[57-60] and surfactant vesicles.[61,62] By these methods, the particle sizes are controlled through variations in the amount of water added to the microemulsions, or through changes in the relative concentrations of ions. Along with their role in the kinetics of ion exchange, the surfactants also act to protect the surface of growing semiconductor particles, preventing agglomeration of particles and macroscopic precipitation. Semiconductor colloids have also been stabilized through passivation of the particle surfaces with organic ligands.[63]

A more recent approach to nanoparticle synthesis has involved the use of synthetic polymers as media for particle growth.[64-75] Several workers have employed ion-containing polymers, in which the inorganic ions are localized in distinct regions of the polymer matrix; these ions are then converted to metallic or semiconducting particles through simple reduction or substitution reactions. In commercial random ionomers such as Nafion[64-69] and Surlyn,[70,71] PbS and CdS nanoparticles of a wide range of sizes have been prepared, using various conditions of ion-loading and annealing.

Other advantages are offered by block copolymer systems, in which metal ions are introduced into ion-complexing microdomains, and subsequently converted to metal or semiconducting particles.[72-76] In these simple chemical conversions, the microdomains, or cores, act as *microreactors*, localizing and containing inorganic reagents in a manner that is analogous to the round-bottom flasks of larger-scale operations. The use of a block copolymer microreactor is represented in Figure 1.8, showing two possible outcomes of the chemical conversion: the *"raspberry"* and *"cherry"* morphologies.[75]

In the early stages of chemical conversion, a number of nucleation sites may form throughout the microdomain, resulting in a raspberry. If, however, a single nucleation site forms in each core, or if the raspberry "seeds" come together following nucleation to form a single particle, then the microreactor and its product will resemble a cherry. The cherry morphology is by no means "the pits", as the formation of a single particle in each core results in a direct correlation between the particle size and the original number of ions in the microreactor. This provides an excellent mechanism of size control, provided that (1) the system can be induced to adopt the cherry morphology, and (2) the number of ions in the microreactor can be controlled in a reliable manner. Both of these conditions are addressed in the present thesis, with a particular emphasis on the second point, where block ionomers offer some unique advantages.

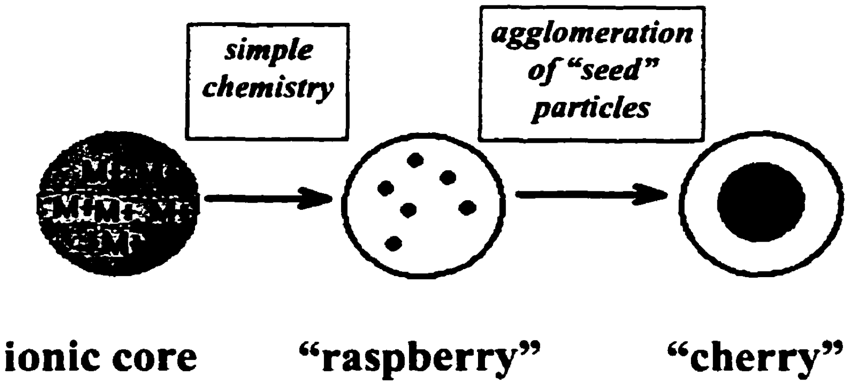

Figure 1.8. Chemical conversion of ions in a block copolymer microreactor, showing "raspberry" and "cherry" morphologies.

1.6. Small-Angle Neutron Scattering

Part of the work described in this thesis has involved the use of small-angle neutron scattering (SANS) to investigate coronal structure in block ionomer micelles. The following section provides a brief introduction to the SANS technique and aspects of instrumentation. First, the principles and terminology of SANS are summarized, with a special emphasis on scattering from polymer chains. Some technical information on both of the spectrometers used for this work is then presented. Details on data analysis and specific experimental parameters are given in subsequent chapters, and are therefore omitted from this introductory discussion.

1.6.1. A Basic Introduction to Small-Angle Neutron Scattering

The scattering of neutrons incident on a sample is attributed to interactions with the nuclei in the system, resulting in secondary waves that are "scattered" in all directions; the scattered waves are out of phase with the incident waves, and have amplitudes that are dependent on the nuclei.[77] The square of the sum of the amplitudes for radiation scattered at all angles gives the scattered intensity function, $I(q)$, where q is the scattering vector, which is the vector difference between incident and scattered neutrons. q is defined as follows:

$$q = \frac{4\pi}{\lambda}\sin\left(\frac{\theta}{2}\right) \tag{12}$$

where λ is the neutron wavelength and θ is the scattering angle.

The scattering function is the sum of two signals, attributed to coherent and incoherent scattering. Coherent scattering is dependent on the scattering vector, and is due to the interference between scattering from individual nuclei; it contains information on the spatial distribution of nuclei and therefore on the structure of the sample. The contribution from incoherent scattering arises from the random distribution of isotopes and nuclear spin states, and results in a constant background that is not dependent on the scattering vector. The incoherent scattering is generally subtracted in the data reduction procedure, and information on structure is obtained from the coherent scattered intensity.

The power of a nucleus to scatter neutrons is defined by its scattering length, b, or the scattering cross section, $\sigma = 4\pi b^2$. Variations in the scattering cross section are not systematic as one moves across the periodic table, and σ can vary significantly between isotopes of the same element. The most common (and most useful) example is hydrogen and deuterium, where deuterium has a significantly higher scattering cross section than the lighter isotope. This permits molecules to be "labeled", by replacing hydrogen atoms with deuterium, such that scattering from labeled molecules contributes most strongly to the scattered signal. For example, in the present work, perdeuterated polystyrene labels are placed in different parts of the micelle corona. Since the entire micelle, with the exception of the labels, is contrast-matched with the surrounding solvent (i.e., has the same scattering cross section as the solvent), only the labels are "visible" to the neutrons. The scattered intensity therefore reveals specific information on the conformation of perdeuterated labels in different regions of the micelle corona.

The coherent scattered intensity, $I(q)$, is the product of the form factor and the structure factor:

$$I(q) = P(q)S(q) \tag{13}$$

where the form factor, $P(q)$, arises from intraparticle interference and the structure factor, $S(q)$, is due to interparticle interference. Since the determination of chain conformations for individual labels is the aim of the present work, the form factor is the more important contribution. Methods of separating form and structure factor contributions will be discussed in a later chapter.

The form factor can be regarded as the Fourier transform of the distribution of pairs of scattering centers (i.e., nuclei) within the particle:

$$P(q) = \int n(r)\left[\frac{\sin qr}{qr}\right]dr \tag{14}$$

where $n(r)$ is a number distribution of scattering pairs separated by distance r; the expression is integrated over the entire particle. For polymer chains, the expression within the integral must also averaged over all possible chain conformations and spatial orientations of the molecule.[77]

Through the Fourier transform, the variables q and r are said to be conjugated; that is, as the scattering vector increases, the dimensions that are probed within the particle decrease. Because of the relatively small wavelengths that are available using neutrons, SANS allows length scales down to < 10 Å to be probed, while light scattering techniques are unable to resolve dimensions smaller than most colloidal particles.

A scattering profile is sometimes regarded as a "microscope", with larger values of q corresponding to smaller length scales and therefore higher magnification.[77] For polymer chains, it is useful to distinguish three regions of "low", "intermediate", and "high" magnification. In the region of small scattering vectors (low magnification), the scattering probes length scales on the order of the radius of gyration R_g of the chains. This region is referred to as the Guinier regime, and is generally defined as $q < 1/R_g$. If the polymer chains are made up of statistical segments of length l, an intermediate region of scattering is defined $1/R_g < q < 1/l$, in which information on chain statistics (e.g., chain "stiffness") can be obtained. This region is of particular interest in subsequent discussions. For very high scattering vectors in the region $q > 1/l$ (high magnification), the neutrons "see" the individual segments that make up the chains, and the profile resembles that of a rigid rod. It should be noted that if a polymer chain is very stiff, the region $q > 1/l$ may correspond to scattering vectors normally associated with the "intermediate" region, suggesting that the chain resembles a rigid rod at relatively large length scales.

1.6.2. Spectrometer Specifications

The four main features of a small-angle neutron spectrometer are the neutron source, the monochromator, the collimator, and the detector. These are discussed briefly below, in reference to both spectrometers used in this work: (1) Beamline H9-B at the High Flux Beam Reactor, Brookhaven National Laboratory (BNL) , Upton, NY and (2) Beamline NG7 at the Cold Neutron Research Facility, National Institute of Standards and Technology (NIST), Gaithersburg, MD.

1.6.2.1. BNL Spectrometer

The High Flux Beam Reactor at BNL uses highly enriched Uranium-235 fuel and a heavy water moderator to sustain a controlled nuclear reaction; the reactor is expressly designed to maximize the number of neutrons available to external beams. Fast and epithermal neutrons from the region of the fuel cells escape to a D_2O reflector surrounding the core, where they are further moderated and converted to thermal neutrons. The useful thermal neutron population peaks in the reflector, where the neutrons are accessible to various beam tubes. In beam tube H9, thermal neutrons from the reflector are scattered within a liquid-hydrogen cold neutron moderator, providing intense beams of low-energy "cold" neutrons (≤ 5 meV).

At beamline H9-B, the cold neutrons pass through a Be-filter, then are guided along a flight path with Ni-coated neutron guides. Monochromatization is achieved with exchangeable Ni-Ti or Fe-Mn multilayers with bilayer spacings between 50 and 150 Å. The monochromatic beam is then collimated over a length of 2 m by a series of apertures of decreasing diameter. The typical diameter of the primary beam at the sample is ca. 6 mm. Scattered intensity from the sample is detected using a high-resolution area detector of 50 x 50 cm^2 consisting of a 128 x 128 pixel grid. To vary the range of the scattering vector, the sample-to-detector distance is variable between 50-200 cm. Beamline H9-B is shown in the schematic in Figure 1.9.

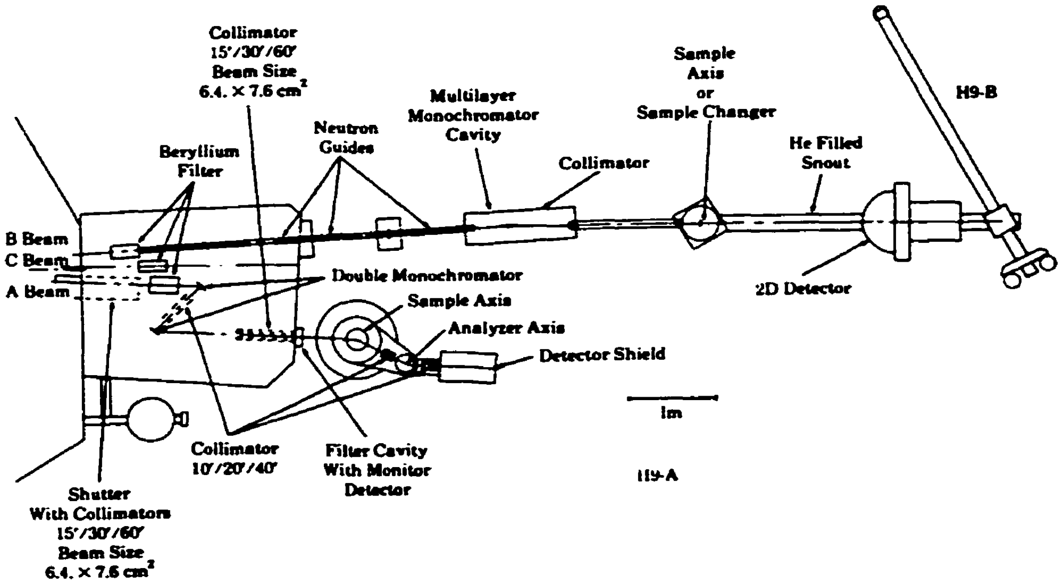

Figure 1.9. Schematic plan of spectrometers installed at H9 (HFBR, Brookhaven National Labs).

1.6.2.2. NIST Spectrometer

The SANS spectrometers at NIST (including NG7) are installed at the end of straight neutron guides in the guide hall of the Cold Neutron Research Facility. Before entering the neutron guide, neutrons from the research reactor are slowed down in a liquid-hydrogen neutron moderator. The mainly "cold" neutrons are then passed through Be and Bi filters, to eliminate residual epithermal neutrons and core gamma radiation, respectively. Monochromatization is accomplished mechanically, using a helical channel velocity selector with variable speed and pitch; this enables both the mean wavelength (5 to 20 Å) and wavelength spread (0.10 to 0.30 FWHM) to be varied.

The monochromated beam is collimated using circular pinhole irises in a 15 m evacuated flight path. Incorporated into this flight path are eight 1.5 m long neutron guides that can be shifted in or out to vary the beam divergence and flux on the sample.

The post-sample flight path consists of a long cylindrical section that forms an evaculated enclosure for a 2D positron-sensitive detector (64 x 64 cm^2 with $1cm^2$ spatial resolution). The sample-to-detector distance can be varied continuously from 1.3 to 15 m. A schematic of the NG7 spectrometer is shown in Figure 1.10.

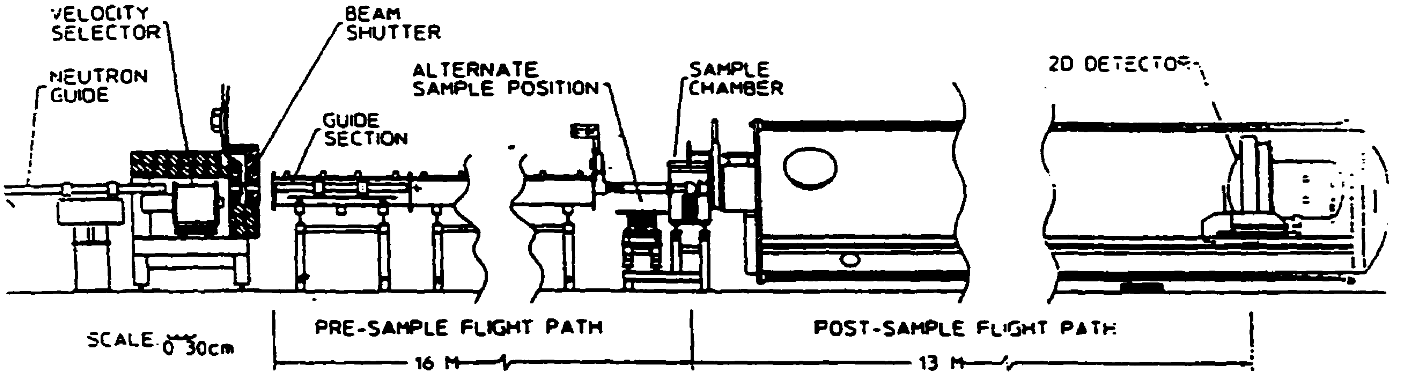

Figure 1.10. Schematic plan of beamline NG7 (Cold Neutron Research Facility, NIST).

1.7. Focus and Scope of the Thesis

As mentioned at the beginning of chapter 1, this dissertation concerns two different aspects of block ionomers. First, the thesis addresses the use of ionic cores in block ionomers as microreactors of controllable size, with an emphasis on semiconducting nanoparticles synthesis. The focus then shifts from the ion-containing cores to the soluble coronae of the micelles; in this context, an investigation of coronal structure by small-angle neutron scattering (SANS) is discussed.

The synthesis and characterization of metal and semiconducting nanoparticles in various media has been an active area of research for about 15 years, in which time attention has gradually shifted from purely fundamental investigations to the search for new and useful materials. The first goal of the present work was to explore the numerous advantages of block ionomers for nanoparticle synthesis, such as size control, stability, and versatility. Earlier studies of random and block ionomers were an important impetus for this research, as these investigations yielded useful information on ion aggregation numbers as a function of ionomer composition. This a priori knowledge provides unique control of ionic aggregate sizes, and its application to the size control of nanoparticles is a central theme of this thesis. The characterization of block ionomer composites has not yet included detailed investigations of their electronic and photocatalytic properties; however, such studies will be an important aspect of future research.

Several workers have investigated the coronal region of block copolymer micelles using small-angle neutron (SANS) and small-angle x-ray scattering (SAXS) techniques.[78-83] These studies described average coronal structure, determined from contrasting the entire micelle corona. In related star polymer systems, perdeuterated labels have been used in conjunction with SANS experiments, in order to obtain selective contrast of spherical polymer brushes at different radial distances.[84-87] It is recognized that such labeling techniques offer detailed and spatially-specific information, and their application to the dense brushes of block copolymer micelles presents some interesting possibilities. The second goal of this work, therefore, was the systematic investigation of coronal structure in block ionomers, using perdeuterated labels situated at various distances from the ionic core.

Chapter 2 of the thesis is a review of recent investigations of ion-containing block copolymers in aqueous and organic media. This article was originally written for *Accounts of Chemical Research*,[30] and is included to supply supplemental information on related research in the growing field of ionic block copolymers. It should be noted that some of the work presented in subsequent chapters is also summarized in this review.

Chapters 3 and 4 concern the synthesis of semiconducting nanoparticles in ionomer "microreactors". Chapter 3 introduces the concept of nanoparticle size control via a series of random ionomers with variable-length spacers; this provides a model for controlled particle growth, in which the mechanism of size control is very similar to that found in block ionomers. In chapter 4, the discussion turns to CdS nanoparticle synthesis in block ionomer micelles, and to the study of the resulting composites with respect to versatility, stability, and processability.

In chapter 5, the system of block ionomer microreactors is expanded to include a broader range of metal ions. The dependence of aggregation numbers and related scaling relations on the choice of metal ion is discussed in the context of nanoparticle synthesis. An extensive study of block ionomers containing different metal ions is presented, including characterization by static light scattering, size-exclusion chromatography, and transmission electron microscopy. As well, an investigation of hydrodynamic behaviour in block ionomer colloids by dynamic light scattering is described.

Chapter 6 concerns the controlled assembly of CdS-containing micelles in aqueous media to form novel, water-soluble aggregates of semiconducting nanoparticles. This work demonstrates the versatility of block ionomer composites, which can serve as "building blocks" for interesting secondary structures.

Chapters 7 and 8 are dedicated to the investigation of coronal structure in block ionomers by SANS. Chapter 7 describes the study of two block ionomer samples with similar aggregation numbers and perdeuterated labels located at slightly different distances from the ionic core. An investigation of chain stiffness under various conditions of solvent and block ionomer concentrations is presented. In chapter 8, the continued investigation of coronal structure, including a wider range of label positions, is described. As a detailed picture of coronal structure emerges, block ionomers are compared with the "blob" model of spherical brushes, and with Gaussian star polymers.

The final chapter includes general conclusions, a discussion of contributions to original knowledge, and suggestions for further work.

References

(1) Cowie, J. M. G. *Polymers: Chemistry & Physics of Modern Materials*, 2nd ed., Chapman & Hall: New York, 1991.

(2) Szwarc, M. *Carbanions, Living Polymers and Electron Transfer Processes*, Interscience Publishers, Inc., 1968.

(3) Hautekeer, J. P.; Varshney, S. K.; Fayt, R.; Jacobs, C.; Jerome, R.; Teyssie, Ph. *Macromolecules* **1990**, *23*, 3893.

(4) Desjardins, A.; Eisenberg, A. *Macromolecules* **1991**, *24*, 5779.

(5) Long, T. E.; Allen, R. D.; McGrath, J. E. In *Chemical Reactions On Polymers*; Benham, J. L.; Kinstel, J. F., Eds.; ACS Symposium Series 364; American Chemical Society: Washington, DC, 1988; chapter 19.

(6) Gauthier, S.; Duschesne, D.; Eisenberg, A. *Macromolecules* **1987**, *20*, 753.

(7) Zhong, X. F.; Varshney, S. K.; Eisenberg, A. *Macromolecules* **1992**, *25*, 7160.

(8) Helfand, E.; Wasserman, Z. R. In *Developments in Block Copolymers*, Goodman, I., ed., Applied Science Publishers: London, 1982.

(9) Meier, D. J. In *Thermoplastic Elastomers: A Comprehensive Review*, Legge, N. R.; Holden, G.; Schroeder, H. E., eds., Hanser: New York, 1987; Chapter 11.

(10) Bates, F. S.; Frederickson, G. H. *Annu. Rev. Phys. Chem.* **1990**, *41*, 525.

(11) Lewis, G. N.; Randall, M. *Thermodynamics*, McGraw-Hill: New York, 1923.

(12) Flory, P. J. *Principles of Polymer Chemistry*, Cornell Univeristy Press: Ithaca, New York, 1953.

(13) Nyrkova, I. A.; Khokhlov, A. R.; Doi, M. *Macromolecules* **1993**, *26*, 3601.

(14) (a) Aggarwal, S. L. *Polymer* **1976**, *17*, 938. (b) Hasegawa, H.; Tanaka, H.; Yamasaki, K.; Hashimoto, T. *Macromolecules* **1987**, *20*, 1651.

(15) (a) Olmstead, P. D.; Milner, S. *Phys. Rev. Lett.* **1994**, *72*, 936; *Phys. Rev. Lett.* **1995**, *74*, 829. (b) Khandpur, A. K.; Forster, S.; Bates, F. S.; Hamley, I. W.; Ryan, A. J.; Bras, W.; Almdal, K.; Mortensen, K. *Macromolecules* **1995**,*28*, 8796.

(16) Leibler, L. *Macromolecules* **1980**, *13*, 1602.

(17) Tuzar, Z., Kratochvil, P. In *Advances in Colloid and Interface Science,* 1976; vol.6,

pp. 201-232

(18) Price, C. In *Developments in Block Copolymers,*Goodman, I., ed., Applied Science Publishers: London, 1982; pp. 39-79.

(19) Tuzar, Z., Kratochvil, P. In *Surface and Colloid Science,* Matijevic, E., ed., Plenum Press: New York, 1993; pp. 1-83.

(20) de Gennes, P. G. In *Solid State Physics*, Liebert, L., ed., Academic Press: New York, 1978; supp. 14, p. 1.

(21) Halperin, A. *Macromolecules* **1987**, *20*, 2943.

(22) Zhang, L.; Eisenberg, A. *Science* **1995**, *268*, 1728; Zhang, L.; Yu, K.; Eisenberg, A. *Science* **1996**, *272*, 1777; Zhang, L.; Eisenberg, A. *J. Am. Chem. Soc.* **1996**, *118*, 3168; Yu, K.; Zhang, L.; Eisenberg, A. *Langmuir* **1996**, *12*, 5980.

(23) Gao, Z.; Eisenberg, A. *Macromolecules* **1993**, *26*, 7353.

(24) Moffitt, M.; Zhang, L.; Khougaz, K.; Eisenberg, A. In *Solvents and Self-Organization of Polymers*, Webber, S. E. et al., eds., Kluwer Academic Publishers: Amsterdam,1996; pp. 53-72.

(25) Whitmore, M.; Noolandi, J. *Macromolecules* **1985**, *18*, 657.

(26) Bluhm, T. L.; Whitmore, M. D. *Can. J. Chem.* **1985**, *63*, 249.

(27) Noolandi, J.; Hong, K. M. *Macromolecules* **1983**, *16*, 1443.

(28) Nagarajan, R.; Ganesh, K. *J. Chem. Phys.* **1989**, *90*, 5843.

(29) Zhulina, E. B.; Birshtein, T. M. *Vysokomol. Soedin.* **1985**, *27*, 511.

(30) Moffitt, M.; Khougaz, K.; Eisenberg, A. *Acc. Chem. Res.* **1996**, *29*, 95.

(31) Khougaz, K.; Zhang, L.; Moffitt, M.; Eisenberg, A. *Vysokomol. Soedin.* **1996**, *38*, 582.

(32) Moffitt, M.; Eisenberg, A. *Macromol. Symp.* **1997**, *117*, 181.

(33) Selb, J., Gallot, Y. In *Developments in Block Copolymers,* Goodman, I., ed., Elsevier Applied Science: London, 1985; vol. 2, p. 27.

(34) Jalal, N.; Duplessix, R. *J. Phys. France* **1988**, *49*, 1775.

(35) Davidson, N. S.; Fetters, L. J.; Funk, W. G.; Graessley, W. W.; Hadjichristidis, N. *Macromolecules* **1988**, *21*, 112; Pispas, S.; Hadjichristidis, N. *Macromolecules*

1994, *27*, 1891; Pispas, S.; Hadjichristidis, N.; Mays, J.M.; *Macromolecules* **1994**, *27*, 6307.

(36) Zhong, X. F.; Eisenberg, A. *Macromolecules* **1994**, *27*, 1751.

(37) Zhong, X. F.; Eisenberg, A. *Macromolecules* **1994**, *27*, 4914.

(38) Gao, Z.; Varshney, S. K.; Wong, S.; Eisenberg, A. *Macromolecules* **1994**, *27*, 7923.

(39) Eisenberg, A.; Rinaudo, M. *Polymer Bulletin* **1990**, *24*, 671.

(40) Ishizu, K.; Kashi, Y.; Fukutomi, T.; Kakurai, T. *Makromol. Chem.* **1982**, *183*, 3099.

(41) Zhou, Z.; Peiffer, D. J.; Chu, B. *Macromolecules* **1994**, *27*, 1428.

(42) Desjardins, A.; van de Ven, T. G. M.; Eisenberg, A. *Macromolecules* **1992**, *25*, 2412.

(43) Nguyen, D.; Williams, C. E.; Eisenberg, A. *Macromolecules* **1994**, *27*, 5090.

(44) Nguyen, D. Ph.D. thesis, McGill University: Montreal, 1994.

(45) Nguyen, D.; Varshney, S. K.; Williams, C. E.; Eisenberg, A. *Macromolecules* **1994**, *27*, 5086.

(46) Gao, Z.; Zhong, X. F.; Eisenberg, A. *Macromolecules* **1994**, *27*, 794.

(47) Gao, Z.; Desjardins, A.; Eisenberg, A. *Macromolecules* **1992**, *25*, 1300.

(48) Khougaz, K.; Gao, Z.; Eisenberg, A. *Langmuir* **1997**, *13*, 623.

(49) Henglein, A. *Chem. Rev.* **1989**, *89*, 1861.

(50) Ostwald, W. *Die Weit der Vernachlassigten Dimensionen*, Steinkopff: Dresden, 1920.

(51) Weller, H.; Koch, V.; Gutierrez, M.; Henglein, A. *Ber. Bunsenges. Phys. Chem.* **1984**, *88*, 649.

(52) Cox, P. A. *The Electronic Structure and Chemistry of Solids*, Oxford University Press: Oxford, 1991.

(53) Brus, L. *J. Phys. Chem.* **1986**, *90*, 2555.

(54) Brus, L. E. *J. Chem. Phys.* **1983**, *79*, 5566.

(55) Brus, L. E. *J. Chem. Phys.* **1984**, *80*, 4403.

(56) Rosetti, R.; Hull, R.; Gibson, J. M.; Brus, L. E. *J. Chem. Phys.* **1985**, *82*, 552.

(57) Meyer, M.; Wallberg, C.; Kurihara, K.; Fendler, J. H.; *J. Chem. Soc., Chem Commun.* **1984**, 90.

(58) Lianos, P.; Thomas, J. K. *Chem. Phys. Lett.* **1986**, *125*, 299.
(59) Petit, C.; Lixon, P.; Pileni, M. P. *J. Phys. Chem.* **1990**, *94*, 1598.
(60) Pileni, M. P.; Motte, L.; Petit, C. *Chem. Mater.* **1992**, *4*, 338.
(61) Tricot, Y.-M.; Fendler, J. H. *J. Phys. Chem.* **1986**, *90*, 3369.
(62) Watzke, H. J.; Fendler, J. H. *J. Phys. Chem.* **1987**, *91*, 854.
(63) Steigerwald, M. L.; Alivisatos, A. P.; Gibson, J. M.; Harris, T. D.; Kortan, R.; Muller, A. J.; Thayer, A. M.; Duncan, T. M.; Douglass, D. C.; Brus, L. E. *J. Am. Chem. Soc.* **1988**, *110*, 3046.
(64) Krishnan, M.; White, J. R.; Fox, M. A.; Bard, A. J. *J. Am. Chem. Soc.* **1983**, *105*, 7002.
(65) Mau, A. W.- A.; Huang, C. B.; Kakuta, N.; Bard, A. J.; Campion, A.; Fox, M. A.; White, J. M.; Webber, S. E. *J. Am. Chem. Soc.* **1984**, *106*, 6537.
(66) Kuczynski, J. P.; Milosavljevic, B. H.; Thomas, J. K. *J. Phys. Chem.* **1984**, *88*, 980.
(67) Wang, Y.; Mahler, W. *Opt. Commun.* **1987**, *61*, 233.
(68) Hilinski, E. F.; Lucas, P. A.; Wang, Y. *J. Chem. Phys.* **1988**, *89*, 3435.
(69) Wang, Y.; Suna, A.; McHugh, J.; Hilinski, E. F.; Lucas, P. A.; Johnson, R. D. *J. Chem. Phys.* **1990**, *92*, 6927.
(70) Wang, Y., Suna, A.; Mahler, W.; Kasowski, R. *J. Chem. Phys.* **1987**, *87*, 7315.
(71) Mahler, W. *Inorg. Chem.* **1988**, *27*, 435.
(72) Möller, M. Synth. Met. 1991, 41-43, 1159.
(73) Cummins, C. C.; Schrock, R. R.; Cohen, R. E. *Chem. Mater.* **1992**, *4*, 27.
(74) Cohen, R. E.; Yue, J. *Supramol. Sci.* **1994**, *1*, 117; Clay, R. T.; Cohen, R. E. *Supramol. Sci.* **1995**, *2*, 183; Kane, R. S.; Cohen, R. E.; Silbey, R. *Chem. Mater.* **1996**, *8*, 1919; Sohn, B. H.; Cohen, R. E. *Chem. Mater.* **1997**, *9*, 264.
(75) Antonietti, M.; Wenz, E.; Bronstein, L.; Seregina, M. *Adv. Mater.* **1995**, *7*, 1000.
(76) Spatz, J.; Roescher, A.; Möller, M. *Adv. Mater.* **1996**, *8*, 337.
(77) Higgins, J. S.; Benoit, H. C. *Polymers and Neutron Scattering*, Oxford University Press: Oxford, 1995.
(78) Cogan, K. A.; Gast, A. P.; Capel, M. *Macromolecules* **1991**, *24*, 6512.
(79) McConnell, G. A.; Gast, A. P.; Huang, J. S.; Smith, S. D. *Phys. Rev. Lett.* **1993**, *71*,

2102.

(80) McConnell, G. A.; Lin, E. K.; Gast, A. P.; Huang, J. S.; Lin, M. Y.; Smith, S. D. *Faraday Discuss.* **1994**, *98*, 121.

(81) Förster, S.; Wenz, E.; Lindner, P. *Phys. Rev. Lett.* **1996**, *77*, 95.

(82) Gast, A. P. *Langmuir* **1996**, *12*, 4060.

(83) McConnell, G. A.; Gast, A. P. *Macromolecules* **1997**, *30*, 435.

(84) Lantman, C. W.; MacKnight, W. J.; Rennie, A. R.; Tassin, J. F.; Monnerie, L. Fetters, L. J. *Macromolecules* **1990**, *23*, 836.

(85) Richter, D.; Farago, B.; Fetters, L. J.; Huang, J. S.; Ewen, B. *Macromolecules* **1990**, *23*, 1845.

(86) Dozier, W. D.; Huang, J. S.; Fetters, L. J. *Macromolecules* **1991**, *24*, 2810.

(87) Willner, L.; Jucknischke; Richter, D.; Roovers, J.; Zhou, L.-L.; Toporowski, P. M.; Fetters, L. J.; Huang, J. S.; Lin M.Y.; Hadjichristidis, N. *Macromolecules* **1994**, *27*, 3821.

CHAPTER 2

Micellization of Ionic Block Copolymers

2.1. Introduction

The investigation of ion-containing block copolymers in solution has revealed that these materials form spherical aggregates, known as micelles, in both water and organic solvents.[1-4] Studies of the formation and characteristics of these aggregates have generated a great deal of interest, as micelles of ionic block copolymers provide an extremely versatile addition to the growing field of molecular self-assembly. Possible applications in the areas of advanced materials and drug delivery have spurred our own interest in this field.

For many years, the phenomenon of micellization has been known to occur in solutions of small molecule amphiphiles (or surfactants) above a concentration known as the critical micelle concentration (cmc). The cmc is a function of both the amphiphile and the solvent environment, and also tends to vary with the method of detection. However, in general terms, we can state that, below the cmc, single amphiphiles exist in solution while, above the cmc, associates (or aggregates) tend to form. Due to differences in the kinetics of exchange between unimers and the self-assembled structures, the term "associate" is generally reserved for surfactant micelles, while micelles of block copolymers are often referred to as "aggregates". This point will be further discussed later on.

To understand the formation of spherical micelles, it is important to realize that amphiphilic molecules consist of both an ionic or nonionic polar moiety, and at least one hydrocarbon chain. Since these two parts of the molecule have very different solubilities, amphiphiles in solution above the cmc will tend to undergo microphase separation. For example, in an aqueous environment, the hydrocarbon chains of a number of Aerosol OT (AOT) molecules will cluster together to form a liquid-like core, surrounded and protected by the solubilized ionic head groups.

The subject of the present article is the self-assembly of ionic block copolymers, which is in many ways analogous to the micellization of surfactants in solution. In our discussion, we hope to show that the combination of extremely high aggregate stability, low cmcs, and a wide range of aggregate sizes gives ionic block copolymers unprecedented versatility, and opens the door to many potential applications. Before embarking on a description of ion-containing block copolymers, however, a more general discussion of block copolymer micellization is required.

It has long been known that block copolymers in selective solvents will form spherical aggregates, with compact cores of insoluble blocks surrounded by a soluble corona composed of soluble blocks. Like their surfactant counterparts, micelles of block copolymers show an extremely narrow size distribution. The term micelle has been applied to these colloidal aggregates, due to the structural similarities with surfactant micelles; however, we shall see that micelles of block copolymers and small molecule surfactants are quite different in terms of their lability and exchange kinetics. For a number of years, block copolymer micelles have been the subject of much interest, and some excellent reviews have been published in the field.[5-7]

Along with a number of experimental studies, block copolymer micelles have been the subject of considerable theoretical treatment in recent years.[8-21] Of particular relevance to the present review are theories proposed by Zhulina and Birshtein[12] and by Halperin[16] for "starlike" micelles. These micelles are spherical with small cores and expanded coronae, which form when the length of soluble block is considerably longer than that of the insoluble block. Conversely, "crew-cut" micelles[22,23] are structures with large cores and short coronal "hair", formed from asymmetric block copolymers with relatively long insoluble blocks. In the former case, theory predicts that the radius of the core (R_{core}) is independent of the soluble block length, and scales as $N_B^{3/5}$, where N_B is the number of units in the insoluble block.

At this point, it is important to mention that the theoretical treatment of block copolymer micelles, resulting in scaling relations such as the one given above, is generally based on thermodynamic considerations, and assumes an equilibrium between single chains and the micellar aggregates. Unlike associates of surfactants, which are extremely labile structures, the kinetics of exchange between block copolymer micelles and single chains in solution are slow, due to the high viscosity of the insoluble blocks within the micelle core. This is especially true in the case of the ionic block copolymer micelles which pertain to the present discussion; these have glassy polystyrene cores in an aqueous environment, or ionic cores with short-range electrostatic interactions in organic environments. In fact, on a reasonable time scale, the micelles of ionic block copolymers may be regarded as "frozen" structures, with no dynamic equilibrium between micelles and single chains. An application of theoretical models to such systems, therefore, requires us to assume that a dynamic equilibrium does exist at some stage of micelle formation, even though the final result is a frozen aggregate. These considerations should be kept in mind throughout the present review, as they serve to qualify our use of the term "micelle" in describing frozen aggregates of block copolymers.

Several theoretical treatments of block copolymers in selective solvents have addressed the phenomenon of the critical micelle concentration.[9,18-20] However, until very recently, the polydispersity of the insoluble blocks had not been properly considered. In a new model for the micellization of block copolymers in solution, Gao and Eisenberg[21] refined the treatment of Holland and Rubingh,[24,25] in order to account for the polydispersity effect of the insoluble blocks on the cmc. The model describes the collapse of insoluble blocks into colloidal spheres below the cmc, such that the driving force for micellization is the van der Waals interaction between spherical particles.

To illustrate the effect of polydispersity on the cmc, a plot of single chain concentration (*S*) as a function of total block copolymer concentration for a polystyrene-*b*-polyisoprene (PS-*b*-PI) / n-hexadecane system is shown in Figure 2.1.[21] For an average insoluble block length of 67 styrene units, the concentration of single chains is plotted for

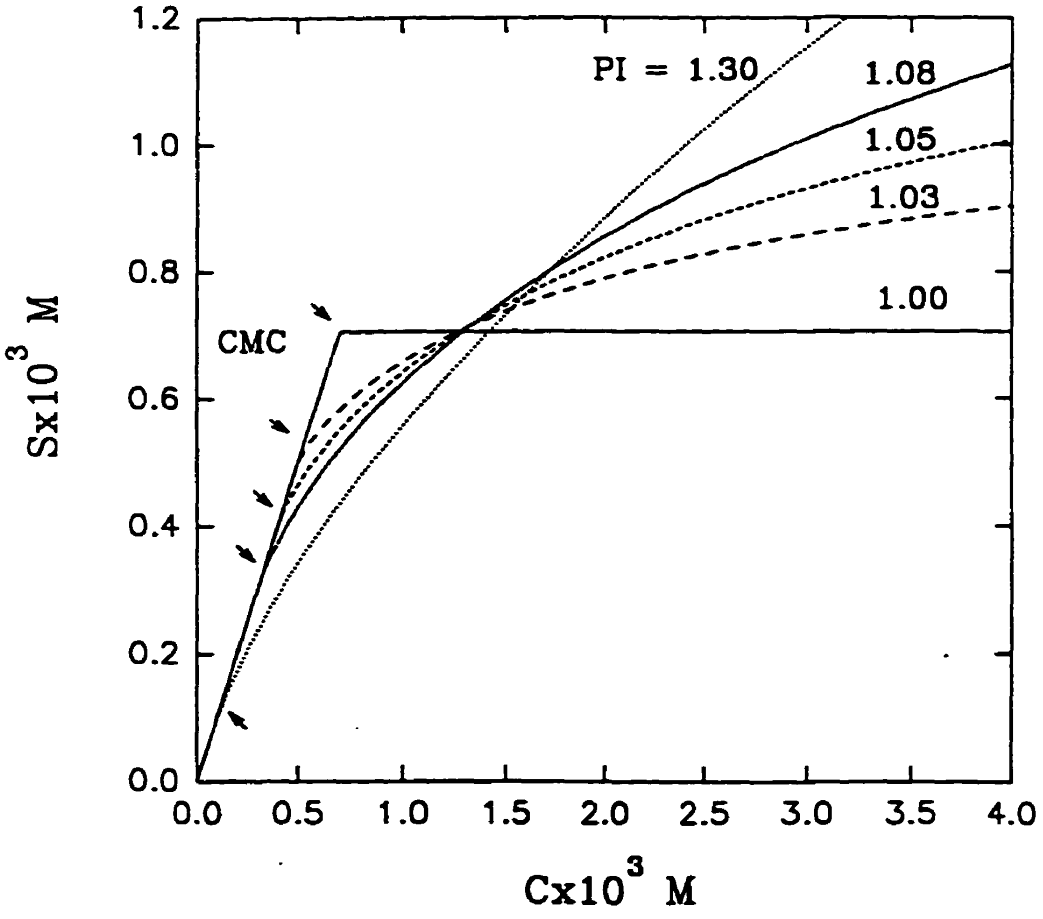

Figure 2.1. Single chain concentration as a function of the total block copolymer concentration at different polydispersity indexes in the PS-*b*-PI/*n*-hexadecance system. The polystyrene block length is 67 units.

various polydispersity indexes (P.I.). The horizontal line above the cmc for P.I. = 1.00 indicates a sharp pseudo-phase transition, which, for polydisperse systems, is replaced by a continued increase in S with concentration above the cmc. As a result, the cmc (denoted by arrows in the figure) decreases with increasing P.I. and becomes much less distinct.

We now turn our attention to the colloidal behaviour of ionic block copolymers, which possess both hydrophilic blocks of ionic repeat units and hydrophobic blocks of nonionic units. In an AB diblock, for example, a block of nonionic A units is covalently linked to a block of ionic B units. Due to the high degree of incompatibility between the ionic and nonionic blocks, ionic block copolymers in solution exhibit extremely low cmcs[26-28] and high aggregate stability.[3,4]

Ionic block copolymers in solution can be divided into two main categories: block polyelectrolytes and block ionomers. According to the definitions of polyelectrolytes and ionomers proposed by Eisenberg and Rinaudo,[29] the properties of block polyelectrolytes are governed by electrostatic interactions over the relatively large distances within the corona and between the micelles, while the properties of block ionomers are governed by short-range interactions within the micelle core.

The classification of ionic block copolymer as either block polyelectrolytes or block ionomers is determined by the nature of the solvent. Ionic block copolymers in water are block polyelectrolytes, forming micelles with nonionic cores and coronae made up of the soluble ionic blocks. In organic solvents, ionic block copolymers can be described as block ionomers, with ionic micelle cores surrounded by the nonionic soluble blocks. Following the terminology adopted for surfactants, ionic block copolymers in aqueous and nonaqueous solvents are sometimes referred to as regular and reverse micelles, respectively. In the starlike micelle regime, block ionomers generally have long nonionic blocks and short ionic blocks, whereas block polyelectrolytes have long ionic blocks and short nonionic blocks. The so-called crew-cut polyelectrolytes, on the other hand, have relatively short ionic blocks, surrounding a large nonionic core. Crew-cut micelles of block ionomers, to our knowledge, have not been investigated.

This chapter presents an overview of the literature on ionic block copolymers in nonaqueous and aqueous solutions, with particular emphasis on work performed in this group. We will begin with a summary of the recent work on block ionomer micelles, followed by a discussion of block polyelectrolytes.

2.2. Ionic Block Copolymers in Organic Solvents

The ionic block copolymers which have been most extensively studied in organic solvents are the polystyrene-based diblock ionomers with long polystyrene blocks joined to relatively short ionic blocks. Diblock ionomers of this type, in which the ionic block is poly(metal acrylate), poly(metal methacrylate), or quaternized poly(4-vinylpyridine), will be the focus of the present discussion. However, it is worth mentioning that an investigation of quaternized polystyrene-*b*-poly(4-vinylpyridine)-*b*-polystyrene (PS-*b*-P4VP-*b*-PS) triblock ionomers in THF has also been reported.[30] Another related system is sodium-neutralized poly(*tert*-butylstyrene)-*b*-lightly sulfonated polystyrene, which has recently been studied by light scattering in nonpolar solvents.[31]

The following section on reverse micelles of ionic block copolymers will be divided into four parts. The first part will deal with the characterization of fundamental parameters of block ionomers using numerous techniques (size-exclusion chromatography, light scattering, small-angle x-ray scattering, etc.). The second part will discuss the problem of cmc determination of block ionomers. Next, nuclear magnetic resonance (NMR) investigations of the solubilization of water into the ionic cores and the dynamics of the soluble corona will be described. Lastly, an interesting application of block ionomers will be presented: the size control of quantum-confined nanoparticles within a polymer host.

2.2.1. Characterization of Fundamental Parameters

Until quite recently, experimental work on the properties of ionic block copolymers in organic solvents was very limited. In the first detailed study of diblock ionomer reverse micelles,[3] the aggregation behaviour of polystyrene-*b*-poly(sodium methacrylate) (PS-*b*-PMANa) and polystyrene-*b*-poly(cesium methacrylate) (PS-*b*-PMACs) copolymers was investigated in solvents selectively good for the polystyrene block (e.g. dimethylformamide (DMF), tetrahydrofuran (THF)). Using size-exclusion chromatography (SEC) coupled with intrinsic viscosity measurements, micellar characteristics such as aggregation number and hydrodynamic radius were investigated systematically as a function of the ionic and polystyrene block lengths.

Typical size-exclusion chromatograms of block ionomers in selective solvents show up to three distinct peaks, attributable to micelles, single chains, and homopolystyrene.[3,32] The micelle peak appears at the lowest elution volume, due to the large size of the micellar aggregates relative to that of the unimers. The relative area under the micelle and single chain peaks depends on the composition of the block ionomer, with longer ionic blocks resulting in a higher percentage of micellized material.

When a mixture of micelles with different molecular weights was injected repeatedly into the SEC column, the bimodal shape of the chromatogram was retained over 3 days, indicating the lack of a dynamic equilibrium between micelles and single chains.[3] The existence of a single chain peak was attributed to a distribution in the length of the ionic block, with single chains having a lower ion content than aggregated chains. Infrared spectroscopy of micelle and single chain fractions supported this hypothesis. Despite the absence of a dynamic equilibrium, the term micelle is used for block ionomers, on the basis of the structural and behavioural similarities with other block copolymer micelles.

A combination of SEC and viscometry was used to determine aggregation numbers and hydrodynamic radii (R_h) of polystyrene-*b*-poly(metal methacrylate) reverse micelles.[4] Both the aggregation number and the hydrodynamic radius were found to increase as the length of the insoluble block increases. However, as the length of the soluble block increases, the aggregation number decreases and the hydrodynamic radius increases. The latter trend is understood on the basis of an increase in the corona thickness as the length of the polystyrene segment increases; thus the overall radius of the micelle increases, despite a lowering of the aggregation number.

The above trends were confirmed by dynamic light scattering (DLS) measurements.[4] DLS was also used to test the stability of reverse micelles by the addition of polar solvents to different solutions of block ionomers. After an initial decrease in R_h

upon addition of the polar solvent, the sizes of reverse micelles were found to remain constant over a period of several months.

One of the attractive features of block ionomer micelles is the wide range of aggregate sizes that are possible in these systems, as micellization is found to occur down to very short ionic block lengths. In fact, when the length of the ionic block is reduced to a single ionic unit, one obtains a useful conceptual bridge between micelles of block copolymers and those of surfactant amphiphiles, which generally possess a single ionic head group. Related to this discussion are the telechelic ionomers,[33] in which single ionic groups or zwitterions are fixed to both ends of the polymer chain, and the monochelic ionomers,[34-37] in which an ionic moiety is fixed to one end of the chain. In the case of monochelics, viscometry and static light scattering (SLS) have been used to determine cmcs and aggregation numbers of carboxylate-terminated polystyrene chains in solvents of low dielectric constant.[36] The aggregation behaviour of 1,2-dicarboxyethyl-terminated polystyrene in cyclohexane has also been studied.[37]

It has been found that small-angle x-ray scattering (SAXS) is a useful technique for obtaining structural information on block ionomer micelles. SAXS has been used to investigate micellar core sizes of polystyrene-*b*-poly(cesium acrylate) (PS-*b*-PACs) and PS-*b*-PMACs in toluene for several ionic block lengths.[38] Typical SAXS profiles for block ionomer micelles (Figure 2.2) are a combination of a shape factor, which characterizes the size and shape of the scatterers (i.e., the ionic cores), and the structure factor, which characterizes distances between scatterers. The structure factor can also be related to order within the micelle solution.

From such scattering profiles, core sizes of the PS-*b*-PACs and PS-*b*-PMACs systems were found to obey the starlike model, scaling as $N_B^{3/5}$, independent of the PS block length. A proportionality constant of 6.5 Å was determined. The applicability of a thermodynamically-derived scaling relation is a good indication that block ionomer micelles, although undoubtedly frozen structures, approach equilibrium in the early stages of micelle formation. These micelles are formed by neutralization of single chains of acid-form block copolymers in organic solvent; before the core-forming blocks are 100% neutralized,[39] it is likely that micelles and single chains are in dynamic equilibrium. At

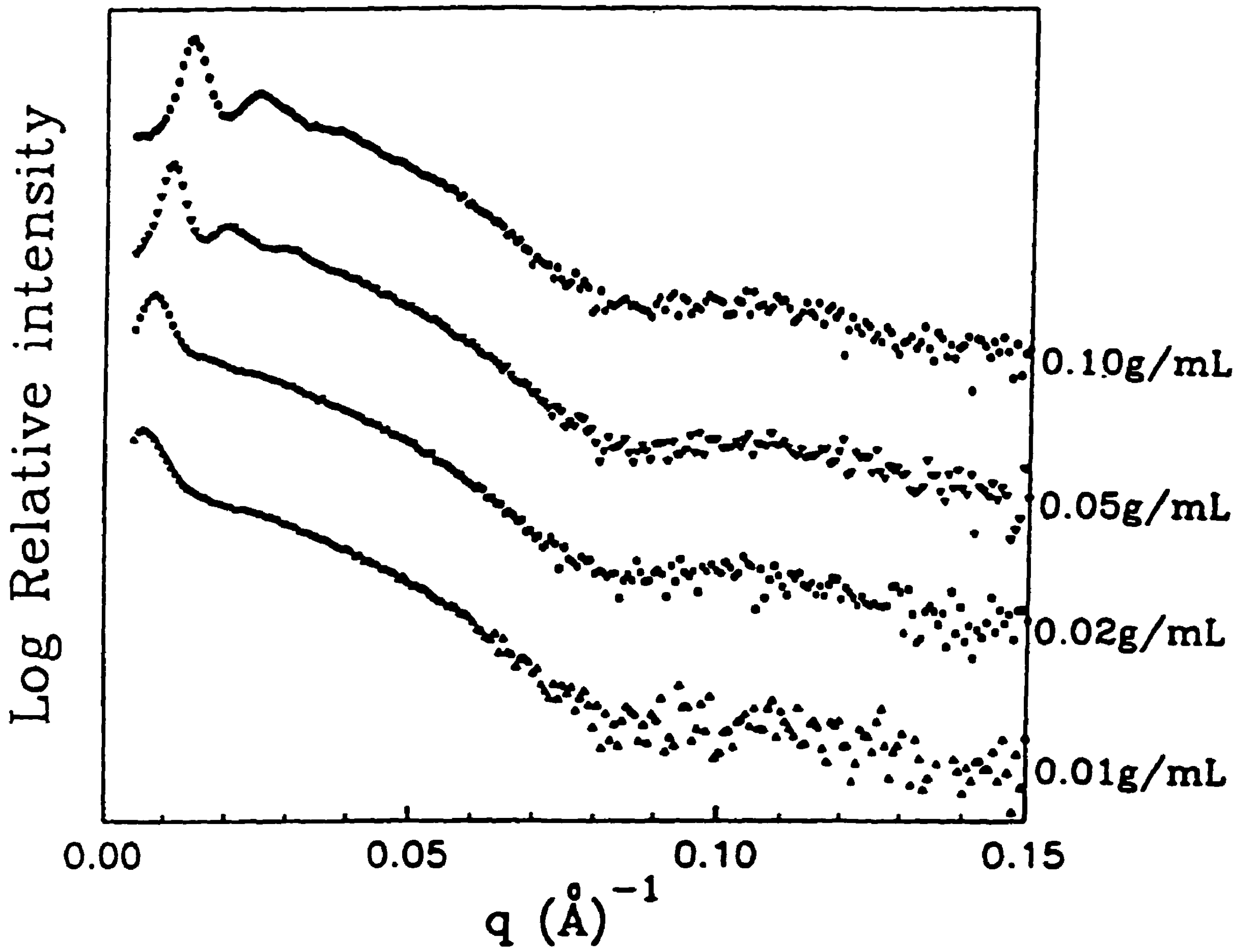

Figure 2.2. SAXS profiles of PS(600)-*b*-PACs(45) diblock ionomer in toluene, for concentrations from 0.01 g/mL to 0.10 g/mL.

some point, the equilibrium structures become frozen as solvent is excluded from an increasingly ionic core.

In further SAXS work,[40] the study of block length dependence was extended to include quaternized PS-*b*-P4VP. The same fit with the Halperin model was obtained, supporting the relationship $R_{core} = 6.5N_B^{3/5}$ Å. High chain extension in the micelle core was observed for both ionic microdomains dispersed in a nonionic matrix and nonionic microdomains dispersed in an ionic matrix.[41] This result proved that chain extension within the cores of block ionomers is due to the minimization of interfacial energy rather than to short-range ionic interactions. SAXS results, together with computer modeling of spherical shape factors, have been used to determine the radii polydispersity indexes (RPI) of ionic cores.[38] These were found to be between 1.02 and 1.04, considerably smaller than the polydispersity indexes of the polymer chains.

2.2.2. Critical Micelle Concentrations of Block Ionomers

A wide range of techniques has been used to determine the critical micelle concentrations of block copolymers in selective solvents, such as fluorescence, osmometry, viscometry, and static light scattering. The latter method is sensitive to changes in the apparent weight-average molecular weight (M_w) of the solution, a quantity which includes contributions from both micelles and single chains. In a typical experiment, the quantity $Kc/R(0)$ (where K is the optical constant and $R(0)$ is the Rayleigh ratio extrapolated to 0 angle) is plotted as a function of concentration; since $Kc/R(0)$ is inversely proportional to the apparent M_w, such a plot shows three distinct regions, corresponding to unimers in solution, a transition region, and micelles in solution.

The extremely low cmcs of block ionomer micelles make their determination by empirical methods difficult, as the unimer region is often at concentrations below the limit of detection. However, the cmcs can be evaluated by fitting the micelle and transition region according to an equation proposed by Debye.[42] For systems with significant polydispersity in the insoluble block, a new method has been developed,[26] based on the micellization model of Gao and Eisenberg.[21] Figure 2.3 shows plots of cmc vs. the insoluble block length for various systems,[43-46] including AOT surfactant in benzene and

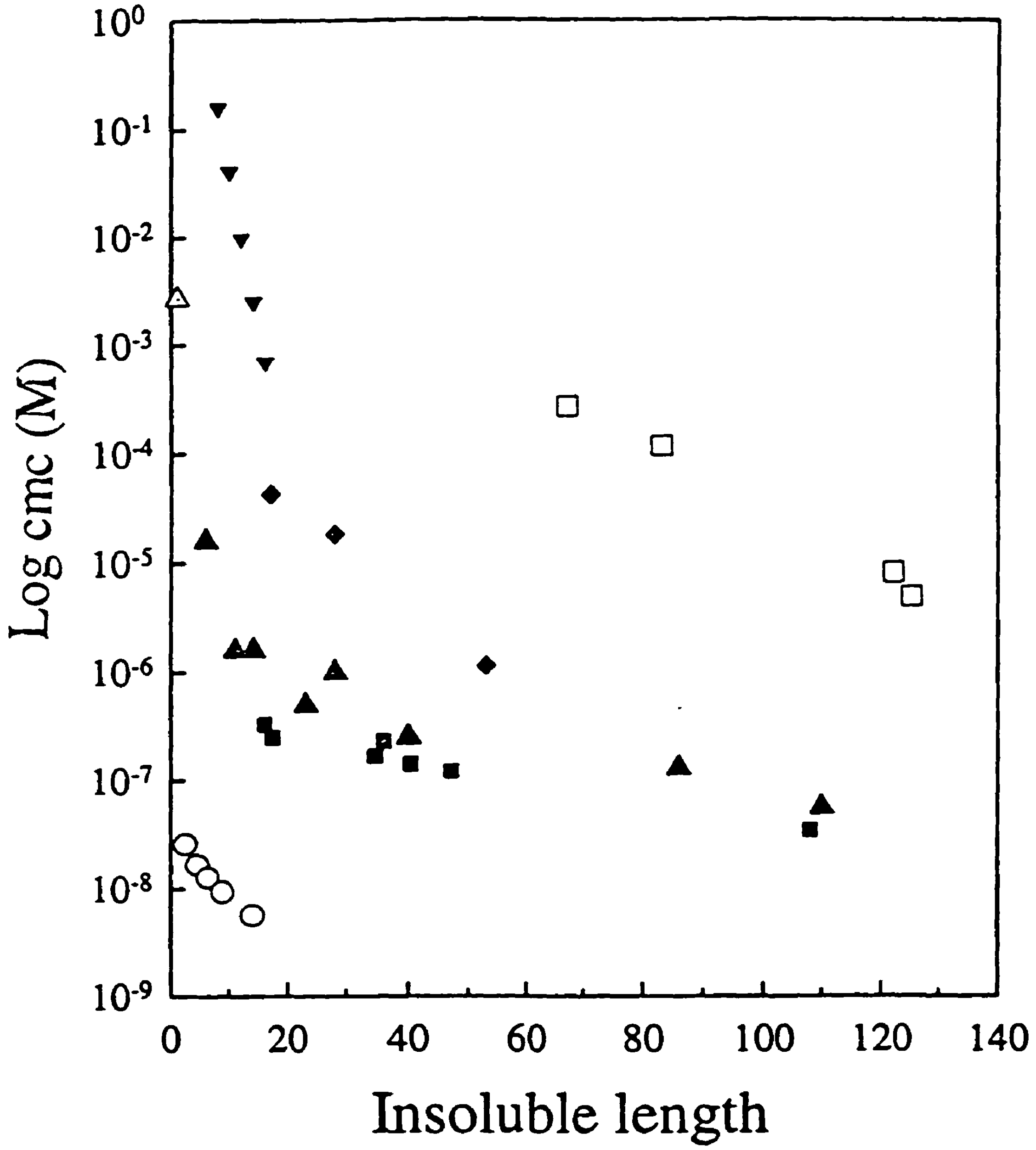

Figure 2.3. cmc values for different micellar systems: AOT (Δ),[44] sodium alkyl sulfonate surfactants (▼),[44] PS-*b*-PI (□),[43] poly(ethylene oxide)-*b*-poly(butylene oxide)-*b*-poly(ethylene oxide) (PEO-*b*-PBO-*b*-PEO) (◆),[46] PS-*b*-PANa (▲),[26] PS-*b*-PEO and PEO-*b*-PS-*b*-PEO (■),[45] and PS-*b*-PANa (○).[27] The filled and hollow symbols represent aqueous and organic mediums, respectively.

nonionic block copolymers in selective solvents. From these plots, one can compare the extremely low cmcs of block ionomer micelles with the wide range of cmcs observed for other self-assembling species.

2.2.3. Characterization of Water Solubilization and Chain Dynamics by NMR

An important feature of surfactant reverse micelles is their ability to solubilize water within the ionic core, creating water pools which can act as "microreactors" for hydrophilic reactants. Block ionomer micelles in nonpolar solvents are also able to solubilize small quantities of water, and the distribution coefficient of water between the ionic core and the solvent has been studied by proton NMR.[47,48] A single chemical shift for the water protons is observed, which is a weighted average of the chemical shift of water in the reverse micelle and in the nonpolar solvent. The appearance of a single chemical shift indicates that the exchange of water between the ionic core and the solvent phase is very fast within the time scale of the NMR experiment. On these grounds, it seems that the ionic core is liquid-like in the presence of water.

From measurements of the observed chemical shift of the water protons,[47] the distribution coefficients in favour of water solubilization in different solvents were found to occur in the following order: cyclohexane > benzene ~ toluene > chloroform >> THF ~ DMF. Distribution coefficients were also investigated for ionic blocks with different functional groups,[48] and at 25 °C they were found to decrease as follows: cesium carboxylate > sodium sulfonate ~ sodium carboxylate >> pyridinium methyl iodide.

NMR has also proven useful in the measurement of coronal chain dynamics at the segmental level. In systems of PS-*b*-PACs in carbon tetrachloride (CCl_4), the mobility of ^{2}H-labeled polystyrene segments was probed at various distances from the ionic core.[49] ^{2}H relaxation times revealed that close to the ionic-nonionic junction there is a definite decrease in segmental mobility with respect to the "free" chain. Further from the ionic block, the segmental mobility is less restricted, and at a distance of ca. 40 units the mobility is close to that of the nonionic homopolymer. It was also found that segmental mobility decreased with increasing length of the ionic block. This result can be explained on the basis of geometrical considerations; for starlike micelles, the segmental density at a particular distance from the core is higher when the ionic core is larger, resulting in a larger number of steric interactions.

2.2.4. Semiconductor Nanoparticles in Block Ionomer Micelles

The control of ionic core sizes through variations in the insoluble block length make block ionomers attractive materials for the formation of polymer-nanoparticle composites. For example, the neutralization of polystyrene-*b*-poly(acrylic acid) (PS-*b*-PAA) block copolymers can introduce a wide range of metal ions into the core; the reduction of these ions, or treatment with H_2S, will effect the formation of ultra-small metal or metal sulfide particles within the cores,[50] with sizes determined by the aggregation number of the block ionomer host.[51]

One such application of block ionomers has been demonstrated by the precipitation of quantum-confined CdS nanoparticles within the cores of polystyrene-*b*-poly(cadmium acrylate) (PS-*b*-PACd).[51] Quantum confinement arises from the extremely small sizes of these crystallites (< 60 Å), and results in excited states which are more energetic than those of bulk CdS. To prepare the composites, the ionic cores were placticized with water, after which the films were treated with H_2S for 8 hours. CdS particle sizes were determined from blue-shifts in the UV-vis spectrum, and these were plotted against the size of the original core ($R_{core} = 6.5\ N_B^{3/5}$ Å). A linear relationship was found between CdS particle sizes and ionic core sizes, up to a particle diameter of 50 Å, where the particle sizes level off (Figure 2.4). Below 50 Å, it appears that excellent size control of CdS particles can be achieved by selecting the appropriate ionic core size. Also shown in the plot are CdS nanoparticles synthesized in the multiplets of random ionomers (dotted circles), which allow for synthesis of particles down to 18 Å.[52]

The stability of the CdS-polymer composites was shown by dissolving the materials in organic solvents (e.g. toluene, THF) to form clear yellow solutions of CdS-containing reverse micelles.[51] The micelles were stabilized by reneutralizing the PAA block with NaOH. The yellow powders were then repeatedly precipitated into MeOH and redissolved, without significant changes in the UV-vis absorption spectrum of the composite.

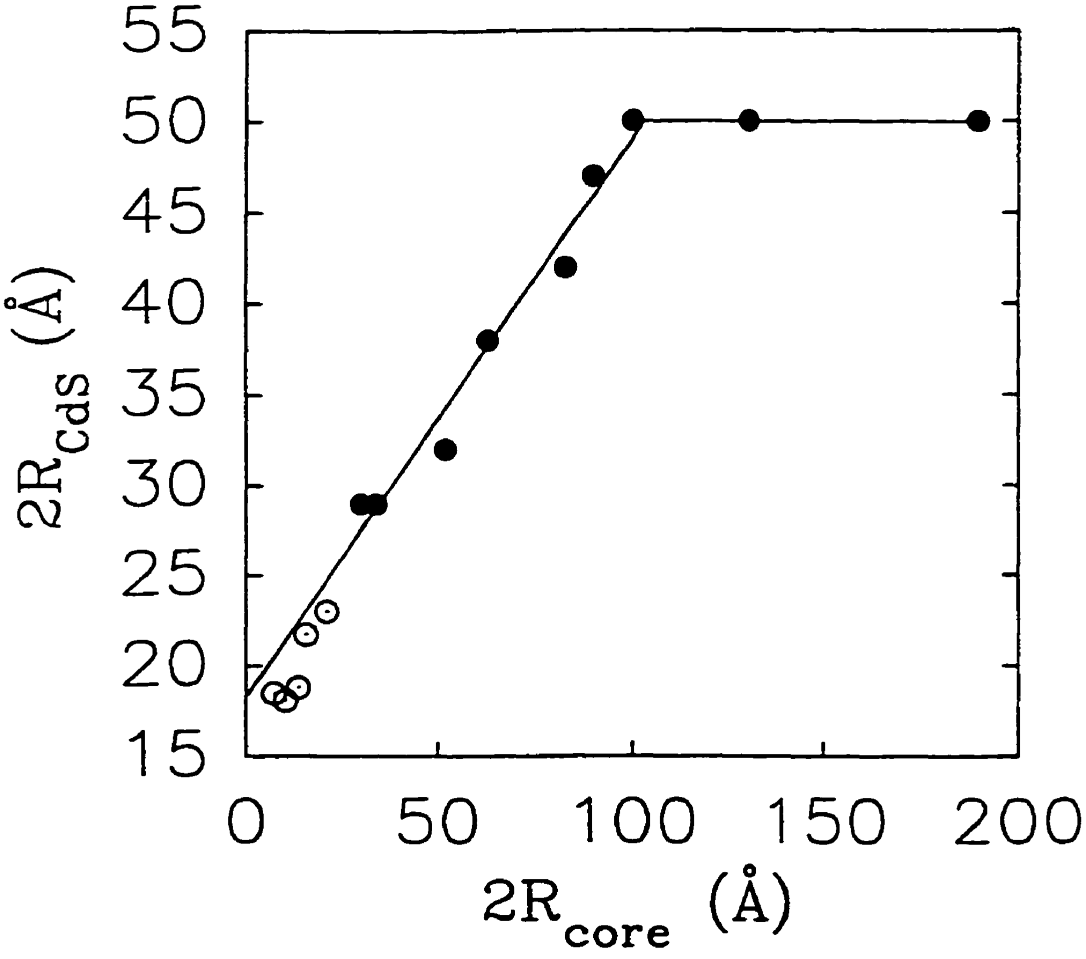

Figure 2.4. Plot of CdS particle diameter vs. diameter of original core (calculated from $R_{core} = 6.5\ N_B^{3/5}$ Å). Dotted circles indicate CdS particles synthesized within the microdomains of random ionomers.

2.3. Ionic Block Copolymers in Aqueous Solutions

In this section, two types of block polyelectrolyte micelles will be discussed, starlike and crew cut micelles. One of the earliest studies of block polyelectrolytes was performed by Schindler and Williams, in which phase separation in films of polystyrene-*b*-poly(vinylpyridinuim methyl bromide) was investigated.[53] Much of the pioneering studies of block polyelectrolyte starlike micelles in solution was performed by Selb and Gallot, and their work has been reviewed.[1,2] It should be mentioned that the micellization of block polyelectrolytes on the surface of water has also been extensively studied.[54-58] However, in general, studies of block polyelectrolyte micelles have been scarce. To date there are two theoretical models dealing with the micellization of block polyelectrolytes.[19,59]

The following section will first focus on the characterization of aqueous starlike micelles by a variety of techniques. The effects of several factors, such as the solvent quality (i.e. salt concentration and temperature), block size, degree of neutralization, and solubilization on the micellization will be discussed. In the second part of this section, an overview of a aqueous crew cut micelles and a number of related morphologies, will be addressed.

2.3.1. Characterization of Starlike Micelles

The solvent quality has been found to influence the micellization of block copolymers. In general, when the solvent quality decreases, the solubility of the chains decreases, resulting in a lowering of the cmc and an increase in the aggregation number of the micelles. The quality of the solvent for block polyelectrolyte chains can be influenced, for example, by the addition of salt or by changing the temperature. The effects of solvent quality on the micellization of two block polyelectrolyte systems, polystyrene-*b*-poly(4-vinyl-N-ethylpyridinium bromide) (PS-*b*-P4VPEtBr) and PS-*b*-PANa, as well as the influence of block lengths, will now be discussed.

The solvent quality for PS(26)-*b*-P4VPEtBr(140) in a water (34 wt. %) / methanol mixture was explored as a function of LiBr concentration by SLS and sedimentation velocity.[1] It was found that the weight fraction of the micelles and the apparent M_w

increased at low salt content and remained essentially constant at and above 0.2 M LiBr concentration. At very low salt concentrations (0.01 M), no micelles were present. For some of the low salt concentrations, a cmc was observed which was found to decrease as the salt concentration increased. This observation corresponds to the transition from micelles to single chains, which occurred at lower concentration as the salt concentration increased. The effect of temperature on the cmc and the apparent M_w was studied for this sample at different salt concentrations. An increase in temperature resulted in an increase in the solvent quality and thus an increase in the cmc and a decrease in the aggregation number.

The effect of the solvent quality on micellization was found to depend on the length of the copolymer blocks. For instance, Selb and Gallot found that for short PS block lengths (< 30 units), the cmc and molecular weight were strongly affected by the salt concentration. However, for larger PS block lengths, (> 30 units), the effects of temperature and salt concentration were less important. Thus, it can be suggested that at high PS block lengths, the micellization process is dominated primarily by the insoluble PS block.

Block polyelectrolytes formed from PS-*b*-PANa in aqueous solutions have also received considerable attention.[26,28,60] In this system, micelle formation occurred when single chains of PS-*b*-PAA were dissolved in methanol, due to microphase precipitation of the polystyrene blocks. The micelles were then neutralized by the addition of NaOH, and the subsequent ionic form precipitated from solution. It has been observed that block copolymers micelles consisting of hydrophobic-hydrophilic segments are difficult to dissolve directly in aqueous solvents.[2] However, in the case of PS-*b*-PANa, heating the aqueous solutions at 100 °C for a period of time rendered the copolymer micelles soluble. This heating process was followed by viscometry and SLS.[26,60] Due to their glassy cores, these aqueous micelles are most likely kinetically-frozen aggregates at normal concentrations, although we shall see that they do exhibit a cmc at very high degrees of dilution.

The cmcs of PS-*b*-PANa in water are shown in Figure 2.3.[26] These values were determined by fluorescence measurements using previously established methods.[45] It was found that the PS block length has a much greater effect on the cmc than the soluble PANa block length. For instance, an increase in the PS block length from 6 to 110 units, for a constant PANa block length of 1000 units, decreased the cmc by a factor of 320, while an increase in the PANa block length from 300 to 1400 lowered the cmc by a less than a factor of 2.[26]

A recent study explored more systematically the effects of the PANa block length and salt concentration on the cmc values.[28] A wide range of samples were investigated, with PS block lengths ranging from 6 to 110 units and PANa block length ranging from 44 to ca. 2400 units. For two series consisting of PS blocks of 11 and 23 units, it was observed that the cmc increased as a function of the PANa block length, passed through a maximum, then decreased as the PANa block length increased further. This maximum can be explained by a balance of solubility effects. The change in the cmc values with increasing PANa block length was found to become less dramatic for longer PS block lengths (e.g. 110 units), in agreement with results of Selb and Gallot.

The effect of NaCl concentrations (c_s) (0.1 to 2.5 M) on the cmc was also investigated for the PS-*b*-PANa system.[28] The cmc values were found to decrease when the salt concentration increased, and log cmc versus $c_s^{1/2}$ was linear for most of the series investigated. The slope, d (log cmc) / d ($c_s^{1/2}$), was found to be a function of the PS block length. For three different series with PS block lengths of 6, 11 and 23 units, d(log cmc) / d($c_s^{1/2}$) plotted against the PANa length exhibited sigmodal behaviour. This relationship was related to conformational changes of the polyelectrolyte chain as a function of the PANa block length.

SLS has also been used to characterize the PS-*b*-PANa system in 2.5 M NaCl.[60] It was found that for short PS block lengths (i.e. 6 units) the micellization was strongly affected by the PANa block length. However, as the PS block length increased, the effect of the PANa block length on the aggregation numbers decreased. Aggregation numbers, calculated core radii, and radii of gyration (R_g) were compared with the scaling predictions of the starlike model. It was found that the scaling relations were a good representation of the R_{core} and R_g values. The calculated R_{core} values for this system in 2.5 M NaCl agreed with the values determined by SAXS for similar samples measured in the solid state.[41]

This result implies that for the present system, the morphology of these micelles is the same in the solid state and in solution.

Micelles of polystyrene-*b*-poly(methacrylic acid) (PS-*b*-PMAA) have been extensively studied in mixed solvents of dioxane/water and water.[61-66] It has been pointed out that such micelles may be kinetically frozen when the solvent is very poor for the PS core (i.e. water rich solvents). The micellization process and coronal structure are influenced by the degree of neutralization (α) of the polyelectrolyte, as observed using DLS, viscosity and SLS by Kiserow et. al.[63] At low concentrations and ionic strengths, the apparent hydrodynamic diameter increased gradually with α, due to the stretching of the ionized carboxylic groups. However, at higher concentrations, a maximum in R_h was observed, corresponding to α values of ca. 0.25-0.35. Similarly, at this α value, a maximum was observed in the viscosity and a minimum in the scattered light intensity. These results imply that a certain amount of ordering in the solutions exists as a result of repulsive interactions between highly charged micelles. Two well defined maxima were determined from DLS, corresponding to the collective mode and the diffusion of clusters of structurally organized micelles. Clusters of micelles have also been seen in such aqueous micellar systems as PS-*b*-PEO[67] and Triton X-100.[68]

Solubilization of organic molecules into block polyelectrolytes is a subject of considerable interest due to numerous potential applications. Morishima et al. investigated the quenching of fluorescence probes in hydrophobic domains formed in poly(9-vinylphenanthrene)-*b*-poly(methacrylic acid) (PVPh-*b*-PMAA) in water.[69] The solubilization of organic molecules into aqueous solutions of PS-*b*-PMAA was also followed by fluorescence spectroscopy[61,63] and DLS.[63] Valint and Bock solubilized toluene in block copolymers of poly(*tert*-butylstyrene)-*b*-poly(styrene sulfonate) (PTBS-*b*-PSS) in water and found an increase in the viscosity.[70]

2.3.2. Characterization of Crew-Cut Micelles

Crew-cut micelles were prepared and characterized from polystyrene-*b*-poly(4-vinylpyrindinium iodide) (PS-*b*-P4VPMeI) in water.[71] These micelles consisting of a large hydrophobic PS core and a relatively thin hydrophilic ionic corona (P4VPMeI) were found to form monodisperse stable micelles in water. Crew cut micelles were prepared by dissolving the polymer in DMF, then adding a selective non-solvent for the PS block. In order to determine the effect of different selective solvents, two procedures were used. In the first, water was added dropwise to the DMF solution; alternatively, methanol was first added, followed by water. In both cases, the solutions were dialyzed against distilled water to remove DMF and methanol. The diameters of the micelle cores were measured by transmission electron microscopy (TEM), and were found to be smaller for the samples prepared by the addition of water, compared with those prepared from water and methanol. Also, the aggregation numbers and polydispersity indexes, calculated from TEM results, were found to be lower for the micelles prepared from the addition of water. The choice of selective solvent is therefore critical to the micellar properties. The higher aggregation number and broader distribution for micelles prepared using methanol and water was attributed to the different compatibility between styrene and water on one hand, and styrene and a methanol/water mixture on the other.

Recently, crew-cut micelles were prepared from PS-*b*-PAA in water.[72,73] Different micellar morphologies were observed by TEM depending on the relative block lengths.[73] Some of these morphologies consist of spheres, rods, lamellae, and vesicles. Typical examples of these structures are shown in Figure 2.5. In addition, compound micelles were observed, in which reverse micelle-like aggregates are contained in up to micrometer-size spheres having hydrophilic surfaces. When the samples were dried, ordered needle-like solids formed spontaneously. After soaking in water, the separated needle-like solids showed birefringence under crossed polaroids. This phenomenon may suggest that the solids have crystal-like structure, in which the repeat unit is the micelle particle which is several tens of nanometers in diameter.

The PS-*b*-PAA spherical crew cut micelles were characterized in water by TEM and DLS for a wide range of block lengths.[72] The R_{core} values scaled as $R_{\mathrm{core}} \sim N_{\mathrm{PS}}^{0.4} N_{\mathrm{PAA}}^{-0.15}$ illustrating an influence of the soluble block length on the R_{core} values. From DLS measurements, the R_{h} values were determined, and the thickness and the degree of extension of the coronal chains were estimated from the R_{core} and R_{h} values. It was found that the ionized form of the PAA chains (at pH ca. 7) in the coronae had a

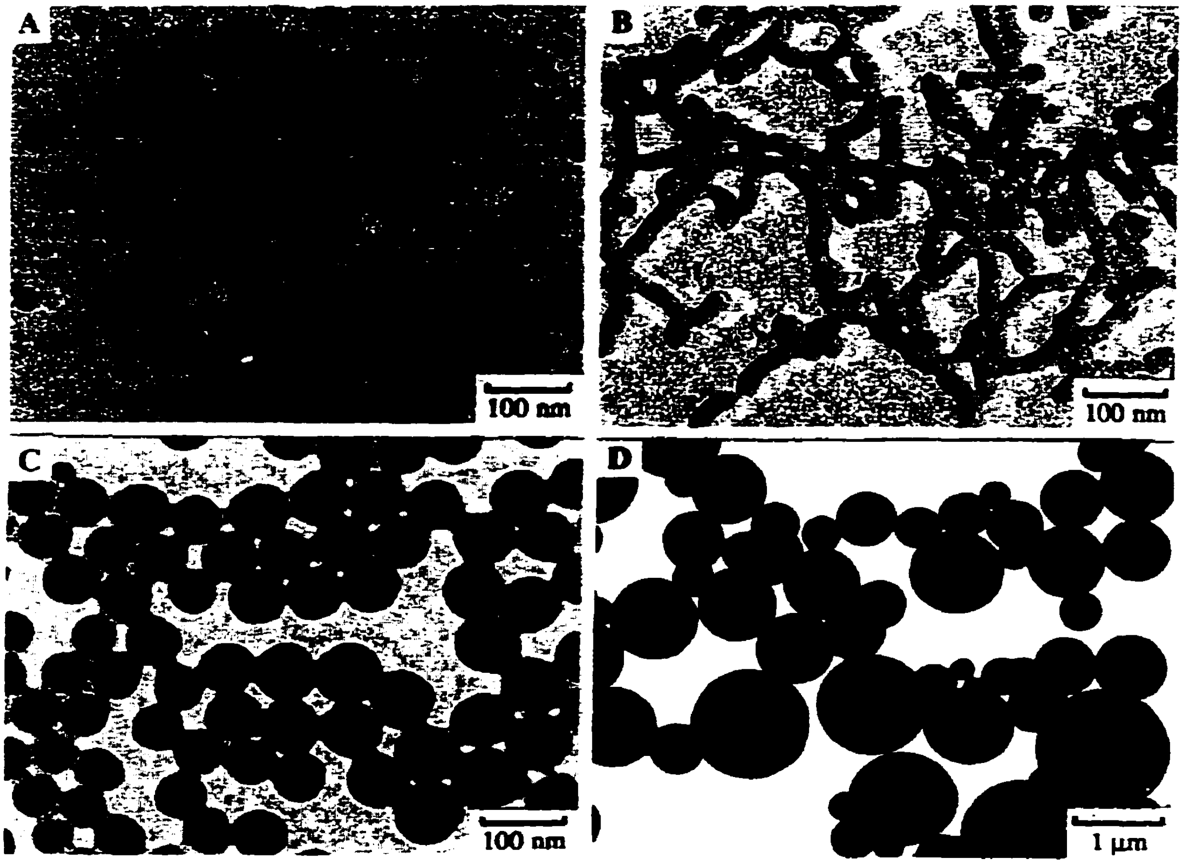

Figure 2.5. Multiple morphologies of crew-cut aggregates formed from PS-*b*-PAA block copolymers having different compositions (a) PS(740)-*b*-PAA(55) (b) PS(180)-*b*-PAA(15) (c) PS(200)-*b*-PAA(8) (d) PS(200)-*b*-PAA(4).

highly extended conformation. This result was attributed to the charged nature of the PAA chains, the low degree of curvature of the core and the relatively low concentration of micelles in the DLS experiment.

2.4. Conclusions

This review has attempted to summarize some recent findings in the field of ionic block copolymer micelles. Both block ionomer micelles and block polyelectrolyte micelles have been characterized extensively by a wide range of techniques. Low cmcs, high micelle stability, and control over aggregate sizes via copolymer composition make ionic block copolymers of interest for a number of possible applications, including drug delivery and material science. The solubilization of water into the cores of reverse micelles and the preparation of quantum-confined CdS nanoparticles of controlled sizes have illustrated the potential of these systems as microreactors in, for example, the controlled precipitation of metallic and semiconducting clusters. Crew-cut micelles have also been discussed as interesting new morphologies, providing further evidence of the versatility which is offered by solutions of ionic block copolymers.

In the next chapter, another type of ionic copolymer, namely a series of random ionomers, is applied to the synthesis of semiconducting nanoparticles. These materials are structurally quite different from the ionic block copolymers described in the present chapter, in that the ionic groups are distributed statistically throughout the chain, rather than in distinct blocks. However, the occurrence of microphase separation in these materials, to form discreet ionic multiplets in a polystyrene matrix, is analogous to block ionomer micelle formation in organic solvents. We begin our detailed discussion of nanoparticle size control with the random ionomer system, before progressing to the wider range of sizes that is accessible using block ionomers.

Acknowledgments

This work was supported by the Natural Sciences and Engineering Research Council of Canada (NSERC) and Le Fonds pour La Formation de Chercheurs et L'Aide à la Recherche (FCAR, Quebec). M.M. and K.K. are grateful for scholarship funding provided from NSERC and FCAR.

References

---

(1) Selb, J.; Gallot, Y. In *Polymeric Amines and Ammonium Salts*. Goethals, E. J. ed., Pergamon Press: New York, 1980, p 205.

(2) Selb, J and Gallot, Y. In *Development in Block Copolymers*; Goodman, I., ed.; Elsevier Applied Science: London, U.K., 1985; Vol 2, pp 27-96.

(3) Desjardins, A.; Eisenberg, A. *Macromolecules* **1991**, *24*, 5779.

(4) Desjardins, A.; van de Ven, T. G. M., Eisenberg, A. *Macromolecules* **1992**, *25*, 2412.

(5) Tuzar, Z.; Kratochvil, P. *Adv. Colloid Interface Sci.* **1976**, *6*, 201.

(6) Price, C. In *Developments in Block Copolymers*, Vol 1; Goodman, I., ed.; Applied Science Publishers: London, 1982, p.39.

(7) Tuzar, Z.; Kratochvil, P. In *Surface and Colloid Science*, Vol 15; Matijevic, E., ed.; Plenum Press: New York, 1993, p.1.

(8) de Gennes, P.-G. In *Solid State Physics*; Leibert, L., Ed.; Academic Press: New York, 1978; Supplement 4.

(9) Noolandi, J.; Hong, K. M. *Macromolecules* **1982**, *15*, 482.

(10) Noolandi, J.; Hong, K. M. *Macromolecules* **1983**, *16*, 1443.

(11) Whitmore, M. D.; Noolandi, J. *Macromolecules* **1985**, *18*, 657.

(12) Zhulina, E. B.; Birshtein, T. M. *Vysokomol. Soedin.* **1985**, *27*, 511.

(13) Fredrickson, G. H.; Helfand, E.; *J. Chem. Phys.* **1987**, *87*, 697.

(14) Bug, A. L. R.; Gates, M. E.; Safran, S. A.; Witten, T. A. *J. Chem. Phys.* **1987**, *87*, 1824.

(15) Marques, C.; Joanny, J. F.; Leibler, L. *Macromolecules* **1988**, *21*, 1051.

(16) Halperin, A. *Macromolecules* **1989**, *22*, 3806.

(17) Halperin, A.; Alexander, S. *Macromolecules* **1989**, *22*, 2403.

(18) Nagarajan, R.; Ganesh, K. *J. Phys. Chem.* **1989**, *90*, 5843.

(19) Marko, J. F.; Rabin, Y. *Macromolecules* **1992**, *25*, 1503.

(20) Yuan, X. F.; Masters, A. J.; Price, C. *Macromolecules* **1992**, *25*, 6876.

(21) Gao, Z.; Eisenberg, A. *Macromolecules* **1993**, *26*, 7353.

(22) Nagarajan, R.; Barry, M.; Ruckenstein, Z. E. *Langmuir* **1986**, *2*, 210.

(23) Nagarajan, R.; Ganesh, C. *Macromolecules* **1989**, *22*, 4312.

(24) Holland, P. M.; Rubingh, D. N. *J. Phys. Chem.* **1983**, *87*, 1984.

(25) Holland, P. M. *Adv. Colloid Interface Sci.* **1986**, *26*, 111.

(26) Astafieva, I.; Zhong, X. F.; Eisenberg, A. *Macromolecules* **1993**, *26*, 7339.

(27) Khougaz, K.; Gao, Z.; Eisenberg, A. *Macromolecules* **1994**, *27*, 6341.

(28) Astafieva, I.; Khougaz, K.; Zhong, X.F.; Eisenberg, A. *Macromolecules* **1995**, *28*, 7127.

(29) Eisenberg, A.; Rinaudo, M. *Polymer Bull.* **1990**, *24*, 671.

(30) Ishizu, K.; Kashi, Y.; Fukutomi, T.; Kakurai, T. *Makromol. Chem.* **1982**, *183*, 3099.

(31) Zhou, Z.; Peiffer, D. J.; Chu, B. *Macromolecules* **1994**, *27*, 1428.

(32) Zhong, X. F.; Varshney, S. K.; Eisenberg, A. *Macromolecules* **1992**, 25, 7160.

(33) Vanhoorne, P.; Jerome, R. In *Ionomers: Characterization, Theory, and Applications*; Schlick, S., Ed.; CRC Press: Boca Raton, Chapter 9, in press .

(34) Jalal, N.; Duplessix, R. *J. Phys.(France)* **1988**, *49*, 1775.

(35) (a) Davidson, N. S.; Fetters, L. J.; Funk, W. G.; Graessley, W. W.; Hadjichristidis *Macromolecules* **1988**, *21*, 112. (b) Pispas, S.; Hadjichristidis, N. *Macromolecules* **1994**, *27*, 1891. (c) Pispas, S.; Hadjichristidis, N.; Mays, J.M. *Macromolecules* **1994**, *27*, 6307.

(36) Zhong, X. F.; Eisenberg, A. *Macromolecules* **1994**, *27*, 1751.

(37) Zhong, X. F.; Eisenberg, A. *Macromolecules* **1994**, *27*, 4914.

(38) Nguyen, D.; Williams, C. E.; Eisenberg, A. *Macromolecules* **1994**, *27*, 5090.

(39) Khougaz, K.; Nguyen, D.; Williams, C. E.; Eisenberg, A. *Can. J. Chem.* In Press.

(40) Nguyen, D.; Williams, C. E.; Eisenberg, A. To be published.

(41) Nguyen, D.; Varshney, S. K.; Williams, C. E.; Eisenberg, A.

Macromolecules **1994**, *27*, 5086.

(42) Elias, H. G., In *Light Scattering from Polymer Solutions;* Huglin, M. B., ed.; Academic Press: New York, 1972, Chapter 9.

(43) Price, C.; Chan, E. K. M.; Stubbersfield, R. B. *Eur. Polym. J.* **1987**, *23*, 649.

(44) Myers, D. *Surfactant Science and Technology;* VCH publishers; New York, 1988.

(45) Wilhelm, M.; Zhao, C. L.; Wang, Y.; Xu, R.; Winnik, M. A.; Mura, J. L.; Riess; G., Croucher, M. D. *Macromolecules* **1991**, *24*, 1033.

(46) Nicolas, C. V.; Luo, Y. Z.; Deng, N. J.; Attwood, D.; Collet, J. H.; Price, C.; Booth, C. *Polymer* **1993**, *34*, 138.

(47) Gao, Z.; Desjardins, A.; Eisenberg, A. *Macromolecules* **1992**, *25*, 1300.

(48) Khougaz, K.; Gao, Z.; Eisenberg, A., To be published.

(49) Gao, Z. Zhong, X. F.; Eisenberg, A. *Macromolecules* **1994**, *27*, 794.

(50) Kunstle, H. PhD Thesis, Twente University, **1993**.

(51) Moffitt, M.; McMahon, L.; Pessel, V.; Eisenberg, A., *Chem. Mater.* **1995**, *7*, 1185.

(52) Moffitt, M.; Eisenberg, A., *Chem. Mater.* **1995**, *7*, 1178.

(53) Schindler, A.; Williams,J.L. *Polym. Prepr. (Am. Chem. Soc., Polym. Chem. Div).* **1968**, *10*, 832.

(54) Zhu, J.; Eisenberg, A.; Lennox, R. B. *J. Am. Chem. Soc.* **1991**, *113*, 5583.

(55) Zhu, J.; Eisenberg, A.; Lennox, R. B.*Langmuir* **1991**, 7, 1579.

(56) Zhu, J.; Eisenberg, A.; Lennox, R. B. *J. Phys. Chem.* **1992**, *96*, 4727.

(57) Zhu, J.; Eisenberg, A.; Lennox, R. B. *Macromolecules* **1992**, *25*, 6547.

(58) Zhu, J.; Eisenberg, A.; Lennox, R. B. *Macromolecules* **1992**, *25*, 6556.

(59) Dan, N.; Tirrell, M. *Macromolecules* **1993**, *26*, 4310.

(60) Khougaz, K.; Astafieva, I.; Zhong, X. F.; Eisenberg, A. *Macromolecules* **1995**, *28*, 7135.

(61) Cao, T.; Munk, P.; Ramireddy, C.; Tuzar, Z.; Webber, S. E. *Macromolecules* **1991**, *24*, 6300.

(62) Prochazka, K.; Kiserow, D.; Ramireddy, C.; Tuzar, Z.; Munk, P.; Webber, S. E. *Macromolecules* **1992**, *25*, 454.

(63) Kiserow, D.; Prochazka, K.; Ramireddy, C.; Tuzar, Z.; Munk, P.; Webber, S. E.

Macromolecules **1992**, *25*, 461.

(64) Tian, M.; Qin, A.; Ramireddy, C.; Webber, S. E.; Munk, P.; Tuzar, Z.; Procházka, K. *Langmuir* **1993**, *9*, 1741.

(65) Tuzar, Z.; Procházka, K.; Zuzková, I.; Munk, P. *Polym. Prepr. (Am. Chem. Soc., Poly. Chem. Div.)* **1993**, *34*, 1038.

(66) Qin, A.; Tian, M.; Ramireddy, C.; Webber, S. E.; Munk, P. *Macromolecules* **1994**, *27*, 120.

(67) Xu, R.; Winnik, M. A.; Hallett, F. R.; Riess, G.; Croucher, M. D. *Macromolecules* **1991**, *24*, 87.

(68) Brown, W.; Rymden, R.; Stam, J.; Almgren, M.; Svensk, G. *J. Phys. Chem.* **1989**, *93*, 2512.

(69) Morishima, Y.; Itoh, Y.; Hashimoto, T.; Nozakura, S.-I. *J. Polym. Sci., Polym.Chem. Ed.* **1982**, *20*, 2007.

(70) Valint, Jr., P. L.; Bock, J. *Macromolecules* **1988**, *21*, 175.

(71) Gao, Z.; Varshney, S. K.; Wong, S.; Eisenberg, A. *Macromolecules* **1994**, *27*, 7923.

(72) Zhang, L.; Barlow, R. J.; Eisenberg, A. *Macromolecules* **1995**, *28*, 6055.

(73) Zhang, L.; Eisenberg, A. *Science* **1995**, *268*, 1728.

CHAPTER 3

Size Control of Nanoparticles in Semiconductor-Polymer Composites: I. Random Ionomer Microreactors

3.1. Abstract

A priori knowledge of ionic aggregate sizes in random ionomers has been applied to the synthesis of semiconducting nanoparticles of predictable sizes. The size control of quantum-confined cadmium sulfide (CdS) and lead sulfide (PbS) particles in the range of $2R$ = 18-23 Å is accomplished within styrene-based random ionomers with ionic groups located at the ends of side-chains of variable lengths. The CdS and PbS nanoparticles are precipitated within the ionic aggregates (multiplets) of the ionomer, to form composites consisting of semiconducting particles dispersed in a polymer matrix. The sizes of the nanoparticles are found to increase linearly with increasing side chain length. A previous study has shown that the sizes of ionic multiplets also increase with the length of the side chain; the present finding therefore suggests that the sizes of nanoparticles are controlled by ionic aggregation numbers in the ionomer. The semiconductor-polymer composites are characterized by UV-vis spectroscopy, small-angle x-ray scattering (SAXS) and transmission electron microscopy (TEM). This is the first of two chapters in which the size control of semiconducting nanoparticles is accomplished through primary ionic aggregate sizes in ionomers.

3.2. Introduction

The study of semiconducting nanoparticles, and their controlled precipitation in various media, has received much attention in recent years. Such nanoparticles exhibit electrical and optical properties different from those of bulk semiconductors, and contain anywhere from several hundred to <10 ion-pair units. In this regime of ultrasmall sizes, the particle diameter is comparable to or less than the diameter of the bulk semiconductor exciton, such that quantum confinement of electron-hole pairs increases the band gap relative to that in the bulk materials.

In the quantum-confined regime, the control of particle sizes allows the band gap to be "tuned" to give the desired electrical and optical properties. For cadmium sulfide (CdS) particle diameters below ca. 60 Å, the absorption spectrum is "blue shifted" from the bulk, and correlations have been made between the absorption threshold and the size of the particles, using both theoretical calculations[1-3] and experimental measurements.[4,5] The control of semiconducting nanoparticle sizes has been achieved in a wide range of colloidal and solid-state media, including reverse micelles,[6-9] surfactant vesicles,[10,11] zeolites,[12] and several types of ion-containing polymers.[13-26]

Ionomers have been recently defined as ion-containing copolymers "in which the bulk properties are governed by ionic interactions in discrete regions of the material (the ionic aggregates)".[27] Microphase separation of ionomers results in the formation of ionic aggregates within a matrix of the nonionic polymer component. It is convenient to distinguish between two types of ionomers: random and block ionomers. In random ionomers, there is a statistical distribution of ionic units along the polymer chain. Block ionomers, on the other hand, consist of strands (or blocks) of ionic units and strands of nonionic units, linked in sequence through covalent bonds; a common case is the AB diblock ionomer, in which a block of nonionic A units is joined to a block of ionic B units. In both random and block ionomers, the relationship between morphological characteristics in the solid state, and the structure or composition of the ionomer, introduces a convenient method of controlling ionic aggregate sizes. As a detailed understanding of ionomer morphology has developed, it has become possible to form ionic aggregates of a specific size, simply by selecting an appropriate ionomer.

In the case of random ionomers, recent advances have greatly increased the understanding of microstructure and physical properties of these systems. A model of random ionomers has been developed by Eisenberg, Hird, and Moore (the EHM model),[28] and is based on ionic aggregates (or multiplets) that are surrounded by regions of restricted mobility in the bulk polymer. At sufficiently high ion contents, these regions overlap to form "clusters" of multiplets, resulting in phase-separated behaviour.

A recent study has shown that it is possible to control aggregate sizes in random ionomers by varying the structure of the ionic unit.[29] For a series of styrene-based ionomers with variable-length side chains between the polymer backbone and the ionic groups, it was found that the ionomers with longer side chains formed larger multiplets; this trend was attributed to decreased steric hindrance to ionic aggregation when the ionic groups are further removed from the backbone. For example, SAXS results showed that the multiplet aggregation numbers increased from ca. 30 to ca. 75, when the length of the side chain was increased by 9 methylene groups.

In diblock copolymers, microphase separation results in a range of morphologies from lamellar to spherical, depending on the volume fractions of the component blocks.[30-32] A number of theories have been developed which allow the morphology of diblock copolymers to be predicted in terms of fundamental parameters;[30,31,33-36] these are based on quantitative expressions for the free energy, which is minimized to determine the equilibrium shape of the microdomains for various relative block lengths. When the volume fraction of one block is relatively low, it has been observed that the microdomains have a spherical morphology.[30,37]

In diblock ionomers, spherical ionic aggregates are formed in a matrix of the nonionic component, even at extremely short ionic block lengths.[38] It is frequently found that Halperin's model for starlike diblock copolymers[39] is well-suited for describing the sizes of spherical ionic microdomains, both in the bulk[40a] and in solution.[40b] In solution, diblock copolymers form micelles, which consist of a core of the insoluble blocks, surrounded by a corona of the soluble blocks. Halperin's model states that the size of the micelle cores (which become spherical microdomain in the solid state), is determined exclusively by the length of the insoluble blocks (N_B), such that the core radius scales as

$N_B^{3/5}$. Other models, such as those developed by Leibler, Orland, and Wheeler[41] and Noolandi and Hong,[42] have also been used to predict the core radii and critical micelle concentrations of block copolymers. Investigations of block ionomers have included detailed SAXS studies of polystyrene-*b*-poly(meth)acrylate systems, which confirm the relationship between the length of the ionic block and the size of the ion-containing core, and demonstrate the control of ionic aggregate sizes through ionomer composition.[40]

From this description of random and diblock ionomers, it is evident that size control of ionic aggregates can be achieved by selecting an ionomer of a particular structure and composition. When both groups of ionomers are considered, a wide range of aggregate sizes is accessible. In random ionomers, aggregation numbers in the neighborhood of 2-75 ion pairs are possible, with multiplet radii in the range of < 5-10 Å.[29] In diblock ionomers with spherical microdomains, the radii of the ionic core can be varied conveniently in the range of 15-100 Å, by selecting the appropriate ionic block length. In such cases, the aggregation numbers of the ionic cores vary from ca. 20 to ca. 200 chains;[40b] this means that the largest spherical cores in block ionomers are ionic aggregates of several thousand ion pairs.

The synthesis of metal sulfide and metallic nanoparticles within ion-containing polymers has been demonstrated by several groups.[13-26] Ion-containing homopolymers, random ionomers, and ion-complexing block copolymers have all been used to synthesize various metallic and semiconducting particles, resulting in composite materials consisting of nanoparticles dispersed in a polymer matrix. Such composites have been shown to exhibit a wide range of interesting optical, electronic, and photocatalytic properties.[13-18,26,43,44]

In studies involving random ionomers, CdS particles have been precipitated in perfluorosulfonate (Nafion) films,[13-18] and PbS particles have been synthesized in ethylene-based (Surlyn) polymers.[19,20] The latter work demonstrated size control of PbS particles within the random ionomer, forming a range of particle sizes from monomolecular to bulk PbS. In these studies, size control was achieved through control of the initial ion concentration and subsequent annealing conditions, and not through control of the primary ionomer aggregate sizes.

Synthesis of inorganic nanoparticles within the metal-complexing microdomains of polystyrene-*b*-poly(2-vinylpyridine) has been reported by Moller.[21] Subsequently, Schrock and coworkers demonstrated the synthesis of CdS and ZnS particles within the microdomains of diblock copolymers formed by ring-opening metathesis polymerization.[22,23] These workers have also used the norborene-based metal-complexing blocks of such polymers to form metallic particles of platinum, palladium, gold and silver in the micro-separated domains.[24,25] TEM results showed that small particles of narrow size distribution were formed preferentially within metal-complexing microdomains of lamellar and cylindrical morphology. Single particles within microdomains of spherical morphology were also observed, suggesting the existence of a "cherry" morphology following nanoparticle synthesis.[25]

This work demonstrates the control of semiconducting nanoparticle particle sizes by the control of primary ionic aggregation numbers in several styrene-based ionomers. Ionomers are prepared by neutralizing the acid-form copolymer with metal acetates or metal hydroxides, such that metallic cations are localized in aggregates of a controlled size. These aggregates are the source of metal ions in metal sulfide formation, and thus serve as "microreactors" for the synthesis of semiconducting particles. The size of the resulting particles should ultimately be limited by the number of cations in the aggregate, which is directly related to the ionic aggregation number. The present chapter investigates random ionomers with variable length side chains as a medium for the synthesis of metal sulfide nanoparticles. The sizes of the semiconducting particles were determined from the absorption edge of UV-vis spectra, and compared with SAXS and TEM measurements.

3.3. Experimental

3.3.1. Polymer Materials

The synthesis of styrene-based ionomers with variable length *para*-methyl alkanoate side chains has been described in a previous publication.[45] Preparation of these materials involved direct attachment of the terminally carboxylated alkyl chains to the para position of the styrene rings through alkyl aryl ether linkages, to produce the following precursors: poly[styrene-*co*-4-[(carbomethoxymethy)oxy]styrene], poly[styrene-*co*-4-

[(carbomethoxybutyl)-1-oxy]styrene], and poly[styrene-*co*-4-[(carbomethoxydecyl)-1-oxy]styrene] .

The precursors were hydrolyzed by refluxing (under nitrogen) with excess sulfuric acid in a 90:10 tetrahydrofuran/water solution for 3-5 days. Structure I (Diagram I) shows the resulting polymers in the acid form, with variable-length spacers (n = 1, termed C_2 ether; n = 4, termed C_5 ether; n = 10, termed C_{11} ether). The carboxylic acid content was determined by titration of the hydrolyzed polymers with a standard 0.05 N methanolic NaOH solution. The acid content of the C_2-C_{11} ether series was determined to be 18 mol %.

The synthesis of poly[styrene-*co*-4-(carboxy)styrene] (acid content 10%, Structure II) was also described in a previous paper.[46] Poly[styrene-*co*-methacrylic acid] (acid content 14%, Structure III) was prepared by standard free radical polymerization techniques.

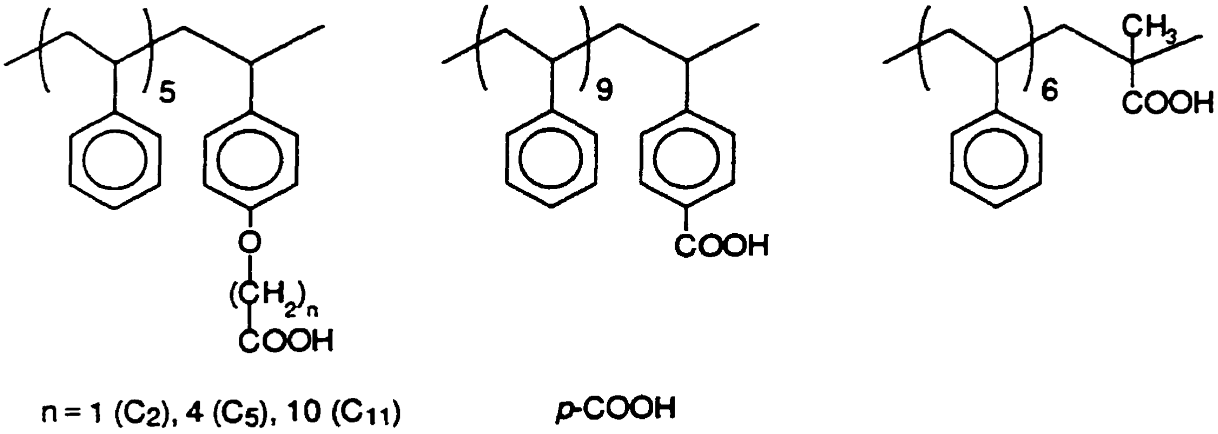

Structure I

Structure II

Structure III

N.B. The numbers outside the brackets indicate styrene units per ionic unit, and represent average values.

Diagram I

3.3.2. Preparation of Cd and Pb-Neutralized Ionomer Films

Transparent films of the Cd and Pb-neutralized ionomers were required for UV-vis analysis of the subsequent CdS and PbS-containing composites. Each polymer was cast in its acid form onto glass slides, from concentrated solutions in N,N-dimethylformamide (DMF). DMF was evaporated under vacuum at 130 °C, and the films were left to dry overnight under the same conditions. The polymer films were neutralized by immersing them for 3 days in a 0.25 M solution of cadmium acetate dihydrate (Aldrich) in 70:30 methanol/toluene (v/v), or in a 0.12 M solution of lead acetate trihydrate (Analar) in 80:20 methanol/toluene (v/v), to obtain Cd and Pb-neutralized films, respectively. The solutions were changed regularly over the 3 day period to remove acetic acid. Small amounts of the C_2, C_5, and C_{11} samples were scraped from the glass slides and mixed with dried KBr. FTIR spectral analysis of these samples indicated between 80% and 90% neutralization by the present method. Following neutralization, the polymer films were soaked for 3 days in methanol/toluene solutions, to wash away excess metal acetate such that all cadmium and lead ions were bound to the ionic groups of the polymer. During neutralization and rinsing, the films were swollen with toluene, facilitating multiplet formation.

The films turned from transparent to cloudy during the rinsing step. After rinsing, the films were heated with a heat gun until transparency returned, then the neutralized polymer films were dried under vacuum at 130 °C for 3 days.

In theory, the ratio of doubly-bound to singly-bound Cd^{2+} and Pb^{2+} ions is determinable from FTIR analysis of the neutralized copolymer films. The quality of the obtained spectra, however, made such quantitative analysis impossible in the present case. This method was more successful with neutralized block ionomer films, and will be discussed further in Chapter 4 of the thesis.

Ionomer films for small-angle X-ray scattering were prepared in an identical manner, except that generally thicker films were cast, and the transparency of the films was no longer critical. Ionomer films were prepared on Teflon sheets, and the subsequent composite films were then stacked to obtain thick films (ca. 1 mm) for SAXS analysis.

3.3.3. Reaction of Ionomer Films with Hydrogen Sulfide

After drying, the Cd and Pb-neutralized films were reacted for 5 hours in a closed flask with dry H_2S at atmospheric pressure and 25 °C. This was assumed to be sufficient time for all of the counterions in the ionic aggregates to be converted to CdS or PbS. Acrylate units were converted to acrylic acid in the course of the reaction. Within the first ten minutes of the reaction, colour changes indicated the formation of metal sulfide particles. CdS-containing films were pale yellow, while PbS-containing films ranged from dark orange to yellow in colour, depending on the host ionomer. Following the reaction, the films were left under vacuum in a desiccator overnight, to remove excess H_2S.

3.3.4. Transmission Electron Microscopy

Electron microscopy was performed on a Phillips EM410 instrument. A film of the CdS-C_{11} polymer composite was prepared for electron microscopy by microtoming (film thickness, ca. 800 Å), and the microtomed sample was then mounted on a copper grid.

3.3.5. UV-Vis Absorption Spectroscopy

UV-vis absorption spectra were obtained on a Hewlett-Packard 8452 diode array spectrophotometer. CdS and PbS-containing films were scanned between 250 and 550 nm, and between 200 and 800 nm, respectively. Absorption from the polymer and the glass slide was subtracted from each spectrum.

3.3.6. Small-Angle X-ray Scattering

Small-angle X-ray scattering experiments were carried out at Laval University, Quebec, on a Rigaku rotating-anode instrument (λ = 1.548 Å). The CdS-containing polymer films were scanned from q = 0.02 to 0.35 Å^{-1}. An "air" background signal was also scanned, and this was subtracted from each scattering profile. Low scattering intensities relative to the background resulted in very low signal to noise ratios. However, for the CdS-C_{11} polymer composite, a Bragg scattering peak was observed, and this was used to calculate the average spacing between scattering centers ($d_{Bragg} = 2\pi/q$). The number of CdS units per particle, n_{CdS}, was then determined by space-filling calculations for a simple cubic lattice, using the appropriate assumptions.[29]

3.4. Results and Discussion

3.4.1. UV-Vis Absorption Data for CdS Particles

Figure 3.1 shows an absorption spectrum for quantum-confined CdS particles synthesized in the 18 mol.% C_{11} ether ionomer. Absorbance from the glass slide and from the polymer before reaction with H_2S was subtracted from the spectrum. The insert shows the absorption spectrum of a styrene-based ionomer before treatment with H_2S. Neither the glass slide nor the polymer show significant absorbance above 300 nm, so the subtraction procedure does not interfere with the relevant spectral features. As indicated in Figure 3.1, the absorption edge, λ_e, is obtained from the intersection of the sharply decreasing region of the spectrum with the baseline. The exciton maximum, λ_m, is an example of spectral structure, and indicates a relatively narrow distribution of particle sizes.[47] For smaller CdS particles, λ_m could not be determined from the absorption spectra, as this feature was obscured by absorption from the polymer and/or glass.

The side chain lengths (L_{sc}) of the host ionomers (Table 3.1) were calculated assuming a fully-extended side chain.[29] Figure 3.2 shows the absorption spectra of CdS nanoparticles in polymers with variable-length spacers. Comparison of these spectra shows that the wavelength of the absorption edge increases with the length of the side chain, suggesting a concomitant increase in nanoparticle sizes.

For all spectra obtained in this study, the absorption edge, λ_e, was converted into an associated CdS particle size, using Henglein's empirical curve which relates the wavelength of the absorption threshold to the diameter of the CdS particles[5] (the curve was digitized, and the best-fitting function was used to calculate particle diameters[48]). For the spectrum shown in Figure 3.1, it was also possible to calculate a particle size corresponding to λ_m. The difference between the particle size calculated from λ_e and that calculated from λ_m gives the quantity $d_{1/2}$,[11] which indicates the width of the size

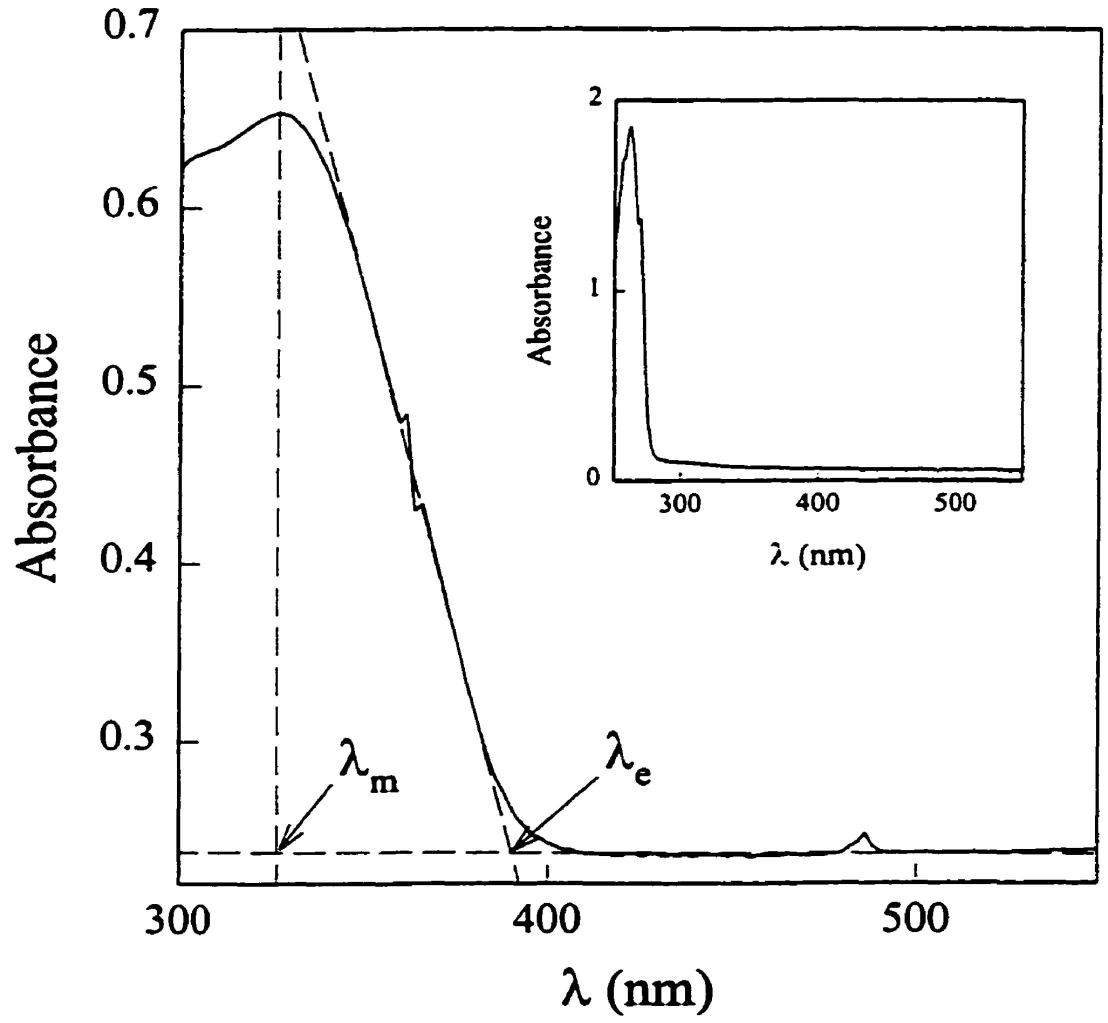

Figure 3.1. UV-vis absorbance spectrum of CdS formed in the 18% C_{11} ionomer. The polymer absorbance has been subtracted from the spectrum. The absorption edge is λ_e = 390 nm and the maximum is λ_m = 332 nm. The absorbance of the untreated polymer is shown in the insert.

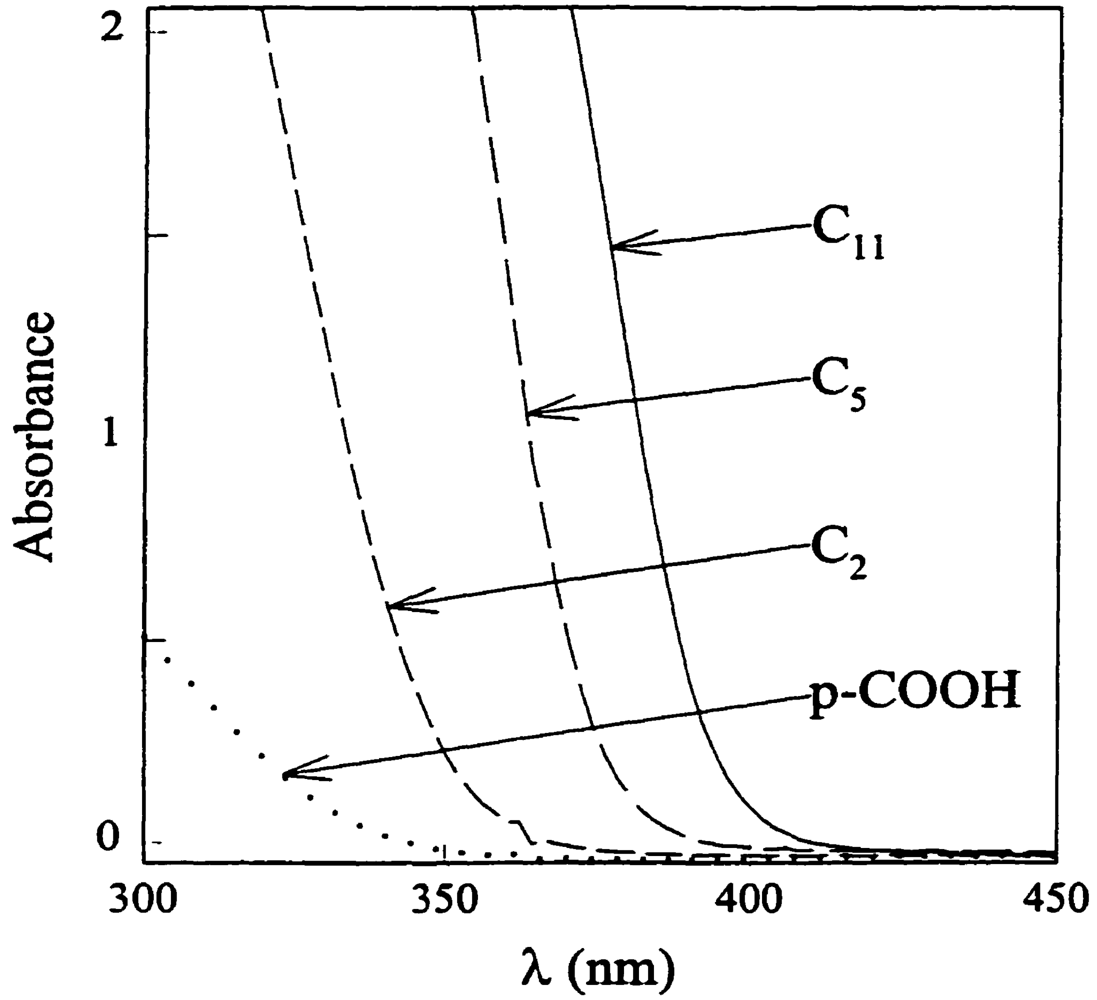

Figure 3.2. UV-vis spectra of CdS formed in a series of styrene-based ionomers with variable-length spacers. The 10% *p*-carboxystyrene ionomer is denoted *p*-COOH. The baselines have been normalized, such that the vertical axis indicates absorbance above the baseline.

distribution. Assuming a Gaussian distribution of particle sizes, $d_{1/2}$, can be used to calculate the radius polydispersity index (RPI), analogous to the polydispersity index (P.I.) of polymer molecular weights. From the spectrum shown in Figure 1, the CdS distribution has an RPI value of 1.03. This is a good indication that the particle sizes have a very narrow distribution.

UV-vis data and corresponding CdS particle diameters ($2R_{CdS}$) are listed in Table 3.1. To test the reproducibility of the results, each composite was prepared three times from the copolymer in the acid form. Average values of repeat preparations are reported in the table. Only two preparations of the methacrylate composite were performed, as the same value of λ_c was obtained both times for this sample.

Table 3.1. Nanoparticle sizes from UV-vis data for CdS and PbS in styrene-based random ionomers with variable-length spacers. The number of CdS and PbS ion pairs in the nanoparticles are compared with aggregation numbers in Cs-neutralized ionomers.

polymer	L_{sc} (Å)	λ_c(CdS) (nm)	λ_c(PbS) (nm)	$2R_{CdS}$ (Å)	$2R_{PbS}$ (Å)	n_{CdS}	n_{PbS}	n_{Cs} [a]
methacrylate, 14%	1.5	340	459	18.5	19.8	66	77	
p-carboxystyrene, 10%	5.3	335	453	18.1	19.6	62	74	
C_2 ether, 18%	8.0	344		18.8		70		28
C_5 ether, 18%	11.5	374	506	21.7	21.9	107	104	44
C_{11} ether, 18%	18.7	388	535	23	23.3	130	125	74

[a] Determined in 14% ether ionomers.

Figure 3.3 shows the CdS particle diameters, $2R_{CdS}$, plotted vs. side chain length, L_{sc}. The error bars indicate standard deviations of repeat preparations. From the *p*-carboxystyrene (L_{sc} = 5.3 Å) to the C_{11} ether (L_{sc} = 18.7 Å), the plot indicates that CdS particle diameters increase linearly with the side chain length (slope = 0.41, correlation coefficient, r^2 = 0.97) from $2R_{CdS}$ = 18 Å to ca. 23 Å. This is in agreement with the previous observation that multiplet sizes increase linearly with the length of the side chain. It is also interesting to note that the slope of the present line (0.41) is identical to that

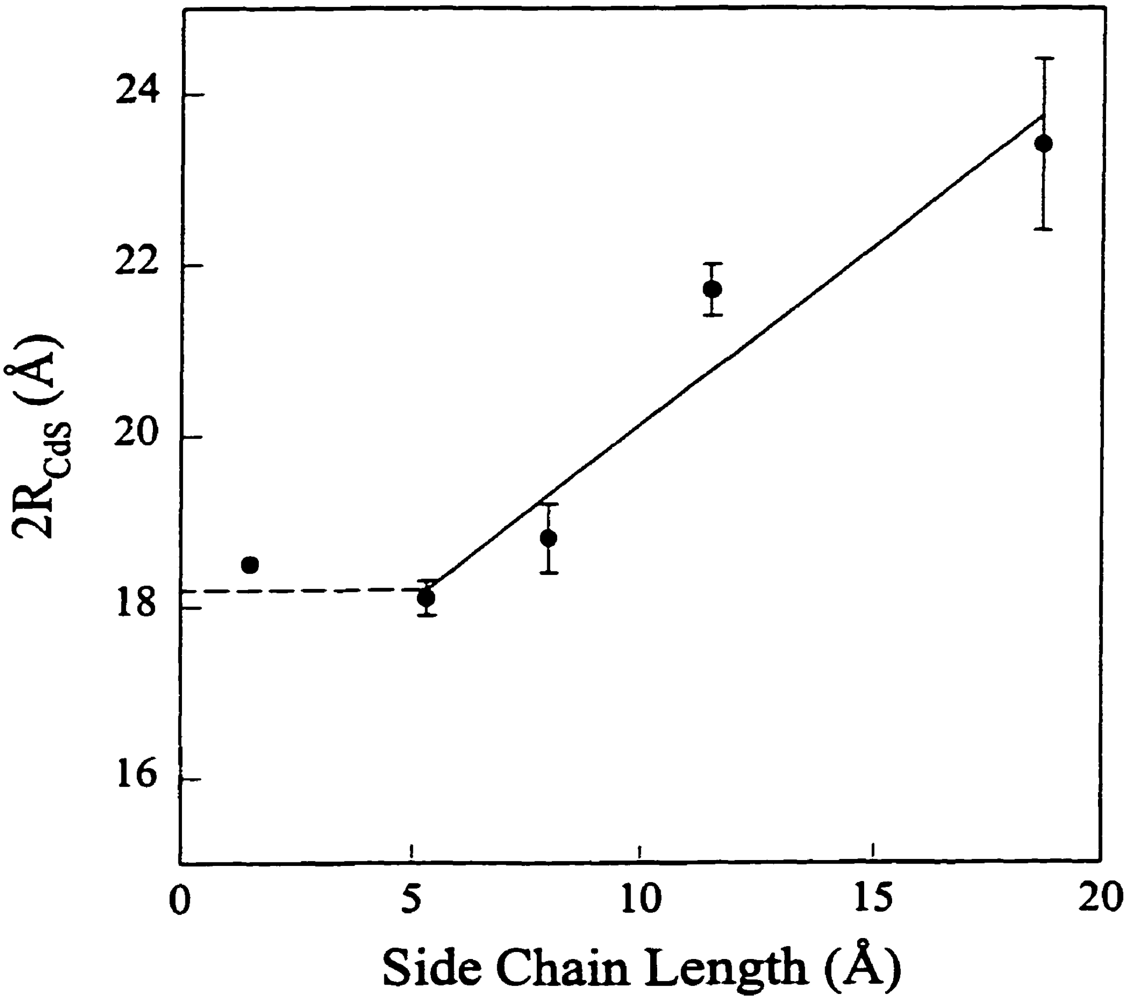

Figure 3.3. Plot of CdS nanoparticle diameters ($2R_{CdS}$) versus ionomer side chain length (L_{sc}). Linear regression was performed (solid line), omitting the methacrylate ionomer (L_{sc} = 1.5 Å). The dotted horizontal line is a guide for the eye and indicates an apparent plateau at small L_{sc} values.

found previously for the plot of ionic aggregate radius of cesium-neutralized ionomers versus side chain length.[29] It should also be noted that the majority of points fall within 1 Å of the particle diameter on the regression line. The similarity in the behaviour of multiplet sizes and nanoparticle sizes with increasing side chain length suggests that multiplet size is the limiting factor in CdS nanoparticle growth; it therefore seems reasonable to conclude that the particle sizes are effectively controlled by the ionomer morphology in "microreactors" of ionic multiplets. It should be noted that the methacrylate and *p*-carboxystyrene copolymers have lower ion percentages than the side-chain ether series, and this will lower their aggregation numbers slightly with respect to the other ionomers used in the study. However, since the effect of variable side-chain lengths has been shown to be more significant than the effect of ion percentage,[29] it was considered valid to plot the results of all five ionomers on the same graph.

The methacrylate point (L_{sc} = 1.5 Å) seems to fall within a plateau region, as $2R_{CdS}$ values level off at ca. 18 Å for small values of L_{sc}. This lower limit may be due to a degree of association or ripening of extremely small CdS particles. It is also possible that the size distributions broaden as the particle sizes decrease, such that, in the plateau region observed in Figure 3.3, the particle sizes calculated from λ_e remain constant while the average sizes continue to decrease. This possibility is supported by previous SAXS data on random ionomers with variable side chain lengths, which show that the size distribution of ionic aggregates is narrower in ionomers with longer side chains.[29]

Table 3.1 also lists the number of CdS units in the nanoparticles, n_{CdS}, calculated from R_{CdS} values. For this calculation, spherical particles ($V = (4/3)\pi R^3$) were assumed; also, the volume per CdS ion pair in the nanoparticles was assumed to be identical to the bulk value, 50 Å^3.

3.4.2. SAXS Data

Figure 3.4 shows a typical air-subtracted SAXS profile for CdS-containing polymer films prepared by the present method. The scattering profile shows a definite peak, related to the Bragg spacing between the scattering centers (the CdS-containing multiplets) by $d_{Bragg} = 2\pi/q$. However, due to low scattering intensities obtained, the

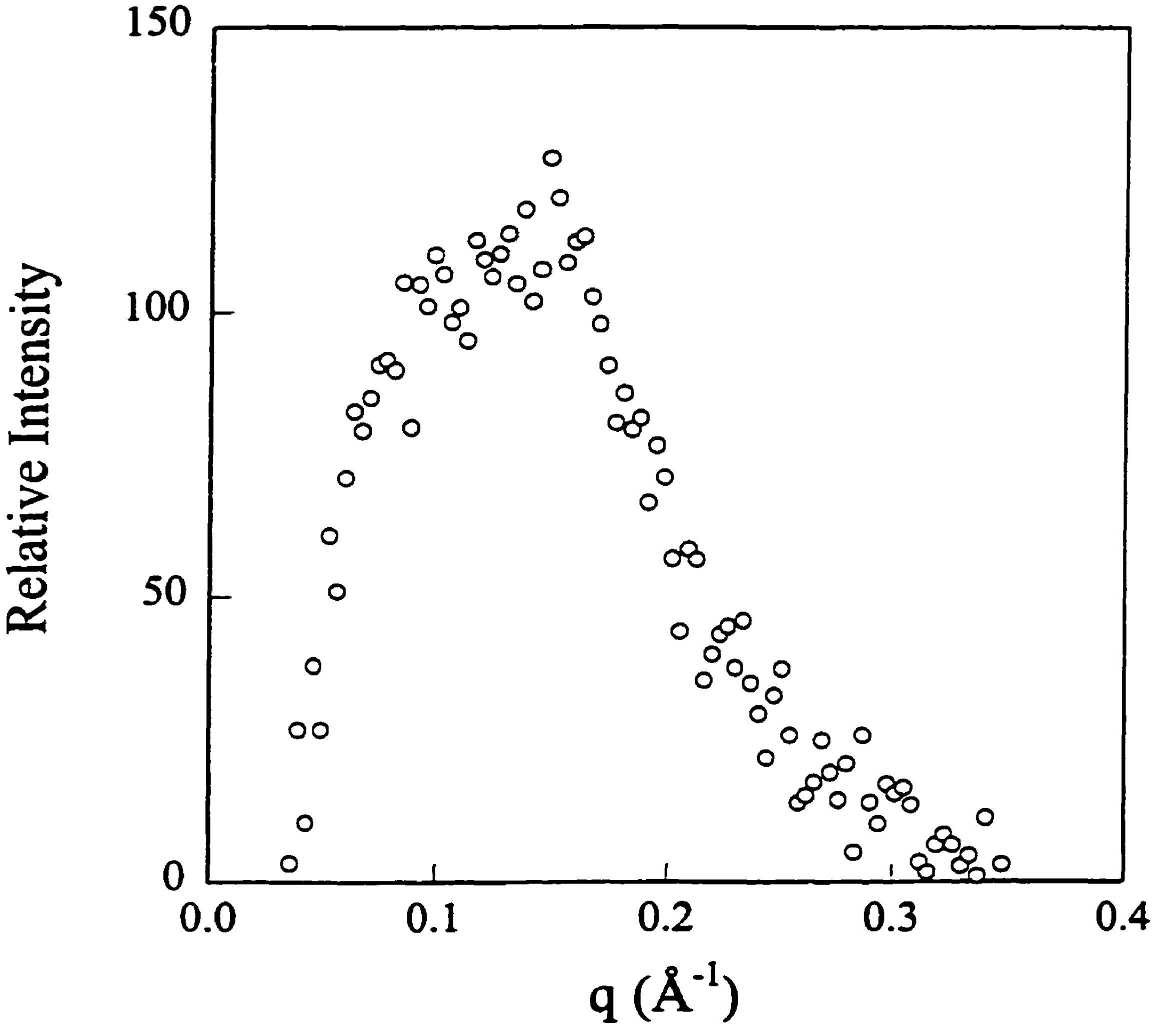

Figure 3.4. SAXS data for the CdS-C_{11} polymer composite. An air background has been subtracted. The position of the Bragg peak is determined to be $q = 0.12$ Å^{-1}.

subtraction procedure resulted in significant negative intensity values (not shown in the figure). As well, the number of counts obtained per scattering vector was relatively low. These factors contributed to a large margin of error in the peak positions. For the CdS-C_{11} polymer composite, which showed the most defined scattering peak, n_{CdS} was calculated from the position of the peak shown in Figure 3.4 (q = 0.12 Å^{-1}), using space-filling calculations for a simple cubic arrangement of multiplets.[29] The use of this particular lattice model is discussed below.

In ref. 40a, the sizes of ionic cores in block ionomers were calculated from the structure factors of SAXS profiles, assuming various arrangements of cores within the polymer matrix. Simple cubic (sc), face-centered cubic (fcc), body-centered cubic (bcc), and hexagonal close packed (hcp) were all applied in space-filling calculations. In general, the assumption of a sc lattice resulted in the best agreement with core sizes calculated directly from the form factor. The simple cubic arrangement of cores (or multiplets) in ionomers is not necessarily the most accurate description; however, it should be noted that the assumptions involved in other lattice models are, most likely, equally unrealistic.

Along with the assumption of a simple cubic arrangement of multiplets, the space-filling calculation involved the assumption of a single CdS unit per carboxylic acid group on the polymer chain. Although cadmium is a divalent counterion, this is not unreasonable, as the polymer films were neutralized with a large excess of cadmium acetate, which should favour the singly bound cadmium acetate counterion, $Cd(Ac)^+$. The value of n_{CdS} calculated from SAXS data for the C_{11} ionomer was 110, compared with n_{CdS} = 134, calculated from UV-vis data for the same ionomer (Table 3.1). This reasonable agreement provides confirmation of particle sizes determined using UV-vis spectroscopy.

3.4.3. Electron Microscopy

Figure 3.5 shows an electron micrograph of CdS particles in the C_{11} polymer. The small dark regions indicate well-defined CdS-containing multiplets, scattered evenly throughout the (grey) polystyrene matrix. The dark regions indicate particle diameters of ca. 25 Å, confirming UV-vis results. It should be noted that the microtomed composite

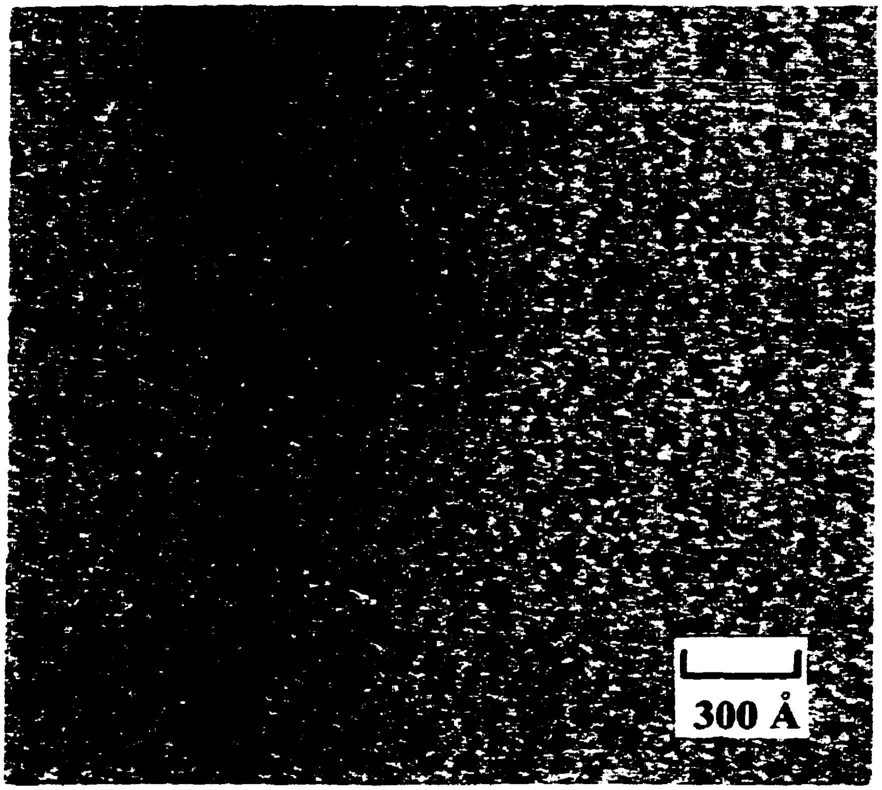

Figure 3.5. Transmission electron micrograph of the CdS-C_{11} polymer composite. The dark regions indicate CdS particles dispersed in the polymer matrix. From the micrograph, average particle diameters are ca. 25 Å.

film (800 Å) does not constitute a monolayer, so a statistical assessment of the size distribution from the micrograph has not been attempted. The monolayer thickness was defined as the dimension of a cube consisting of a single CdS-containing aggregate and the surrounding styrene (simple cubic arrangement of multiplets), and was calculated to be ca. 60 Å. This value corresponds to an average of 13 monolayers in the microtomed film.

3.4.4. UV-Vis Absorption Data for PbS Particles

Data for PbS nanoparticles formed in the same series of ionomers are listed with the CdS data in Table 3.1. These values were obtained from a single preparation of each PbS-polymer composite. The correlation between absorption edge values and PbS particle diameters was made using a theoretical model developed by Wang et al.[19,49] The number of PbS units in the nanoparticles, n_{PbS}, was calculated from the spherical particle volume and the volume of a single PbS unit in bulk, 53 Å^3. Data for PbS particles within the C_2 polymer are not reported, as a reliable absorption edge could not be determined from the spectrum of this composite. Comparison between n_{PbS} and n_{CdS} values for the same ionomers shows good agreement, which lends further support to the claim that particle sizes are controlled by the size of the ionic multiplet. It seems possible to use a selected polymer host to form nanoparticles of different materials containing identical numbers of ion pairs, assuming that the nature of the counterion does not significantly affect the size of the multiplets.

3.4.5. Comparison with Aggregation Numbers in Cs-neutralized Ionomers

Table 3.1 also lists multiplet aggregation numbers for 14% Cs-neutralized ether ionomers (n_{Cs}), determined from SAXS data by Moore and coworkers using space-filling calculations.[29] Despite differences in ion content and method of preparation, it is still interesting to compare n_{CdS} and n_{PbS} with n_{Cs}. This is, in effect, a comparison of ionomer aggregation numbers for different counterions, assuming that n_{CdS} and n_{PbS} correspond to the aggregation numbers of the Cd and Pb-neutralized multiplets prior to reaction with H_2S. This assumption requires 100% conversion of the metal counterions into the semiconductor particles. The results for the Cd and Pb-neutralized C_2-C_{11} ether series, determined by UV-vis spectroscopy of the semiconductor particles, are within a factor of 2 of SAXS-determined results for the Cs-neutralized samples. It is not surprising that aggregation numbers determined from UV-vis data (n_{CdS}, n_{PbS}) are generally larger than those determined from SAXS (n_{Cs}), since, in a distribution of particle sizes, the UV-vis absorption edge corresponds to particles larger than the mean.[4] SAXS results, on the other hand, are based on the average spacing between scattering centers, and therefore reflect average particle sizes. The lower ion percentage in the Cs-neutralized samples will also contribute to lower aggregation numbers compared with Cd and Pb-neutralized ionomers prepared in this study. A more thorough comparison of the dependence of aggregation numbers on the nature of the counterion is discussed in chapter 5, in the context of block ionomers.

3.4.6. Long-term Stability

To test for long-term stability, the CdS-polymer composites were stored under ambient conditions for a period of 7 months, after which UV-vis spectra were obtained. Values of λ_e and $2R_{CdS}$ after 7 months storage are listed in Table 3.2, along with the original data for the same composites. In most cases, an increase in particle diameter from 1-3 Å was observed, possibly due to long-term ripening under ambient conditions.

Table 3.2. UV-Vis absorption data and CdS nanoparticle sizes before and after 7 months storage under ambient conditions.

polymer	λ_e *after 24h* (nm)	$2R_{CdS}$ *after 24h* (Å)	λ_e *after 7 months* (nm)	$2R_{CdS}$ *after 7 months* (Å)
methacrylate,14%	340	18.5	349	19.3
p-carboxystyrene,10%	332	17.9	353	19.6
C_2 ether, 18%	344	18.8	354	19.7
C_5 ether, 18%	376	21.9	381	22.5
C_{11} ether, 18%	390	23.6	411	26.7

3.5. Conclusions

This investigation has shown that size control of semiconducting nanoparticles can be achieved through a knowledge of primary multiplet aggregation numbers in the host ionomer. A linear relationship between the ionomer side chain length and the resulting CdS particle diameter has been found, along with excellent agreement between values of n_{CdS} and n_{PbS} determined independently for the same ionomers. Agreement between n_{CdS} values determined by UV-vis and SAXS data was found for the C_{11} ionomer. TEM results show CdS particles evenly dispersed in the polymer matrix. It has been inferred that CdS or PbS precipitation is restricted to the ionic multiplets of the polymer host, which act as "microreactors" in nanoparticle formation. Multiplet size is therefore the limiting factor in particle growth. In random ionomers, the multiplet sizes are controlled by varying the length of the ionomer side chain, with longer side chains resulting in larger multiplets and thus larger semiconducting particles. With an understanding of the relationship between ionomer structure and morphology, the use of predictable multiplet sizes to control the sizes of nanoparticles within ionomers may have the advantages of precision and convenience over other methods of size control, such as controlling the initial ion concentration and/or thermal annealing of particles following precipitation.[19,20] This method of size control, of course, is not limited to semiconducting quantum dots, and other types of nanoparticles (e.g. magnetic, catalytic, etc.) within random ionomer aggregates are also conceivable.

This chapter has shown size control in the narrow range of 18-23 Å using random ionomers of various side chain lengths. In the next chapter, a similar mechanism of size control is investigated in block ionomers, by the synthesis of semiconducting nanoparticles in the larger ion aggregates of these materials. Along with the wider range of aggregate sizes that is accessible in block ionomers, microreactors of this type offer the unique advantage of solution stability, as they can be suspended in organic solvents in the form of reverse micelles. Stability to other methods of composite processing is also investigated in this work, and other aspects of system versatility are demonstrated.

Acknowledgments

The authors gratefully acknowledge Dr. G. Bazuin for the use of SAXS facilities, and assistance with the instrument, and Dr. J.-S. Kim for helpful discussions. This work was supported by the Natural Sciences and Engineering Research Council of Canada (NSERC). M.M. also acknowledges the financial support of NSERC.

References

(1) Brus, L. E. *J. Chem. Phys.* **1983**, *79*, 5566.
(2) Brus, L. E. *J. Chem. Phys.* **1984**, *80*, 4403.
(3) Lippens, P. E.; Lannoo, M. *Phys. Rev. B* **1989**, *39*, 10935.
(4) Weller, H.; Schmidt, H. M.; Koch, U.; Fojtik, A.; Baral, S.; Henglein, A.; Kunath, W.; Weiss, K.; Dieman, E. *Chem. Phys. Lett.* **1986**, *124*, 557.
(5) Spanhel, L.; Haase, M.; Weller, H.; Henglein, A. *J. Am. Chem. Soc.* **1987**, *109*, 5649.
(6) Meyer, M.; Wallberg, C.; Kurihara, K.; Fendler, J. H.; *J. Chem. Soc., Chem. Commun.* **1984**, 90.
(7) Lianos, P.; Thomas, J. K. *Chem. Phys. Lett.* **1986**, *125*, 299.
(8) Petit, C.; Lixon, P.; Pileni, M. P. *J. Phys. Chem.* **1990**, *94*, 1598.
(9) Pileni, M. P.; Motte, L.; Petit, C. *Chem. Mater.* **1992**, *4*, 338.
(10) Tricot, Y.-M.; Fendler, J. H. *J. Phys. Chem.* **1986**, *90*, 3369.
(11) Watzke, H. J.; Fendler, J. H. *J. Phys. Chem.* **1987**, *91*, 854.
(12) Wang, Y.; Herron, N. *J. Phys. Chem.* **1987**, *91*, 257.
(13) Krishnan, M.; White, J. R.; Fox, M. A.; Bard, A. J. *J. Am. Chem. Soc.* **1983**, *105*, 7002.
(14) Mau, A. W.- A.; Huang, C. B.; Kakuta, N.; Bard, A. J.; Campion, A.; Fox, M. A.; White, J. M.; Webber, S. E. *J. Am. Chem. Soc.* **1984**, *106*, 6537.
(15) Kuczynski, J. P.; Milosavljevic, B. H.; Thomas, J. K. *J. Phys. Chem.* **1984**, *88*, 980.
(16) Wang, Y.; Mahler, W. *Opt. Commun.* **1987**, *61*, 233.
(17) Hilinski, E. F.; Lucas, P. A.; Wang, Y. *J. Chem. Phys.* **1988**, *89*, 3435.

(18) Wang, Y.; Suna, A.; McHugh, J.; Hilinski, E. F.; Lucas, P. A.; Johnson, R. D. *J. Chem. Phys.* **1990**, *92*, 6927.

(19) Wang, Y., Suna, A.; Mahler, W.; Kasowski, R. *J. Chem. Phys.* **1987**, *87*, 7315.

(20) Mahler, W. *Inorg. Chem.* **1988**, *27*, 435.

(21) Möller, M. *Synth. Met.* **1991**, *41-43*, 1159.

(22) Cummins, C. C.; Schrock, R. R.; Cohen, R. E. *Chem. Mater.* **1992**, *4*, 27.

(23) Yue, J.; Sankaran, V.; Cohen, R. E.; Schrock, R. R. *J. Am. Chem. Soc.* **1993**, *115*, 4409.

(24) Ng Cheong Chan, Y.; Craig, G. S. W.; Schrock, R. R.; Cohen, R. E. *Chem. Mater.* **1992**, *4*, 885.

(25) Ng Cheong Chan, Y.; Schrock, R. R.; Cohen, R. E. *J. Am. Chem. Soc.* **1992**, *114*, 7295.

(26) Im, S. S.; Lee, J. S.; Kang, E. Y. *J. Appl. Polym. Sci.* **1992**, *45*, 827.

(27) Eisenberg, A.; Rinaudo, M. *Polymer Bulletin* **1990**, *24*, 671

(28) Eisenberg, A.; Hird, B.; Moore, R. B. *Macromolecules* **1990**, *23*, 4098.

(29) Moore, R. B.; Bittencourt, D.; Gauthier, M.; Williams, C. E.; Eisenberg, A. *Macromo lecules* **1991**, *24*, 1376.

(30) Molau, G. E. In *Block Polymers*, Aggarwal, S. L., ed., Plenum: New York, **1970**, p.79.

(31) Helfand, E.; Wasserman, Z. R.; In *Developments in Block Copolymers*, Goodman, I., ed., Applied Science Publishers: London, **1982**.

(32) Aggarwal, S.L. In *Processing, Structure and Properties of Block Copolymers*, Folkes, M. J., ed., Elsevier: London, **1985**.

(33) Folkes, M.; Keller, A. In *Physics of Glassy Polymers*, Haward, R. N., ed., Applied Science Publishers: London, **1973**.

(34) Meier, D. J. In *Thermoplastic Elastomers: A Comprehensive Review*, Legge, N. R.; Holden, G.; Schroeder, H. E., eds., Hanser: New York, **1987**, Chapter 11.

(35) Bates, F. S.; Fredrickson, G. H. *Annu. Rev. Phys. Chem.***1990**, *41*, 525.

(36) Richards, R. W. In *Multicomponent Polymer Systems*, Miles, I. S.; Rostami, S., eds., Longman Scientific & Technical: U. K., **1992**, Chapter 4.

(37) Hashimoto, T.; Fujimura, M.; Kawai, H. *Macromolecules* **1980**, *13*, 1660

(38) Gouin, J. P.; Williams, C. E.; Eisenberg, A. *Macromolecules* **1989**, *22*, 4573.

(39) Halperin, A. *Macromolecules* **1987**, *20*, 2943.

(40) a. Nguyen, D.; Varshney, S. K.; Williams, C. E.; Eisenberg, A. *Macromolecules* **1994**, *27,* 5086 b. Nguyen, D.; Williams, C. E.; Eisenberg, A. *Macromolecules* **1994**, *27,* 5090.

(41) Leibler, L.; Orland, H.; Wheeler, J. C. *J. Chem. Phys.* **1983**, *79*, 3550.

(42) Noolandi, H.; Hong, K. M. *Macromolecules* **1983**, *16*, 1443.

(43) Meissner, D.; Memming, R.; Kastening, B. *Chem. Phys. Lett.* **1983**, *96*, 34.

(44) Misawa, K.; Yao, H.; Hayashi, T.; Kobayashi, Y. *Chem. Phys. Lett.* **1991**, *183*, 113.

(45) Gauthier, M.; Eisenberg, A. *J. Polym. Sci.* **1990**, *28*, 1549.

(46) Hird, B.; Eisenberg, A. *Macromolecules* **1992**, *25*, 6466.

(47) Henglein, A. *Chem. Rev.* **1989**, *89*, 1861.

(48) The equation used to calculate CdS nanoparticle diameters was: $2R_{\mathrm{CdS}} = 1/(0.1338 - 0.0002345\lambda)$. The number of significant figures shown is that necessary to arrive at the reported results.

(49) The equation used to calculate PbS nanoparticle diameters was: $2R_{\mathrm{PbS}} = \exp(0.9587 + 0.09468\lambda^{1/2})$. The number of significant figures shown is that necessary to arrive at the reported results.

CHAPTER 4

Size Control of Nanoparticles in Semiconductor-Polymer Composites: II. Diblock Ionomer Microreactors

4.1. Abstract

The size control of semiconducting nanoparticles via primary aggregate sizes in ionomers has been extended to include the precipitation of cadmium sulfide (CdS) within the spherical ionic cores of PS-*b*-PACd diblock ionomers of various ionic block lengths. This procedure yields nanoparticles in the range of $2R$ = 29-50 Å, using ionic block lengths of 4 to 32 repeat units. The sizes of quantum-confined CdS particles formed in water-plasticized ionic cores, determined by UV-vis spectroscopy, are found to increase linearly with the size of the original core (correlation coefficient $r^2 = 0.99$), and scale with the ionic block length as $N_B^{3/5}$, in agreement with the Halperin model of starlike micelles. Comparisons between the number of ion pairs in CdS particles and the number of countercations in the original cores are used to show that, except in the largest ionic cores, a single particle per core is obtained (cherry morphology). The stability of the CdS-containing micelles in a selective solvent is enhanced considerably by re-neutralizing the poly(acrylic acid) layer surrounding the nanoparticle within the core. These stabilized micelles can be dissolved in an organic solvent, precipitated into methanol, and redissolved several times, without significant changes in the UV-vis absorption spectrum. It is also

found possible to process the CdS-polymer composites by casting from toluene or compression molding at 130 °C, without affecting the nanoparticle sizes. Particle sizes can be increased by re-neutralizing the CdS-containing micelle cores with cadmium acetate, followed by secondary treatment with H_2S. Thus by successively "reloading" the microreactor, nanoparticles of 37 Å in diameter are enlarged to 56 Å in two steps.

4.2. Introduction

The controlled precipitation of quantum-confined semiconductor particles such as cadmium sulfide has been achieved in a wide range of media, including surfactant micelles,[1-4] vesicles,[5,6] zeolites,[7] random ionomers,[8-15] and ion-complexing block copolymers.[16-20] Several studies have been concerned with the control of nanoparticle sizes by variations in the methods of preparation, though techniques of synthesizing monodisperse particles of predictable, thermodynamically-controlled sizes are still quite rare. The aim of this work is to apply a priori knowledge of ionic aggregate sizes in a wide range of ionomers, in order to use these materials as hosts for the precipitation of semiconducting nanoparticles of predictable sizes.

In the previous chapter, CdS particle sizes were controlled in the narrow range of 18-23 Å in diameter, using the relatively small aggregates of styrene-based random ionomers.[21] The sizes of these aggregates are controlled via the length of the spacers which separate the backbone from the ionic functional groups, with longer spacers resulting in larger aggregates.[22] The present chapter describes the size control of nanoparticles by precipitation of CdS within the spherical microdomains of cadmium-neutralized polystyrene-*b*-poly(acrylic acid) copolymers with variable ionic block lengths. As in the case of random ionomers, this size control, in principle, is thermodynamic in origin, as the sizes of growing particles are limited by the number of ions within the original aggregate. The ionic aggregates in block ionomers are very much larger than those in random ionomers, and these materials therefore allow the size control of CdS nanoparticles to be extended into a range of sizes not accessible with random ionomers.

It is well known that the morphology of microphase-separated regions in bulk-phase diblock copolymers (spherical, cylindrical, or lamellar) is determined by the relative volume fraction of the component blocks, while the size of these regions is determined by the absolute length of the microdomain-forming block.[23-25] For highly asymmetric AB diblock copolymers, the shorter block forms spherical microdomains within a matrix of the major component.[23,26]

Microphase separation into spherical microdomains in the bulk is analogous to the formation of diblock copolymer micelles in a selective solvent, in which the short insoluble blocks form a spherical core, surrounded by a corona of the soluble major component. Halperin's model of starlike diblock copolymer micelles,[27] among other theories, addresses the sizes of the spherical cores. The model states that the core radius scales as $N_B^{3/5}$, where N_B is the number of units in the short insoluble block. Small-angle X-ray scattering studies of block ionomer reverse micelles with relatively short ionic blocks were found to agree well with the Halperin model, and a proportionality constant of 6.5 Å was determined by fitting the measured ionic core radii ($R_{core} = 6.5\text{Å}\ N_B^{3/5}$).[28]

The predictability of core radii in microphase-separated diblock ionomers allows a desired core size to be obtained simply by selecting the length of the ionic block. Using anionic polymerization, polystyrene-*b*-poly(*tert*-butyl acrylate) diblock copolymers with specific poly(*tert*-butyl acrylate) block lengths can be synthesized routinely, and subsequent hydrolysis and neutralization allows a particular type of metal ion (or combination of ions) to be incorporated into cores of controlled sizes. Cadmium-neutralized polystyrene-*b*-poly(acrylic acid) ionomers are converted into CdS-copolymer composites by reaction with H_2S; simple chemistry within the "microreactor" core effects the precipitation of CdS nanoparticles and the re-protonation of the carboxylate groups. The acrylic acid layer then offers the possibility of performing further chemistry close to the surface of the semiconductor particle. For example, reneutralizing the acrylic acid units with sodium hydroxide should increase the stability of the composites in solution, as the solubility of poly(sodium acrylate) is much lower than that of poly(acrylic acid) in organic solvent. Along with stabilizing, or "fixing", the CdS-containing micelle, reneutralization allows a wide range of ions to be incorporated at the surface of the CdS particles. The following schematic shows particle formation (cherry morphology) and subsequent "fixing" within the block ionomer microreactor:

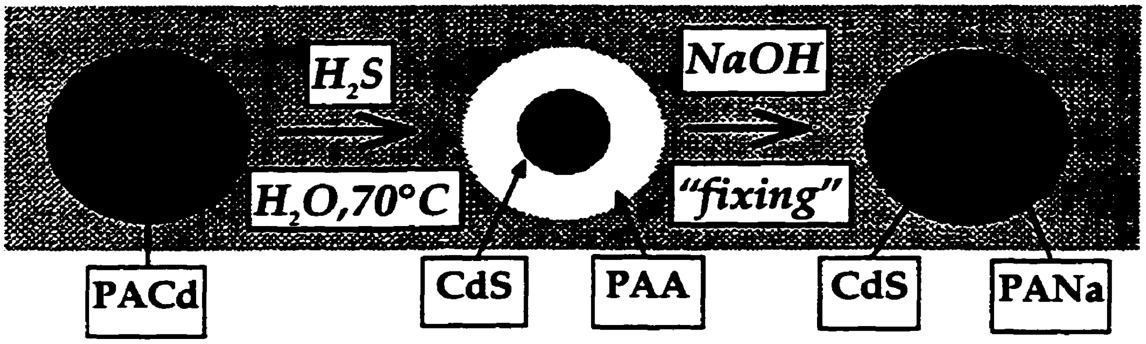

In organic solvents, the polystyrene blocks (represented by the grey background in the schematic) will constitute the soluble coronae of reverse micelles, protecting the CdS particles from agglutination and macroscopic precipitation. Isolated CdSe nanoparticles, soluble in organic solvent, have previously been formed by functionalizing the surface of the particles with phenyl ligands.[29] As well, ion-containing polymers have been used to stabilize CdS nanoparticles in aqueous solution, and to isolate the materials as re-dispersible powders.[30] The present study of semiconducting nanoparticles within the cores of diblock ionomer reverse micelles demonstrates a novel combination of selected aspects of past work, in the form of polymer-stabilized nanoparticles of predictable sizes that are highly stable and soluble in a wide range organic solvents. The stability of these materials is of interest in view of potential applications; for example, CdS particles have been used for the photochemical reduction of water both in colloidal solutions of reverse surfactant micelles[31] and in polymer films.[32,9] A CdS-polymer composite that can be dissolved in organic solvents and then recovered as a solid, without changes in fundamental properties, offers the unique possibility of a photocatalytic material that is equally effective in colloidal and bulk media.

4.3. Experimental

4.3.1. Synthesis of Diblock Copolymers

The synthesis of the block ionomers used in the present study was performed according to known procedures;[33-35] hence, only a brief summary is presented here. Series of polystyrene-*b*-poly(*tert*-butyl acrylate) with polystyrene blocks of constant length and poly(*tert*-butyl acrylate) blocks of variable length were synthesized by anionic polymerization. The initiator used in the synthesis was sec-butyllithium capped with a few units of α-methylstyrene. The block copolymers in the ester form were then hydrolyzed to polystyrene-*b*-poly(acrylic acid) (PS-*b*-PAA) by refluxing overnight in toluene solution with *p*-toluenesulfonic acid as the catalyst. The polymers were recovered by precipitation into methanol and were then dried in a vacuum oven at 70° C for 24 h. The molecular weight of the polystyrene blocks and the polydispersity indexes of all copolymers were determined by SEC. Polydispersity indexes of block copolymers used in the present study varied between 1.04 and 1.10. The composition of the copolymers was determined by FTIR, using the copolymers in the ester form.

The copolymers PS-*b*-PAA were dissolved in benzene/methanol (5% methanol w/w) at a concentration of about 1% (w/w). The acid blocks were neutralized by addition of excess cadmium acetate dihydrate in methanol (1.5 mol cadmium acetate dihydrate : 1 mol acrylic acid repeat units). The solutions were stirred for 3-4 h, then the block ionomers were recovered by freeze drying. They were subsequently dried in a vacuum oven at 70 °C for 24 h to remove any remaining solvent and acetic acid by-product. Excess cadmium acetate was removed by repeated washings of the block ionomers in methanol; the washed polymers were dried overnight under vacuum at 70 °C. FTIR was used to confirm that the polymers were 100% neutralized. The composition of each of the diblock ionomers used in this work is presented in Table 4.1, using the following nomenclature: PS(300)-*b*-PACd(4.0) indicates a diblock copolymer consisting of a polystyrene block of 300 repeat units covalently linked to a poly(cadmium acrylate) block of 4.0 repeat units.

4.3.2. Determination of the Degree of "Bridged" Cadmium in Neutralized Diblock Copolymer Films

The percentage of bridged Cd^{2+} ions within neutralized and rinsed polymer films was calculated from the length of the ionic block and the total number of carbonyl moieties (both acetate and acrylate) in the polymer chain. The latter quantity was determined by FTIR, using the following calibration procedure. Known quantities of cadmium acetate dihydrate and polystyrene-*b*-poly(*tert*-butyl acrylate) (PS(50)-*b*-PtbA(330)) were dissolved in methanol, and films were cast from the mixed solutions onto KBr windows. For various mole percentages of cadmium acetate carbonyl moieties, the ratio of carbonyl absorbance (1550 cm^{-1}) to polystyrene absorbance (700 cm^{-1}) was calculated from the obtained spectrum. A calibration curve was plotted, and this was used to analyze spectra of Cd-neutralized block copolymers.

4.3.3. Preparation of Cadmium Sulfide-Diblock Copolymer Films

Thin, optically transparent films of polystyrene-*b*-poly(cadmium acrylate) (PS-*b*-PACd) with various ionic block lengths were cast onto glass slides by spin coating from toluene solution, or by casting from tetrahydrofuran solution. The ionic core sizes in the polymer films are not affected by the solvent or method of casting. CdS-diblock copolymers composite films were then prepared by two methods, which shall be called "dry" and "wet" preparations. In the dry preparation method, the films were dried in a vacuum oven at 130° C for 4 days to remove all traces of water. The dried films of PS-*b*-PACd were then treated with dry hydrogen sulfide (H_2S) for 5 h at 25 °C. After about 15 min, the transparent films turned from colourless to light yellow. The H_2S-treated films were stored overnight in a desiccator under vacuum, to remove excess H_2S. In the wet preparation method, the PS-*b*-PACd films after casting were dried in a vacuum oven at 130 °C overnight to remove any remaining solvent. They were subsequently exposed to an atmosphere of 100% humidity for several days, by storing over water in a closed container at ca. 70 °C. The "wet" ionomer films were then exposed to "wet" H_2S (bubbled through water at 70 °C) for periods of 4 h, 5 h, and 8 h. After 8 h exposure to H_2S, FTIR was used on the treated films to confirm 100% conversion of poly(cadmium acrylate) to poly(acrylic acid). The transparent yellow films of CdS-diblock copolymer composites were then stored overnight in a desiccator under vacuum to remove excess H_2S.

4.3.4. UV-Vis Absorption Spectroscopy

UV-vis absorption spectra of the CdS-diblock copolymer composites (yellow transparent films) were obtained on a Hewlett-Packard 8452 diode array spectrophotometer, by scanning between 250 and 550 nm. A clean glass slide was run as a blank, such that any absorbance from the glass was subtracted from each spectrum. The absorption edge, λ_e, was determined for each spectrum as described in the preceding chapter. For quantum-confined CdS nanoparticles ($2R_{CdS}$ < ca. 60Å), the absorption edge is known to be blue-shifted relative to the bulk material, with smaller particles showing a greater blue shift. Semiconductor particle sizes, $2R_{CdS}(\lambda_e)$, can thus be determined from the absorption edge of the blue-shifted spectra, using the appropriate correlation curve.[36] Along with a characteristic absorption edge, all spectra possessed either a distinct maximum, λ_m, or shoulder, λ_{sh}, and these features were also used to calculate CdS particle sizes ($2R_{CdS}(\lambda_{m,sh})$). Table 4.1 lists relevant spectral features and associated CdS particle sizes for several PS-*b*-PACd ionomers of varying poly(cadmium acrylate) block lengths.

4.3.5. Transmission Electron Microscopy

Electron microscopy was performed on a Phillips EM410 instrument. CdS-diblock copolymer composite films were prepared for electron microscopy by microtoming (microtomed film thickness = ca. 800Å), and the microtomed sample was then mounted on a copper grid.

4.3.6. Preparation of Cadmium Sulfide-Diblock Copolymer Micelles in Solution

CdS-containing micelles in toluene solution were prepared by a method analogous to the preparation of the CdS-diblock copolymer films. PS-*b*-PACd samples in the powder form were exposed to an atmosphere of 100% humidity for a period of 1 week. They were then treated with "wet" H_2S for 8h; during exposure to H_2S, the powders turned from white to yellow, with samples of longer ionic block lengths becoming more intense yellow in colour. To form micelles in solution, the yellow powder was dissolved in toluene; a clear yellow solution was obtained. Alternatively, to reneutralize the poly(acrylic acid) block, the yellow powder was dissolved in tetrahydrofuran, and a selected amount of sodium hydroxide (NaOH) or cadmium acetate dihydrate in methanol solution was added with stirring. The yellow composite was recovered by evaporation of the solvent. A solution of reneutralized CdS-containing micelles was then obtained by dissolving the solid in toluene.

The micelles with and without reneutralization were repeatedly precipitated from toluene into methanol, filtered, dried under vacuum at 70 °C for 4 h, then redissolved in toluene. The solution stability of CdS-block copolymer composites was monitored, by preparing constant weight percent solutions of the yellow powders in toluene after each recovery, and comparing the absorbance and absorption edge of the obtained UV-vis spectra.

Following nanoparticle formation, the microreactors were also "reloaded" with cadmium, in order to increase the semiconductor particle sizes by secondary exposure to H_2S. For this experiment, the CdS-containing micelles of PS(320)-*b*-PAA(14) were reneutralized by stirring with cadmium acetate (1 mol cadmium acetate : 1 mol acrylic acid repeat units) in THF solution for a week. The reneutralized micelles were then recovered by precipitation into methanol, and the powder was dried at 70 °C for at least 4 h. The yellow powder was then exposed to "wet" H_2S for 8 h. The absorption edge of the micelles in toluene solution was determined. This process was repeated by neutralizing with cadmium acetate once again, then exposing the powder to "wet" H_2S for a third time.

4.4. Results and Discussion

4.4.1. Control of CdS Particle Sizes in Diblock Copolymer Films

The absorption spectra of CdS nanoparticles prepared by the "dry" method in the series of ionomers PS(300)-*b*-PACd(x) (x = 4.0, 10, 25, 44) revealed very similar absorption edges, corresponding to a particle size of $2R_{CdS}$ = ca. 21 Å. The CdS absorbance was generally higher for longer ionic block lengths, although this trend was somewhat obscured by slight differences in film thickness. For the dry preparation, it appears that ionic core sizes do not influence the sizes of CdS particles that precipitate within the core; restricted diffusion within the high viscosity PACd core may contribute to the kinetic control of particle growth and a small particle size common to all copolymer compositions. This results in a raspberry morphology, with small (ca. 21 Å) CdS "seeds" dispersed throughout the core. Of course, materials with larger cores will have a greater number of seeds in each core, and therefore a higher concentration of CdS within the composite; this explains the higher absorbance values for CdS prepared in block copolymers with longer ionic blocks, despite marked similarity in the values of the absorption edge.

Table 4.1. UV-vis absorption data and sizes of CdS nanoparticles in block ionomers.

polymer	λ_e (±2 nm)	$2R_{CdS}(\lambda_e)$ (±1 Å)	$\lambda_{m,sh}$ (±2 nm)	$2R_{CdS}(\lambda_{m,sh})$ (±1 Å)	$d_{1/2}$ (Å)	RPI
PS(300)-*b*-PACd(4.0)	421	29	353	20	9	1.05
PS(470)-*b*-PACd(5.0)	421	29	353	20	9	1.05
PS(300)-*b*-PACd(10)	435	32	394	24	8	1.03
PS(320)-*b*-PACd(14)	457	38	421	29	9	1.02
PS(730)-*b*-PACd(22)	469	42	435	31	11	1.03
PS(300)-*b*-PACd(25)	479	47	438	32	15	1.05
PS(470)-*b*-PACd(32)	485	50	459	38	12	1.02
PS(300)-*b*-PACd(44)	485	50	459	38	12	1.02
PS(730)-*b*-PACd(84)	485	50	459	38	12	1.02

In contrast, absorption spectra of quantum-confined CdS particles prepared by the wet method revealed spectral features with a clear dependence on the ionic block length of the host polymer. Figure 4.1 shows a series of spectra of wet-prepared CdS nanoparticles

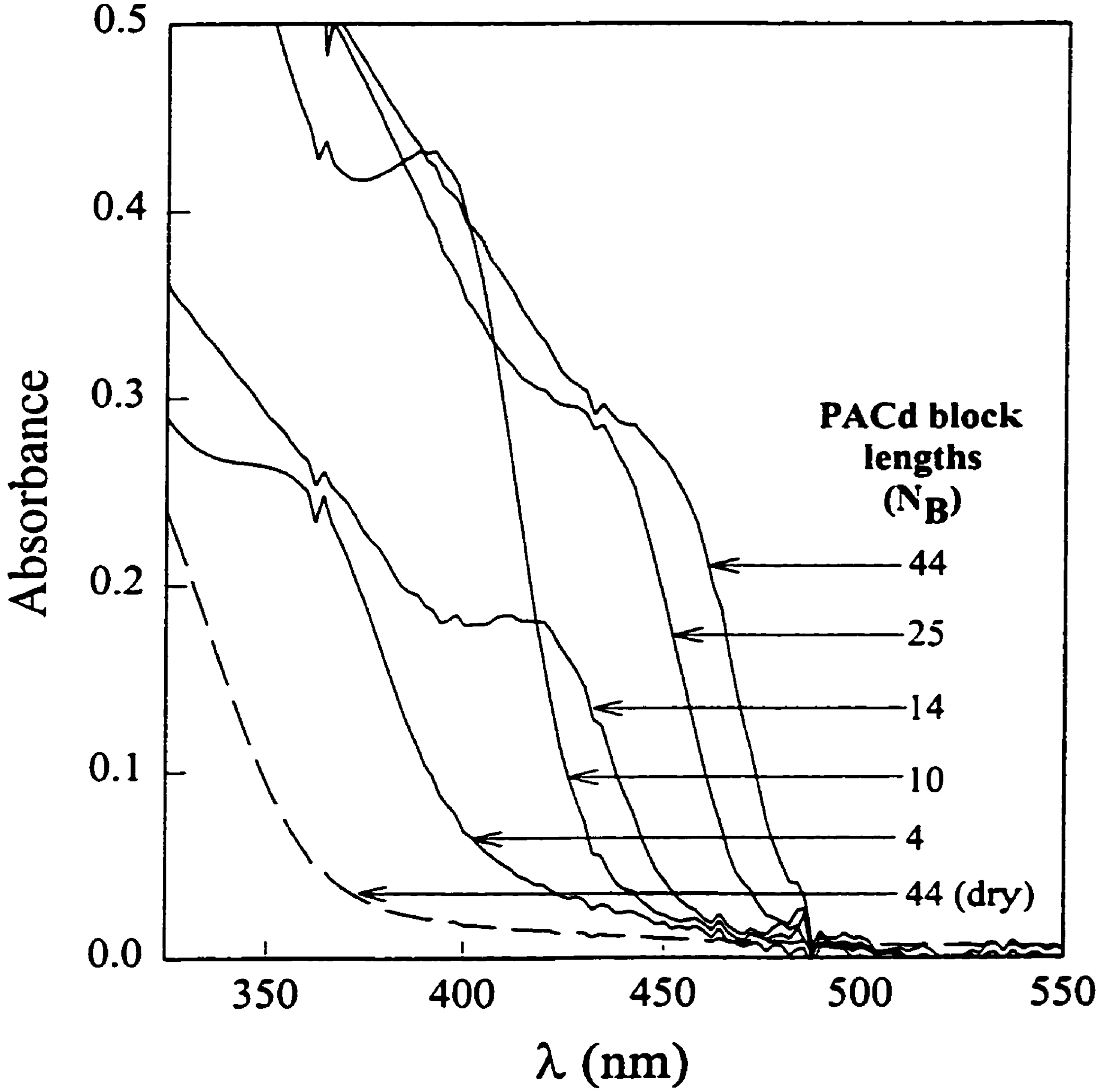

Figure 4.1. Absorbance spectra of CdS in PS-*b*-PAA copolymers with variable poly(acrylic acid) block lengths for wet (solid lines) and dry (dotted line) preparations. All samples were treated with H_2S for 5 h. The baselines have been normalized, such that the vertical axis indicates absorbance above the baseline.

in the diblock copolymers PS(300)-*b*-PAA(x) (x = 4.0, 10, 25, 44) and PS(320)-*b*-PAA(14), along with a spectrum of dry-prepared CdS in PS(300)-*b*-PAA(44). Each spectrum exhibits a distinct exciton shoulder or maximum, which is an indication of relatively narrow size distributions.[37] The "blips" at ca. 360 nm are due to a filter change in the instrument; other irregularities arise from nonuniformities in the films. It is clear from the absorption edges that the wet-prepared CdS particles are larger than the dry-prepared particles, and that the wet-prepared particles show an increase in size with increasing acrylic acid block lengths. This is attributed to plasticization of the cores with water, which decreases the viscosity of the medium in which CdS precipitation occurs.

Two mechanisms of particle formation in the plasticized core can be imagined. In the first case, small seed particles of cadmium sulfide form initially as H_2S diffuses into the ionic core; the mobility within the core then allows these particles to diffuse and associate. In the second case, the increased mobility in the plasticized core results in an increase in the rate of particle growth with respect to the rate of nucleation, restricting nucleation to a single site per core. In both cases, the end result is a cherry morphology, with a single CdS particle in each water-plasticized core. The size of the particles should thus be dependent on the number of cadmium ions in the original ionic core.

The relationship between wet-prepared CdS particle sizes (after treatment with H_2S for 8 h) and original ionic core sizes in the host polymer (before H_2S treatment) is shown in Figure 4.2. CdS particle sizes (Table 4.1) were calculated from λ_e values using Henglein's correlation curve; ionic core diameters were calculated from ionic block lengths, using the scaling relation ($R_{core} = 6.5\ N_B^{3/5}$Å). The validity of this equation for cadmium-neutralized diblock ionomers is suggested by initial SAXS results.[38] Results for polymers with various polystyrene block lengths are plotted on the same graph, as the length of the nonionic block is known to have little influence on the size of the spherical core.[27] As shown in Figure 4.2, CdS nanoparticle diameters increase linearly with the ionic core diameters (slope = 0.31 correlation coefficient, r^2 = 0.99), indicating that the particle sizes are indeed controlled by the sizes of the original ionic aggregates up to a core diameter of ca. 100 Å. CdS nanoparticles prepared in random ionomers[21] are also

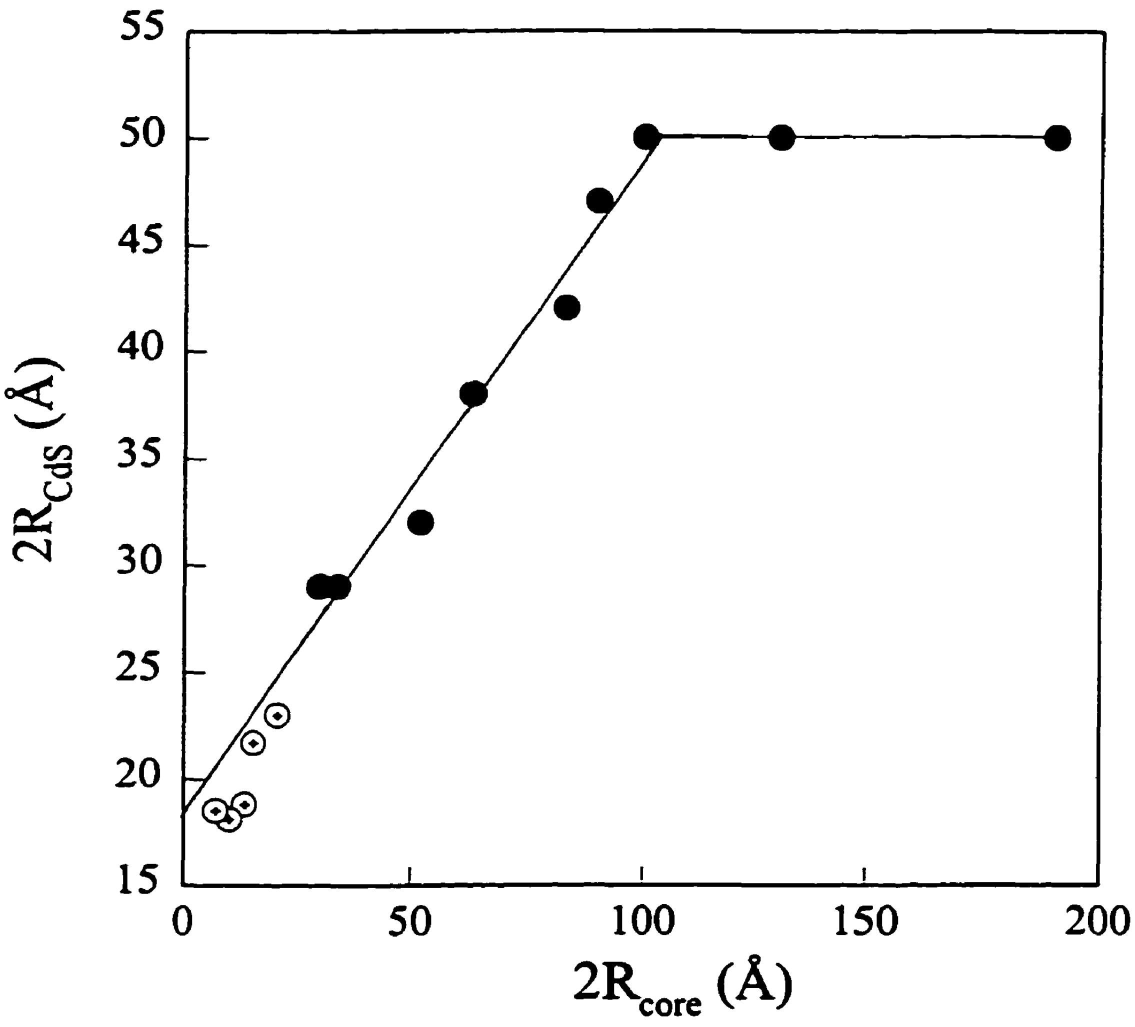

Figure 4.2. Plot of CdS nanoparticle diameters ($2R_{CdS}$) versus the diameter of the original ionic core ($2R_{core}$), calculated from the scaling relation $2R_{core} = 6.5N_B^{3/5}$ Å. Crossed circles represent nanoparticles synthesized in random ionomers. The regression line is through the solid circles (excluding $2R_{core} > 100$ Å), but has been extended manually to include the random ionomer data. The horizontal line is a guide for the eye.

included in Figure 4.2, with particle sizes plotted versus multiplet radii (reported for cesium-neutralized ionomers of variable chain lengths[22]). The linear regression for particles prepared in diblock ionomers (closed circles) is found to pass very close to the random ionomer samples (crossed circles); this suggests that the control of nanoparticle sizes via ionic aggregate sizes in diblock ionomers is an extension of the same type of size control observed in random ionomers. The smaller CdS particle sizes calculated from λ_m or λ_{sh} (Table 4.1) were also plotted against R_{core}, and a linear correlation was found with a correlation coefficient of $r^2 = 0.98$.

For ionic core sizes $2R_{core} > 100$ Å, the size control described above is lost, and the CdS particle size levels off at ca. 50 Å. The observed plateau in Figure 4.2 may be explained in the following way. In very large ionic cores, the diffusion of material through large volumes results in relatively slow rates of particle growth with respect to the rates of nucleation, such that several particles per core are formed. This results in a kinetically-controlled particle size, dependent on the viscosity of the plasticized core, within a raspberry morphology. It should be noted that the CdS spectra in the plateau region are still blue-shifted from the bulk material, which starts to absorb near 515 nm.[37] The two regions of Figure 4.2, therefore, indicate two kinds of size control over quantum-confined CdS particles: up to $2R_{core} = 100$ Å, the sizes of CdS particles are limited by the sizes of ionic aggregates (thermodynamic control, cherry morphology), while for $2R_{core} > 100$ Å, the viscosity within the cores is the limiting factor (kinetic control, raspberry morphology), independent of the sizes of aggregates.

The CdS particle radii (excluding the plateau region of Figure 4.2) were also plotted against the ionic block length, and these points were fitted to the Halperin[27] scaling relation $R \sim N_B^{3/5}$ using the equation $R_{CdS} = aN_B^{3/5} + b$; a and b were found to be 1.9 Å and 9.4 Å, respectively. The fit is shown in Figure 4.3, along with a linear approximation, which does not deviate significantly from the Halperin scaling relation in the region of interest. Unlike the scaling relation for ionic core radii, the equation for R_{CdS} does not pass through the origin. It is noteworthy that the value of the y intercept, $R_{CdS} = 9.4$ Å, which represents a limiting case for block lengths tending to 0 units, corresponds very closely to our previously determined CdS particle diameter in the polystyrene-

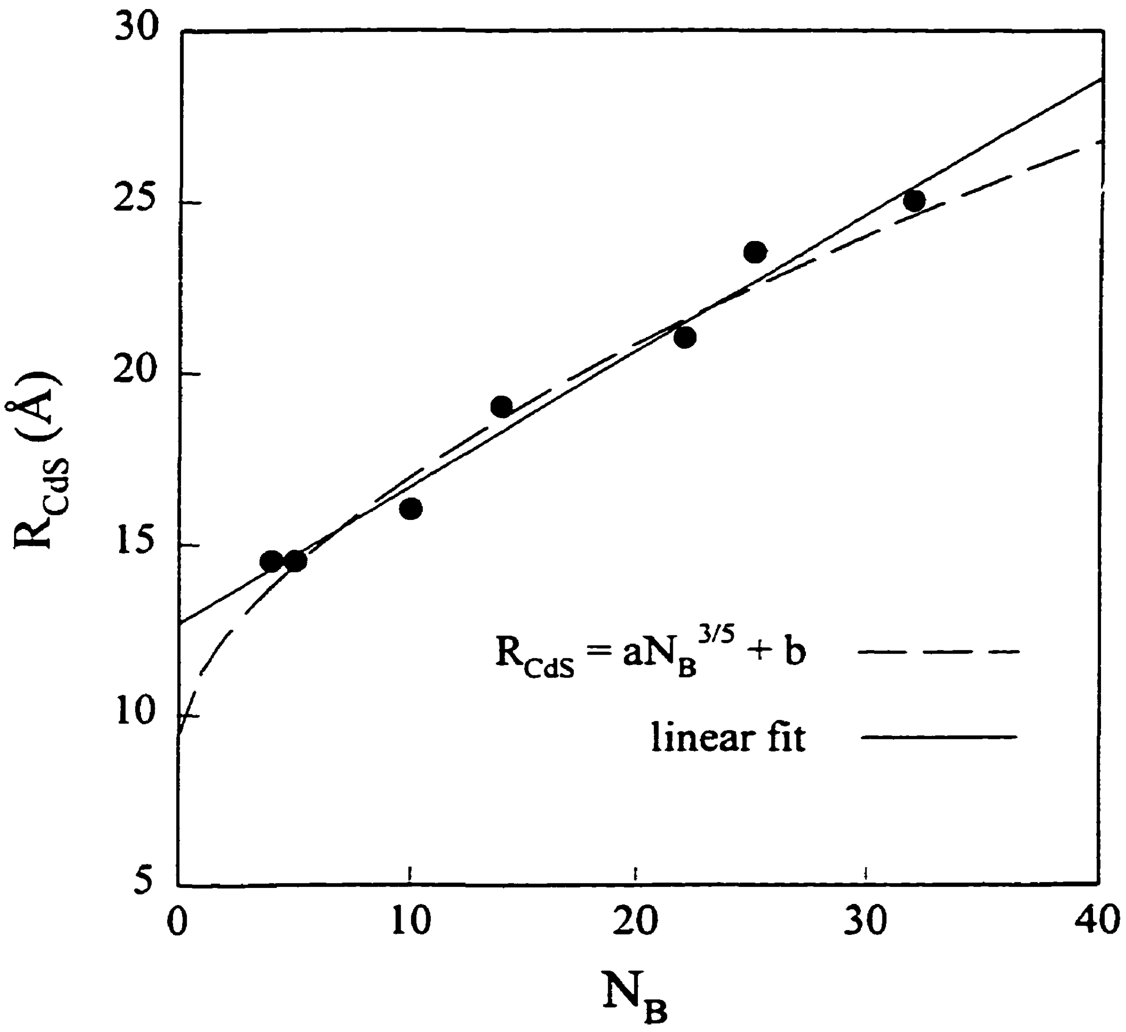

Figure 4.3. Plot of CdS nanoparticle radii (R_{CdS}) versus the number of repeat units in the ionic block (N_B). The dotted line shows the best fit to the $N_B^{3/5}$ relation, with a = 1.9 and b = 9.4 Å. A linear regression through the data is also shown (solid line).

poly(cadmium methacrylate) random ionomer ($2R_{CdS} = 18.5$ Å).[21] This lends further credence to the claim that the size control of CdS particles in block ionomers is an extension of the same type of size control, based on the size of the original ionic aggregate, which has been demonstrated in random ionomers.

Within the region of apparent thermodynamic control (R_{core} = 30-100 Å), it has been assumed that all cadmium ions in the core become incorporated into a single cadmium sulfide particle (cherry morphology). The validity of this assumption can be tested by determining the number of cadmium ions in the ionic core, and comparing this to the number of cadmium ions in the subsequent CdS particle. Assuming spherical cores and nanoparticles, these numbers were calculated using values of R_{core} and R_{CdS}, along with the unit volumes the ionic core material and monomolecular CdS. The volume of a single unit of CdS was calculated from its bulk density and molecular weight to be 50 Å^{3}· There are two possibilities for the unit volume of the ionic core, depending on the binding of countercations following neutralization with cadmium acetate. In the first case, Cd^{2+} cations are each bound to two carboxylate anions, resulting in one counterion shared between two units of acrylate. In the second case, the singly bound Cd(Ac)$^{+}$ cation is invoked, such that there is one counterion for each acrylate unit. The core radius was assumed to be independent of the nature of cadmium binding, as implied by the equation $R_{core} = 6.5N_B^{3/5}$ Å. Quantitative FTIR analysis of the neutralized copolymers showed combinations of doubly and singly bound counterions, with percentages of Cd^{2+} bridging ranging from 100% in PS(300)-*b*-PACd(4.0) to 24% in PS(730)-*b*-PACd(84). In Table 4.2, the two extreme cases have been considered independently, so that the number of cadmium ions within a core containing 100% doubly bound cadmium, n_{Cd}(II), and the number of cadmium ions within a core containing 100 % singly bound cadmium, n_{Cd}(I), are reported separately. The unit volumes of the ionic core material for both cases were calculated approximately, starting from the experimentally-determined density of poly(cesium acrylate) (d = 2.0 g/ml).[39]

Table 4.2 also lists two sets of numbers for the CdS nanoparticles; $n_{CdS}(\lambda_e)$ corresponds to larger particles in the distribution, while $n_{CdS}(\lambda_{m,sh})$ corresponds to particle sizes closer to the mean.[6] For the two shortest block lengths, n_{Cd}(I) and n_{Cd}(II) are in reasonable agreement with $n_{\mathrm{CdS}}(\lambda_{\mathrm{m,sh}})$; for longer block lengths, $n_{\mathrm{Cd}}(\mathrm{I})$ and $n_{\mathrm{Cd}}(\mathrm{II})$ show better agreement with $n_{\mathrm{CdS}}(\lambda_{\mathrm{e}})$. The copolymers PS(300)-*b*-PACd(44) and PS(730)-*b*-PACd(84) result in n_{CdS} values significantly lower than the number of cadmium ions in the original core. This is not a surprising result, if we assume that there are several CdS particles in ionic cores which are >100 Å in diameter, as is suggested by the plateau region observed in Figure 4.2. For other polymers, however, reasonable agreement between the numbers of cadmium ions in the microreactor and the number of CdS units in subsequent nanoparticles suggests that a cherry morphology is obtained.

Table 4.2. Calculated number of cadmium ions in the ionic cores and comparison with the number of ion pairs in subsequent CdS nanoparticles.

polymer	$n_{\mathrm{Cd}}(\mathrm{I})$	$n_{\mathrm{Cd}}(\mathrm{II})$	$n_{\mathrm{CdS}}(\lambda_{\mathrm{e}})$	$n_{\mathrm{CdS}}(\lambda_{\mathrm{m,sh}})$
PS(300)-*b*-PACd(4.0)	56	47	260	84
PS(470)-*b*-PACd(5.0)	82	68	260	84
PS(300)-*b*-PACd(10)	290	240	340	150
PS(320)-*b*-PACd(14)	520	430	580	260
PS(730)-*b*-PACd(22)	1200	990	780	310
PS(300)-*b*-PACd(25)	1500	1300	1100	340
PS(470)-*b*-PACd(32)	2100	1700	1300	580
PS(300)-*b*-PACd(44)	4600	3800	1300	580
PS(730)-*b*-PACd(84)	14000	12000	1300	580

A TEM micrograph of CdS-containing PS(470)-*b*-PAA(32) is shown in Figure 4.4. The dark regions are the CdS nanoparticles, which appear evenly dispersed in the polymer matrix. The particle size measured from the micrograph is ca. 50 Å, confirming the value determined from the UV-vis spectrum. The irregular shape of some of the dark

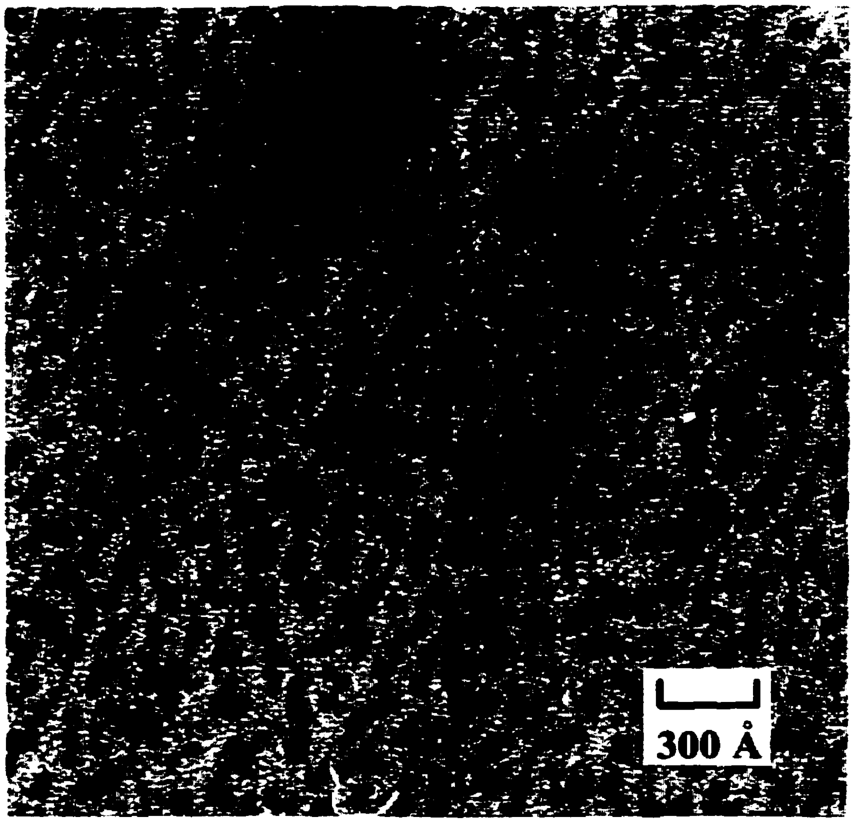

Figure 4.4. Transmission electron micrograph of CdS nanoparticles in PS(470)-*b*-PAA(32). The dark regions are CdS particles dispersed in the polymer.

regions is probably due to overlapping particles in different layers of the microtomed film. A total micelle diameter of 200 Å has been calculated for the solid state, which indicates that the microtomed film (thickness = ca. 800 Å) contains about 4 overlapping monolayers.

4.4.2. Polydispersity of CdS Particle Sizes

In UV-vis studies of quantum confined semiconductors, absorption spectra which exhibit distinct maxima and/or shoulders are generally associated with relatively monodisperse size distributions. A useful measure of the polydispersity of the sample is obtained by calculating $d_{1/2}$,[6] defined as

$$d_{1/2} = 2R_{CdS}(\lambda_e) - 2R_{CdS}(\lambda_{m,sh}) \qquad (1)$$

If a Gaussian distribution of particles is assumed, $d_{1/2}$ can be taken to be twice the standard deviation ($2\sigma_{2R}$), and $2R_{CdS}(\lambda_{m,sh})$ will approximate the mean particle diameter. A radius polydispersity index (RPI) can thus be defined for each distribution:

$$RPI = (\sigma_{2R} / \overline{2R}_{CdS})^2 + 1 \qquad (2)$$

As shown in Table 4.1, RPI values for the CdS particles obtained in block ionomers are low, between 1.02 and 1.05. Very similar polydispersities have been found for the radii of ionic cores in block ionomers, as determined by SAXS.[30] It should be noted that the assumption of a Gaussian distribution may not be entirely realistic, and therefore the RPIs listed in Table 4.1 are only approximate values. In some cases, it is conceivable that the polydispersities of CdS particles would be higher than the polydispersities of the original ionic cores. Such a situation would arise, for example, from slight non-uniformities in the degree of conversion throughout the composite; smaller particles in the distribution could therefore represent incomplete conversion from Cd^{2+} in the core to a single particle of CdS. Incomplete conversion would explain some of the results in Table 4.2; for example, in some cases, the number of CdS units that make up larger particles in the distribution ($n_{CdS}(\lambda_e)$) show the best agreement with ion aggregation numbers in the original core.

4.4.3. Solution Stability and "Fixing" of CdS-Containing Block Copolymer Micelles

Normalized absorbance values (A_{norm}) for CdS-containing micelles of PS(1100)-*b*-PAA(23) in toluene (identical weight percentages) versus the number of sequential recoveries are shown in Figure 4.5. The absorbance was determined at 400 nm, close to the shoulder of the absorption spectrum; the polymer host in toluene shows no absorbance at this wavelength, so that only the absorbance of the CdS nanoparticles was monitored. Absorbance values were normalized by dividing the absorbance after each recovery by the value that was determined prior to the first precipitation of the micelles into methanol. Thus, a normalized absorbance value of 1 is obtained for "0 recoveries" on the horizontal axis. Since micelle solutions of identical weight percentages were prepared after each recovery, a drop in the absorbance of the solution may be interpreted as a drop in the CdS concentration of the composite. A normalized absorbance value of 0.5, for example, indicates (according to Beer's law) a 50% loss of CdS from the micelles.

Three different methods of preparation were used prior to the first precipitation of the micelle solution into methanol. In the first case, the yellow powders were simply dissolved in toluene, without reneutralization of the poly(acrylic acid) block; this resulted in a nearly linear drop in the absorbance (Figure 4.5), with a 60% loss of CdS after 4 recoveries from toluene. It is possible that this loss is due to the presence of a micelle-single chain equilibrium for PS-*b*-PAA in toluene, which results in the partial dissociation of the micelles upon dissolution. The CdS-micelles that were reneutralized by overnight stirring in excess NaOH, however, showed a greatly improved stability with respect to the normalized absorbance. After an initial rise to 1.1 and a subsequent drop to about 0.9, the normalized absorbance was found to plateau, indicating that no further CdS was lost until the seventh recovery. This enhanced stability with respect to the concentration of CdS in the composite may be attributed to the enhanced solution stability of the micelles

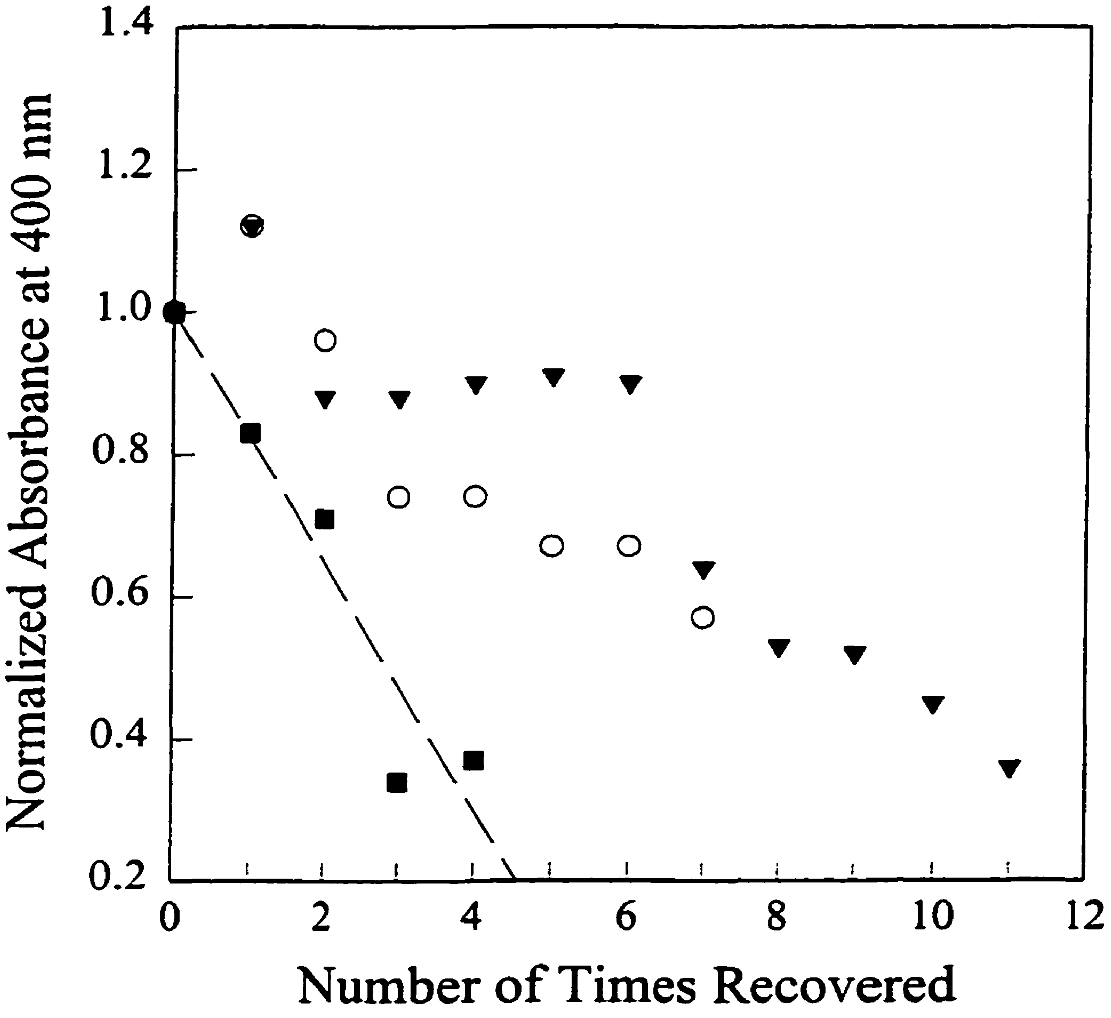

Figure 4.5. Normalized absorbance values for CdS-containing PS(1100)-*b*-PAA(23) micelles in toluene solution plotted versus number of recoveries by precipitation into methanol. Symbols indicate the preparation of micelles prior to the first recovery: (■) no reneutralization, (○) reneutralization with excess NaOH and 15 min. stirring, (▼) reneutralization with excess NaOH and overnight stirring.

following reneutralization; thus, reneutralization of the poly(acrylic acid) block can be said to "fix" the micelles. Since poly(sodium acrylate) has a much lower solubility in toluene than poly(acrylic acid), it is likely that single chains of PS-*b*-PANa have a much lower critical micelle concentration (or cmc) than single chains of PS-*b*-PAA. Considering the kinetics of the system, it is also possible that "fixing" results in an effective freezing of the core, such that the characteristics of the micelle approach those of a stable, non-equilibrium aggregate.

Following the plateau region (Figure 4.5), after 6 recoveries, a clear drop in the normalized absorbance is observed for the sample reneutralized with overnight stirring in NaOH. This observation can be explained by the following chemical reactions, which will partially convert the poly(sodium acrylate) back to poly(acrylic acid) after several precipitations in methanol:

$$\begin{gathered} H_2O + CO_2 \leftrightarrow H_2CO_3 \\ RCOO^-Na^+ + H_2CO_3 \leftrightarrow RCOOH + HCOO^-Na^+ \end{gathered} \qquad (3)$$

As shown in Figure 4.5, an intermediate degree of stability was found for micelles reneutralized by 15 min. stirring with NaOH.

Table 4.3 shows the spectral features for CdS-containing micelles of another polymer, PS(320)-*b*-PAA(14), after sequential recoveries from toluene by the same method. In this case, the reneutralized micelles were prepared by stirring with cadmium acetate (1 mol cadmium acetate : 1 mol acrylic acid repeat units), either overnight or for a period of 1 week. An interesting result is the greater stability of the normalized absorbance (determined at 400 nm) for unneutralized micelles of PS(320)-*b*-PAA(14), compared with unneutralized micelles of PS(1100)-*b*-PAA(23). Unlike the linear drop in absorbance which was observed for the PS(1100)-*b*-PAA(23) composite without reneutralization (Figure 4.5), Table 4.3 shows that the composite of PS(320)-*b*-PAA(14), prepared in an identical manner, suffered only a 3% drop in absorbance after 4 recoveries. This result points to a greater tendency for micelles of PS(1100)-*b*-PAA(23) to dissociate into single chains upon dissolution in toluene. This can be explained by the much longer soluble blocks in the PS(1100)-*b*-PAA(23) copolymer, which increases the solubility of its single chains compared with those of PS(320)-*b*-PAA(14). For both reneutralized micelle preparations of PS(320)-*b*-PAA(14), impressive solution stability is shown by the normalized absorbance values in Table 4.3; up to 10 recoveries into methanol were achieved with only a 25% drop in the CdS absorbance.

Table 4.3. UV-vis absorption data for CdS-containing micelles of PS(320)-*b*-PAA(14), after sequential recoveries from toluene by precipitation into methanol.

number of recoveries	λ_e[a] (nm)	A_{norm}[a]	λ_e[b] (nm)	A_{norm}[b]	λ_e[c] (nm)	A_{norm}[c]
0	449	1.00	452	1.00	456	1.00
1	456	1.10	452	0.99	456	0.98
2	456	1.26	454	0.91	457	0.96
3	453	1.01	454	1.01	457	0.97
4	455	0.97	453	0.92	457	1.09
5	455	0.66	453	0.87	456	0.97
6			454	0.83	458	0.78
7			454	0.85		
8			453	0.80		
9			455	0.77		
10			453	0.75		

[a] No reneutralization. [b] Reneutralized by stirring with excess cadmium acetate overnight.
[c] Reneutralized by stirring with excess cadmium acetate for 1 week.

The slight increase in the absorption edge, λ_e, after the first recovery of the unneutralized composites (from $\lambda_e = 449$ nm to 456 nm) may be attributed to a certain of degree of Ostwald ripening (Table 4.3). The reneutralized materials, on the other hand, show impressive stability in the absorption edge, indicating that the sizes of CdS particles within the micelles do not change, even after repeated precipitation of the composite into methanol. Comparing λ_e values before the first recovery for different methods of micelle preparation, it is found that the absorption edge increases slightly with stirring time in the reneutralizing solution; from this information, it seems that some ripening occurs as the micelles are reneutralized over an extended period of stirring in THF. However, it should be noted that the increase in λ_e from 449 to 456 nm, after 1 week stirring in THF, represents only a 2 Å increase in the CdS particle diameter.

4.4.4. Composite Stability Under Various Methods of Processing

To test the stability of semiconducting nanoparticle sizes under different methods of processing the composite powder, the CdS absorption edge in micelles of PS(300)-*b*-PAA(4.0) was obtained in the following three ways. First, a spectrum was obtained in solution by dissolving the powder in toluene (without reneutralization). Second, a transparent film of the composite was prepared by compression molding the powder at 130 °C (above the T_g of the polystyrene matrix) for 7 minutes. Finally, the CdS-containing micelles were cast from a 10% toluene solution onto a glass slide, and a spectrum of the transparent film was obtained. The absorption spectra for the three preparations are shown in Figure 4.6; despite obvious difference in the quality of the spectra, all three spectra show identical absorption edges, indicating that the nanoparticle sizes are insensitive to various methods of composite processing. This indicates a definite advantage for such composites, which could be cast as films or molded into various devices, without changes in the photo-electrical properties of the material.

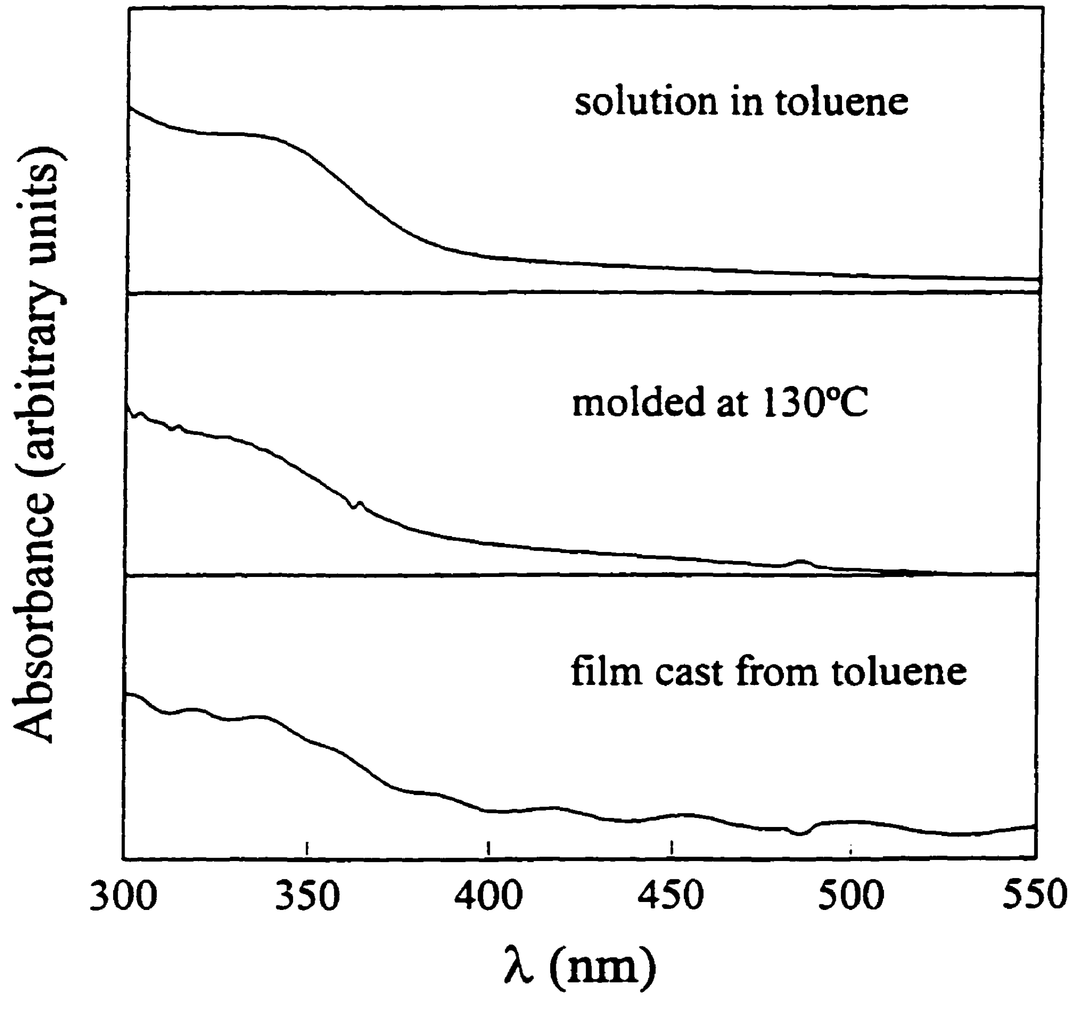

Figure 4.6. UV-vis spectra of CdS nanoparticles in PS(300)-*b*-PAA(4.0), obtained by three different methods of processing the composite.

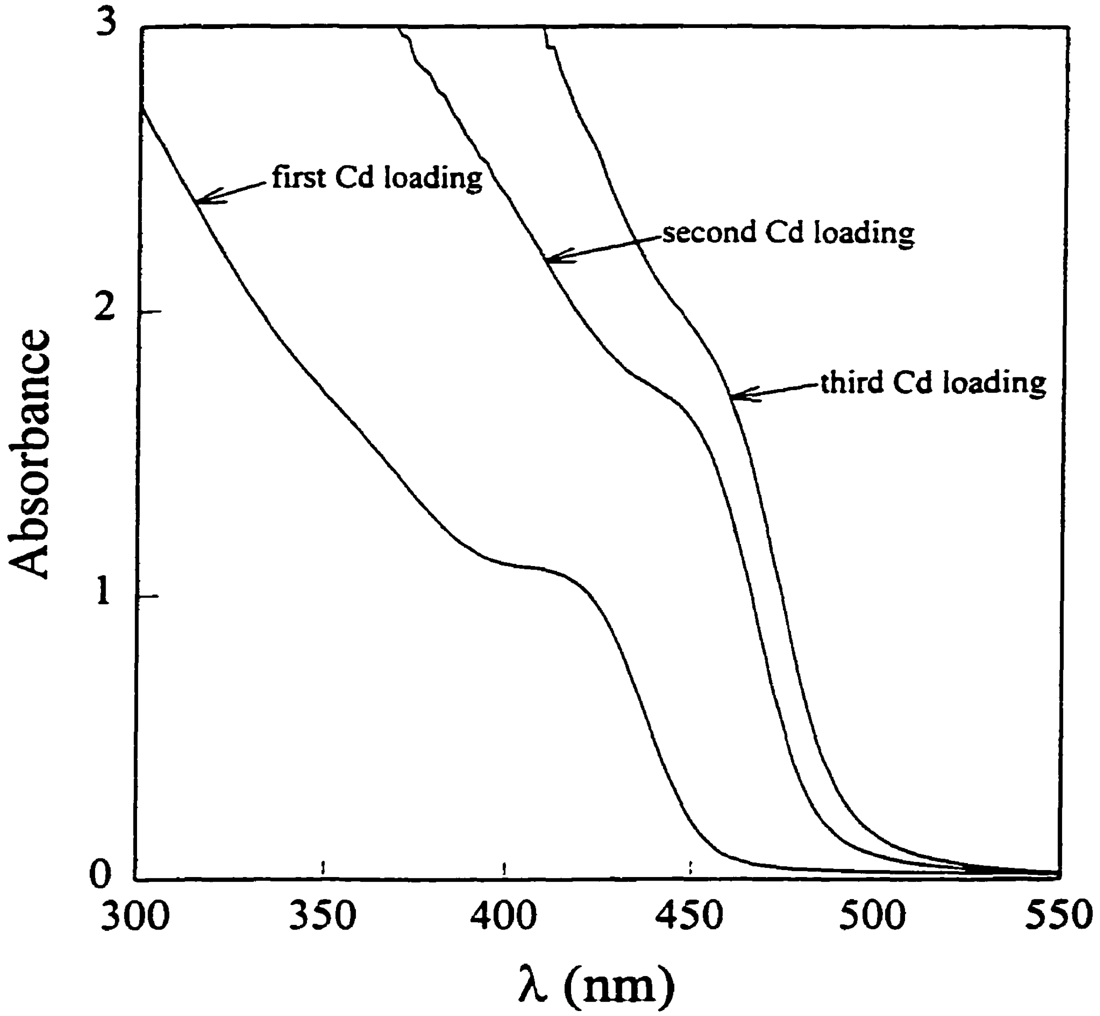

Figure 4.7. Controlled continued growth of CdS nanoparticles in PS(320)-*b*-PAA(14), by successive loadings of the microreactor and reaction with H_2S. The observed red-shift in the absorption spectra with each loading indicates growth of the particle.

4.4.5. Controlled Continued Particle Growth

It was also found possible to "reload" the microreactors with Cd^{2+} ions, by reneutralization of the acetic acid layer with cadmium acetate. This strategy allowed the sizes of nanoparticles to be increased in a controlled manner, as shown in the following schematic:

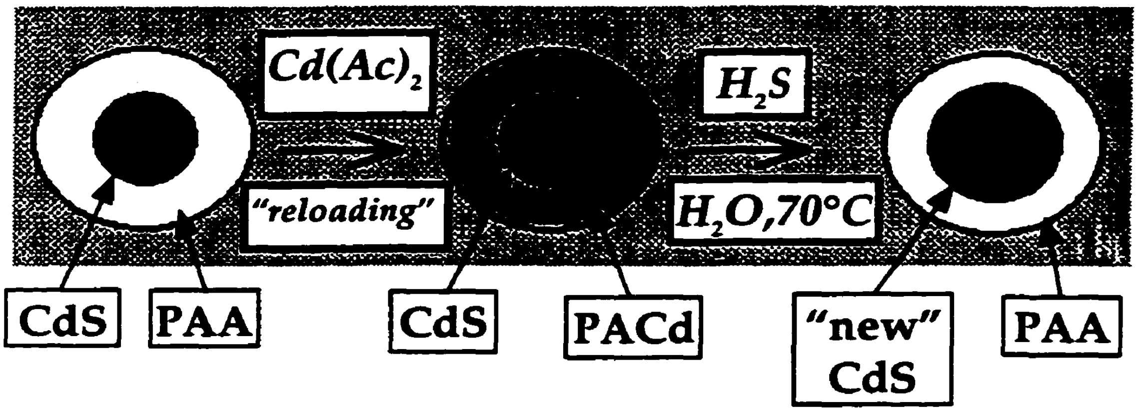

For the CdS-containing PS(320)-*b*-PAA(14) micelles, reneutralization and secondary H_2S treatment resulted in a noticeable increase in the intensity of the yellow colour of the composite powder. Comparison of UV-vis spectra after 1 and 2 loadings of the microreactors showed a red-shift in the absorption edge from 456 nm to 488 nm (Figure 4.7); this corresponds to an increase in the particle diameter from $2R_{CdS}$ = 37 Å to 52 Å, or an increase in the spherical particle volume from V_{CdS} = 27000 $Å^3$ to 74000 $Å^3$. This increase in nanoparticle size is attributed to counterions in the reloaded microreactor being converted to CdS upon treatment with H_2S; the newly-formed CdS deposits on the surface of the original particle, thus increasing its diameter. Since the volume of the particle more than doubled, it is seems that all of the counterions in the reneutralized PACd layer became incorporated into the growing CdS particle; excess cadmium acetate in the core may also have been involved. The next reneutralization/H_2S treatment (third loading) resulted in further growth of the particle to $2R_{CdS}$ = 56 Å (λ_e = 494 nm, Figure 4.6), corresponding to an increase in the particle volume of 18000 $Å^3$. This result suggests that, after the third loading, about 2/3 of the counterions in the microreactor became incorporated into the growing particle. It is possible that the remaining 1/3 of the cadmium ions were converted into small CdS seed particles surrounding the larger particle.

4.5. Conclusions

This work has demonstrated the size control of CdS nanoparticles in the range of $2R_{\mathrm{CdS}}$ = 29-50 Å, within the water-plasticized cores of diblock ionomers. For ionic cores up to 100 Å in diameter, the sizes of quantum-confined CdS particles increased linearly with the sizes of the original cores, while for cores with diameters > 100 Å, a particle size of 50 Å was obtained, independent of the original core size. In completely dry ionic cores, CdS particles of ca. 21 Å were obtained for all ionic block lengths. This size control of CdS nanoparticles through a priori knowledge of primary ionic aggregate sizes is an extension of earlier work in styrene-based random ionomers, in which size control in the range of $2R_{\mathrm{CdS}}$ = 18-23 Å was accomplished.

The solution stability of CdS-containing diblock copolymer micelles has also been shown by repeated precipitation of the micelles into methanol and redissolution of the recovered powder in organic solvent. By "fixing" the micelles (reneutralization of the acid block), the solution stability of the composites was significantly improved. For solutions of "fixed" micelles, numerous sequential recoveries of the composite were performed without significant changes in the CdS nanoparticle sizes, or losses in CdS absorbance. By reneutralizing the CdS-containing micelles with cadmium acetate (reloading the microreactor) and subsequent exposure to H_2S, it was found that the original particle sizes could be increased. By this method, particles up to 56 Å in diameter were obtained, demonstrating the possibility of "secondary" size control for CdS nanoparticles with diameters > 50 Å.

This combination of precise size control, solution and melt stability, and controlled continued growth makes PS-*b*-PAA-based diblock ionomers unique polymer hosts for the formation of quantum-confined CdS-polymer composites, or similar materials containing other types of particles. This system combines the advantages of semiconductor particles evenly dispersed in a polymer matrix with those of particles stabilized in colloidal solution. As well, it should be noted that, unlike other work involving small particles in block copolymers,[16-20] the incorporation of metal ions into the core of PS-*b*-PAA involves simple carboxylate-counterion associations, and does not rely on the coordination of metals to the core-forming blocks. Therefore, metal ions that do not undergo complex formation (e.g. group IA and IIA metals) can also be incorporated into the core by neutralizing the poly(acrylic acid) block with the appropriate reagents. Subsequent chemistry within the core could then be carried out to form a wide range of metallic nanoparticles of predictable sizes and varying composition.

An important question arises from the possibility of incorporating different metal ions into the cores of block ionomers: How does our choice of metal ion affect the sizes of the aggregates? Or, perhaps more importantly: Can reliable scaling relations be determined, in order to control the sizes of aggregates containing different metal ions? The next chapter seeks to answer these questions, for series of starlike block ionomers neutralized with six different metal ions. Although the main thrust of this work is the potential for nanoparticle size control, the chapter concentrates on the characterization of aggregate sizes, rather than the application of microreactors to inorganic particle synthesis.

Acknowledgments

The authors gratefully acknowledge Drs. Mark Andrews and Xing Fu Zhong for helpful discussions. This work was supported by the Natural Sciences and Engineering Research Council of Canada (NSERC). M.M. also acknowledges the financial support of NSERC.

References

(1) Meyer, M.; Wallberg, C.; Kurihara, K.; Fendler, J. H.; *J. Chem. Soc., Chem. Commun.* **1984**, 90.

(2) Lianos, P.; Thomas, J. K. *Chem. Phys. Lett.* **1986**, *125*, 299.

(3) Petit, C.; Lixon, P.; Pileni, M. P. *J. Phys. Chem.* **1990**, *94*, 1598.

(4) Pileni, M. P.; Motte, L.; Petit, C. *Chem. Mater.* **1992**, *4*, 338.

(5) Tricot, Y.-M.; Fendler, J. H. *J. Phys. Chem.* **1986**, *90*, 3369.

(6) Watzke, H. J.; Fendler, J. H. *J. Phys. Chem.* **1987**, *91*, 854.

(7) Wang, Y.; Herron, N. *J. Phys. Chem.* **1987**, *91*, 257.

(8) Krishnan, M.; White, J. R.; Fox, M. A.; Bard, A. J. *J. Am. Chem. Soc.* **1983**, *105*, 7002.

(9) Mau, A. W.- A.; Huang, C. B.; Kakuta, N.; Bard, A. J.; Campion, A.; Fox, M. A.; White, J. M.; Webber, S. E. *J. Am. Chem. Soc.* **1984**, *106*, 6537.

(10) Kuczynski, J. P.; Milosavljevic, B. H.; Thomas, J. K. *J. Phys. Chem.* **1984**, *88*, 980.

(11) Wang, Y.; Mahler, W. *Opt. Commun.* **1987**, *61*, 233.

(12) Hilinski, E. F.; Lucas, P. A.; Wang, Y. *J. Chem. Phys.* **1988**, *89*, 3435.

(13) Wang, Y.; Suna, A.; McHugh, J.; Hilinski, E. F.; Lucas, P. A.; Johnson, R. D. *J. Chem. Phys.* **1990**, *92*, 6927.

(14) Wang, Y., Suna, A.; Mahler, W.; Kasowski, R. *J. Chem. Phys.* **1987**, *87*, 7315.

(15) Mahler, W. *Inorg. Chem.* **1988**, *27*, 435.

(16) Möller, M. *Synth. Met.* **1991**, *41-43*, 1159.

(17) Cummins, C. C.; Schrock, R. R.; Cohen, R. E. *Chem. Mater.* **1992**, *4*, 27.

(18) Yue, J.; Sankaran, V.; Cohen, R. E.; Schrock, R. R. *J. Am. Chem. Soc.* **1993**, *115*, 4409.

(19) Ng Cheong Chan, Y.; Craig, G. S. W.; Schrock, R. R.; Cohen, R. E. *Chem. Mater.* **1992**, *4*, 885.

(20) Ng Cheong Chan, Y.; Schrock, R. R.; Cohen, R. E. *J. Am. Chem. Soc.* **1992**, *114*, 7295.

(21) Moffitt, M.; Eisenberg, A. *Chem. Mater.* **1995**, *7*, 1178.

(22) Moore, R. B.; Bittencourt, D.; Gauthier, M.; Williams, C. E.; Eisenberg, A. *Macromolecules* **1991**, *24*, 1376.

(23) Molau, G. E. In *Block Polymers*, Aggarwal, S. L., ed., Plenum: New York, **1970**, p.79.

(24) Helfand, E.; Wasserman, Z. R.; In *Developments in Block Copolymers*, Goodman, I., ed., Applied Science Publishers: London, **1982**.

(25) Aggarwal, S.L. In *Processing, Structure and Properties of Block Copolymers*, Folkes, M. J., ed., Elsevier: London, **1985**.

(26) Hashimoto, T.; Fujimura, M.; Kawai, H. *Macromolecules* **1980**, *13*, 1660

(27) Halperin, A. *Macromolecules* **1987**, *20*, 2943.

(28) Nguyen, D.; Williams, C. E.; Eisenberg, A. *Macromolecules*, **1994**, *27*, 5086

(29) Steigerwald, M. L.; Alivisatos, A. P.; Gibson, J. M.; Harris, T. D.; Kortan, R.; Muller, A. J.; Thayer, A. M.; Duncan, T. M.; Douglass, D. C.; Brus, L. E. *J. Am. Chem. Soc.***1988**, *110*, 3046.

(30) Fojtik, A.; Weller, H.; Koch, U.; Henglein, A. *Ber. Bunsenges. Phys. Chem.* **1984**, *88*, 969.

(31) Meyer, M.; Wallberg, C.; Kurihara, K.; Fendler, J. H. *J. Chem. Soc., Chem. Commun.* **1984**, 90.

(32) Meissner, D.; Memming, R.; Kastening, B. *Chem. Phys. Lett.* **1983**, *96*, 34.

(33) Desjardins, A.; Eisenberg, A. *Macromolecules* **1991**, *24*, 5779.

(34) Long, T. E.; Allen, R.D.; McGrath, J. E. In *Chemical Reactions On Polymers*; Benham, J. L.; Kinstel, J. F., eds.; ACS Symposium Series364; American Chemical Society: Washington, DC, **1988**; Chapter 19.

(35) Gauthier, S.; Duchesne, D.; Eisenberg, A. *Macromolecules* **1987**, *20*, 753.

(36) Spanhel, L.; Haase, M.; Weller, H.; Henglein, A. *J. Am. Chem. Soc.* **1987**, *109*, 5649.

(37) Henglein, A. *Chem. Rev.* **1989**, *89*, 1861.

(38) Nguyen, D. et al. Results to be published.

(39) Nguyen, D. *PhD thesis* McGill University: Montreal, **1994**.

CHAPTER 5

Scaling Relations and Size Control of Block Ionomer Microreactors Containing Different Metal Ions

5.1. Abstract

Block ionomer micelles of polystyrene-*b*-poly(metal acrylate) containing a wide range of metal ions have been characterized, in order to establish a priori size control for this system of inorganic microreactors. A variety of techniques have been employed, including size exclusion chromatography (SEC), static light scattering (SLS), dynamic light scattering (DLS), and transmission electron microscopy (TEM). Scaling relations for aggregation numbers (Z) and ionic core radii (R_{core}) as a function of the ionic block length (N_B) are determined: $Z \sim N_B^{0.74 \pm 0.08}$; $R_{core} \sim N_B^{0.58 \pm 0.03}$, where the proportionality constants $K_{Z,av}$ and $K_{R,av}$ are dependent on the metal ion, and decrease as $Ni^{2+} > Cs^{+} > Co^{2+} > Ba^{2+} > Cd^{2+} > Pb^{2+}$. For most metal ions, linear plots of R_{core} vs. $N_B^{0.58}$ yield correlation coefficients of r^2 of ca. 0.99, indicating excellent size control of ionic core radii. It is also found that $K_{Z,av}$ decreases linearly with the crystal ionic radius (r_{ion}) for block ionomers neutralized with metal acetates. The role of the metal ion on micelle growth is discussed. Comprehensive scaling laws are also determined to include the soluble block length dependence, and similar exponents are found for most metal ions. DLS results show R_g/R_h values between those of stars and compact spheres. The coronal brush height (H) is found

to scale $H \sim Z^{0.3 \pm 0.1} N_A^{0.9 \pm 0.2}$, in reasonable agreement with the Daoud and Cotton model for starlike systems.

5.2. Introduction

It has been known for some time that block copolymers tend to self-assemble in selective solvents, forming aggregates that are structurally analogous to micelles of associated surfactant molecules.[1-3] The driving force for micellization is generally attributed to microphase precipitation of the insoluble blocks, although the final structure of the micelle is an expression of both enthalpic and entropic factors. When there are relatively small differences between the polymer-solvent interaction parameters of the two blocks (χ_{AS}, χ_{BS}), the micelles exist in the weak segregation limit, with low interfacial tension between the micelle core and the surrounding solvent.

More recently, an increasing amount of attention has focused on the micellization of ionic diblock copolymers, which consist of an ionic block covalently linked to a nonionic block.[4-6] These materials can be classified as polymeric amphiphiles, with large solubility differences between hydrophilic and hydrophobic moieties. Two types of ionic diblock copolymer micelles can be distinguished, depending on the nature of the selective solvent. In aqueous media, ionic diblock copolymers exist as block polyelectrolyte micelles, sometimes referred to as "regular micelles", with hydrophobic cores solubilized by ionic coronae. In organic media, the insolubility of the hydrophilic ionic blocks results in block ionomer (or "reverse") micelles. Compared with their nonionic counterparts, both classes of ionic diblock copolymers are characterized by extremely low critical micelle concentrations (cmcs), indicative of strong driving forces for micellization. The interfacial tension between the cores and the solvent (and between ionic and nonionic blocks) is relatively high, and the micelles exist in the strong or perhaps even superstrong segregation limit.

The present chapter concerns the detailed study of diblock ionomer micelles in organic solvents, specifically micelles of polystyrene-*b*-poly(metal acrylate) ionomers. These aggregates generally consist of block copolymers in which the number of insoluble ionic repeat units (N_B) is very small compared with the number of soluble styrene repeat units ($N_B << N_A$), and fall into the category of "starlike" micelles due to their small, compact cores and large, extended coronae. An interest in these materials has been spurred by the potential applications of poly(metal acrylate) ionic cores as inorganic microreactors of controllable size, in which various metal counterions can be converted via simple chemistry to metallic or semiconducting nanoparticles. The size of the inorganic particles growing in such microreactors will be determined by the aggregation number of the block ionomer; after chemical conversion, the core regions will then protect the particles dispersed in the matrix phase from growth mechanisms such as agglomeration and Ostwald ripening.

In chapter 4, the synthesis of CdS nanoparticles within reverse micelles of polystyrene-*b*-poly(cadmium acrylate) (PS-*b*-PACd) was described.[7] In this work, chemical conversion within inorganic microreactors involved the simple reaction of ion-containing cores with hydrogen sulfide (H_2S). The particle sizes showed excellent correlation with the sizes of the original ionic cores, demonstrating that size control of CdS particles is possible. The CdS-polymer composites were reneutralized with NaOH to increase micelle stability, after which the materials could be repeatedly dissolved in organic solvents and precipitated into methanol, or compression-molded above 100 °C, without the observation of Ostwald ripening or particle agglomeration. The CdS nanoparticles were found to be relatively monodisperse, with radius polydispersity indexes (RPI) of ca. 1.04. Controlled secondary growth of CdS nanoparticles within the micelle cores was also demonstrated, by "reloading" the PAA blocks with cadmium acetate, followed by secondary reaction with H_2S.

Other groups have also employed ion-containing polymers in the synthesis of nanoparticles,[8-12] although clear correlations between the composition of the polymer host and the size of the particles are still rare. In most polymer systems, the strategy for nanoparticle synthesis involves the formation of micelles with metal-complexing insoluble blocks, followed by the incorporation of metal ions into the cores and their subsequent conversion to metals or semiconductors. Block copolymers with such core-forming blocks as poly(2-vinylpyridine),[8] norborene-based polymers,[9,10] poly(4-vinylpyridine),[11] and poly(ethylene oxide)[12] have all been applied to synthesize a wide range of metallic and semiconducting nanoparticles.

In the present work, the preparation of microreactors employs a different approach to the incorporation of metal ions into the micelle cores. To form reverse micelles of polystyrene-*b*-poly(metal acrylate) ionomers, single chains of polystyrene-*b*-poly(acrylic acid) (PS-*b*-PAA) are neutralized with various metal ions, which induces self-assembly of insoluble ionic blocks. In contrast to the methods employed in ref.'s 8-12, micellization and the incorporation of ions into the micelle core do not occur in separate steps; rather, these are simultaneous and mutually dependent processes arising from the neutralization of acid units. Along with the inherent stability of the micelles, it is proposed that the present strategy offers several other advantages over other systems, such as: (1) the controlled introduction of metal ions by acid-base titration, (2) the effective localization of ions within the micelle core, and (3) the wide range of complexing and non-complexing metals that can be incorporated into the core. It is important to note that, since micellization is initiated by the neutralization of the acid block, the effect of the nature of the counterion on self-assembly must be considered, and is of fundamental importance to the quest for a priori size control.

From the point of view of material science, the control of nanoparticle sizes within a polymer matrix is of great interest, as a means of producing composites with specific electronic and optical properties. These properties are largely determined by the sizes of metallic or semiconducting nanoparticles within the matrix, through various quantum-confinement and surface effects.[13,14] Thus, if nanoparticle sizes are controlled by the composition of the matrix, a situation arises in which the properties of a polymer/inorganic composite are easily "tuned" through the selection of an appropriate polymer host. The control of block copolymer composition can be achieved by well-established techniques of sequential anionic polymerization. However, in order to establish relationships between the composition of the block copolymer and the ultimate sizes of the guest nanoparticles, two conditions must be met. First, a priori knowledge of micelle aggregation numbers as a function of soluble and insoluble block lengths should be obtained for the system of interest. Second, the complete conversion of ions to a single particle in each core should be achieved, such that the size of the particles and the micelle aggregation number are closely correlated. Single particles in the cores of block copolymer micelles are described in the literature, and are generally formed by heating[10,12] or placticizing[7] the ion-containing microdomains. In the field of material science, however, little attention has been given to the first of these conditions.

This work continues earlier investigations of polystyrene-*b*-poly(methacrylic acid) (PS-*b*-PMAA) and PS-*b*-PAA-based block ionomers, in which cesium and sodium were the counterions of the neutralized acid block.[15-17] In these systems, gel-permeation chromatography, viscometry, dynamic and static light scattering, transmission electron microscopy, and small-angle x-ray scattering were used to probe micelle aggregation numbers and ionic core sizes as a function of block lengths. Here, a wider range of counterions from across the periodic table are used, in order to establish scaling relationships between block copolymer composition and micelle aggregation numbers for a variety of potential inorganic microreactors. Simple reduction chemistry within one type of microreactor is also demonstrated, through the production of Pb^0 particles in the cores of Pb^{2+} block ionomer micelles. Along with such applications to material science, this investigation is also of interest on a more fundamental level, as it is the first detailed study of block ionomer micellization as a function of counterion.

5.3. Experimental

5.3.1. Synthesis of PS-b-PAA Diblock Copolymers

The diblock copolymers used in the present study (Table 5.1) were synthesized by known procedures;[15,18,19] therefore, only a brief summary is presented here. In the table, $x = N_A$, and $y = N_B$.

Table 5.1. Molecular characteristics of polystyrene-*b*-poly(acrylic acid) copolymers.

PS(x)-*b*-PAA(y)	mol % PAA	M_n (g mol^{-1})	P.I.
370-*b*-3	0.8	38800	1.04
370-*b*-7	1.9	39000	1.04
370-*b*-11	2.9	39300	1.04
370-*b*-15	3.9	39600	1.04
370-*b*-19	4.9	39900	1.04
370-*b*-26	6.6	40400	1.06
730-*b*-84	10.3	82100	1.08
300-*b*-44	12.8	34600	1.05

Sequential anionic polymerization was used to prepare series of polystyrene-*b*-poly(*tert*-butylacrylate) (PS-*b*-PtbA) with polystyrene blocks of constant length and poly(*tert*-butylacrylate) blocks of variable length. In this procedure, the styrene monomer is polymerized first, then a precise amount of the second monomer is added to the solution of "living" polymer chains. A sample of block copolymer is extracted from the flask, followed by the next addition of the second monomer. Thus, six samples of diblock copolymers with identical polystyrene blocks of 370 units and six different PtbA block lengths, ranging from 3 to 26 repeat units, were prepared in a single synthetic run. The other two diblock copolymers used in this study, PS(300)-*b*-PtbA(44), and PS(730)-*b*-PtbA(84), were individual samples from two independent series.

For all series of diblock copolymers, anionic polymerization in tetrahydrofuran (THF) was initiated by *sec*-butyllithium capped with a few units of α-methylstyrene. The molecular weights of the polystyrene blocks, and the polydispersity indexes of each block copolymer, were determined by size-exclusion chromatography (SEC) in THF. As shown in Table 5.1, all block copolymers used in the present study had polydispersity indexes between 1.04 and 1.08. The length of the *tert*-butylacrylate blocks were determined by quantitative Fourier-transform infrared spectroscopy (FTIR) of samples dissolved in carbon tetrachloride. Block copolymers in the ester form were then hydrolyzed, by refluxing overnight in toluene with small amounts of *p*-toluenesulfonic acid catalyst. The polymers in the acid form were precipitated into methanol, then dried in a vacuum oven at 70 °C for at least 24 h. A few samples showed incomplete hydrolysis, and these were subsequently hydrolyzed to completion by dissolving the polymers in an 80/20 mixture of toluene/acetic acid (v/v) and refluxing for 2 h with methanesulfonic acid catalyst.[20]

5.3.2. Preparation of Block Ionomer Micelles

Block copolymers in the acid form were dissolved in benzene/methanol (10% methanol v/v) to obtain solutions of 2% polymer (w/w). To form micelles containing Cs^+, Ba^{2+}, Cd^{2+}, Pb^{2+}, Ni^{2+}, and Co^{2+}, single chains of PS-*b*-PAA were neutralized by the addition of methanolic solutions (0.10 or 0.25 M) of cesium hydroxide monohydrate ($Cs(OH)\cdot H_2O$), barium hydroxide octahydrate ($Ba(OH)_2\cdot 8H_2O$), cadmium acetate dihydrate ($Cd(Ac)_2\cdot 2H_2O$), lead acetate trihydrate ($Pb(Ac)_2\cdot 3H_2O$), nickel acetate tetrahydrate ($Ni(Ac)_2\cdot 4H_2O$), and cobalt acetate tetrahydrate ($Co(Ac)_2\cdot 4H_2O$), respectively.

For the neutralization of PS-*b*-PAA with $Cs(OH)\cdot H_2O$, a stoichiometric quantity of neutralizing agent was added. Neutralizing agents with divalent cations were added in excess (R = moles of neutralizing reagent / moles of acrylic acid repeat units), such that $R = 1.5$. It should be noted that, in the case of divalent counterions, this represents an excess of 3 equivalents (i.e. moles of acetate or hydroxide ions) per mole of acrylic acid units.

After addition of the neutralizing agent, all solutions were stirred for at least 1 h. Neutralized block ionomers (reverse micelles) were recovered by freeze-drying, then dried under vacuum at 70 °C to remove remaining solvent and acetic acid. Excess metal acetate or metal hydroxide was removed by repeated washings of the micelles in methanol, and the washed polymers were dried overnight under vacuum at 70 °C. FTIR spectra confirmed that the ionomers were 100% neutralized.

5.3.3. Size-Exclusion Chromatography of Block Ionomers

Size-exclusion chromatography (SEC) measurements of the reverse micelles were performed using a Varian Model 5000 liquid chromatograph equipped with a refractive index detector. The data were collected and analyzed on a Varian DS-604 computer with appropriate SEC software. After freeze drying and washing of the neutralized samples, small amounts of block ionomer were dissolved in THF. These solutions were filtered through membrane filters with a nominal pore size of 0.45 μm, then diluted to a concentration of about 2 g/L before injection into the SEC columns. Chromatograms generally showed two peaks at high and low elution volumes, attributed to single chains and micelles, respectively. The weight percentage of micellized chains was calculated from the relative areas under the two peaks. The error on the values, determined from three repeat measurements, was typically ca. 1%.

5.3.4. Static Light Scattering

Static light scattering (SLS) experiments were performed on a Dawn-F multi-angle laser photometer (Wyatt Technology) fitted with a He-Ne laser (632.8 nm). Data acquisition and Zimm plot processing utilized DawnF and Aurora (Wyatt) software, respectively. Stock solutions of block ionomers were prepared by dissolving the neutralized polymers in toluene. To eliminate dust from all samples, stock solutions were filtered twice through membrane filters with a nominal pore size of 0.45 μm, transferred to a dust-free scintillation vial, then diluted with filtered solvent. After each set of five repeat measurements, the micelle solutions were diluted with a known quantity of filtered toluene and allowed to sit for 10 minutes. Measurements were obtained at five different concentrations, in the range of 2.0 - 0.1 mg/mL. The exact range of concentrations for each sample depended on the molecular weight of the reverse micelles, and was selected such that reasonable scattered intensity was obtained without saturation of the detectors.

5.3.5. Dynamic Light Scattering

Dynamic light scattering (DLS) experiments were performed on a Brookhaven Instruments photon correlation spectrometer equipped with a BI-2030 digital correlator and a He-Ne laser (632.8 nm) from Spectra Physics. The angle of detection was varied between 50 and 145° using a goniometer apparatus. All measurements were made at 25 °C over a range of concentrations and detection angles. Five repeat measurements of $\Gamma(s^{-1})$ (the relaxation rate of the autocorrelation function, $g_1(\tau)$) were made at each angle and concentration and average values were taken.

To ensure that DLS measurements were not affected by dust, all glassware was rinsed, first with filtered reagent-grade acetone then with acetone condensed from the vapour. Stock solutions of selected block ionomers in toluene were prepared, and these were filtered through membrane filters with a nominal pore size of 0.45 μm. Successive dilutions of sample solutions were performed by the addition of known quantities of toluene, filtered through 0.20 μm membrane filters.

5.3.6. Transmission Electron Microscopy

Transmission Electron Microscopy (TEM) was performed on a Phillips EM410 instrument. Solid-state block ionomers were prepared by casting solutions of reverse micelles from THF, followed by the evaporation of solvent. The films were then microtomed to a thickness of ca. 800 Å and mounted on a copper grid. Of the ionomers prepared in the present study, those containing metal ions with the highest atomic numbers (Pb^{2+}, Cs^{+}, Ba^{2+}, and Cd^{2+}) were investigated by TEM, in order to obtain adequate contrast of electron density from ions within the polymer.

5.4. Results and Discussion

The following Results and Discussion section is divided into four parts. In section 5.4.1, size-exclusion chromatography (SEC) and static light scattering (SLS) results are described, including the calculation of aggregation numbers and ionic core radii for a wide range of block ionomers. The determination of scaling relations for micellar parameters as a function of ionic and nonionic block lengths is then discussed in section 5.4.2. Scaling relations for block ionomers containing different metal ions are compared, and speculation upon the role of the counterion in micellar growth is made. Section 5.4.3 pertains to dynamic light scattering (DLS) results; the hydrodynamic behaviour of block ionomers is discussed, especially in connection with its relevance to micellar structure. Finally, in section 5.4.4, transmission electron micrographs (TEM) of selected block ionomers containing different metal ions are considered, including one in which Pb^{2+} ions have been partially converted into metal particles.

5.4.1. SEC and SLS of Block Ionomers

5.4.1.1. Basic SLS Theory

If colloidal particles are of sufficient size (>λ/20), they are found to scatter light according to the following relation:[21]

$$\frac{Kc}{R(\theta)} = \frac{1}{P(\theta)M_w} + 2A_2c \qquad (1)$$

where $R(\theta)$ is the Rayleigh ratio at the angle of measurement, $P(\theta)$ is the particle scattering function, M_w is the weight-average molecular weight of the particle, and A_2 is the second virial coefficient. The optical constant, K, is defined:

$$K = 4\pi^2(n\ dn/dc)^2/\lambda_0^4 N_A \qquad (2)$$

where n is the refractive index of the particle, dn/dc is the specific refractive index increment at constant chemical potential, N_A is Avogadro's number, and λ_0 is the wavelength of scattered light in a vacuum.

For SLS of block copolymer micelles, dn/dc is a function of the refractive indexes of both blocks; Zimm plot analysis yields an apparent molecular weight, $M_{w,app}$, which must be adjusted according to the chemical heterogeneity of the block copolymer to determine a true molecular weight.[22,23] However, for block ionomer micelles of the type studied in the present work, it has been found that dn/dc is identical to that of polystyrene in the appropriate solvent, such that $M_{w,app}$ is close to the true value of M_w.[24] In eq 2, the specific refractive index increment for polystyrene in toluene, $dn/dc = 0.11$, was therefore used to calculate K for all reverse micelles in this work. The low weight fraction of the ionic block and the compact nature of the small micelle core are both factors which make the chemical heterogeneity negligible in these materials.

5.4.1.2. SEC and SLS Results

The weight fraction of micelles, f_{mic}, was determined for each sample using SEC chromatography, from the relative areas of the micelle and single chain peaks; these values are listed in Table 5.2. In block ionomers, which do not exhibit significant dissociation-association equilibria on a reasonable time scale, the single chain fraction is attributed to a mixture of homopolymer and diblocks with ionic segments that are too short to self-assemble.[15] For the shortest ionic blocks ($y = 3$ repeat units), f_{mic} values are found to be lowest in the Cd^{2+} ($f_{mic} = 0.04$) and Pb^{2+} ($f_{mic} = 0.08$) ionomers, indicating higher single-chain solubility and weaker ionic interactions for these two counterions. Ionomers neutralized with Cs^+ exhibit an intermediate micelle fraction for the shortest ionic block ($f_{mic} = 0.13$), while Ba^{2+}, Ni^{2+}, and Co^{2+} ionomers show the lowest solubility ($f_{mic} = 0.37 \pm 0.02$). For all counterions, single-chain solubility is found to decrease dramatically when $y > 3$, as evinced by a marked increase in f_{mic}.

Table 5.2. Characteristics of block ionomer micelles from SEC and SLS data.

polymer composition	Type of Metal Ion								
	Cs			Ba			Cd		
PS(*x*)-*b*-PAA(*y*)	f_{mic}	$M_{w,tot} \times 10^{-6}$ (g mol^{-1})	$M_{w,mic} \times 10^{-6}$ (g mol^{-1})	f_{mic}	$M_{w,tot} \times 10^{-6}$ (g mol^{-1})	$M_{w,mic} \times 10^{-6}$ (g mol^{-1})	f_{mic}	$M_{w,tot} \times 10^{-6}$ (g mol^{-1})	$M_{w,mic} \times 10^{-6}$ (g mol^{-1})
370-*b*-3	0.13	0.68	5.0	0.35	0.81	2.2	0.04	0.26	6
370-*b*-7	0.74	1.28	1.72	0.80	1.2	1.5	0.72	0.94	1.29
370-*b*-11	0.86	2.04	2.37	0.87	1.65	1.89	0.85	1.9	2.2
370-*b*-15	0.89	2.95	3.3	0.89	1.90	2.13	0.89	1.59	1.78
370-*b*-19	0.90	3.35	3.7	0.90	2.55	2.83	0.91	2.01	2.20
370-*b*-26	0.91	3.99	4.38	0.90	3.95	4.38	0.90	3.7	4.1
730-*b*-84	0.75	12.4	16.5	0.73	10.7	14.6	0.77	9.7	12.6
300-*b*-44	0.87	8.08	9.3	0.72	13.3	18.5	0.88	11.0	12.5
	Pb			Ni			Co		
PS(*x*)-*b*-PAA(*y*)	f_{mic}	$M_{w,tot} \times 10^{-6}$ (g mol^{-1})	$M_{w,mic} \times 10^{-6}$ (g mol^{-1})	f_{mic}	$M_{w,tot} \times 10^{-6}$ (g mol^{-1})	$M_{w,mic} \times 10^{-6}$ (g mol^{-1})	f_{mic}	$M_{w,tot} \times 10^{-6}$ (g mol^{-1})	$M_{w,mic} \times 10^{-6}$ (g mol^{-1})
370-*b*-3	0.08	0.29	3.1	0.39	0.41	0.98	0.36	0.27	0.68
370-*b*-7	0.74	0.62	0.82	0.83	1.07	1.28	0.83	1.00	1.20
370-*b*-11	0.85	1.43	1.68	0.88	2.20	2.49	0.87	1.35	1.55
370-*b*-15	0.89	1.31	1.47	0.89	2.64	2.96	0.89	2.25	2.52
370-*b*-19	0.90			0.91	3.85	4.23	0.90	3.48	3.86
370-*b*-26	0.92	2.23	2.42	0.91	4.22	4.63	0.91	4.3	4.7
730-*b*-84	0.78	8.69	11.1	0.77	13.5	17.5	0.76	18.3	24.1
300-*b*-44	0.88	5.47	6.21	0.84	11.0	13.1	0.85	29	34

From Zimm plot analysis,[21] the total molecular weights of block ionomers in toluene, $M_{w,tot}$, were determined (Table 5.2). Since there are both single chain and micellar fractions present in solution, $M_{w,tot}$ is a weighted average of these two components:

$$M_{w,tot} = f_{mic}M_{w,mic} + f_{sc}M_{w,sc} \tag{3}$$

where f_{mic} and $M_{w,mic}$ are the weight fraction and molecular weight of micelles in solution, and f_{sc} and $M_{w,sc}$ are the weight fraction and molecular weight of the single chains.

With values of f_{mic} determined from SEC, and $M_{w,tot}$ from SLS measurements, the micellar molecular weights, $M_{w,mic}$, were calculated using eq 3 and are listed in Table 5.2. For these calculations, the average molecular weight of the single chains, $M_{w,sc}$, was assumed to be equal to that of the polystyrene block.

Aggregation numbers were calculated from values of $M_{w,mic}$, and the molecular weights of unimers making up the micelles. In general, the molecular weights of micellized chains depend on the final chemical state of the insoluble block, i.e. the percentage of "bridged" counterions in the micelle core. In the case of neutralization with metal acetates, two equilibria for counterion binding are possible:

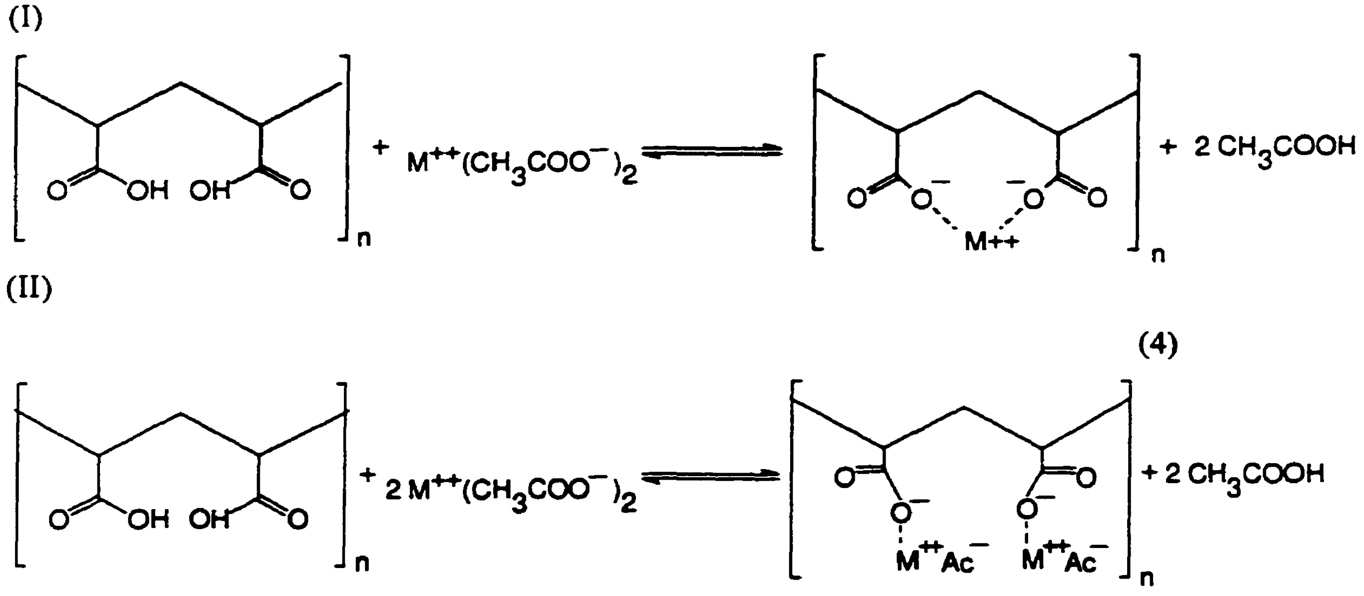

For any PAA block neutralized with metal acetate, a mixture of I and II is the most probable state,[7] though for the purpose of comparison it is generally assumed that one of these two equilibria is dominant. In the cases of Ba^{2+} and Cs^{+}, which were introduced in the form of metal hydroxides, these chemical equilibria are not operative, and all counterions are either bridged or unbridged, depending on the ionic valence.

It should be noted that, since the ionic content in these block ionomers is very low, the molecular weight of the micellized chains is only weakly dependent on the extent of counterion bridging. Even for samples with the highest ionic content, aggregation numbers of 100%-bridged and 100%-unbridged micelles differ by only 10%; for most samples, the differences are much smaller. For the sake of simplicity, therefore, aggregation numbers for block ionomers containing all bridged divalent counterions are reported (Table 5.3). Aggregation numbers for each counterion show a general increase with ionic block length, though exceptions are found for the shortest ionic blocks. The diblock PS(370)-*b*-PAA(3), neutralized with Cs^{+}, Ba^{2+}, Cd^{2+}, and Pb^{2+} gave anomalously large aggregation numbers, indicating the possibility of supermicellar agglomeration or nonspherical aggregate formation. Large aggregation numbers for extremely short ionic block lengths were observed previously in block ionomers containing univalent ions.[24] The four anomalous samples were omitted from all scaling analyses.

Table 5.3. Aggregation numbers of block ionomer micelles containing different metal ions.

polymer composition	Type of Metal Ion					
PS(*x*)-*b*-PAA(*y*)	Cs^{+}	Ba^{2+}	Cd^{2+}	Pb^{2+}	Ni^{2+}	Co^{2+}
370-*b*-3	127	58	140	80	25	18
370-*b*-7	43	38	33	21	33	31
370-*b*-11	58	47	56	41	63	39
370-*b*-15	80	52	44	36	74	63
370-*b*-19	88	69	54		105	95
370-*b*-26	100	104	98	56	113	115
730-*b*-84	177	167	145	123	207	285
300-*b*-44	230	490	340	159	360	950

The aggregation number, Z, is related to the total volume of the micelle core by $V_{\mathrm{core}} = ZN_{\mathrm{B}}v$, where N_{B} is the number of units in the insoluble block and v is the volume of a single repeat unit. The radius of a spherical ionic core can then be calculated:

$$R_{core} = \sqrt[3]{\frac{3V_{core}}{4\pi}} \tag{5}$$

To determine v, the density of metal acrylate cores were calculated from the known value for cesium acrylate (d = 2 g/mL),[25] assuming that core and bulk densities were identical; considering the extremely high interfacial tension between soluble and insoluble blocks,[26] solvent-swelling in the core is very unlikely, and this assumption is believed to be valid. A more problematic question, however, is that of bridged or unbridged counterions; the volume per repeat unit in the bridged and unbridged cases are quite different and, consequently, the core radii will also be different for a given aggregation number. Although FTIR has allowed for qualitative comparisons of the extent of counterion bridging for different methods of preparation, this is not considered to be a quantitative technique; future experiments will therefore involve more precise elemental analysis of our block ionomers. For the time being, two sets of ionic core radii are reported for all samples prepared using metal acetates (Table 5.4): one for the case of 100%-bridged counterions, $R_{\mathrm{M}^{2+}}$, and another for the case of 100%-unbridged counterions, $R_{\mathrm{M(Ac)}^{+}}$. It should be noted that the true chemical state of the core material, and the true core radius, should lie somewhere between these extreme cases; however, given the appropriate assumptions with regard to the chemical state of the core, the "extreme" radii can be calculated to up to three significant figures, which makes them more useful quantities for the purpose of scaling analysis.

Table 5.4. Ionic core radii (Å) of block ionomer micelles containing different metal ions.

polymer composition PS(x)-b-PAA(y)	Type of Metal Ion Cs	Ba	Cd		Pb		Ni		Co	
	R_{Cs^+}	$R_{Ba^{2+}}$	$R_{Cd(Ac)^+}$	$R_{Cd^{2+}}$	$R_{Pb(Ac)^+}$	$R_{Pb^{2+}}$	$R_{Ni(Ac)^+}$	$R_{Ni^{2+}}$	$R_{Co(Ac)^+}$	$R_{Co^{2+}}$
370-*b*-3	24.9	18.6	29	25	24.3	20.7	16.4	14.0	14.5	12.4
370-*b*-7	23.0	21	23.8	20.2	20.4	17.5	23.6	20.2	23.1	19.7
370-*b*-11	29.5	26.8	33.0	28.1	29.7	25.6	34.1	29.2	29.1	24.9
370-*b*-15	36.4	30.8	33.7	28.8	31.2	27.0	39.8	34.2	37.7	32.4
370-*b*-19	40.7	36.4	38.8	33.3			48.2	41.5	46.8	40.3
370-*b*-26	47.2	46.4	52.3	45.1	43.1	37.7	54.6	47.3	55.0	47.6
730-*b*-84	84.4	80	87.0	76.0	81.4	72.4	98.0	85.6	109	95.2
300-*b*-44	74.2	93	92	81	70.8	63.6	95	83	130	115

5.4.2. Dependence of Micellar Parameters on Insoluble and Soluble Block Lengths

Both theoretical and empirical methods have been used to determine relationships between micellar parameters and block lengths. In the theoretical approach,[27-31] expressions for the total free energy of the micelle, including terms pertaining to the core, the coronae, and the core/coronae interface, are minimized with respect to such variables as aggregation number and core radius, in order to determine the dependence of these variables on characteristics of the block copolymer. Empirical studies, on the other hand, involve the determination of micellar characteristics for several block copolymer compositions, followed by the selection of scaling laws that best fit the data.[32] The latter approach is the focus of the present study, along with the additional goal of investigating the relationship between scaling laws and the metal ions in the core.

In their general form, scaling laws for the aggregation numbers and core radii of block copolymer micelles can be written

$$\begin{aligned} Z &\sim N_B^{\alpha} N_A^{-\beta} \\ R_{core} &\sim N_B^{\kappa} N_A^{-\gamma} \end{aligned} \qquad (6)$$

This trend, where aggregation numbers and core radii increase with the insoluble block length and decrease with the soluble block length, is predicted by theory and corroborated by experimental evidence in a wide range of systems. The values of the exponents vary from system to system, depending on such factors as the chemical nature of the blocks, the type of solvent, and the relative block lengths.

This analysis of scaling behaviour begins with the six block copolymers that constitute the series PS(370)-*b*-PAA(*y*), in order to determine the scaling of aggregation numbers and ionic radii as a function of the insoluble block length (section 5.4.2.1). The values of the exponents and the proportionality constants are compared for different neutralizing ions. The contribution of the soluble block length to scaling behaviour is then estimated, using aggregation numbers and ionic core radii for all eight block copolymer compositions (section 5.4.2.2).

5.4.2.1. Insoluble Block Length Dependence

From the scaling relations in eq 6, the following equations are obtained when the length of the soluble block is a constant:

$$\begin{aligned} Z &= K_Z N_B^{\alpha} \\ R_{core} &= K_R N_B^{\kappa} \end{aligned} \qquad (7)$$

where K_Z and K_R are proportionality constants, into which any N_A dependence has been absorbed. Taking the logarithm of these equations yields:

$$\begin{aligned} \log Z &= \log K_Z + \alpha \log N_B \\ \log R_{core} &= \log K_R + \kappa \log N_B \end{aligned} \qquad (8)$$

Plots of log Z and log R_{core} vs. log N_B for a constant soluble block length are therefore linear, with slopes equal to the scaling exponents, α and κ, respectively; the proportionality constants, K_Z and K_R, are determined from the y-intercepts. Figure 5.1 shows examples of such log-log plots for block ionomer micelles in the PS(370)-*b*-PANi(y) series; a least-squares regression algorithm was used to determine the slopes and y-intercepts, along with the standard deviations on these values. Similar log-log plots were obtained for each of the other five counterions, using aggregation numbers and core radii from Tables 5.3 and 5.4, respectively.

Table 5.5 lists exponents and proportionality constants for the relation $Z = K_Z N_B^{\alpha}$, describing aggregation number as a function of ionic block length for reverse micelles containing different counterions. Since all data included in this part of the analysis were obtained from samples with identical polystyrene block lengths, differences in K_Z and α could be attributed exclusively to counterion effects. The analogous relations for core radii, $R_{core} = K_R N_B^{\kappa}$, were similarly characterized for each counterion, and values of K_R

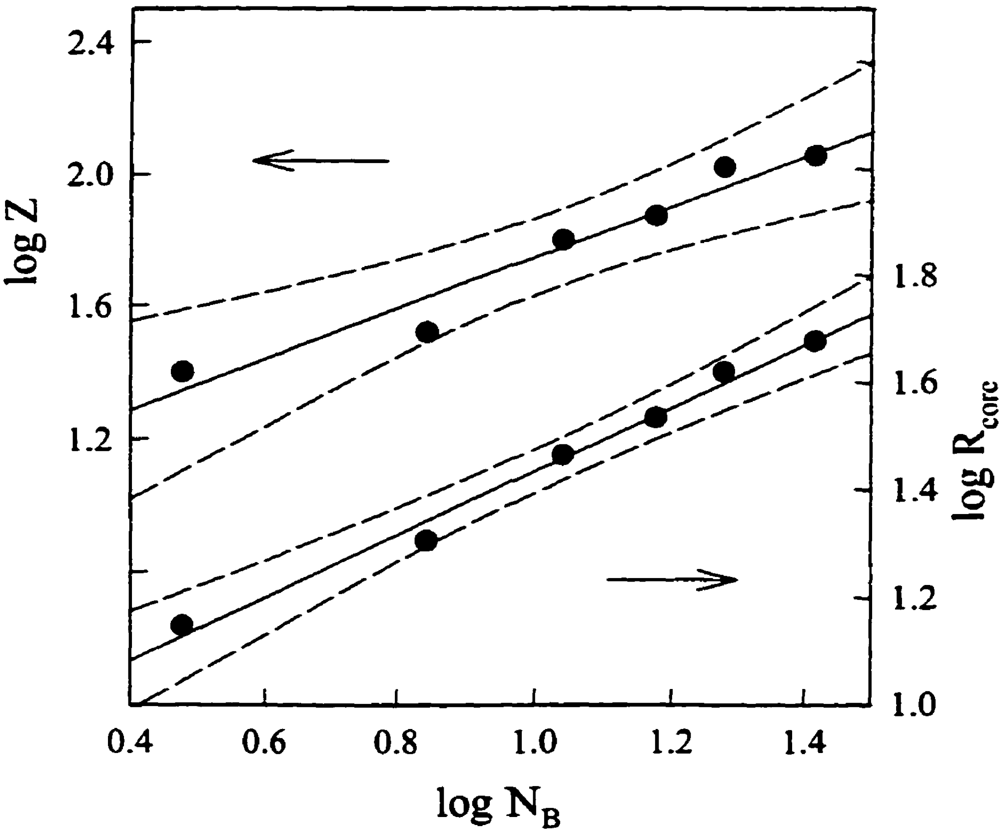

Figure 5.1. Plots of log aggregation number (Z) (top) and log core radii (R_{core}) (bottom) versus log N_B, for block ionomer micelles of the series PS(370)-*b*-PANi(y). Arrows indicate the appropriate axis for each set of data. For the relation $Z = K_Z N_B^{\alpha}$, the upper plot yields $\alpha = 0.77 \pm 0.09$ and $K_Z = 9.5 \pm 1.3$. Similarly, for $R_{core} = K_R N_B^{\kappa}$, the lower plot yields $\kappa = 0.59 \pm 0.03$, and $K_R = 7.0 \pm 1.1$ Å. The dotted lines are 99% confidence intervals.

Table 5.5. Ionic block length dependence of aggregation numbers according to the expressions $Z = K_Z N_B^{\alpha}$ and $Z = K_{Z,av} N_B^{0.74}$, for micelles of PS(370)-*b*-PAA(*y*) neutralized with different metal ions.

metal ion	r_{ion}[a] (Å)	K_Z	α	r^2 [b]	$K_{Z,av}$	r^2 [c]
Cs^+	1.67	12.0 ± 1.2	0.67 ± 0.06	0.96	9.71 ± 0.07	0.96
Ba^{2+}	1.34	8.3 ± 1.4	0.74 ± 0.13	0.92	8.36 ± 0.09	0.92
Cd^{2+}	0.97	8.9 ± 1.9	0.68 ± 0.24	0.74	7.63 ± 0.15	0.74
Pb^{2+}	1.20	6.3 ± 1.8	0.68 ± 0.22	0.84	5.27 ± 0.07	0.84
Ni^{2+}	0.69	9.5 ± 1.3	0.77 ± 0.09	0.95	10.49 ± 0.10	0.95
Co^{2+}	0.72	6.0 ± 1.3	0.89 ± 0.10	0.96	9.49 ± 0.15	0.95

[a] From: *CRC Handbook of Chemistry and Physics*, 60th edition; CRC Press: Boca Raton, FL.

[b] Correlation coefficient for linear regression of Z versus N_B^{α}.

[c] Correlation coefficient for linear regression of Z versus $N_B^{0.74}$.

Table 5.6. Ionic block length dependence of ionic core radii according to the expressions $R_{core} = K_R N_B^{\kappa}$ and $R_{core} = K_{R,av} N_B^{0.58}$, for micelles of PS(370)-*b*-PAA(*y*) neutralized with different metal ions.

Counterion	K_R (Å)	κ	r^2 [a]	$K_{R,av}$ (Å)	r^2 [b]
Cs^+	7.8 ± 1.1	0.56 ± 0.02	0.99	7.33 ± 0.02	0.99
Ba^{2+}	6.5 ± 1.1	0.59 ± 0.04	0.99	6.73 ± 0.02	0.99
$Cd(Ac)^+$	8.2 ± 1.2	0.55 ± 0.08	0.94	7.54 ± 0.05	0.94
Cd^{2+}	6.8 ± 1.2	0.56 ± 0.08	0.94	6.47 ± 0.04	0.94
$Pb(Ac)^+$	7.4 ± 1.2	0.55 ± 0.08	0.97	6.67 ± 0.03	0.97
Pb^{2+}	6.1 ± 1.2	0.56 ± 0.08	0.97	5.79 ± 0.03	0.97
$Ni(Ac)^+$	8.3 ± 1.1	0.58 ± 0.03	0.99	8.37 ± 0.03	0.99
Ni^{2+}	7.0 ± 1.1	0.59 ± 0.03	0.99	7.21 ± 0.03	0.99
$Co(Ac)^+$	7.0 ± 1.1	0.63 ± 0.03	0.99	8.05 ± 0.05	0.99
Co^{2+}	5.9 ± 1.1	0.63 ± 0.03	0.99	6.93 ± 0.04	0.99

[a] Correlation coefficient for linear regression of R_{core} versus N_B^{κ}.

[b] Correlation coefficient for linear regression plot of R_{core} versus $N_B^{0.58}$.

and κ are listed in Table 5.6; scaling exponents and proportionality constants for both bridged and unbridged counterions are reported.

Aggregation numbers and ionic core radii for each counterion (constant soluble block length) were plotted vs. N_B^α and N_B^κ, respectively, using the exponents listed in Tables 5.5 and 5.6; Figure 5.2 shows sample plots of Z (top) and R_{core} (bottom) for micelles of Ni^{2+} block ionomers in the series PS(370)-*b*-PANi(*y*). Correlation coefficients (r^2) for plots of Z vs. N_B^α (Table 5.5) and R_{core} vs. N_B^κ (Table 5.6) indicate excellent linear correlation for most metal ions. Ionic core radii show considerably less scatter than aggregation numbers (Table 5.6); five of the six metal ions gave a linear correlation with $r^2 \geq 0.97$. With these scaling relations, therefore, it appears that the sizes of ionic cores containing a wide range of metal ions can be controlled a priori through variations in the ionic block length. For materials applications, size control within this limited range of ionic block lengths is extremely important, as microreactors with radii < 100 Å are best suited to nanoparticle formation.

When the scaling exponents for aggregation numbers are compared (Table 5.5), it is found that the differences between values of α for the six counterions are mostly within experimental error. Along with reporting the six exponents individually, therefore, values of α have been averaged to obtain $\alpha_{av} = 0.74 \pm 0.08$. Assuming an N_B dependence of $N_B^{0.74}$, aggregation numbers for different counterions were then plotted on the same ordinate scale. Sample plots of Z vs. $N_B^{0.74}$ for the Ni^{2+}, Ba^{2+}, and Pb^{2+} series are shown (Figure 5.3, top). The slopes on the average ordinate scale, $K_{Z,av}$, were determined from regression lines forced through the origin; these values, listed in Table 5.5, are proportionality constants for the equation $Z = K_{Z,av}N_B^{0.74}$. Although aggregation numbers for various counterions scale similarly with $N_B^{0.74}$, the proportionality constants are clearly dependent on the nature of the counterion. A similar strategy was applied to the ionic core radii, as the scaling exponents κ were also found to be the same for different counterions, within experimental error. An average exponent $\kappa_{av} = 0.58 \pm 0.03$ was calculated, and from linear regression of R_{core} vs. $N_B^{0.58}$ (Figure 5.3, bottom), proportionality constants $K_{R,av}$ were determined for each counterion (Table 5.6).

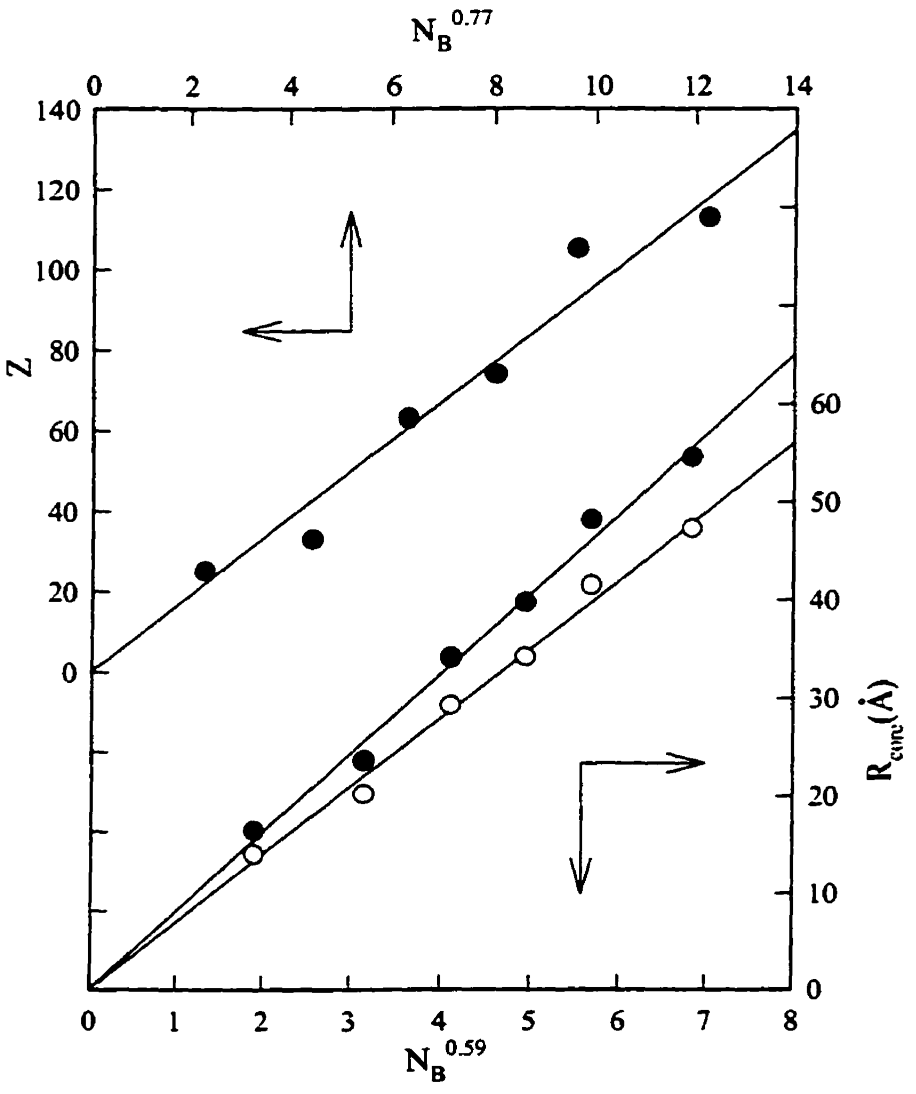

Figure 5.2. Plots of aggregation numbers (Z) versus N_B^{α} (where $\alpha = 0.77$) (top) and ionic core radii (R_{core}) versus N_B^{κ} (where $\kappa = 0.59$) (bottom) for micelles of PS(370)-*b*-PANi(*y*). Arrows indicate the appropriate axes for each set of data. For the lower plots, open circles represent radii of cores with 100% bridged counterions, $R_{Ni^{2+}}$, and closed circles represent radii of cores with 100% unbridged counterions, $R_{Ni(Ac)^+}$.

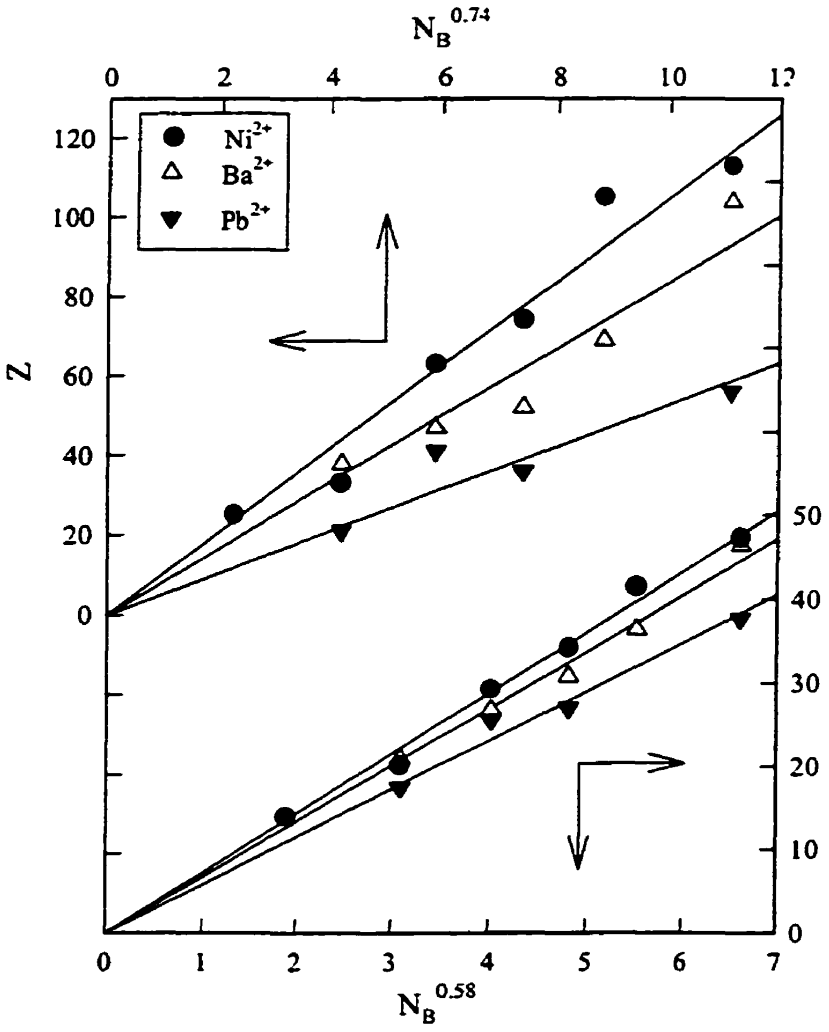

Figure 5.3. Plots of aggregation numbers (Z) versus $N_B^{0.74}$ and ionic core radii (R_{core}) versus $N_B^{0.58}$ for micelles of PS(370)-*b*-PAX(y), where X = Ni, Ba, and Pb. Arrows indicate the appropriate axes for each set of data. For the purpose of illustration, $R_{M^{2+}}$ values have been used to represent the core radii for all metal ions.

Although the scaling exponents for each counterion, α and κ, were obtained using only a small number of data points (five or six), the similarity of these values for different counterions suggests that the average exponents represent reliable trends within this range of ionic block lengths.

If it is assumed that the scaling exponents α and κ are independent of the neutralizing ion within experimental error, the effects of the counterion on Z and R_{core} are contained within the proportionality constants $K_{\mathrm{Z,av}}$ and $K_{\mathrm{R,av}}$, respectively. Values of $K_{\mathrm{Z,av}}$, listed in Table 5.5, indicate that aggregation numbers of block ionomer micelles containing different counterions decrease in the following order: $\mathrm{Ni}^{2+} > \mathrm{Cs}^{+} > \mathrm{Co}^{2+} > \mathrm{Ba}^{2+} > \mathrm{Cd}^{2+} > \mathrm{Pb}^{2+}$. It is noteworthy that Pb^{2+} and Cd^{2+} ionomers, which show the lowest fraction of micelles by SEC, also have the lowest aggregation numbers. At this point, it is stressed that any counterion dependence in the aggregation number is a consequence of the influence of the ion on micelle formation. This is not a trivial statement, considering that most ion-containing block copolymers described in the literature were prepared by the introduction of metal ions after the micelle had formed.[8-12] In the present system, however, it is the exchange between protons and counterions that initiates the self-assembly of insoluble blocks, such that metal ions play an important role in the early stages of micellization.

For the divalent metal acetates, a linear decrease in $K_{\mathrm{Z,av}}$ is found as the crystal ionic radius (r_{ion}) of the divalent species increases (Figure 5.4). To explain the linear relation between micelle aggregation number and the radius of the metal ions, it is considered that, as r_{ion} decreases, stronger interactions are expected between the counterions and the charged polymer units.[33] Stronger ionic interactions between (and within) poly(metal acrylate) blocks will tend to increase the surface tension of the core-solvent interface. In order to minimize this thermodynamic penalty, the system will form larger micelles as the counterions become smaller. For the Cs^{+} and Ba^{2+} ionomers, prepared using metal hydroxides, it is clear that the $K_{\mathrm{Z,av}}$ values (9.71 and 8.36, respectively) fall significantly above the regression line, and these two series therefore do not appear to obey the trend. The unexpectedly high values of $K_{\mathrm{Z,av}}$ for Cs^{+} and Ba^{2+}, given their relatively large ionic radii (1.67 Å and 1.34 Å, respectively) may be related to

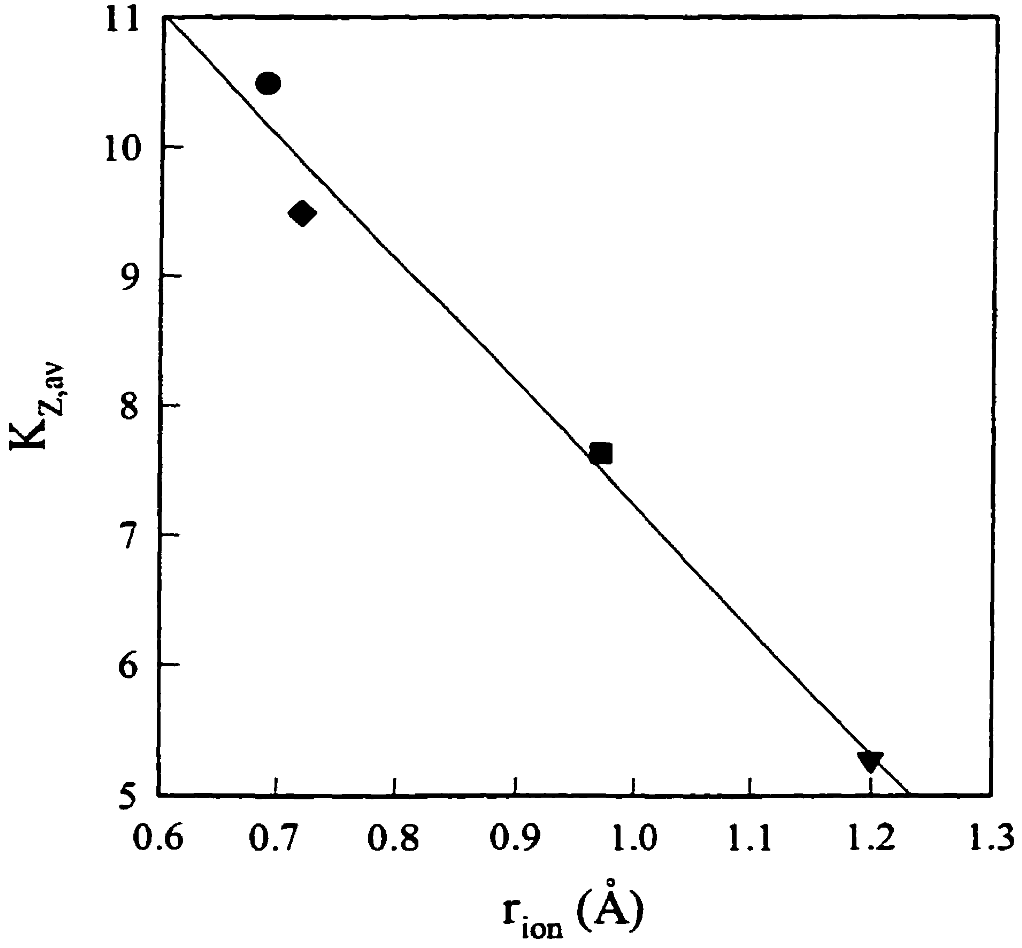

Figure 5.4. Plot of $K_{Z,av}$ versus the crystal ionic radii (r_{ion}) for block ionomers containing various divalent metal ions: Ni^{2+} (●), Co^{2+} (◆), Cd^{2+} (■) and Pb^{2+} (▼).

the strong basicity of cesium and barium hydroxide compared with that of the metal acetates.

A brief comparison was made between the N_B dependence observed in the present system ($Z \sim N_B^{0.74 \pm 0.08}$, $R_{core} \sim N_B^{0.58 \pm 0.03}$) and other empirical and theoretical scaling relations. The scaling laws determined here are most similar to theoretical relations for starlike micelles, $Z \sim N_B^{0.8}$, $R_{core} \sim N_B^{0.6}$.[30,31] This agrees with earlier data on the core sizes of Cs-neutralized block ionomers, which also scaled as $N_B^{0.6}$.[17] The relation determined by Zhang et al. for aqueous crew-cut micelles[32] ($R_{core} \sim N_B^{0.4}$) showed a somewhat weaker N_B dependence than was determined in the present work.

It is important to note that the starting point of theoretical approaches to self-assembly is the thermodynamic equilibrium between single chains and the micellar pseudophase. As previously stated, it has been found that block ionomer micelles, in their final state, are kinetically-frozen aggregates that do not exhibit dynamic equilibrium, even under high-temperature conditions.[15] However, it is believed that rapid exchange between micelles and unimers does exist in the early stages of micellization, when the ion content of the insoluble blocks is relatively low, and micelle lability is enhanced by solvent swelling.[34] As the degree of neutralization increases, solvent is expelled from the micelle and the core becomes increasingly viscous and compact. At some point, the high viscosity of the core prevents the facile movement of unimers to and from the micelle, such that the dynamic equilibrium between micelles and single chains is kinetically stalled. Although the movement of small molecules to and from the micelle cores, together with the chemical equilibria of eq 4, will allow further neutralization or changes in the degree of ion-bridging, the aggregate can no longer adjust to these chemical changes, and aggregation numbers are effectively frozen in. (It is stressed that all micelles were completely neutralized in their final form, as determined by FTIR spectra.) The scaling relations observed in the frozen aggregates, therefore, are actually "snapshots" of earlier thermodynamic states.

To summarize, Z and R_{core} scale with the insoluble block in a similar manner for all counterions, with an N_B dependence that agrees well with thermodynamically-based models of micellization. As well, aggregation numbers and ionic core radii both show counterion dependence through their respective proportionality constants. To rationalize these various observations, it is pointed out that the factors which give rise to counterion dependence of micellar parameters (e.g., the crystal ionic radius) are not accounted for in general theories of block copolymer micelles. These "counterion factors" are unique to block ionomer systems, and clearly have an influence on the overall size of the aggregates. At the same time, it appears that the power of N_B scaling is still governed by the more conventional factors of micellization (e.g., chain stretching, interfacial tension),[27-31] such that a single scaling relation can be applied equally well to a wide range of block ionomers containing different metal ions.

5.4.2.2. Soluble Block Length Dependence

Along with the N_B dependence described above, several theoretical[27-29,31] and empirical[32] scaling laws have predicted an N_A dependence for aggregation numbers and core radii of block copolymer micelles. Although theories of starlike micelles predict that scaling with N_A is negligible, it has been found that the ionic core radii of starlike PS-*b*-PACs micelles show improved linear correlation when the length of the soluble block is considered; the possibility of N_A dependence was therefore not ruled out in the present system. Along with data obtained at constant N_A, values of Z and R_{core} for different soluble block lengths have been included in comprehensive scaling relations for each counterion. Aggregation numbers and ionic core radii for each metal ion were plotted vs. $N_B^{\alpha}N_A^{-\beta}$ and $N_B^{\kappa}N_A^{-\gamma}$, respectively. N_B exponents, determined previously, were held constant, while the N_A exponents, β and γ, were varied until the best linear correlation was obtained.

It was found that Z and R_{core} values for block ionomers prepared from the copolymer PS(300)-*b*-PAA(44) were unusually large, such that scaling plots could not be linearized without selecting unrealistic N_A exponents. The mole percentage of the ionic block is somewhat higher in these micelles (ca. 13%), which may account for their anomalous behaviour relative to the other samples. Block ionomers of the copolymer PS(300)-*b*-PAA(44) were rejected from further scaling analysis, which left only two different soluble block lengths for the determination of scaling with N_A; the exponents β

and γ are therefore considered to be very approximate values. Figure 5.5 shows scaling plots for the Ni^{2+} reverse micelles, including both N_A and N_B dependence.

For the complete scaling relations $Z \sim N_B^{\alpha} N_A^{-\beta}$ and $R_{core} \sim N_B^{\kappa} N_A^{-\gamma}$, N_A exponents determined for Cs^+, Ba^{2+}, Cd^{2+}, and Ni^{2+} micelles were all in the range of $\beta = 0.42 \pm 0.06$ and $\gamma = 0.14 \pm 0.02$, while Pb^{2+} and Co^{2+}-neutralized samples showed considerably weaker scaling with the soluble block length ($\beta = 0.10 \pm 0.05$ and $\gamma = 0.04 \pm 0.02$). The observation of lower β and γ values for the latter two counterions may not be physically meaningful, considering the poor statistics in the determination of N_A dependence.

5.4.3. DLS of Block Ionomers

5.4.3.1. Basic DLS Theory

The diffusion of monodisperse, noninteracting particles in a colloidal solution results in the exponential decay of the normalized electric field autocorrelation function, $g_1(\tau)$:

$$g_1(\tau) = \exp(-\Gamma\tau) \qquad (9)$$

where τ is the correlation time and Γ is the relaxation rate; Γ is related to the particle diffusion coefficient (D) by

$$\Gamma = Dq^2. \qquad (10)$$

The scattering vector q is defined:

$$q = (4\pi n/\lambda)\sin(\theta/2) \qquad (11)$$

where n is the refractive index of the solvent, λ is the wavelength of the incident light, and θ is the angle at which scattered light is measured. The simple linear relationship

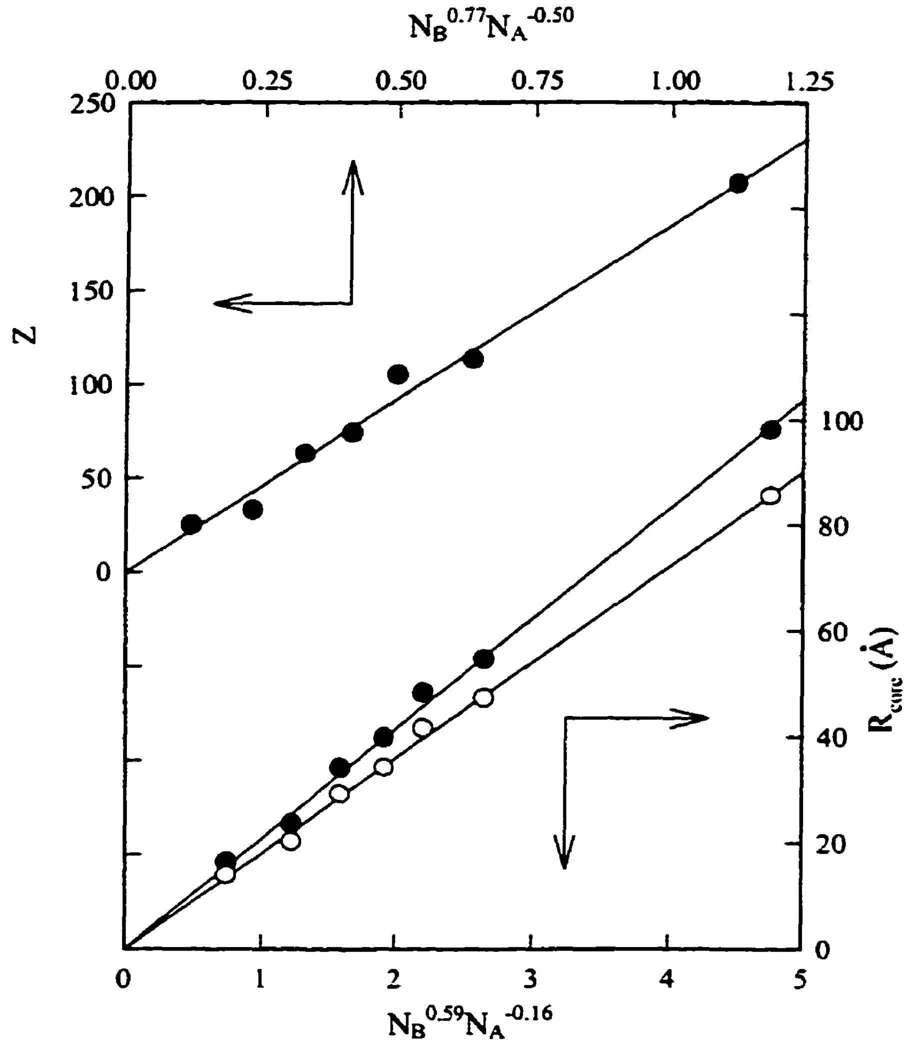

Figure 5.5. Plots of aggregation numbers (Z) versus $N_B^{0.77}N_A^{-0.50}$ (top) and ionic core radii (R_{core}) versus $N_B^{0.59}N_A^{-0.16}$ (bottom) for micelles of Ni^{2+} block ionomers. Arrows indicate the appropriate axes for each set of data. The full scaling relations for Z and R_{core} were determined for each metal ion as described in the text.

between Γ and q^2 (eq 10) holds for diffusive relaxation modes, and may be disrupted by interactions between particles which inhibit free diffusion.

For colloidal solutions containing a distribution of particle sizes, the resultant autocorrelation function will be made up of a distribution of relaxation rates. Detailed information on the distribution can be extracted from the autocorrelation function using sophisticated analysis techniques such as Provencher's CONTIN method.[35] For the purposes of this study, however, the simpler cumulant method of Koppel[36] has been used; this describes the total autocorrelation function as an expansion about the z-average relaxation rate, Γ_z :

$$\ln g_1(\tau) = 1 - \Gamma_z\tau + \frac{\mu}{2!}\tau^2 - \ldots \qquad (12)$$

where μ is the second moment of the distribution, and the ratio μ/Γ_z^2 is related to the polydispersity of the particles.

Γ_z, determined at a finite concentration of particles, is related via eq 10 to an effective z-average diffusion coefficient, $D_{z,\mathrm{eff}}$. In some cases, $D_{z,\mathrm{eff}}$ will show concentration dependence in the form of the expansion

$$D_{z,eff} = D_z(1 + k_D c + \ldots)\,. \qquad (13)$$

The mutual z-average diffusion coefficient, D_z, is obtained by extrapolation to infinite dilution. The slope, k_D, of the linear extrapolation is a measure of interparticle correlations, which are a balance of direct and hydrodynamic interactions. In general, positive values of k_D arise from repulsive interactions between particles (e.g. hard sphere, electrostatic), while negative k_D values connote attractive interactions (e.g. Van der Waals).

Perhaps the most fundamental parameter to describe colloidal particles is their hydrodynamic radius, R_h, which is obtained by substitution of D_z into the Stokes-Einstein relation:

$$(R_h)_z = kT / 6\pi\eta D_z \qquad (14)$$

where k is the Boltzmann constant, T is the temperature of the experiment, and η is the solvent viscosity at temperature T. As indicated in eq 14, R_h derived from cumulant analysis is a *z*-average value.

5.4.3.2. DLS of Block Ionomers in Toluene

Several solutions of block ionomers were investigated by dynamic light scattering, in order to obtain some information on the hydrodynamic behaviour of the reverse micelles. Limitations of sample availability prevented the acquisition of DLS data on all the block ionomers that were investigated by SLS; representative samples were therefore selected, covering a range of metal ions and block copolymer compositions.

Cumulant analysis of autocorrelation functions for all block ionomer micelles gave values of μ/Γ_z^2 in the range 0.05-0.20, indicating a distribution of relaxation times. It should be noted that, in some cases, low scattering intensity makes the fitting of autocorrelation functions less accurate, which often results in high values of the second cumulant; actual polydispersities may therefore be much lower than those suggested by μ/Γ_z^2. In some cases, more detailed information on colloidal polydispersities can be obtained from CONTIN analysis of the autocorrelation function; however, such an analysis was beyond the scope of the present work.

For several concentrations of micelles in toluene, values of Γ_z were plotted as a function of q^2. Figure 5.6a shows examples of such plots for aggregates of Cd-neutralized PS(302)-*b*-PAA(44); the linearity of Γ_z vs. q^2 is indicative of free diffusion of micelles, and was observed for the vast majority of reverse micelles. The concentration dependence of the slope ($D_{z,\mathrm{eff}}$) is plotted in Figure 5.6b. In most cases, the diffusion coefficients of block ionomer micelles showed relatively low concentration dependence, although values of k_D were consistently negative. This suggests weak attractive interactions between the micelles in toluene, most likely of the Van der Waals variety.

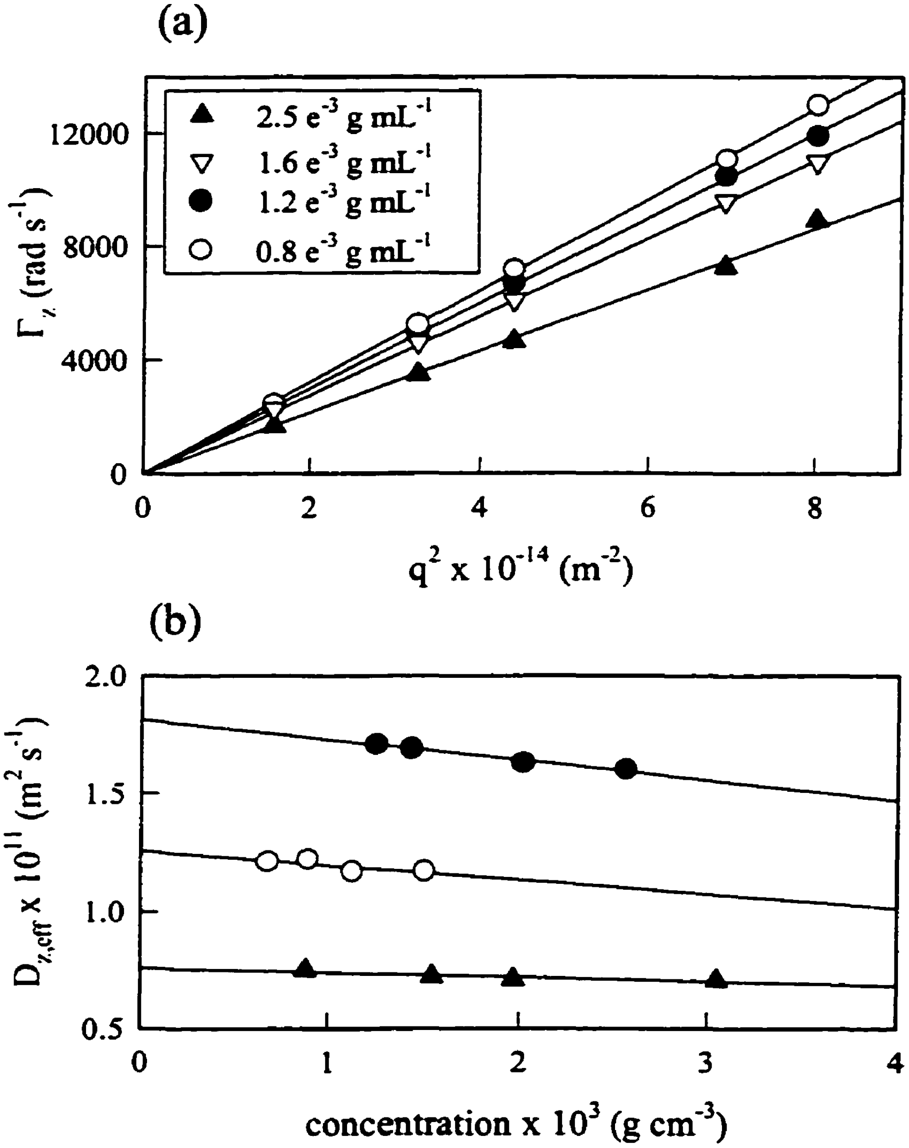

Figure 5.6. (a) Plots of the *z*-average relaxation rate (Γ_z) versus the square of the scattering vector (q^2) for different concentrations of micellar solutions of the block ionomer PS(300)-*b*-PACd(44). (b) Plots of the effective *z*-average diffusion coefficient ($D_{z,\text{eff}}$) versus concentration for the following block ionomers: PS(730)-*b*-PACs(84) (▲), PS(300)-*b*-PACs(44) (○), and PS(370)-*b*-PACs(15) (●). Extrapolation of each line to infinite dilution yields the *z*-average mutual diffusion coefficients (D_z).

Table 5.7 lists hydrodynamic radii, R_h, calculated from D_z at infinite dilution for selected ionomers. The ratio R_g/R_h is also shown, as this parameter gives useful information on the micellar structure.[37] For hard spheres, R_g/R_h has a value of 0.775, while for star polymers, $R_g/R_h \approx 1.10$ for most aggregation numbers, and increases rapidly at low Z. With certain exceptions, most of the block ionomers investigated show R_g/R_h ratios between the values for hard spheres and star polymers, in agreement with recent results by Förster for strongly-segregated block copolymer micelles.[38] These findings are consistent with our assumption of spherical ionic cores..

Daoud and Cotton developed a scaling model for star polymers,[39] which can be applied to features of the corona in starlike block copolymer micelles. They predicted that the polymer brush height, H, scales as $H \sim Z^{0.2}N_A^{0.6}$ in good solvents. In the present system, H is the height of the corona, calculated from $H = R_h - R_{core}$, Z is the aggregation number of the micelle, and N_A is the number of units in the polystyrene block. For block ionomers with a constant soluble block length of PS = 370, log H vs. log Z was plotted, including data for all counterions (Table 5.7), to obtain $H \sim Z^{0.3 \pm 0.1}$. This agrees with the theoretical scaling of brush height with aggregation number, indicating that coronal segment density profiles of block ionomer micelles are starlike, irrespective of the metal ions in the core. The N_A dependence of H was also estimated from a limited number of data points to obtain the full scaling relation $H \sim Z^{0.3 \pm 0.1}N_A^{0.9 \pm 0.2}$; this suggests stronger soluble block length dependence than is predicted by theory, possibly due to more extensive steric perturbations in the corona than are described by Daoud and Cotton for star polymers.

Table 5.7. Structural data for block ionomer micelles in toluene.

metal ion	PS(*x*)-*b*-PAA(*y*)	Z	R_h (nm)	H (nm)	R_g (nm)	R_g / R_h
Cs^+	370-*b*-3	127	15	12.5	25	1.67
Cs^+	370-*b*-15	80	22	18.4	19	0.86
Cs^+	370-*b*-19	88	25	20.9	19	0.76
Cs^+	370-*b*-26	100	26	21.3	25	0.96
Cs^+	730-*b*-84	177	52	43.6	46	0.88
Cs^+	300-*b*-44	230	31	23.6	32	1.03
Cd^{2+}	370-*b*-15	44	18	15.1	20	1.11
Cd^{2+}	370-*b*-19	54	18	14.7	17	0.94
Cd^{2+}	370-*b*-26	98	23	18.5	19	0.83
Cd^{2+}	300-*b*-44	340	21	12.9	44	2.10
Ba^{2+}	370-*b*-15	52	20	16.9	30	1.50
Ba^{2+}	370-*b*-26	104	21	16.4	24	1.14
Ba^{2+}	730-*b*-84	167	42	34.0	32	0.76
Co^{2+}	370-*b*-15	63	16	12.8	20	1.25
Co^{2+}	370-*b*-19	95	20	16.0	22	1.10
Co^{2+}	730-*b*-84	285	43	33.5	58	1.35
Ni^{2+}	370-*b*-15	74	19	15.6	25	1.32
Ni^{2+}	730-*b*-84	207	44	35.4	45	1.02
Pb^{2+}	370-*b*-26	56	20	16.2	23	1.15
Pb^{2+}	730-*b*-84	123	46	38.8	32	0.70

5.4.4. TEM of Block Ionomer Films Containing Different Metal Ions

TEM micrographs of PS(703)-*b*-PAA(84) neutralized with Ba^{2+} and Pb^{2+} ions are shown in Figure 5.7. In both cases, the dark regions of high electron density are ion-containing microdomains dispersed in a polystyrene matrix (grey background), confirming that metal ions are localized in the micelle cores. In the Ba^{2+} block ionomer, spherical cores of low polydispersity are observed, with a radius of 80 Å, identical to R_{core} calculated from SLS data. The RPI value for the core distribution is 1.04, indicating low polydispersity. In the Cd^{2+} and Cs^+ films (not shown), the ionic cores appeared somewhat elongated; holes and cracks in the polystyrene matrix of these films were also observed. Both elongated cores and aberrations in the matrix phase are attributable to the microtoming of these samples, and may reflect differences in the mechanical properties of ionomers containing different metal ions. The elongated cores of Cd^{2+} and Cs^+ micelles both showed distinct orientation, which is evidence that the original cores were stretched in the direction of microtoming. DLS results for the Cs^+ sample gave $R_g/R_h = 0.88$, supporting spherical micellar structure in solution, prior to TEM sample preparation. The micrograph of Pb^{2+} reverse micelles reveals the formation of small metal particles within micelle cores, probably due to the reduction of Pb^{2+} ions within the electron beam. Close inspection of the micrograph reveals that some of the cores have formed a single lead particle (indicated with an arrow), while other cores contain clusters of smaller particles; in the latter case, the overall shape of the dark regions, while roughly spherical, is somewhat irregular. The average radius of the Pb-containing microdomains is 63 Å with an RPI of 1.02, which is about 15% lower than R_{Pb2+} calculated from SLS aggregation numbers. The low value of R_{core} determined from TEM can be explained by the migration of Pb "seed" particles toward the center of the core in the process of reduction and single particle formation. As well, the average radius of the single lead particles in the micrograph have been measured, and these are found to be ca. 40 Å. Assuming that the density of the particles is identical to the bulk value (11.4 g/mL), this corresponds to 9800 Pb atoms per particle. From the SLS-determined aggregation number, it has been calculated that the original ionic core contains between 5200 and 10300 Pb^{2+} ions,

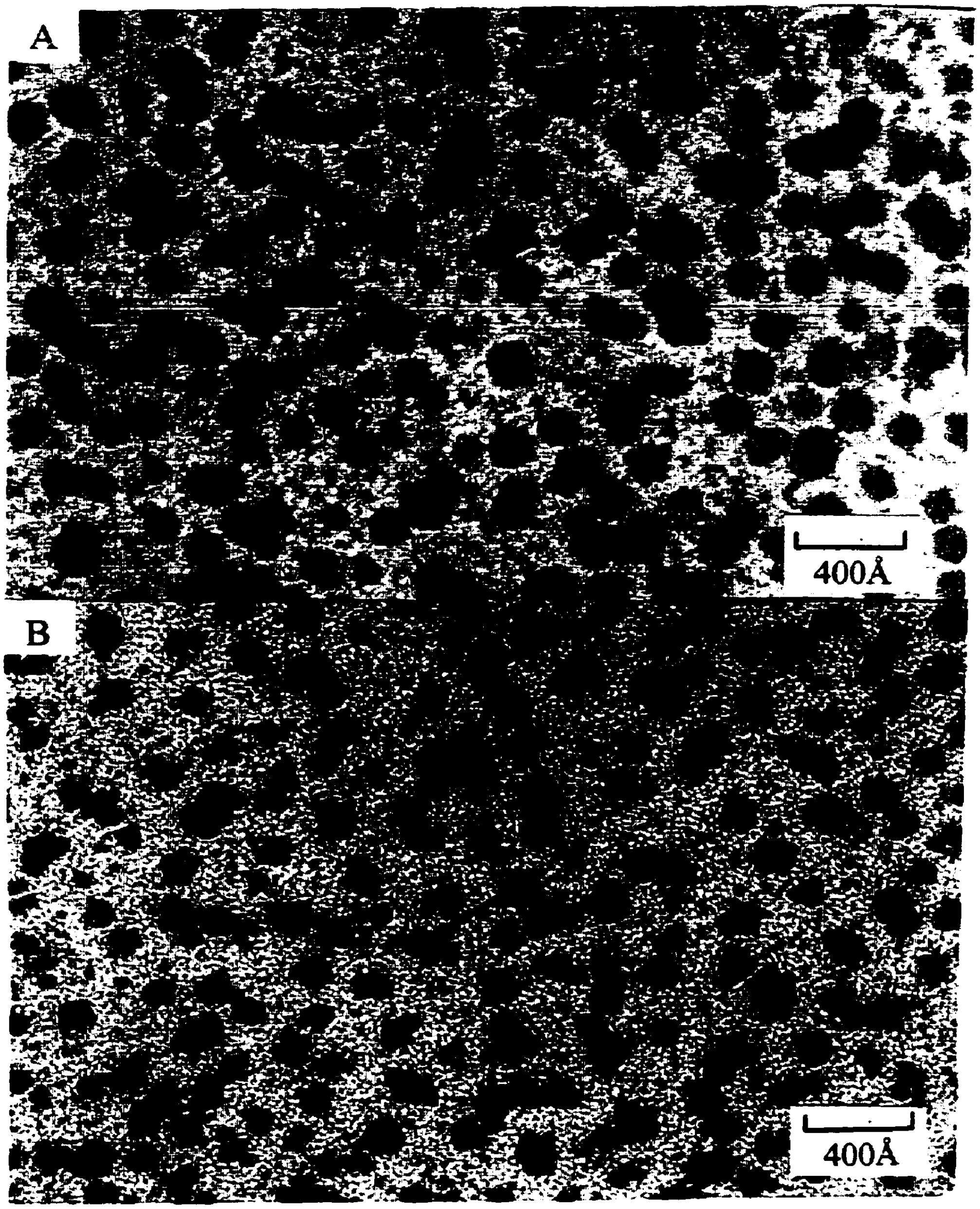

Figure 5.7. Transmission electron micrographs of PS(730)-*b*-PAA(84) neutralized with (A) Ba^{2+} and (B) Pb^{2+}. Dark regions indicate ionic cores dispersed in a matrix of polystyrene. Pb^{2+}-neutralized sample (B) shows evidence of metal reduction, with some cores containing single lead particles (indicated with an arrow) of ca. 80 Å in diameter.

depending on the extent of counterion bridging. This suggests that the size of the Pb single particles is indeed restricted by the number of Pb^{2+} ions in the cores, supporting the claim that the ionic cores can be used as true inorganic microreactors.

5.5. Conclusions

Scaling relations have been determined for block ionomer reverse micelles of PS-*b*-PAA, in which the acid block was neutralized with a wide range of metal ions. Micelle aggregation numbers for all counterions were found to scale with the insoluble block length as $Z \sim N_B^{0.74 \pm 0.08}$, while ionic core radii scaled as $R_{core} \sim N_B^{0.58 \pm 0.03}$; both scaling relations are in agreement with theories for starlike block copolymer micelles. For most metal ions, aggregation numbers and core radii also showed significant N_A-dependence, and approximate exponents were determined. Although scaling exponents, within experimental error, were independent of the counterion, aggregation numbers and core radii were found to show metal ion dependence through the proportionality constants, decreasing in the order $Ni^{2+} > Cs^{+} > Co^{2+} > Ba^{2+} > Cd^{2+} > Pb^{2+}$. For divalent counterions introduced via metal acetates, a linear relationship was found between aggregation numbers and the crystal ionic radii. R_g/R_h ratios, calculated from combined SLS and DLS data, are between the values for stars and compact spheres. The coronal brush height was found to scale as $H \sim Z^{0.3 \pm 0.1} N_A^{0.9 \pm 0.2}$.

The determination of reliable scaling laws for aggregation numbers and core radii is a critical step toward the use of block ionomer cores as inorganic micoreactors of controllable size. The present work has shown that the radii of these microreactors can be controlled, with excellent linear correlation, in the range of ca. 10 - 100 Å, by variations in the length of either block, or by selecting the appropriate counterion. Such control in the range of small sizes is especially important for the synthesis of metal and semiconductor nanoparticles in the ionic core; these particles of ultrasmall dimensions have interesting optical and electronic properties which can be tuned through variations in the particle size.

Reverse micelles of PS-*b*-PAA block ionomers appear to offer numerous advantages over other systems of ion-containing block copolymers, including compatibility with a large variety of counterions, facile and controllable ion addition, high stability of aggregates, and now well-characterized core sizes for a selection of different metal ions. With an understanding of scaling relations and counterion dependence, it is relatively easy to prepare inorganic microreactors of a desired size, containing a wide range of ionic precursors for small particle synthesis. The reader may recognize the potential of a wide range of composite materials derived from block ionomers, with properties that can be controlled through a priori knowledge of self-assembly in the ionomer host.

In the next chapter of the thesis, we return to the composites of CdS-containing reverse micelles described in chapter 4, and show how the quantum dots of controlled microreactor synthesis can be further used as "building blocks" to form secondary water-solubility aggregate structures. This work extends the possibilities of composite formation to another level, providing a means whereby the behaviour of materials is tailored, not only through the controlled growth of nanoparticles, but through subsequent assembly in aqueous solutions. The water-solubility of the secondary aggregates is shown to be another great advantage, as it allows our reverse micelle microreactors to be incorporated into environmentally-friendly media.

Acknowledgments

This work was supported by the Natural Sciences and Engineering Research Canada (NSERC). M.M. is grateful for scholarship funding provided by NSERC and Le Fonds pour la Formation de Chercheurs et L'Aide à la Recherche (FCAR, Quebec).

References

(1) Tuzar, Z.; Kratochvil, P. *Adv. Colloid and Interface Sci.* **1976**, *6*, 201.

(2) Price, C. In *Developments in Block Copolymers,* Vol 1; Goodman, I., Ed.; Applied Science Publishers: London, 1982, p.39.

(3) Tuzar, Z.; Kratochvil, P. In *Surface and Colloid Science*, Vol 15; Matijevic, E., Ed.; Plenum Press: New York, 1993, p.1.

(4) Selb, J.; Gallot, Y. In *Polymeric Amines and Ammonium Salts.* Goethals, E. J. Ed., Pergamon Press: New York, 1980, p 205.

(5) Selb, J and Gallot, Y. In *Development in Block Copolymers*; Goodman, I., Ed.; Elsevier Applied Science: London, U.K., 1985; Vol 2, pp 27-96.

(6) Moffitt, M.; Khougaz, K.; Eisenberg, A. *Acc. Chem. Res.* **1996**, *29*, 95.

(7) Moffitt, M.; McMahon, L.; Pessel, V.; Eisenberg, A. *Chem. Mater.* **1995**, *7*, 1185.

(8) Möller, M. *Synth. Met.* **1991**, *41-43*, 1159.

(9) Cummins, C. C.; Schrock, R. R.; Cohen, R. E. *Chem. Mater.* **1992**, *4*, 27.

(10) Ng Cheong Chan, Y.; Craig, G. S. W.; Schrock, R. R.; Cohen, R. E. *Chem. Mater.* **1992**, *4*, 885; Ng Cheong Chan, Y.; Schrock, R. R.; Cohen, R. E. *J. Am. Chem. Soc.* **1992**, *114*, 7295; Yue, J.; Sankaran, V.; Cohen, R. E.; Schrock, R. R. *J. Am. Chem. Soc.* **1993**, *115*, 4409; Cohen, R. E.; Yue, J. *Supramolecular Science* **1994**, *1*, 117.

(11) Antonietti, M.; Wenz, E.; Bronstein, L.; Seregina, M. *Adv. Mater.* **1995**, *7*, 1000.

(12) Spatz, J.; Roescher, A.; Möller, M. *Adv. Mater.* **1996**, *8*, 337.

(13) Brus, L. E. *J. Chem. Phys.* **1983**, *79*, 5566; Brus, L. E. *J. Chem. Phys.* **1984**, *80*, 4403.

(14) Henglein, A. *Chem. Rev.* **1989**, *89*, 1861.

(15) Desjardins, A.; Eisenberg, A. *Macromolecules* **1991**, *24*, 5779.

(16) Desjardins, A.; van de Ven, Th., Eisenberg, A. *Macromolecules* **1992**, *25*, 2412.

(17) Nguyen, D.; Williams, C. E.; Eisenberg, A. *Macromolecules* **1994**, *27*, 5090.

(18) Long, T. E.; Allen, R.D.; McGrath, J. E. In *Chemical Reactions On Polymers*; Benham, J. L.; Kinstel, J. F., eds.; ACS Symposium Series364; American Chemical

Society: Washington, DC, **1988**; Chapter 19.

(19) Gauthier, S.; Duchesne, D.; Eisenberg, A. *Macromolecules* **1987**, *20*, 753.

(20) DePorter, C. D.; Ferrence, G. M.; McGrath, J. E.; *Polym. Prepr.* **1993**, p.574.

(21) Zimm, B. H. *J. Chem. Phys.* **1948**, *16*, 1093.

(22) Benoit, H.; Froelich, D. In *Light Scatterig from Polymer Solutions*; Huglin, M. B., Ed.; Academic Press: New York, 1972; Chapter 11.

(23) Renliang, X.; Winnik, M. A.; Hallett, F. R.; Riess, G.; Croucher, M. D. *Macromolecules* **1991**, *24*, 87.

(24) Khougaz, K.; Zhong, X. F.; Eisenberg, A. Macromolecules **1996**, *29*, 3937-3949.

(25) Nguyen, D. *PhD thesis* McGill University: Montreal, **1994**.

(26) Nguyen, D.; Varshney, S. K.; Williams, C.E.; Eisenberg, A. *Macromolecules*, **1994**, *27*, 5086.

(27) Whitmore, M.; Noolandi, J. *Macromolecules* **1985**, *18*, 657.

(28) Bluhm, T. L.; Whitmore, M. D. *Can. J. Chem.* **1985**, *63*, 249.

(29) Nagarajan, R.; Ganesh, K. *J. Chem. Phys.* **1989**, *90*, 5843.

(30) Halperin, A. *Macromolecules* **1987**, *20*, 2943.

(31) Zhulina, E. B.; Birshtein, T. M. *Vysokomol. Soedin.* **1985**, *27*, 511.

(32) Zhang, L.; Barlow, R. J.; Eisenberg, A., *Macromolecules* **1995**, *28*, 6055.

(33) Hird, B.; Eisenberg, A. *Macromolecules* **1992**, *25*, 6466.

(34) Khougaz, K.; Nguyen, D.; Williams, C. E.; Eisenberg, A. *Can. J. Chem.* **1995**, *73*, 2086.

(35) Provencher, S. W. *Comput. Phys. Comm.* **1982**, *27*, 213.

(36) Koppel, D. E. *J. Chem. Phys.* **1972**, *57*, 4814.

(37) Burchard, W. *Adv. Polym. Sci.* **1983**, *48*, 1.

(38) Förster, S.; Zisenis, M.; Wenz, E.; Antonietti, M. *J. Chem. Phys.* **1996**, *104*, 9956.

(39) Daoud, M.; Cotton, J. P. *J. Phys.* **1982**, *43*, 531.

CHAPTER 6

Assemblies of Semiconducting Nanoparticles in Water-Soluble Block Copolymer Aggregates

6.1. Abstract

Novel spherical assemblies of CdS-containing block copolymer reverse micelles in aqueous solution have been formed, by the slow addition of water to mixtures of the reverse micelles and a polystyrene-*b*-poly(acrylic acid) stabilizer. The structures are large compound micelles (LCMs) consisting of quantum-confined CdS nanoparticles dispersed throughout a spherical PS matrix, which is stabilized in water by a layer of solubilized hydrophilic chains. The size of the CdS particles ($2R_{\mathrm{CdS}}$ = ca. 30 Å) is controlled by the ionic block length, N_{B}, of the block copolymer making up the reverse micelle. LCM formation is found to be dependent on the amount of added stabilizing copolymer. When the weight of stabilizer relative to the total polymer weight is 12% for the specific system under study, a single population of LCMs is formed with an average diameter of $D_{\mathrm{agg}} = 64$ nm; each of these LCMs consists of an average of 58 reverse micelles and 87 stabilizing chains, with an average surface area per stabilizing chains of 148 nm^2. At 10% stabilizer, two LCM populations, $D_{\mathrm{agg}} = 52$ nm and $D_{\mathrm{agg}} = 152$ nm, are formed. When the concentration of stabilizing copolymer is increased to 21 and 35%, regular micelles with no internal structure coexist with LCMs. Without added stabilizing copolymer, most

reverse micelles undergo macroscopic precipitation upon water addition, although some LCMs are observed in the remaining solution.

6.2. Introduction

The synthesis of metallic and semiconducting nanoparticles has become a topic of extreme interest in the field of material science, due in part to the wide range of optical and electronic properties that are accessible in the regime of ultrasmall sizes. The unique properties of such nanoparticles are attributed to quantum-confinement or surface effects, which become operative when the particle is too small to exhibit bulk behaviour.[1,2] Since optical and electronic properties can be "tuned" through variations in the sizes of clusters, a synthetic medium producing monodisperse particles of controllable size is highly desirable.

Block copolymers have long been known to self-assemble in selective solvents, forming stable aggregates known as micelles or micelle-like aggregates.[3-5] Quite recently, various types of block copolymers have been applied to the synthesis of metallic and semiconducting particles.[6-11] In these systems, particle growth is restricted to ionic or highly polar microdomains, providing a mechanism for both size control and particle stabilization. In particular, CdS quantum dots of low polydispersity have been synthesized within the spherical ionic cores of polystyrene-*b*-poly(cadmium acrylate) (PS-*b*-PACd) reverse micelles.[10] Excellent correlation was found between the micelle ionic core radii and the resultant sizes of the semiconducting particles. As well, the polymer-semiconductor composites were found to be extremely stable, and could be suspended indefinitely in organic solvents, or precipitated into polar solvents, without agglomeration or significant ripening of CdS particles within the polymer "host". In other work, relationships between ionic block length and core radius were determined for a wide range of polystyrene-*b*-poly(acrylic acid) (PS-*b*-PAA)-based reverse micelles, where the acid block was neutralized with several different counterions (Cs^{+}, Ba^{2+}, Ni^{2+}, Co^{2+}, Cd^{2+}, Pb^{2+}).[12] This provides a versatile system of "tunable" inorganic microreactors, in which precursor ions can be converted to a variety of metallic and semiconducting particles of a specific size at the nanometer scale.

Another aspect of amphiphilic block copolymers that has been investigated extensively in recent years is their tendency to form interesting aggregate morphologies in aqueous solutions.[13-19] Through variations in such parameters as relative block lengths, polymer concentration, solvent composition, and acid or electrolyte addition, a wealth of morphologies, including spheres, rods, vesicles, and several unprecedented bilayer structures, has been observed. Another new morphology found in these systems is the so-called large compound micelle (LCM).[13-15] These are solid, micron-size spheres, generally with large polydispersities, consisting of assemblies of reverse micelles stabilized in water by a thin layer of hydrophilic chains. It has been observed that aqueous suspensions of LCMs do not coalesce, and can be easily resuspended when the larger particles settle to the bottom of the container. In typical LCM-forming systems (e.g. PS-*b*-PAA[13,14] or polystyrene-*b*-poly(ethylene oxide) (PS-*b*-PEO)[15]), the large compound micelles are formed from a single type of block copolymer amphiphile, with most of the hydrophilic chains making up the reverse micelle cores and the remainder stabilizing the assemblies in water.

The present chapter describes the synthesis of quantum-confined CdS nanoparticles within block ionomer reverse micelles, followed by the assembly of the reverse micelles to form aqueous suspensions of LCMs. LCM formation is initiated by the slow addition of water to solutions of CdS-containing reverse micelles and a stabilizing copolymer (PS-*b*-PAA). This is in contrast to previous examples of LCM-forming systems, in which aggregates were prepared from solutions containing only single chains of block copolymer; here, the primary "building blocks" are previously-formed reverse micelles. It should also be noted that the reverse micelles and the stabilizing chains are comprised of different block copolymers, another feature that distinguishes this system from past approaches to LCM formation. The present work can be divided into three distinct steps: (1) self-assembly of block ionomer single chains in organic solvent, (2) synthesis of CdS nanoparticles within the resultant reverse micelles, and (3) "secondary" self-assembly of reverse micelles in aqueous solution. The final structures are comprised of many hydrophilic regions, each containing a semiconducting nanoparticle, dispersed throughout a hydrophobic sphere which is solubilized by a hydrophilic outer shell.

Another approach to the solubilization of hydrophobic micelles in aqueous solutions is demonstrated in onion-type micelles, recently reported by Procházka et al.[20]

Assemblies of quantum dots within a polymer matrix, spatially confined to spherical geometry at the nanometer to micron scale, may have interesting non-linear or electro-optical applications. The aqueous nature of these suspensions is very appealing from the point of view of possible biological applications, and also makes them well-suited to the conversion of water-soluble reagents; in such cases, CdS quantum dots could be replaced by catalytic metal particles. This study represents the first example of quantum-confined semiconductors assembled in a system of water-soluble block copolymers.

6.3. Experimental

6.3.1. Synthesis of PS-b-PAA Diblock Copolymers

The synthesis of PS-*b*-PAA diblock copolymers used in the present study was performed by sequential anionic polymerization of styrene and *tert*-butyl acrylate; since this procedure is described in detail elsewhere,[21-23] only a brief summary is presented here. Polymerization reactions were performed in tetrahydrofuran (THF), using *sec*-butyllithium initiator capped with a few units of α-methylstyrene. The molecular weights and polydispersity indexes (P.I.) of the PS blocks were determined using size-exclusion chromatography (SEC); a small amount of PS was therefore extracted from the reaction solution before addition of the *tert*-butyl acrylate monomer and injected into an SEC column. The molecular weights of the ester blocks were determined by quantitative FTIR of the diblock copolymer. The block copolymers in the ester form were hydrolyzed to PS-*b*-PAA, by refluxing overnight in toluene with *p*-toluenesulfonic acid catalyst. The polymers were then recovered by precipitation into methanol, followed by drying under vacuum at 70 °C for 24 h. Two diblock copolymers were prepared in this manner: PS(240)-*b*-PAA(15) (i.e. 240 PS repeat units and 15 PAA repeat units; P.I. = 1.04) was used to prepare diblock ionomer micelles, in which CdS clusters were synthesized; PS(1100)-*b*-PAA(170) (i.e. 1100 PS repeat units and 170 PAA repeat units; P.I. = 1.06) was used as a stabilizing agent in the preparation of CdS-containing LCMs.

6.3.2. Preparation of PS-b-PACd Reverse Micelles

The copolymer PS(240)-*b*-PAA(15) was dissolved in benzene/methanol (10% methanol v/v) to obtain a 2% polymer solution (w/w). To initiate reverse micelle formation, the acid blocks were neutralized by the addition of excess cadmium acetate dihydrate in methanol (1.5 mol of $CdAc_2{\cdot}2H_2O$: 1 mol acrylic acid repeat units). A slight increase in turbidity indicated the presence of micelles, although a low aggregation number resulted in a relatively clear solution. The solution was stirred for 3-4 h, then the solvent was removed by freeze drying. The diblock ionomer (white powder) was dried at 70 °C overnight in a vacuum oven to remove residual solvent and acetic acid byproduct. Excess cadmium acetate was removed from the ionomer sample by repeated washings in methanol; the washed sample was dried under vacuum at 70 °C. A transparent film of the sample was cast on a KBr window, and FTIR was used to confirm that the acid block was completely neutralized; 100% neutralization was indicated by the disappearance of the carboxylic acid doublet at 1738 and 1710 cm^{-1}.

6.3.3. Preparation of CdS-Diblock Copolymer Composite

Diblock ionomer micelles of polystyrene-*b*-poly(cadmium acrylate) (PS(240)-*b*-PACd(15)) in the powder form were exposed to an atmosphere of 100% humidity for a period of 1 week. The powder was then placed in a closed container, into which "wet" H_2S (H_2S bubbled through water at 70 °C) was introduced. The ionomer powder was thus exposed to an H_2S environment for 8 h, during which time the sample turned yellow in colour; excess H_2S was then removed from the powder by leaving the sample for 12 h under active vacuum.

In the process of CdS particle formation, the ionic blocks become protonated to PAA; it has been found that the stability of the CdS-containing micelles can be greatly improved by "fixing", i.e. reneutralization of the acid blocks.[10] To this end, the reverse micelles were resuspended in THF and a stoichiometric quantity of NaOH was added. The solution was stirred for a least 4 h, then the yellow powder was recovered by precipitation into methanol. The CdS-block copolymer composite after "fixing" was designated CdS-MIC.

6.3.4. Quantum Dot Assemblies: LCM Formation

The composite material, CdS-MIC (yellow powder), was codissolved in N,N-dimethylformamide (DMF) with various quantities of the stabilizing copolymer, PS(1100)-*b*-PAA(170). Four solutions were prepared, in which the amount of stabilizing polymer relative to the total amount of polymer (stabilizing polymer + CdS-MIC) was 10, 12, 21 and 35% (w/w); in all cases, the concentration of CdS-MIC in DMF was 0.7% (w/w). Solutions prepared in this manner were comprised of CdS-containing reverse micelles suspended in a medium of DMF and PS-*b*-PAA single chains. A fifth solution of CdS-MIC without the stabilizing copolymer was also prepared.

The formation of micellar aggregates is generally induced by the addition of a precipitant for the PS blocks (water) to solutions of block copolymers in DMF. In the present case, deionized (Milli Q) water was added slowly to the clear yellow solutions (1 drop every 30 s), with rapid stirring; a dramatic increase in turbidity was observed at a water content of ca. 5% (v/v), indicating the onset LCM formation. In the solution without stabilizing polymer, a significant amount of yellow precipitate formed as water was added; all other solutions appeared to be stable. The addition of water was continued to ca. 40% water, then the turbid solutions were dialyzed against distilled water to remove all DMF. Aqueous solutions prepared with 0, 10, 12, 21, and 35% stabilizing copolymer were designated LCM0, LCM10, LCM12, LCM21, and LCM35, respectively.

6.3.5. UV-Vis Absorption Spectroscopy

UV-Vis absorption spectroscopy of the composite CdS-MIC was performed in toluene solution, in order to characterize the sizes of quantum-confined CdS nanoparticles. Spectra were obtained on a Hewlett-Packard 8452 diode array spectrophotometer, by scanning between 250 and 550 nm. From the spectral absorption edge (λ_e), the CdS nanoparticle diameter was calculated, using Henglein's empirically-determined correlation curve.[24, 25]

6.3.6. Transmission Electron Microscopy

Transmission electron microscopy was performed on a Phillips EM410 instrument, and on a JEOL FX200 instrument with energy-diffusive x-ray diffraction (EDAX) capability. Both instruments were operated at an accelerating voltage of 80 kV.

For the determination of CdS nanoparticle sizes in the "unassembled" reverse micelles, a drop of CdS-MIC in dilute benzene solution (ca. 1 mg/mL) was placed on carbon-coated copper grids (J. B. EM Services Inc); excess solution was immediately removed with a piece of lens paper.

For the observation of LCM aggregates, aqueous solutions were diluted to ca. 1 mg/mL, and deposited onto carbon-coated EM grids; the grids had been precoated with a thin film of Formvar (J. B. EM Services) and then coated with carbon using an Edwards evaporator. A drop of solution was left on each grid for 20 minutes under ambient conditions, after which the remaining solution was blotted away with a piece of lens tissue. To improve contrast for the observation of aggregate particle sizes and distributions, the samples were then shadowed with palladium/platinum alloy at a shadowing angle of 45°. Samples of each LCM solution were also prepared without shadowing, such that the internal structure of the aggregates could be observed. The beam was focused on one of the aggregates, to obtain EDAX elemental analysis of the internal particles. The detection of LCM internal structure was optimized in the under-focus mode, with $\Delta f = 100\text{-}150$ nm. Features of both shadowed and unshadowed micrographs are discussed in the following section.

6.4. Results and Discussion

The absorption spectrum of CdS-containing reverse micelles prior to LCM formation (CdS-MIC) is shown in Figure 6.1A. Since the block copolymer is not expected to show absorbance to the red of 300 nm, the spectrum can be attributed exclusively to the semiconductor particles. The clear appearance of an exciton shoulder and blue-shift of the absorption onset indicate that the CdS particles are quantum-confined, suggesting

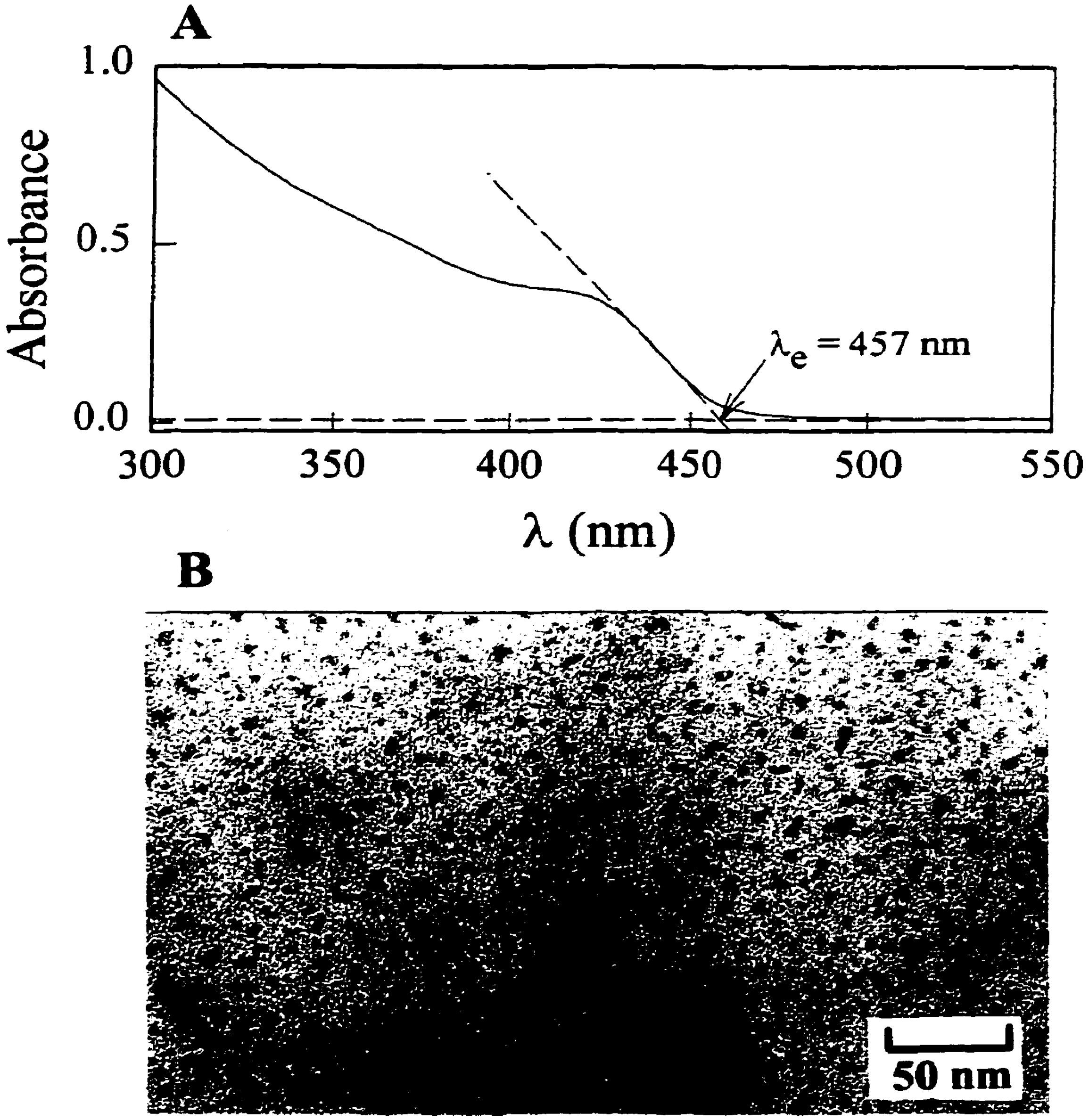

Figure 6.1. (A) UV-vis absorption spectrum of CdS-MIC, showing an absorption edge (λ_e) of 457 nm for the CdS nanoparticles. The semiconductor particle diameter calculated from λ_e is 38 Å. (B) Transmission electron micrograph of CdS-MIC. The dark particles are CdS, with an average diameter of ca. 30 Å.

particle diameters less than 60 Å.[2] From the position of the absorption edge (λ_e), 457 nm, an actual CdS particle diameter of 38 Å was calculated.

An electron micrograph of CdS-MIC (Figure 6.1B) shows an even dispersion of dark semiconductor particles on the grey background of the polymer matrix. The average diameter of the particles is ca. 30 Å, in approximate agreement with UV-vis data. It should be noted that CdS particle sizes calculated from the onset of the absorption spectrum generally represent the larger end of the size distribution, which explains the slightly smaller particle size determined from TEM.

In previous work,[10] the size control of CdS particles in block ionomers was demonstrated, and the following equation, describing the relationship between ionic block lengths and the radii of nanoparticles synthesized in the micelle core, was determined:

$$R_{CdS} = 1.9 N_B^{3/5} + 9.4\text{Å} \qquad (1)$$

where N_B is the number of repeat units in the ionic block and R_{CdS} is in units of Å. Applying eq 1 to the block ionomer "host" used in this study (N_B = 15), a CdS particle radius of 19 Å ($2R_{CdS}$ = 38 Å) is calculated, which agrees exactly with the UV-Vis results. This suggests that the mechanism of size control described previously, involving complete conversion of ions in the micelle core to a single semiconductor particle, is operative in the present case.

When water is slowly added to mixtures of CdS-containing micelles and stabilizing copolymer in DMF, the turbidity of the clear yellow solutions increased markedly at a water concentration of ca. 5% (v/v). The solutions remained turbid, though stable, as the water concentration was increased further and the DMF was removed by dialysis. No macroscopic precipitation of the reverse micelles was observed, suggesting that they had been successfully solubilized in water. TEM of the aqueous solution revealed populations of spherical aggregates; the average size of the aggregates and the number of populations observed in the samples were dependent on the amount of stabilizing copolymer, with most solutions showing two distinct populations. Possible reasons for these dependencies are described later; for now, the discussion turns to one sample, LCM12 (12% stabilizing copolymer), in which a single population of spherical aggregates was observed.

Spherical aggregates in sample LCM12, with and without shadowing, are shown in the transmission electron micrographs of Figure 6.2. In the shadowed picture (Figure 6.2A), the Pd/Pt coating significantly increases the contrast of the whole aggregates relative to the background, and a single population of spheres is clearly visible. Distribution analysis of a larger sample than that shown in the figure reveals an average particle diameter, D_{agg}, of 64 nm, with a standard deviation of 8 nm. A micrograph of the same sample without shadowing (Figure 6.2B) reveals the internal structure of the aggregates, suggesting that they are large compound micelles (LCMs), rather than regular spherical micelles. The dark particles dispersed in the aggregates (unshadowed micrograph) are believed to be CdS nanoparticles in the cores of assembled reverse micelles; this is supported by (1) the yellow colour of the turbid solution, indicating that the CdS particles of CdS-MIC have been incorporated into the aqueous aggregates (2) the size of the dark particles (30 Å), which matches that of CdS particles in CdS-MIC (Figure 6.1B), and (3) energy-dispersive x-ray diffraction results (Figure 6.3), which show both Cd and S bands when the electron beam is focused inside one of the aggregates. The prominent Cu and Si bands are due to the EM grid and trace quantities of stopcock grease, respectively. The LCMs in Figure 6.2A are relatively monodisperse, compared with those formed from single chains of PS-*b*-PAA or PS-*b*-PEO.[13-15]

A schematic diagram of a large compound micelle such as that found in sample LCM12 (Figure 6.4) depicts a spherical assembly of reverse micelles, each with a hydrophilic core consisting of a single CdS particle and a thin layer of poly(sodium acrylate); PS chains radiate from these cores into the surrounding melt. The driving force for LCM formation is mainly enthalpic: the continuous addition of water to a solution of reverse micelles makes interactions between the solvent and the PS corona increasingly unfavourable; the reverse micelles eventually coprecipitate with the long PS blocks of the stabilizing copolymer. This process can be termed "secondary" self assembly, to distinguish it from the original formation of reverse micelles via "primary" self-assembly of ionic block copolymers in organic solvent.

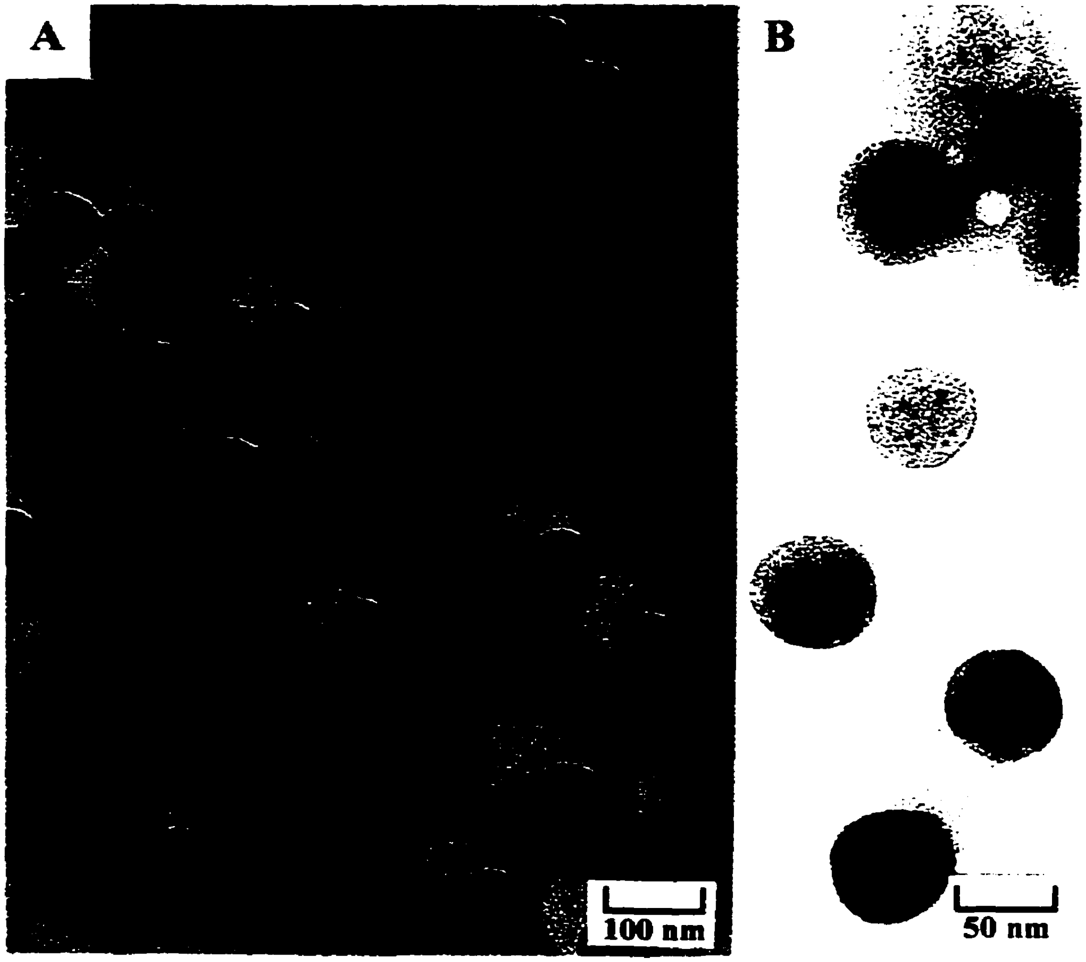

Figure 6.2. (A) Transmission electron micrograph of spherical aggregates in LCM12, with Pd/Pt shadowing and (B) without shadowing. The dark particles inside the spheres are CdS nanoparticles.

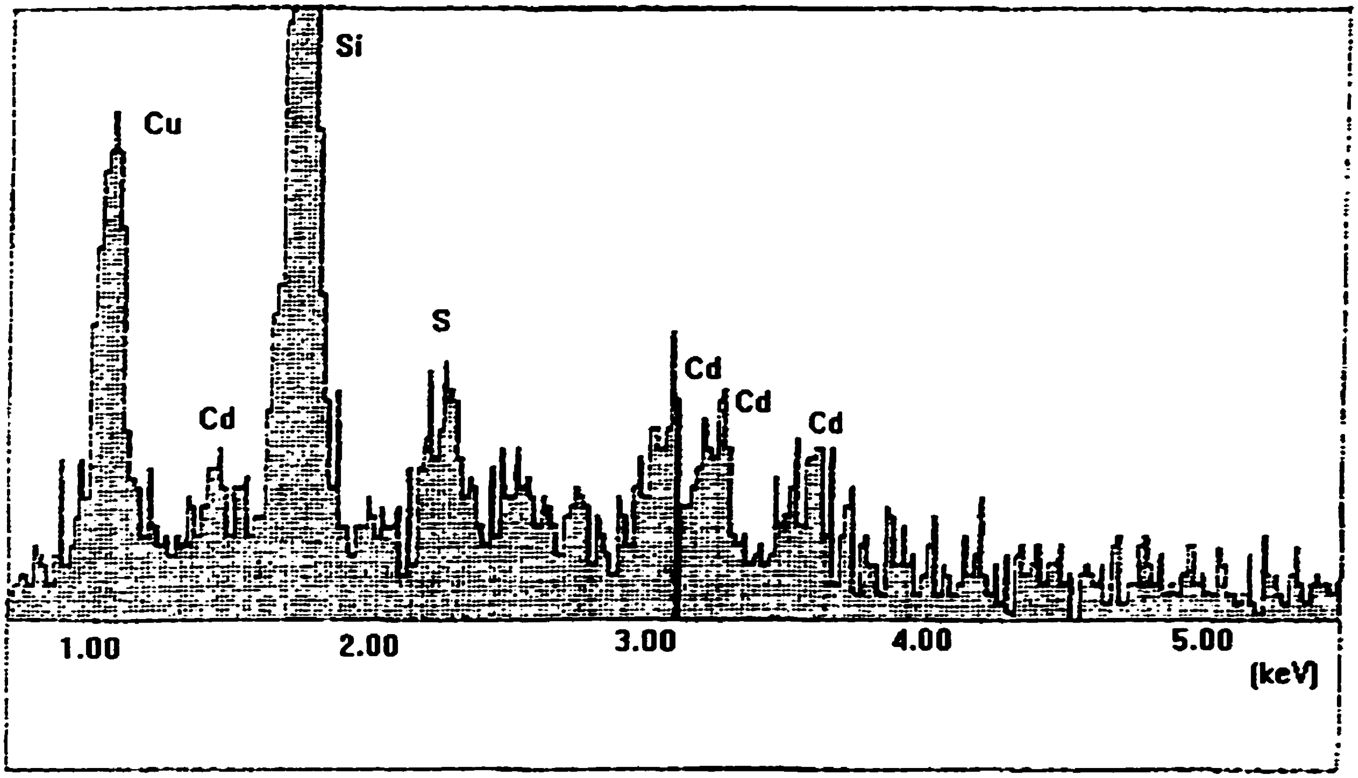

Figure 6.3. Energy-dispersive X-ray diffraction (EDAX) pattern of one of the aggregates containing dark particles, showing Cd and S bands.

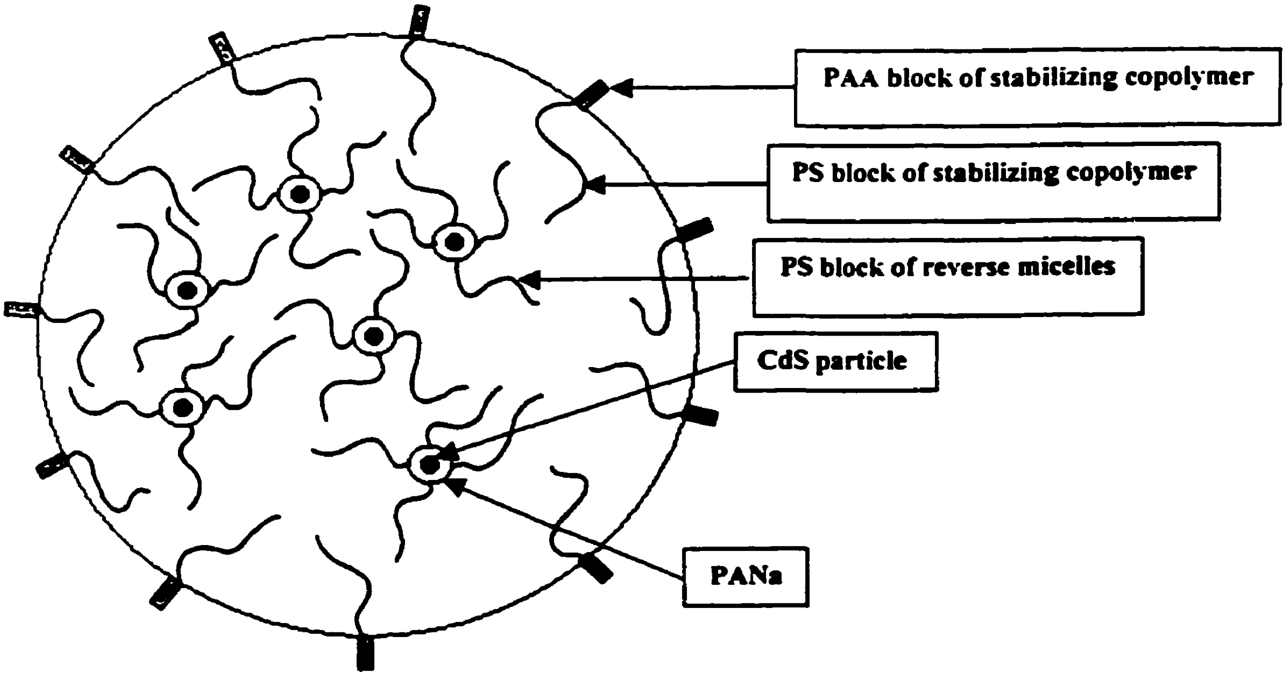

Figure 6.4. Schematic diagram of a large compound micelle (LCM) containing CdS nanoparticles. The spherical aggregate is an assembly of reverse micelles, stabilized with added block copolymer.

As shown in Figure 6.4, single chains of the stabilizing copolymer distribute themselves at the surface of the LCM, minimizing interfacial tension through favourable interactions between water and the "free" PAA blocks; this, in effect, prevents flocculation of the aggregates and macroscopic precipitation of the reverse micelles. The copolymer chains which constitute the reverse micelles are essentially locked into the hydrophilic cores through strong ionic interactions, and are therefore unable to play a stabilizing role. The low polydispersity of the LCMs may be related to the restricted movement of these chains, which is governed by the movement of reverse micelles during secondary self-assembly.

From the average radius of the aggregates, R_{agg}, it is possible to calculate the average number of reverse micelles, N_{rm}, and stabilizing copolymer chains, N_{sc}, which make up the LCMs in Figure 6.2. The average volume of the aggregates is calculated from

$$V_{agg} = \frac{4}{3}\pi R_{agg}^3 \qquad (2)$$

The LCM volume is the sum of the total volume of reverse micelles and stabilizing copolymer in the aggregate, such that

$$V_{agg} = N_{rm} V_{rm} + N_{sc} V_{sc} \qquad (3)$$

where V_{rm} and V_{sc} are the volumes of reverse micelles and stabilizing copolymer chains, respectively; these values can be calculated from the composition of both block copolymers and the aggregation number of the reverse micelles, Z:

$$\begin{aligned} V_{rm} &= Z[240 v_{PS} + 15 v_{PANa}] + V_{CdS} \\ V_{sc} &= 1100 v_{PS} + 170 v_{PAA} \end{aligned} \qquad (4)$$

where v_{PS}, v_{PANa}, and v_{PAA} are the bulk volumes of individual repeat units of polystyrene, poly(sodium acrylate), and poly(acrylic acid), respectively, and V_{CdS} is the average volume of a CdS nanoparticle within each reverse micelle. The aggregation number of the reverse micelles, Z, is determined from published scaling relations to be ca. 50.[12] Similarly, the masses of the reverse micelles and stabilizing copolymer chains can be calculated from:

$$\begin{aligned} m_{rm} &= Z[240 m_{PS} + 15 m_{PANa}] + m_{CdS} \\ m_{sc} &= 1100 m_{PS} + 170 m_{PAA} \end{aligned} \qquad (5)$$

where m_{PS}, m_{PANa}, and m_{PAA} are the masses of polystyrene, poly(sodium acrylate), and poly(acrylic acid) repeat units, and m_{CdS} is the average mass of CdS nanoparticles.

Assuming that all of the stabilizing copolymer in sample LCM12 is evenly distributed throughout the population of aggregates, N_{rm} and N_{sc} can also be expressed in terms of the following equation:

$$\frac{N_{sc} m_{sc}}{N_{rm} m_{rm} + N_{sc} m_{sc}} = 0.12 \qquad (6)$$

where 0.12 is the mass fraction of stabilizing copolymer in LCM12.

Combining eqs 2-6 for an LCM radius of $R_{agg} = 32$ nm, it was determined that an average aggregate in sample LCM12 is an assembly of 58 reverse micelles ($N_{rm} = 58$) and 87 chains of the stabilizing copolymer ($N_{sc} = 87$). This implies that an average of 58 quantum-confined CdS particles are evenly distributed throughout the mainly-polystyrene spheres. From the volume of reverse micelles within the aggregates (V_{rm}), an average spacing of 12 nm between CdS particles was calculated. The spacings between particles within the aggregates should be quite monodisperse, as they are mainly governed by the bulk volume of the reverse micelle coronal layers. It should also be noted that particle-particle spacing could be easily "tuned" by using reverse micelles with different PS block lengths.

A fundamental parameter in aggregate formation is the interfacial area per stabilizing copolymer chain, A_{sc}.[14] For the single population of aggregates in sample LCM12, A_{sc} is calculated from N_{sc} and the average LCM surface area ($A_{agg} = 4\pi R_{agg}^2$) to be 148 nm^2 per chain. This value can be compared with A_{sc} calculated for regular spherical micelles formed from the stabilizing copolymer alone (i.e. PS(110)-*b*-PAA(170) without reverse micelles), which is 38 nm^2 per chain. Other work on PS-*b*-PAA morphologies have also found that A_{sc} values are significantly higher in LCMs than in regular micelles, resulting in larger surface tension contributions to the total free energy of the larger structures.[14]

In the early stages of LCM formation, when the PS regions are sufficiently swollen with DMF, a dynamic equilibrium is assumed to exist between the aggregates and their components (reverse micelles and stabilizing copolymer), such that the structures are an expression of a free energy minimum. As more DMF is forced out by the addition of water, however, the mobility of PS chains in the aggregates decreases, and the LCMs become essentially frozen. The final surface area per chain, A_{sc}, will therefore reflect a minimization of surface energy at a stage when both the polymer aggregates and the surrounding medium contain a considerable amount of organic solvent.

Table 6.1. Spherical aggregate populations from mixtures of CdS-MIC and PS-*b*-PAA stabilizing copolymer

sample	wt. % PS-*b*-PAA[a]	observed aggregate populations[b]
LCM0	0	1. LCMs (CdS); D_{agg} = 100 nm[c]
LCM10	10	1. LCMs (CdS); D_{agg} = 152 nm 2. LCMs (CdS); D_{agg} = 52 nm
LCM12	12	1. LCMs (CdS); D_{agg} = 64 nm
LCM21	21	1. LCMs (CdS); D_{agg} = 63 nm 2. PS-*b*-PAA micelles; D_{agg} = 21 nm
LCM35	35	1. LCMs (CdS); D_{agg} = 50 nm 2. PS-*b*-PAA micelles; D_{agg} = 21 nm

[a] Weight percentage is relative to total polymer in solution. [b] "CdS" in brackets indicates that aggregates contain CdS particles. [c] Extensive macroscopic precipitation of CdS-MIC also observed in LCM0.

As the amount of stabilizing copolymer is varied, TEM reveals distinct changes in the LCM populations; a summary of observed populations for different amounts of added PS-*b*-PAA is presented in Table 6.1. Micrographs of shadowed and unshadowed EM grids are shown in Figure 6.5, for samples prepared with 10, 21, and 35% of the copolymer PS(1100)-*b*-PAA(170). Whereas a single population (D_{agg} = 64 nm) was found with 12% stabilizing polymer, the sample prepared with 10% stabilizing polymer, LCM10 (Figure 6.5A), clearly contains two populations of spheres, with average diameters of 52 and 152 nm. Figure 6.5B shows a portion of the unshadowed grid, with several of the smaller spheres and a typical large sphere; the micrograph reveals that large and small aggregates both contain CdS particles, suggesting that both populations were formed by a mechanism of reverse micelle assembly. When the amount of stabilizing copolymer is increased to 21% (LCM21, Figure 6.5C), we find a population of spheres, D_{agg} = 63 nm, very similar to those formed at 12%, along with a second, much smaller, population (D_{agg} = 21 nm). Microscopy of the unshadowed grid of LCM21 (Figure 6.5D) shows the larger spheres to have internal structure, while the 21 nm particles appear as featureless "blotches" against the background, indicating that they do not contain any semiconductor particles. The situation is very similar when the amount of stabilizing copolymer is increased to 35% (Figure 6.5E), though the larger population has shifted to slightly smaller spheres (D_{agg} = 50 nm), compared with those in LCM21. The smaller population (D_{agg} = 21 nm) is identical to that found with 21% stabilizer, and again does not show evidence of internal structure (Figure 6.5F). Qualitative comparison of LCM21 and LCM35 suggests a greater number of smaller spheres on grids of the latter sample.

These results suggest that a single distribution of aggregates can only be obtained in a narrow window of conditions, i.e. ca. 12% of stabilizing copolymer for the concentration of reverse micelles used in this study. On the other hand, similar populations of spheres, with average diameters in the range 50-64 nm, are observed in all four samples containing stabilizing copolymer. This is not surprising, since the size of the CdS-containing aggregates will depend on the number of nucleation sites during secondary self-assembly, and is therefore largely governed by the initial concentration of reverse micelles. The additional presence of larger LCMs in sample LCM10 (Figure 6.5A

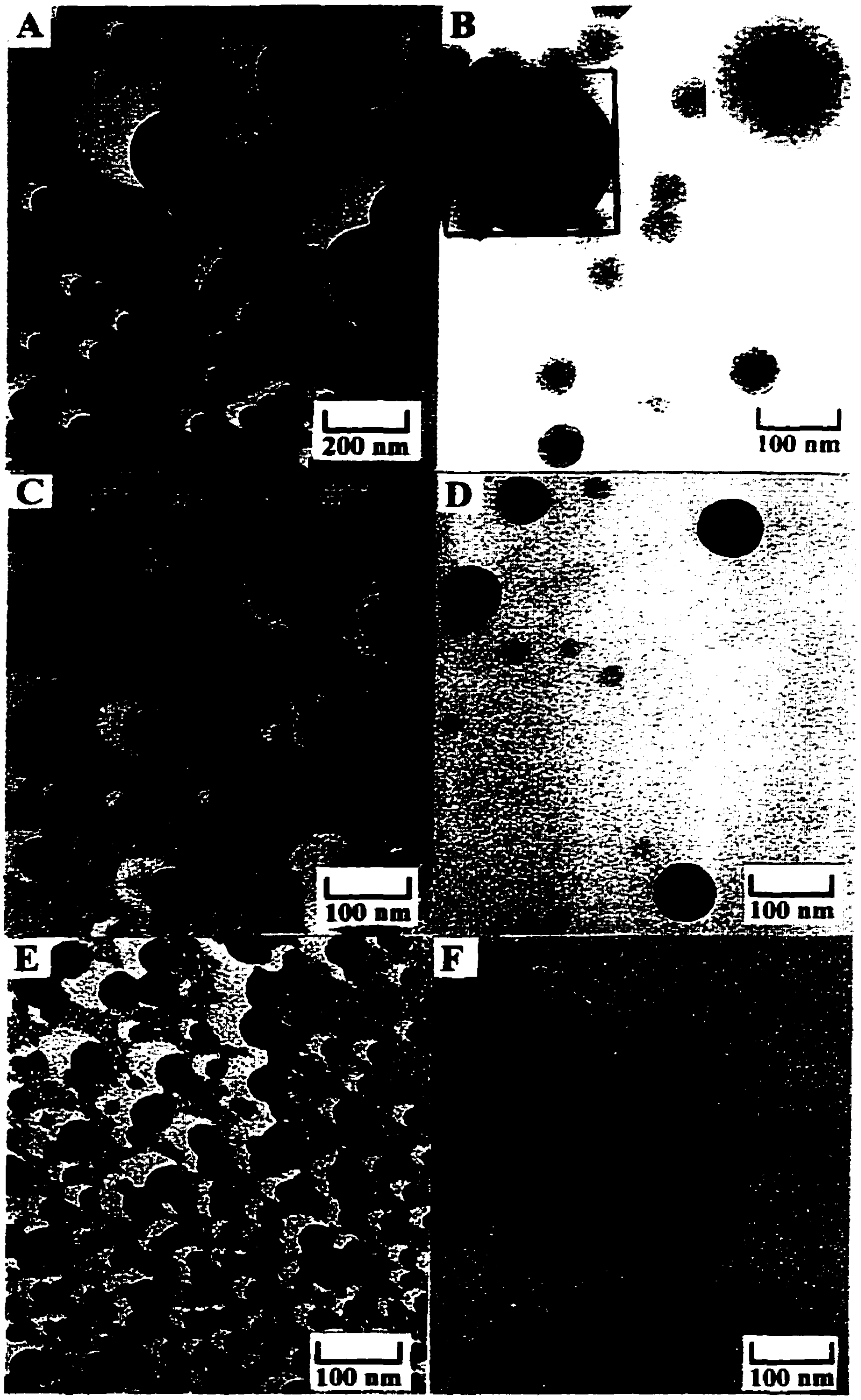

Figure 6.5. Transmission electron micrographs of LCM10, (A) with shadowing and (B) without shadowing; LCM21, (C) with shadowing and (D) without shadowing; LCM35, (E) with shadowing and (F) without shadowing. In B, the insert shows the boxed region at a lower exposure time, revealing the internal structure of the large spherical aggregate.

and B) suggests the crossing over of a phase boundary between 10 and 12% stabilizing copolymer. In the 10% sample, the initial formation of nucleation sites depends only on the concentration of reverse micelles, which accounts for the presence of the smaller spheres (D_{agg} = 52 nm); a lack of stabilizing copolymer, however, necessitates the clustering of some nucleation sites to decrease the total surface area of the system, resulting in a second population of much larger spheres (D_{agg} = 152 nm).

In the 21 and 35% samples, not all of the added block copolymer is required to stabilize the assemblies of reverse micelles; the "excess" copolymer, PS(1100)-*b*-PAA(170), therefore forms regular micelles with polystyrene cores and a poly(acrylic acid) corona. These are the small spheres (D_{agg} = 21 nm) in samples LCM21 and LCM35 that do not contain CdS particles. Since the amount of stabilizing copolymer is greater in LCM35 than in LCM21, a greater concentration of regular micelles is found in the former sample. It is also noteworthy that the average diameter of the LCM population (larger spheres) decreases between 21 and 35%, which suggests that some of the "excess" stabilizer in LCM35 is actually incorporated into the large compound micelles, allowing a decrease in particle size via a lowering of the surface energy. It therefore appears likely that, below a certain concentration of added water, the equilibrium between single chains and regular micelles exists in tandem with the equilibrium between LCMs and their reverse micelle and single chain components.

In the absence of stabilizing copolymer (LCM0), most of the reverse micelles precipitated from solution as water was added. The yellow material settled to the bottom of the vial, though the remainder of the solution was found to be extremely turbid. Following dialysis, electron microscopy of the turbid solution revealed a number of CdS-containing LCMs, with an average diameter of ca. 100 nm. It has been found that a low concentration of single chains will exist in any solution of block ionomer reverse micelles, due to the small number of chains with ionic blocks too short to undergo self-assembly.[22] It is thought that, without added copolymer, these single chains are able to act as stabilizers, allowing the reverse micelles that do not precipitate from solution to form spherical assemblies.

6.5. Conclusions

Novel spherical assemblies of quantum-confined semiconductors in aqueous solution have been prepared, by the slow addition of water to reverse micelles and a stabilizing block copolymer in organic solvent. The assemblies are best described as large compound micelles (LCMs), consisting of CdS nanoparticles ($2R_{\mathrm{CdS}} \sim 30$ Å) dispersed throughout a PS sphere which is stabilized in water by a layer of hydrophilic PAA chains. When the amount of stabilizing copolymer relative to the total amount of polymer was 12% (w/w), a single population of LCMs ($D_{\mathrm{agg}} =$ 64 nm) was observed; it was determined that these aggregates consist of an average of 58 reverse micelles and 87 stabilizing chains. At 10% stabilizing copolymer, two populations of LCMs were observed ($D_{\mathrm{agg}} = 52$ nm and $D_{\mathrm{agg}} = 152$ nm); the larger population is attributed to the agglomeration of nucleation sites due to a lack of stabilizer. When the concentration of stabilizing copolymer was sufficiently high (21 and 35%), regular micelles with no internal structure were found to coexist with LCMs. The amount of stabilizing copolymer required to obtain a given population is believed to be dependent on both the concentration and composition of the reverse micelles; this implies an inherent versatility in the system, through variations in several adjustable parameters. In the absence of stabilizing copolymer, most reverse micelles were found to precipitate upon water addition, although a number of LCMs were observed in the remaining solution; these are thought to be stabilized by single chains of low ionic content in the solution of reverse micelles.

Along with being a novel morphology, assemblies of semiconducting or metallic nanoparticles confined to polymer spheres of small dimensions may have numerous applications to nonlinear optics, electro-optical devices, or catalysis. For some applications, the PS matrix could be easily replaced by conducting or semiconducting organic polymers. Since the spheres are suspended in aqueous solution, they are also amenable to biological systems, in which catalytic or photocatalyic properties could be exploited.

This ends our discussion of block ionomers as tunable microreactors; the next two chapters are devoted to the study of structure within the nonionic coronae of block ionomer micelles. Just as the starlike composition regime (small cores, long coronal chains) is interesting from the point of view of nanoparticle synthesis, it is also interesting in terms of solution stability, as it is the coronal segment density profile of a starlike "brush" that governs the interactions between particles. The study of structure in starlike polymer brushes, such as those found in the coronae of block ionomer micelles, has been a topic of both theoretical and experimental interest, although direct empirical studies on these systems are still quite limited. We recognize that starlike block ionomers are a useful model system for the fundamental investigation of brush structure, due in part to their similarity to polymer-stabilized colloidal particles of many commercial applications. For the use of block ionomers as inorganic microreactors, a knowledge of coronal structure is also helpful, as it may provide clues on interactions between micelle-encased nanoparticles in organic solvents.

Acknowledgments

This work was supported by the Natural Sciences and Engineering Research Council of Canada (NSERC). M.M. is grateful for scholarship funding provided by NSERC and Le Fonds pour la Formation de Chercheurs et L'Aide à la Recherche (FCAR, Quebec). The authors gratefully acknowledge Dr. L. Zhang for useful discussions and for providing the stabilizing copolymer sample.

References

(1) Brus, L. E. *J. Chem. Phys.* 1983, *79*, 5566; Brus, L. E. *J. Chem. Phys.* 1984, *80*, 4403.

(2) Henglein, A. *Chem. Rev.* 1989, *89*, 1861.

(3) Tuzar, Z.; Kratochvil, P. *Adv. Colloid and Interface Sci.* 1976, *6*, 201.

(4) Price, C. In *Developments in Block Copolymers,* Vol 1; Goodman, I., Ed.; Applied Science Publishers: London, 1982, p.39.

(5) Tuzar, Z.; Kratochvil, P. In *Surface and Colloid Science*, Vol 15; Matijevic, E., Ed.; Plenum Press: New York, 1993, p.1.

(6) Möller, M. *Synth. Met.* 1991, *41-43*, 1159.

(7) Cummins, C. C.; Schrock, R. R.; Cohen, R. E. *Chem. Mater.* 1992, *4*, 27.

(8) Ng Cheong Chan, Y.; Craig, G. S. W.; Schrock, R. R.; Cohen, R. E. *Chem. Mater.* 1992, *4*, 885; Ng Cheong Chan, Y.; Schrock, R. R.; Cohen, R. E. *J. Am. Chem. Soc.* 1992, *114*, 7295; Yue, J.; Sankaran, V.; Cohen, R. E.; Schrock, R. R. *J. Am. Chem. Soc.* 1993, *115*, 4409; Cohen, R. E.; Yue, J. *Supramolecular Science* 1994, *1*, 117.

(9) Antonietti, M.; Wenz, E.; Bronstein, L.; Seregina, M. *Adv. Mater.* 1995, *7*, 1000.

(10) Moffitt, M.; McMahon, L.; Pessel, V.; Eisenberg, A. *Chem. Mater.* 1995, *7*, 1185.

(11) Spatz, J.; Roescher, A.; Möller, M. *Adv. Mater.* 1996, *8*, 337.

(12) Moffitt, M.; Eisenberg, A. *Macromolecules* 1997, *in press.*

(13) Zhang, L.; Eisenberg, A. *Science* 1995, *268*, 1728.

(14) Zhang, L.; Eisenberg, A. *J. Am. Chem. Soc.* 1996, *118*, 3168.

(15) Yu, K.; Eisenberg, A. *Macromolecules* 1996, *29*, 6359.

(16) Yu, K.; Zhang, L.; Eisenberg, A. *Langmuir* 1996, *12*, 5980.

(17) Zhang, L.; Yu, K.; Eisenberg, A. *Science* 1996, *272*, 1777.

(18) Zhang, L.; Eisenberg, A. *Macromolecules* 1996, *29*, 8805.

(19) Yu, Y.; Eisenberg, A. *J. Am. Chem. Soc.* 1997, *in press.*

(20) Procházka, K.; Martin, T. J.; Webber, S. E.; Munk, P. *Macromolecules* 1996, *29*, 6526.

(21) Gauthier, S.; Duchesne, D.; Eisenberg, A. *Macromolecules* 1987, *20*, 753.

(22) Desjardins, A.; Eisenberg, A. *Macromolecules* 1991, *24*, 5779.

(23) Zhong, X. F.; Varshney, S. K.; Eisenberg, A. *Macromolecules* 1992, *25*, 7160.

(24) Spanhel, L.; Haase, M.; Weller, H.; Henglein, A. *J. Am Chem. Soc.* 1987, *109*, 5649.

(25) The data in ref. 24 has been digitized, to obtain the equation:

$2R_{CdS} = 1/(0.1338\text{-}0.0002345\lambda_e)$.

CHAPTER 7

Coronal Structure and Interparticle Overlap in Starlike Block Ionomer Micelles

7.1. Abstract

Small-angle neutron scattering (SANS) is used to investigate the stiffness of perdeuterated polystyrene (dPS) labels within the polystyrene (PS) coronae of starlike block ionomer micelles. Measurements are made in both good and near-θ solvents, at polymer concentrations near and above the micelle overlap concentration (c^*). Two micelle samples are investigated, in which dPS labels are located at either 820 or 1080 PS units from the ionic core. Scattering profiles are analyzed for intermediate values of q, and information on chain statistics is obtained from the scaling relation $I \sim q^{-\alpha}$. In toluene (good solvent) at 3 wt. % polymer, Kratky plots of $Iq^{5/3}$ vs. q indicate $q^{-1.7}$ scaling for scattered intensity in the intermediate region, above a minimum vector, q^*. q^* is found to decrease as the distance from the core increases. These results are in qualitative agreement with the "blob" model for starlike spherical brushes. At 5 wt. % in toluene, the stiffness of dPS labels increases; this observation is attributed to steric crowding at the extremities of the coronae, as the overlap of neighbouring micelles becomes considerable. In cyclohexane at 40 °C (near-θ conditions) at 3 wt. % polymer, dPS labels are highly extended, and scattered intensity shows the q^{-1} scaling of rigid rods for $q > 0.1$ Å^{-1}. This "worm-like" behaviour of the coronal labels is found to disappear at 5 wt. %, where chain statistics begin to resemble a polymer melt. Hydrodynamic radii (R_h) are also determined

under dilute conditions using dynamic light scattering (DLS), and percentages of coronal extension are calculated from these results.

7.2. Introduction

The self-assembly of block copolymers in selective solvents has generated a great deal of interest in recent years, and the resulting cooperative structures have been studied by a range of techniques, both in solution and in the solid state.[1-3] In particular, scattering methods (e.g. static and dynamic light scattering, small-angle x-ray scattering, small-angle neutron scattering) have proven invaluable for the elucidation of detailed structural information on block copolymer micelles (and other aggregate morphologies) at various length scales. Although light scattering techniques can be used to determine such fundamental micellar parameters as aggregation numbers, radii of gyration, and hydrodynamic radii, the spatial resolution of these methods is ultimately limited by the wavelength of visible light. To obtain more detailed information on aggregate morphologies, core radii, and coronal chain conformations, investigators have relied on the structural resolution available from small-angle scattering (SAS) techniques, such as small-angle x-ray scattering (SAXS)[3, 4-8] and small-angle neutron scattering (SANS).[3, 5, 9, 10] In the latter experiment, the large difference between the scattering lengths of deuterium and hydrogen nuclei can be used to advantage, through various methods of deuterium labeling and contrast-matching. In this manner, SANS opens the door to detailed and spatially-specific information on the structure of block copolymer micelles. The study of coronal chain conformations in block copolymer micelles and related systems has largely been spurred by the industrial applications of spherical polymer brushes, which have been employed in the stabilization and surface modification of colloids.[11]

In the interpretation of small-angle scattering profiles for polymer chains, information on chain statistics is extracted from the scaling of intensity with the scattering vector, q, in the intermediate region.[12] At intermediate values of q, the scattering behaviour of a polymer does not depend on molecular weight, and scattered intensity is found to scale as $q^{-\alpha}$, where the characteristic exponent, α , yields crucial information on chain stiffness. In general, α decreases as the chains become more extended, or perturbed from their "random-walk" behaviour: for Gaussian chains, $\alpha = 2$; for swollen coils, $\alpha = 5/3$; for "worm-like" or fully extended chains, $\alpha = 1$.

Starlike spherical brushes have been described by Daoud and Cotton as a semidilute solution of polymer chains, where the segment density decreases with distance from the center of the star.[13] In a semidilute polymer solution, steric correlations between neighbouring chains result in the overall extension of polymer chains; these correlations act over distances ξ_E, known as the Edwards screening length.[14] deGennes[15] has described semidilute solutions using the concept of "blobs", which are spherical regions of diameter $\xi(\varphi)$ in which local single chain behaviour is found; the size of the blob depends only on the local volume fraction of polymer segments (φ).

Both the screening length and blob concepts imply that the scattering profile of a semidilute polymer solution will have a minimum scattering vector for the intermediate region, q^*, above which the scattering is identical to that from single chains (or dilute solutions).[5] This follows from the reciprocal relation between the scattering vector and distance; for $q > q^*$, the scattered intensity probes distances in the semidilute solution shorter than the screening length or blob size. As the density of polymer segments increases, interchain correlations act over shorter distances[15], resulting in a decrease in the screening length (or the blob size) and a concurrent increase in q^*.

In the Daoud and Cotton model, a polymer chain in a starlike brush is represented by a string of blobs with diameters $\xi(r)$.[13] As the radial distance from the center of the brush, r, decreases, the segment density increases and the blob size becomes correspondingly smaller. This suggests that polymer chains are more perturbed by neighbouring chains near the center of a starlike brush, where steric crowding is more severe. The model is represented in the following diagram:

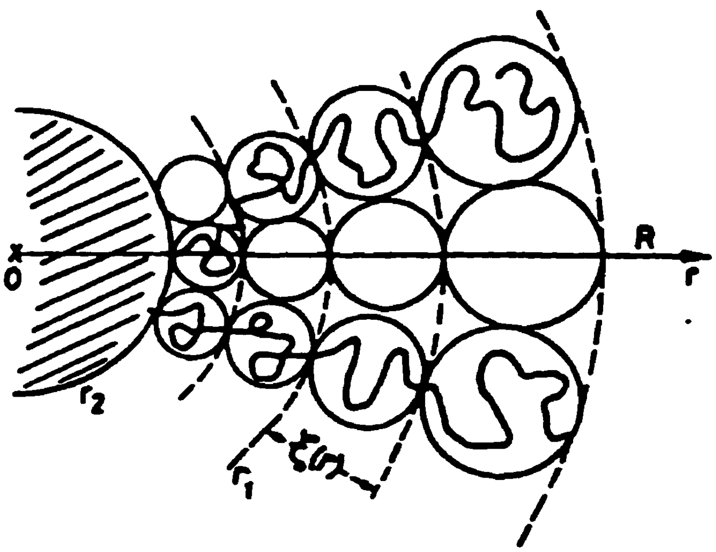

Gast and coworkers used SAXS and SANS to investigate the coronal structure of polystyrene-*b*-poly(ethylene oxide) (PS-*b*-PEO) micelles in both cyclopentane and deuterated cyclohexane (selective solvents for the PS block).[5] The Daoud and Cotton model of starlike brushes was applied to interpret SAXS data for block copolymer micelles with short core-forming blocks and large aggregation numbers. For such systems, Kratky plots (Iq^{α} vs. q, where $\alpha = 2$ under θ conditions) revealed single chain scaling behaviour at scattering vectors larger than q^*, and average blob sizes for the coronae were determined. In micelles of symmetric PS-*b*-PEO, it was found that the coronal chains were more highly perturbed than in starlike structures, such that single chain correlations were not observed on any length scale. The authors noted that severe chain stretching in symmetric systems reflects a high density of polymer segments close to the micelle core, where the concept of blobs, valid for semidilute solutions, does not seem to hold.

Another example of starlike brushes are solutions of star polymers, which have also been the subject of small-angle neutron experiments.[16-19] This work has included the elegant use of labeling techniques, in which the inner cores and outer shells of star polymers were selectively deuterated.[16, 17] Since only the deuterated polymer is in contrast with the surrounding solvent (and therefore "seen" by the neutrons), the authors were able to show that star polymers are more severely stretched close to their center, where the correlation between arms is strongest.

Along with the structure of individual starlike brushes, small-angle scattering techniques can be used to probe star-star interactions at high polymer concentrations. These effects have been monitored primarily at low q values (i.e. large length scales), revealing the influence of interparticle interactions on the radius of gyration and solution structure. In polymer micelle solutions above a critical volume fraction, scattering profiles have shown disorder to order transitions in the structure factor.[6] In solutions of star polymers, correlations between particles were found to influence the low-q Guinier region of the scattering profiles, even below the overlap concentration c^*.[18] At smaller length scales (higher q values), however, the scattering did not change significantly at high concentrations, suggesting that chain statistics were not influenced by interparticle effects. In another study, the radii of gyration of star polymers were plotted as a function of concentration. For this system, R_g was found to be constant up to c^*, and then to decrease at higher concentrations.[19]

In the present work, SANS has been used to investigate the stiffness of perdeuterated PS "labels" within starlike reverse micelles of polystyrene-*b*-poly(cesium acrylate) (PS-*b*-PACs), at polymer concentrations near and above the micelle overlap concentration c^*. Both "good" and near-θ solvent conditions are explored. Block ionomer micelles are ideal species for studies of this type, since they are extremely stable, and can therefore be dissolved in different organic solvents without changes in aggregation number or swelling of the core. Detector distances have been chosen to optimize data collection at intermediate q values, so that the effects of micelle-micelle interactions on coronal chain statistics could be studied. Due to large uncertainties in low-q intensities under these conditions, R_g values of the deuterated labels could not be determined from SANS data.

Two species of block ionomers have been prepared, with perdeuterated polystyrene (dPS) labels of ca. 200 units located at slightly different positions relative to the ionic core. Both samples consist of four blocks: a PS tail, a dPS label, a PS spacer, and the PACs core-forming block. Calculations of scattering cross sections indicate that only the high-contrast labels contribute significantly to coherent scattering profiles. For the two ionomer samples, the PACs blocks make up only ca. 5 mol % of the total diblock, such that the PS coronae behave in the manner of a starlike brush.

7.3. Experimental

7.3.1. Synthesis of PS-b-dPS-b-PS-b-PAA Block Copolymers

PS-*b*-dPS-*b*-PS-*b*-PtBuA block copolymers were prepared by the sequential anionic polymerization of styrene, perdeuterated styrene, and *tert*-butylacrylate in tetrahydrofuran solvent (THF). *sec*-Butyllithium was used as the initiator, and lithium chloride (LiCl) and α-methyl styrene were capping agents. The degree of polymerization of PS and dPS blocks, and the total polydispersity indexes of the block copolymers, were determined by size-exclusion chromatography (SEC). The P.I. values for the two samples were as follows: sample I, P.I. = 1.07; sample II, P.I. = 1.08. Poly(*tert*-butylacrylate) block lengths were determined by quantitative FTIR (Perkin-Elmer 16 PC apparatus) of block copolymers dissolved in carbon tetrachloride. The poly(*tert*-butylacrylate) blocks were subsequently hydrolyzed to poly(acrylic acid) (PAA), by dissolving the polymers in an 80/20 (v/v) mixture of toluene/acetic acid and refluxing for 2 h with methane sulfonic acid catalyst. Hydrolyzed samples were precipitated into methanol, then dried under vacuum at 70 °C for ca. 24 h.

7.3.2. Preparation of Block Ionomer Micelles

To form reverse micelles from the block copolymers, samples in the acid form were dissolved in a 90/10 (v/v) mixture of benzene/methanol to a polymer concentration of 2 wt. %. In this solvent mixture, both the styrene and acid portions of the copolymer are soluble, and the solution therefore contained only single chains. Micellization was then induced by stoichiometric neutralization of the PAA blocks with a 0.25 M methanolic solution of cesium hydroxide monohydrate ($CsOH \cdot H_2O$). The solutions were stirred for 2 h, followed by the removal of solvent by freeze drying. The block ionomer micelles were recovered as a white powder, which was dried under vacuum at 70 °C for at least 4 h. FTIR spectroscopy was used to confirm that both samples were completely neutralized.

The two block ionomer samples are designated sample I and sample II, and have the following compositions: sample I, PS(70)-**dPS(210)**-PS(820)-*PACs(50)* and sample II, PS(250)-**dPS(220)**-PS(1080)-*PACs(77)*. Numbers in brackets represent the number of repeat units in each block. For the sake of clarity, the dPS label is indicated in bold characters and the PACs block is italicized. In later sections of this paper, the polymer compositions are displayed using only degrees of polymerization for each block, e.g. sample I (70-**210**-820-*50*).

7.3.3. Size-Exclusion Chromatography of Block Ionomers

Size-exclusion chromatography (SEC) measurements of the reverse micelles were performed using a Waters Model 510 liquid chromatograph equipped with a Varian RI-4 refractive index detector and the Millenium 2010 software package. Small quantities of block ionomer samples I and II were dissolved in THF, and these solutions were filtered through membrane filters with a nominal pore size of 0.45 μm, then diluted to a concentration of about 2 g/L before injection into the SEC columns. Chromatograms showed two peaks at high and low elution volumes, attributed to single chains and micelles, respectively. The weight percentages of micellized chains were calculated from the relative areas under the two peaks.

7.3.4. Static Light Scattering

Static light scattering (SLS) experiments were performed on a Dawn-F multi-angle laser photometer (Wyatt Technology) equipped with a He-Ne laser (632.8 nm). Data acquisition and Zimm plot processing utilized DawnF and Aurora (Wyatt) software, respectively. Stock solutions of block ionomers were prepared by dissolving the neutralized polymers in toluene, then filtered through membrane filters with a nominal pore size of 0.45 μm and transferred to a dust-free scintillation vial. Micelle solutions were diluted with filtered solvent. Measurements were obtained at five different concentrations, in the range of 0.2 - 0.1 mg / mL.

7.3.5. Dynamic Light Scattering

Dynamic light scattering (DLS) experiments were performed on a Brookhaven Instruments photon correlation spectrometer equipped with a BI-9000AT digital correlator and a Micro Green diode-pumped laser (532 nm) from Uniphase. Measurements were made in toluene at 22 °C and cyclohexane at 40 °C, over a range of concentrations 1.1 - 0.4 mg / mL. Stock solutions were filtered through membrane filters with a nominal pore size of 0.45 μm and transferred to dust-free vials. The angle of detection for all measurements was 90°. Effective diffusion coefficients were determined from the first cumulant, which represents a z-average relaxation rate, $\Gamma_z(s^{-1})$, of the autocorrelation function, $g_1(\tau)$. The second cumulant, μ/Γ_z^2, was generally < 0.05 for all measurements, indicating relatively low polydispersities. Since effective diffusion coefficients did not appear to vary significantly in this range of dilute concentrations, they were assumed to be equivalent to D_0, which is the diffusion coefficient at infinite dilution. R_h values were calculated from diffusion coefficients using the Stokes-Einstein relation for diffusing spheres.

7.3.6. Small-Angle Neutron Scattering

SANS experiments were performed on a small-angle neutron scattering spectrometer, at beamline H9-B in the high-flux beam reactor (HFBR) at Brookhaven National Laboratory. A neutron wavelength of $\lambda = 7.54$ Å was used with monochromatization of < 10 %. The two-dimensional detector was positioned at a distance of 110 cm from the samples. Samples I and II were investigated at two concentrations, 3% and 5% polymer (w/w) in toluene at 22 °C and cyclohexane at 40 °C. The sample solutions were placed in capped quartz cells with 1 mm path lengths.

Scattering profiles were corrected for detector nonlinearity and variations in incident neutron intensity through normalization with a water standard. A solvent background was subtracted from all corrected profiles, followed by normalization with cell path lengths and sample transmission.

7.4. Results and Discussion

7.4.1. Weight Fraction of Micellized Chains

Size-exclusion chromatography (SEC) was used to determine the weight fractions of micelles and single chains in both ionomer samples, by calculating relative areas of the corresponding peaks. It has been shown that single chains in solutions of block ionomer reverse micelles do not result from a dynamic equilibrium between micellized and unmicellized chains, as the ionomer aggregates are kinetically frozen.[20] FTIR spectra of the two fractions suggest that single chains are mostly due to PS homopolymer, an impurity that arises in the early stages of block copolymer synthesis. The weight fractions of micellized chains, f_{mic}, were found to be very similar for samples I and II: $f_{mic} = 0.73$ and $f_{mic} = 0.78$, respectively. It should be noted that, in solutions of samples I and II used for SANS (≤ 5 wt. % polymer), the single chain concentrations are extremely low (< 1 wt. %), and are not expected to contribute significantly to the total incoherent scattering. The pure solvent was therefore considered to be an appropriate subtracted background in all cases.

7.4.2. Static and Dynamic Light Scattering Results

Static light scattering measurements in toluene were used to construct Zimm plots for samples I and II. These plots yielded micelle radii of gyration, $R_{g,tot}$ (Table 7.1), along with the total molecular weight of the block ionomers in solution, $M_{w,tot}$. The latter quantity is a weight average of the micelle molecular weight, $M_{w,mic}$, and the molecular weight of the single chains, $M_{w,sc}$:

$$M_{w,tot} = f_{mic} M_{w,mic} + f_{sc} M_{w,sc} \qquad (1)$$

where f_{sc} is the weight fraction of single chains, which is $1\text{-}f_{mic}$. Micelle aggregation numbers, Z, (Table 7.1) were determined from $M_{w,mic}$ and the molecular weights of unimers making up the micelles. Assuming a spherical, compact poly(cesium acrylate) core and using the measured density of poly(cesium acrylate) (2 g/mL),[7] the core radii,

R_{core}, were then calculated from Z values. Although the micelle radius of gyration is solvent dependent, aggregation numbers and core radii are expected to be identical in different solvents. This follows from the strength of ionic interactions within the core, which prevents the free exchange between aggregates and single chains once the micelles have formed. Aggregation numbers and core radii, determined in toluene, are therefore considered to be "universal" values, applicable to both solvent systems used in this study. Along with the radius of gyration, any micelle parameter that is dependent on polymer-solvent interactions, including all aspects of coronal structure, will vary with the solvent.

Table 7.1. Characteristics of block ionomer micelles from light scattering data.

PS-*b*-**dPS**-*b*-PS-*b*-*PACs*	Z	R_{core} (nm)	$R_{g,tol}$ (nm)	$R_{h,tol}$ (nm)	$R_{g,tol}/R_{h,tol}$	coronal extension in tol (%)	$R_{h,ch}$ (nm)	coronal extension in ch (%)
sample I (70-**210**-820-*50)*	67	5	44	58	0.76	19	43	14
sample II (250-**220**-1080-*77)*	58	6	46	63	0.73	15	45	10

A simple fingerprint of coronal structure is the hydrodynamic radius, from which the average extension of chains within the micelle corona is obtained.[21] Hydrodynamic radii in toluene at 22 °C, $R_{h,tol}$ (Table 7.1), were determined from dynamic light scattering measurements in dilute solution, and therefore reflect the overall radii of isolated, non-interacting micelles. Also listed in Table 7.1 are the ratios $R_{g,tol}/R_{h,tol}$, which yield information on the structure of the micelles in toluene.[22] The ratios for samples I and II are very similar (0.76 and 0.73, respectively), and are close to the expected value for hard spheres ($R_g/R_h = 0.775$). To determine the average extension of coronal chains, the height of the spherical brush, H, was calculated:

$$H = R_h - R_{core} \qquad (2).$$

The percent coronal extension (Table 7.1) was then calculated by comparison of the brush height with the fully extended contour length of the PS chains:

$$\% \text{ extension} = \frac{100H}{aN_{PS}} \qquad (3)$$

where a is the length of one PS repeat unit (ca. 0.25 nm), and N_{PS} is the total number of PS and dPS units in a single coronal chain. The average coronal extension of sample I in toluene (19 %) is found to be significantly greater than that of sample II (15 %). Since chain extension in a starlike brush is expected to decrease with increasing distance from the center, it is clear that a micelle corona made up of longer chains will, on average, be less severely stretched than a corona made up of shorter chains. This explains the greater average extension in sample I, which has a soluble block length of 1100 units, compared with that of sample II, in which the soluble blocks are ca. 40 % longer, i.e. 1550 units. Although variation in the aggregation number will also affect the average chain extension, ref. 13 predicts that the scaling of brush height with Z is actually quite weak: $H \sim Z^{0.2}$. It is therefore reasonable to assume that the small difference in the aggregation numbers of samples I and II (67 and 58, respectively) do not contribute significantly to differences in coronal structure.

Hydrodynamic radii were also determined in cyclohexane at 40 °C ($R_{h,ch}$), and these were used in eqs 2 and 3 to calculate corresponding percentages of coronal extension (Table 7.1). Since this represents near-θ conditions for the PS coronal chains, the spherical brushes are less swollen than in the "good" solvent (toluene), and the coronae are therefore less extended. As was found in toluene, the shorter coronal chains in sample I result in a more extended PS corona, compared with that in sample II (14 % vs. 10 %).

7.4.3. Micelle Overlap Concentrations

An important parameter in this study of concentration effects is the micelle overlap concentration, c^*, which is defined as the concentration at which the coronae of neighbouring micelles begin to overlap. This concentration is related to the hydrodynamic radius in a given solvent, and can be calculated approximately by assuming a certain packing model for spheres with radius R_h. In this manner, overlap concentrations in toluene at 22 °C, c^*_{tol}, and in cyclohexane at 40 °C, c^*_{ch}, have been calculated for two lattice types: face-centered cubic (fcc), or cubic close packed, and body-centered cubic (bcc) (Table 7.2). The calculations consider variations in solvent density with temperature, along with the presence of single chains in both samples. As expected, c^* values for the more closely-packed fcc lattice are somewhat higher than those obtained assuming bcc packing of micelles. Since the lattice type at high polymer concentration is not known, values in Table 7.2 should serve only as rough estimates of actual overlap concentrations.

Table 7.2. Micelle overlap concentrations calculated for fcc and bcc packing lattices.

PS-*b*-**dPS**-*b*-PS-*b*-*PACs*	c^*_{tol}, fcc (wt. % poly.)	c^*_{tol}, bcc (wt. % poly.)	c^*_{ch}, fcc (wt. % poly.)	c^*_{ch}, bcc (wt. % poly.)
sample I (70-**210**-820-*50*)	2.0	1.8	5.5	5.0
sample II (250-**220**-1080-*77*)	1.8	1.7	5.5	5.0

7.4.4. Coronal Chain Stretching in Toluene

Kratky representations of SANS profiles ($Iq^{5/3}$ vs. q) are shown for 3 wt. % solutions of samples I and II in toluene (Figure 7.1a). Both of these plots plateau at sufficiently high values of q, which indicates that the scattering of the deuterated labels is consistent with dilute or semidilute solutions of swollen polymer chains. The important difference in the two profiles is the minimum scattering vector of the intermediate region, q^*, which is marked by the beginning of the plateau on the Kratky plots (indicated with arrows). The values of q^* for labels located at 820 and 1080 units away from the micelle core are 0.05 and 0.04 Å^{-1}, respectively. This suggests an increase in the average blob size as the distance from the core increases, in qualitative agreement with the Daoud and

Cotton model for starlike micelles.[13] In this study, the positions of the labels with respect to the ionic cores differ by only 260 PS units; a wider range of label positions was investigated in a subsequent study (chapter 8).

Figure 7.2 (top) shows log-log representations of the scattering profiles for 3 % solutions of samples I and II in toluene. In the region of intermediate q, the plots are found to be linear, and the characteristic exponent, α, can be obtained from the slope. Both plots give α values of 1.7, as expected for swollen coils; this is consistent with the observed plateau regions in Kratky plots of $Iq^{5/3}$ vs. q (Figure 7.1a). Characteristic exponents determined from log-log plots yield scaling laws for scattered intensity at intermediate q, and these are presented in Table 7.3.

The effect of total polymer concentration at intermediate q values has been explored by comparing Kratky plots of the deuterated labels at 3 wt. % and 5 wt. % in toluene. As shown in Figure 7.1b, the Kratky plot for sample I (70-**210**-820-*50*) at 5 % reaches a plateau at $q^* = 0.05$ Å^{-1}, which is qualitatively similar to its behaviour at 3 %. In contrast, sample II (250-**220**-1080-*77*) at 5 % shows a Kratky plot that is significantly different from that obtained at 3 %; above $q = 0.04$ Å^{-1}, where the plot reaches a plateau at the lower polymer concentration, $Iq^{5/3}$ continues to increase steadily. This behaviour indicates a characteristic exponent that is significantly lower than the value for swollen coils, suggesting a stiffening of the deuterated label as the polymer concentration increases from 3 % to 5 %. The Kratky plot at 5 % does not appear to reach a plateau for any value of q; this indicates a breakdown of semidilute behaviour for the dPS labels, such that they do not show single chain correlations on any length scale.

To obtain more detailed information on the stiffness of the deuterated labels at 5 % polymer, characteristic exponents, α, were determined from log-log representations of the scattering profiles (Figure 7.2, bottom); the resulting intensity scaling laws are listed in Table 7.3. Regression analysis of the curves in the linear region yields $\alpha = 1.6$ and $\alpha = 1.3$ for samples I (70-**210**-820-*50*) and II (250-**220**-1080-*77*), respectively. Comparison of the characteristic exponents for sample I at 3 % ($\alpha = 1.7$) and 5 % ($\alpha = 1.6$) reveals only a slight increase in the stiffness of the deuterated labels with increasing concentration, which

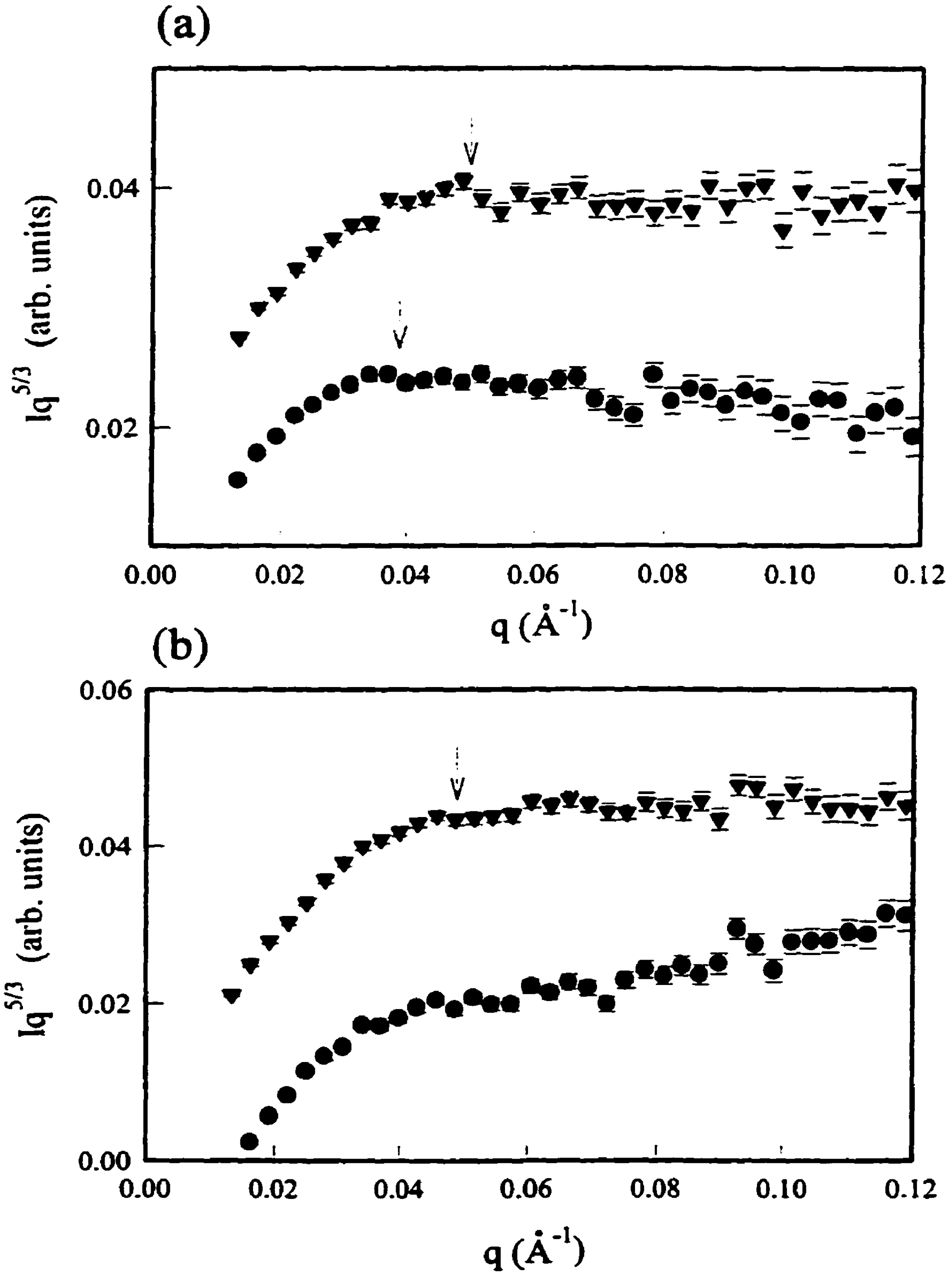

Figure 7.1. Kratky representations of scattering data for sample I (70-210-820-50) (▼) and II (250-220-1080-77) (●) in toluene. (a) 3 wt. % polymer. (b) 5 wt. % polymer. Arrows indicate the beginning of the plateau region.

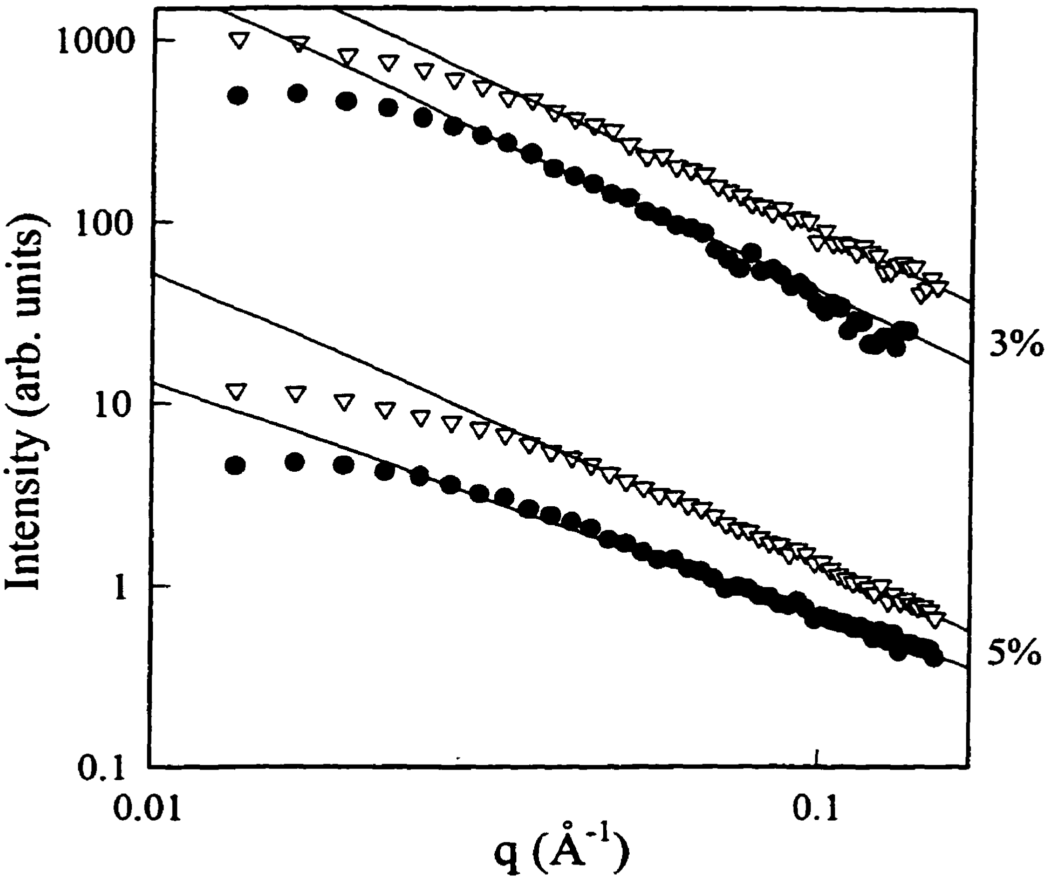

Figure 7.2. Log-log plots of scattering profiles for sample I (70-210-820-*50*) (▽) and II (250-220-1080-*77*) (●) in toluene at 3 and 5 wt. % polymer. Solid lines show linear regression for intermediate *q* values.

Table 7.3. $I(q)$ scaling at intermediate scattering vectors for deuterated labels in block ionomer micelles.

PS-*b*-**dPS**-*b*-PS-*b*-*PACs*	*c* (wt. % poly.)	solvent	scattered intensity scaling
sample I (70-**210**-820-*50*)	3	tol, 22°C	$q > 0.05$ Å^{-1}, $I \sim q^{-1.7}$
sample II (250-**220**-1080-*77*)	3	tol, 22°C	$q > 0.04$ Å^{-1}, $I \sim q^{-1.7}$
sample I (70-**210**-820-*50*)	5	tol, 22°C	$q > 0.05$ Å^{-1}, $I \sim q^{-1.6}$
sample II (250-**220**-1080-*77*)	5	tol, 22°C	$q > 0.05$ Å^{-1}, $I \sim q^{-1.3}$
sample I (70-**210**-820-*50*)	3	ch, 40°C	0.05 Å^{-1} $< q <$ 0.10 Å^{-1}, $I \sim q^{-1.6}$; $q > 0.10$ Å^{-1}, $I \sim q^{-1.1}$
sample II (250-**220**-1080-*77*)	3	ch, 40°C	0.03 Å^{-1} $< q <$ 0.10 Å^{-1}, $I \sim q^{-1.5}$; $q > 0.10$ Å^{-1}, $I \sim q^{-0.9}$
sample I (70-**210**-820-*50*)	5	ch, 40°C	$q > 0.06$ Å^{-1}, $I \sim q^{-1.7}$
sample II (250-**220**-1080-*77*)	5	ch, 40°C	$q > 0.04$ Å^{-1}, $I \sim q^{-1.9}$

was not easily detected from the Kratky plots. For sample II, however, the characteristic exponent decreases markedly between 3 % ($\alpha = 1.7$) and 5 % ($\alpha = 1.3$), suggesting an internal stiffening of the labels. This increase in chain stiffness may be attributed to the overlap of coronal segment density profiles above the micelle overlap concentration, c^*. For an individual micelle (infinite dilution), the blob model describes an increase in local segment densities with increasing radial distance from the core; steric effects thus result in more severe restrictions to chain conformations closer to the micelle core. At concentrations sufficiently greater than c^*, the overlap of neighbouring micelles will result in increased local segment densities within the coronae, especially at relatively large radial distances.[23] The present observations seem to indicate a resulting increase in steric crowding and, consequently, a stiffening of chains at the outer edge of the micelle. This does not address the question of interdigitation or compression of coronal chains as micelles begin to overlap; both possibilities are consistent with increased steric crowding in the neighbourhood of deuterated labels situated near the ends of the coronal chains.

Values of c^* (Table 7.2) show that, even at 3 % polymer in toluene, the reverse micelles of both samples may be above their overlap concentrations; however, no evidence of overlap-induced chain stiffening is observed at the lower concentration, at least insofar as the scattering is consistent with the blob model for individual spherical brushes. This result is not surprising, if the polydispersity of chain lengths within the micelles is considered. Since c^* values were calculated from the hydrodynamic radii, they represent the overlap of micellar regions occupied mainly by solvent molecules, plus only the very longest chains within the neighbouring coronae. Thus the micelles at 3 %, though nominally above c^*, are not sufficiently crowded to exhibit chain stiffening at the outer edge. At 5 %, however, coronal overlap is sufficient to give rise to significant increases in local segment densities, such that overlap-induced stiffening of the deuterated labels is observed. The scaling relations in Table 7.3 show that chain stiffening between 3 % and 5 % polymer concentration is more pronounced in sample II (250-**220**-1080-*77*) than in sample I (70-**210**-820-*50*). This observation is explained by the longer coronal chains in the former sample, which give rise to a slightly lower overlap concentration (Table 7.2).

The absence of single chain correlations at intermediate scattering vectors, such as that found in sample I at 5 % polymer concentration, generally occurs when the chains are more severely stretched than those in a semidilute environment. This has been previously observed for deuterated labels located at the interior of a polymer star.[17] In the present case, however, the labels are located near the outer extremity of the starlike profiles, where steric effects are relatively weak in individual micelles. The present observations, therefore, indicate the considerable effect of micellar overlap on the stretching of coronal chains. In further work, the concentration effects were be studied in more detail as a function of distance from the core (chapter 8). At this point, it seems reasonable to predict that, for micelles with identical c^* values, the conformation of deuterated labels situated closer to the ionic core will be less influenced by the total polymer concentration; for small radial distances, the effects of micelle overlap are more likely to be screened by already high local segment densities.

7.4.5. Coronal Chain Stretching in Cyclohexane

Samples I (70-**210**-820-*50*) and II (250-**220**-1080-*77*) were also investigated in cyclohexane at 40 °C, which represents near-θ conditions for the PS chains.[5] Log-log plots of the resulting scattering profiles are shown in Figure 7.3. At 3 % (Figure 7.3, top), two different regions of intensity scaling are observed for both samples, as shown by the inflection points at q = 0.10 Å^{-1} (indicated with arrows) followed by a decrease in the slopes of the log-log plots. Characteristic exponents in the first region were determined from linear regression over the specified q values, and these were found to be nearly identical for both samples: α = 1.6 and 1.5 for samples I and II, respectively (Table 7.2). More importantly, linear regression in the second region (q > 0.10 Å^{-1}), shown in the insert to Figure 7.3, yields characteristic exponents of $\alpha \approx 1$ for both samples. Scattered intensity is expected to show q^{-1} scaling at scattering vectors greater than $3.82/l$, where the rigidity of individual statistical units is probed;[24] for Gaussian PS chains under θ conditions, this crossover occurs at q = 0.25 Å^{-1}. In the present case, the beginning of q^{-1} scaling at 0.10 Å^{-1} suggests that the deuterated labels are highly extended, showing rod-

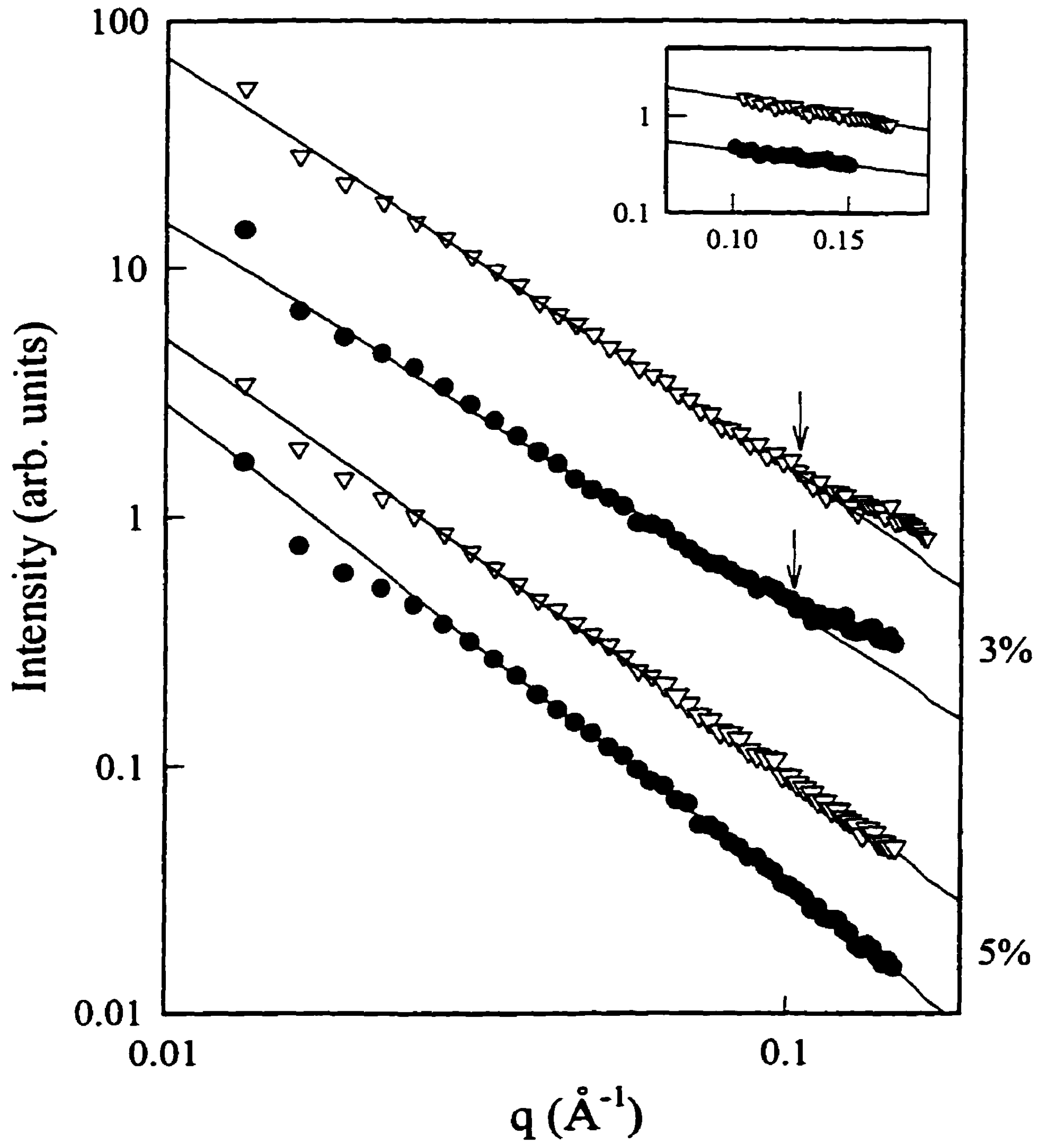

Figure 7.3. Log-log plots of scattering profiles for sample I (70-210-820-*50*) (▽) and II (250-220-1080-*77*) (●) in cyclohexane (40 °C) at 3 and 5 wt. % polymer. Solid lines show linear regression for intermediate q values. At 3 %, the beginning of q^{-1} scaling is indicated with arrows. Linear regression for $q > 0.1$ Å^{-1} (3 %) is show in the insert.

like behaviour over relatively large length scales (i.e. statistical units of ca. 38 Å in length). Since the contour (fully extended) length of the deuterated labels is ca. 500 Å, each label contains only 13 statistical units under these conditions. The labels are therefore best described as "worm-like", and bear little resemblance to the "random walk" of Gaussian chains.[25]

For individual starlike micelles under θ conditions, the scattered intensity from coronal chains is expected to scale as q^{-2} in the intermediate domain, in the manner of a semidilute solution of Gaussian chains.[5] The observed stiffness of the deuterated labels in cyclohexane at 3 % polymer concentration is therefore attributed to intermicellar effects near c^*. As discussed earlier, the overlap of neighbouring micelles in toluene results in the stiffening of deuterated labels, although this effect was found only at 5 % polymer concentration, and was significant only for micelles of sample II (250-**220**-1080-*77*), which have a larger hydrodynamic radius. In cyclohexane at 40 °C (near-θ conditions), however, the effect of micelle-micelle interactions on chain stiffness is operative at 3 % polymer, which, according to c^* values in Table 7.2, is well below the overlap concentration of the micelles in cyclohexane. As well, the deuterated labels in both samples I (70-**210**-820-*50*) and II (250-**220**-1080-*77*) are found to be highly extended at this concentration. These differences in concentration effects likely arise from the very different polymer-polymer interaction parameters in the two solvent systems. In a good solvent such as toluene, solvent-polymer interactions are enthalpically more favourable than those between coronal segments, and attractive forces between the coronal chains of neighbouring micelles are therefore highly unlikely. On the other hand, such interactions may exist under near-θ conditions or, more precisely, at temperatures slightly below T_θ. In the present system, it is possible that, at relatively high concentrations, the mutual attraction between PS segments on neighbouring micelles results in the outward extension of coronal chains. The influence of such attractive forces should be strongest at the outer edge of the corona, where interactions between segments on neighbouring micelles are less screened by segment densities within individual micelles. This explains the observed stiffness of the labels at 3 %. Unlike chain stiffening in toluene at high polymer concentrations, this effect does not involve the overlap of micelle neighbours, and actually appears to be strongest at concentrations below c^*. Coronal stiffness in cyclohexane is therefore observed at a lower polymer concentration than in toluene, and is nearly equivalent for both samples, irrespective of their different hydrodynamic radii. We further note that attractive forces between neighbouring micelles would be operative only for temperatures slightly below T_θ, where the second virial coefficient is negative. This criterion appears to be met in the present system, even though the experiment was done at nominal θ conditions for PS homopolymer. In previous studies, A_2 values for PS-*b*-PANa reverse micelles were found to be significantly lower than those of linear PS of equivalent molecular weight.[26]

When the polymer concentration in cyclohexane was increased from 3 % to 5 %, a surprising decrease in the stiffness of the labels was found. At the higher concentration, rod-like q^{-1} scaling of $I(q)$ is no longer observed for $q > 0.10$ Å^{-1} (Figure 7.3, bottom), and linear regression of the log-log plots reveals characteristic exponents of 1.7 and 1.9 for samples I and II, respectively. The latter exponent suggests nearly Gaussian behaviour for the deuterated label in sample II. The label in sample I is somewhat more extended ($\alpha = 1.7$), though much less so than at 3 % polymer, as evinced by the loss of q^{-1} scaling above 0.10 Å^{-1}.

The observed loss of "worm-like" behaviour as the concentration is increased to the micelle overlap concentration in cyclohexane (ca. 5 %) reflects a decrease in chain stretching. This result is somewhat unexpected, although not unreasonable when the origin of chain stiffening under near-θ conditions is considered. Although the mutual attraction of polymer segments is still operative as the micelles begin to overlap, the resulting force no longer acts to extend coronal chains in a radially-outward direction. Instead, as the micelles are brought into closer proximity and the total concentration of polymer segments increases, the environment of coronal chains approaches that of a polymer melt. This situation appears to exist for sample II (250-**220**-1080-*77*) at 5 % polymer concentration, in which the deuterated label exhibits Gaussian q^{-2} scaling in the intermediate domain (Table 7.3). The greater extension of the label in sample I (70-**210**-820-*50*) ($I(q) \sim q^{-1.7}$) at the same concentration may again reflect the slightly shorter hydrodynamic radii of these micelles. It may be noted that the chain statistics of a polymer melt were not observed for either sample in toluene when the polymer concentration was increased to 5 %. In a good solvent such as toluene, polymer-solvent interactions are dominant even for high volume fractions of PS segments, such that solvent molecules continue to influence chain statistics and preclude melt-like behaviour.

7.5. Conclusions

The stiffness of deuterated labels within the PS corona of starlike block ionomer micelles has been investigated as a function of solvent conditions and polymer concentration. In a good solvent at 3 wt. % polymer, the scattered intensity for both samples I (70-**210**-820-*50*) and II (250-**220**-1080-*77*) scales as $I \sim q^{-1.7}$ in the intermediate domain, indicating a semidilute environment for the labels. The minimum vector of the intermediate region, q^*, decreases as the label's distance from the core increases, in agreement with the blob model for starlike spherical brushes. When the polymer concentration in toluene is increased to 5 wt. %, the stiffness of the labels is found to increase, as evinced by a decrease in the characteristic exponent α. Chain stiffening within the corona is attributed to the significant overlap of neighbouring micelles at concentrations well above c^*. In cyclohexane at 40 °C, which represents near-θ conditions, the labels show worm-like behaviour at 3 wt. % polymer. This suggests highly extended chains at the micelle extremity, possibly due to attractive micelle-micelle interactions below c^*. At 5 wt. % in cyclohexane, near the micelle overlap concentration, the worm-like behaviour of the labels collapses, and chain statistics begin to resemble a polymer melt.

The study of block ionomer coronal structure is continued in the next chapter, using samples with perdeuterated labels located at a three different distances from the ionic core. With these samples, the inner part of the spherical brush is probed in more detail, and a comprehensive picture of block ionomer coronal structure begins to emerge.

Acknowledgments

This work was supported by the Natural Sciences and Engineering Research Council of Canada (NSERC). M.M. is grateful for scholarship funding provided by NSERC and Le Fonds pour la Formation de Chercheurs et L'Aide à la Recherche (FCAR, Quebec).

References

(1) Tuzar, Z.; Kratochvil, P. *Adv. Colloid and Interface Sci.* **1976**, *6*, 201.

(2) Price, C. In *Developments in Block Copolymers,* Vol 1; Goodman, I., Ed.; Applied Science Publishers: London, 1982, p.39.

(3) Tuzar, Z.; Kratochvil, P. In *Surface and Colloid Science*, Vol 15; Matijevic, E., Ed.; Plenum Press: New York, 1993, p.1.

(4) Plestil, J.; Baldrian, J. *Makromolek. Chem.* **1975**, *176*, 1009.

(5) Cogan, K. A.; Gast, A. P.; Capel, M. *Macromolecules* **1991**, *24*, 6512.

(6) McConnell, G. A.; Gast, A. P.; Huang, J. S.; Smith, S. D. *Phys. Rev. Lett.* **1993**, *71*, 2102.

(7) Nguyen, D.; Williams, C. E.; Eisenberg, A. *Macromolecules* **1994**, *27*, 5090.

(8) Nguyen, D.; Varshney, S. K.; Williams, C. E.; Eisenberg, A. *Macromolecules* **1994**, *27*, 5086.

(9) Chu, B. *Langmuir* **1995**, *11*, 414.

(10) Mortensen, K. *J. Phys.: Condens. Matter* **1996**, *8*, A103.

(11) Förster, S.; Wenz, E.; Linder, P. *Phys. Rev. Lett.* **1996**, *77*, 95.

(12) Higgins, J. S.; Benoit, H. C. *Polymers and Neutron Scattering*, Oxford University Press: Oxford, 1995.

(13) Daoud, M.; Cotton, J. P. *J. Phys.* **1982**, *43*, 531.

(14) Edwards, S. F. *Proc. Phys. Soc.* **1966**, *88*, 265.

(15) De Gennes, P.G. *Scaling Concepts in Polymer Physics*, Cornell University Press, 1979.

(16) Lantman, C. W.; MacKnight, W. J.; Rennie, A. R.; Tassin, J. F.; Monnerie, L.;

Fetters, L.J. *Macromolecules* **1990**, *23*, 836.

(17) Richter, D.; Farago, B.; Fetters, L. J.; Huang, J. S.; Ewen, B. *Macromolecules* **1990**, *23*, 1845.

(18) Dozier, W. D.; Huang, J. S.; Fetters, L. J. *Macromolecules* **1991**, *24*, 2810.

(19) Willner, L.; Jucknischke, O.; Richter, D.; Roovers, J.; Zhou, L.-L.; Toporowski, P.M.; Fetters, L. J.; Huang, J. S.; Lin, M. Y.; Hadjichristidis, N. *Macromolecules* **1994**, *27*, 3821.

(20) Desjardins, A.; Eisenberg, A. *Macromolecules* **1991**, *24*, 5779.

(21) Zhang, L.; Barlow, R. J.; Eisenberg, A., *Macromolecules* **1995**, *28*, 6055.

(22) Burchard, W. *Adv. Polym. Sci.* **1983**, *48*, 1.

(23) McConnell, G. A.; Gast, A. P. *Macromolecules* **1997**, *30*, 435.

(24) Kratky, O. *Pure Appl. Chem.* **1966**, *12*, 483.

(25) Kratky, O.; Porod, G. *Rec. Trav. Chim.* **1949**, *68*, 1106.

(26) Khougaz, K.; Zhong, X.-F.; Eisenberg, A. *Macromolecules* **1996**, *29*, 3937.

CHAPTER 8

Coronal Structure of Starlike Block Ionomer Micelles: an Investigation by Small-Angle Neutron Scattering

8.1. Abstract

Coronal structure of starlike block ionomer micelles has been probed directly by small-angle neutron scattering (SANS), using specific contrast labeling of different regions of the corona. Solutions of PS-*b*-**dPS**-*b*-PS-*b*-*PACs* starlike block ionomer micelles in toluene are studied; contrast is provided by perdeuterated polystyrene labels situated at different distances from the ionic core. For deuterated labels situated at 390 PS units from the core, the scattered intensity is found to scale as $I \sim q^{-1.7}$ at intermediate q, suggesting a semidilute environment for the labels and local swollen coil behaviour. For labels 180 PS units from the core, steric perturbations are more extensive than are found under semidilute conditions, such that single chain scaling is not observed at any length scale; scattered intensity is found to scale as $I \sim q^{-1.3}$ at intermediate q. The stiffness of coronal chains next to the core is even greater, as indicated by $I \sim q^{-1.0}$ scaling for dPS labels attached directly to the ionic core; these probes exhibit rigid-rod behaviour at length scales less than ca. 76 Å. In Kratky representations of the three samples, a maximum characteristic of polymer stars becomes more pronounced as the distance of the dPS labels from the core decreases, indicating greater contributions from interchain scattering. Increases in chain stiffness and interchain scattering suggest a significant increase in local

segment densities with decreasing distance from the ionic core. Interparticle scattering as a function of polymer concentration is also investigated. The position of the Bragg peak scales with concentration as $c^{1/3}$, suggesting liquid ordering of the solution. Radii of gyration determined from Guinier analysis agree well with light scattering results, with the exception of micelles in which dPS probes are attached directly to the core. In this case, the neutrons "see" only the inner part of the spherical brush, and R_g from SANS data is less than R_g for the whole micelle.

8.2. Introduction

The structure of spherical polymer brushes has received a considerable amount of attention in recent years, spurred by industrial applications of such systems to colloid stabilization and surface modification. In several studies, model systems of star polymers[1-4] and starlike block copolymer micelles[5-10] have been employed in the investigation of spherical brushes, using small-angle x-ray scattering (SAXS) and small-angle neutron scattering (SANS). The latter experiment offers the advantage of deuterium labeling techniques, allowing for the determination of spatially-specific information on brush structure. This strategy has been used to probe the structure of star polymers in which the inner cores and outer shells were selectively deuterated.[1,2] However, apart from the work described in chapter 7,[11] no other studies have used deuterated labels to probe coronal structure in block copolymer micelles.

Due to the high stability of block ionomer micelles, these materials provide an ideal system for the investigation of coronal structure. After micellization and complete neutralization of the ionic cores, the aggregates are essentially frozen structures, with no detectable equilibrium between micelles and single chains on a reasonable time scale.[12] It is therefore possible to study the spherical brushes under various conditions of solvent and polymer concentration without changes in the micelle aggregation numbers and core radii. Block ionomer micelles are thus very suitable models for polymer-protected colloidal particles, in which the ionic cores represent small spheres of ionic material, with soluble stabilizing polymer (coronal chains) end-tethered to the particle surface.

In the first part of this study, the stiffness of deuterated labels within polystyrene-*b*-poly(cesium acrylate) (PS-*b*-PACs) star-like reverse micelles was investigated as a function of both solvent conditions and polymer concentration.[11] Two block ionomer samples were studied, with perdeuterated PS labels of ca. 200 units situated at 820 and 1080 units from the core. At 3 wt. % polymer concentration in a good solvent (toluene), both samples showed intensity scaling as $I \sim q^{-1.7}$ in the intermediate region of scattering vectors, indicating a semidilute environment for the labels. The average "blob" size appeared to be slightly larger for the labels that were more removed from the ionic core, as determined by the minimum vector of the intermediate region, q^*; this observation is in agreement with the Daoud and Cotton model for starlike spherical brushes.[13] When the polymer concentration was increased to 5 wt. % in toluene, the stiffness of the labels was found to increase, a phenomenon that was attributed to micelle overlap and a concomitant increase in the local segment density of the deuterated probes. Under near-θ conditions (cyclohexane at 40 °C) at a polymer concentration of 3 wt. %, the labels were found to be extremely stiff, with intensity scaling characteristic of worm-like behaviour. At 5 wt. % in the same solvent, this worm-like behaviour was found to collapse, and the chain statistics of the probes resembled a polymer melt.

In the present chapter, the coronal structure of starlike block ionomers is investigated in more detail, using deuterated labels at a wider range of distances from the ionic core. Using small-angle neutron scattering, three micelle samples with total coronal block lengths of ca. 800 units are studied; deuterated polystyrene (dPS) labels are situated at 0, 180, and 390 units from the core, such that the inner region of the polymer brush is probed in detail. This work therefore compliments the samples investigated in the preceding chapter, in which the dPS probes were located near the outer edge of the spherical brush. All reverse micelles are studied under good solvent conditions; the effect of polymer concentration on the scattering profile in low and intermediate regions of the scattering vector is determined, providing insight into both spherical brush structure and interparticle correlations.

8.3. Experimental

8.3.1. Synthesis of PS-b-dPS-b-PS-b-PAA Block Copolymers

Block copolymers of the type PS-*b*-dPS-*b*-PS-*b*-PtBuA were prepared by the sequential anionic polymerization of styrene, perdeuterated styrene, and *tert*-butylacrylate in tetrahydrofuran (THF). The initiator was *sec*-butyllithium; lithium chloride (LiCl) and α-methyl styrene were added as capping agents for the "living" chains, to regulate anionic polymerization and prevent side reactions. Further details on sequential anionic polymerization of this type are described in the literature.[12, 14-16]

The degrees of polymerization of PS and dPS blocks, and the polydispersity indexes of the block copolymer samples (P.I.), were determined by size-exclusion chromatography (SEC). For all samples, P.I. values were between 1.08 and 1.13, indicating relatively low polydispersities for the polymer chains. The number of units in the poly(*tert*-butylacrylate) blocks were determined using quantitative FTIR (Perkin-Elmer 16 PC apparatus) of block copolymers dissolved in carbon tetrachloride. The poly(*tert*-butylacrylate) blocks were then hydrolyzed to the acid form, poly(acrylic acid) (PAA), by dissolving the polymers in toluene (5 % polymer (w/w)) and refluxing for ca. 12 h in the presence of a *p*-toluenesulfonic acid catalyst. The hydrolyzed samples were precipitated into methanol, then dried under vacuum at 70 °C for ca. 24 h.

8.3.2. Preparation and Fractionation of Block Ionomer Micelles

Block copolymers in the acid form were dissolved in a 90/10 (v/v) mixture of benzene/methanol to obtain a solution of 2 wt. % polymer. Micellization was induced by stoichiometric neutralization of the PAA blocks with a 0.25 M methanolic solution of cesium hydroxide monohydrate ($CsOH \cdot H_2O$). The block ionomer micelles were then recovered by freeze drying, followed by further drying of the samples under vacuum at 70 °C. Complete neutralization of the acid blocks to poly(cesium acrylate) (PACs) was confirmed by FTIR spectroscopy.

The reverse micelles in THF solutions were characterized by size-exclusion chromatography (SEC), using a Waters Model 510 liquid chromatograph equipped with a

Varian RI-4 refractive index detector and the Millennium 2010 software package. Chromatograms revealed two populations at high and low elution volumes, attributed to single chains and micelles, respectively. The percentage of single chains with respect to the total weight of polymer was calculated from the relative areas under the two peaks. For the samples investigated, single chain fractions were between 15-28 wt. %.

Single chain fractions in these block ionomers were attributed mainly to dPS-labeled polystyrene (i.e. no ionic block). Labeled, unmicellized chains will contribute to the coherent SANS scattering, and may partially obscure the effects of coronal structure; it was therefore desirable to fractionate these materials, in order to obtain relatively pure micelle samples. Fractionation of the samples was accomplished by dissolving the samples to 2 wt. % polymer in THF, followed by the addition of Milli-Q water (ca. 15% (w/w)); a white precipitate formed, and this was allowed to settle to the bottom of the container. Since micelles have a lower solubility in THF/water mixtures than single chains, the precipitate was assumed to contain mainly micellized material. The precipitate was isolated by vacuum filtration, dried under vacuum, then characterized by SEC in THF solutions. SEC chromatograms revealed a significantly lower single chain fraction following fractionation. For some samples, the material was fractionated twice; final single chain fractions were ≤ 4 wt. % in all cases.

The average lengths of the ionic blocks were significantly affected by the removal of the single chain fractions. For each sample, the average ionic block length was therefore recalculated, using FTIR data for the polymers in the ester form, and accounting for the weight percentage of labeled PS that was removed.

Three block ionomer samples were prepared for SANS experiments; these were designated samples I, II and III, and had the following compositions: sample I, PS(240)-**dPS(190)**-PS(390)-*PACs(48)*; sample II, PS(370)-**dPS(250)**-PS(180)-*PACs(79)*; and sample III, PS(590)-**dPS(270)**-*PACs(60)*. Numbers in brackets designate degrees of polymerization for each block, with dPS labels indicated in bold characters and PACs blocks italicized for the sake of clarity. In later sections of this chapter, polymer compositions will be shown using only degrees of polymerization for each block, e.g., sample I (240-**190**-390-*48*).

8.3.3. Static Light Scattering

Static light scattering experiments were performed on a Dawn-F multi-angle laser photometer (Wyatt Technology) equipped with a He-Ne laser (632.8 nm). Data acquisition and Zimm plot processing was carried out using DawnF and Aurora (Wyatt) software, respectively. Stock solutions of samples I, II and III were prepared by dissolving the white solids in toluene. These solutions were then filtered through membrane filters with a nominal pore size of 0.45 μm and transferred to a dust-free scintillation vial. Micelle solutions were diluted with filtered toluene, such that measurements were obtained at five different concentrations, in the range of 0.2 - 0.1 mg / mL.

8.3.4. Dynamic Light Scattering

Dynamic light scattering (DLS) experiments were performed on a Brookhaven Instruments photon correlation spectrometer equipped with a BI-9000AT digital correlator and Micro Green diode-pumped laser (532 nm) from Uniphase. All measurements were made in toluene at 22 °C over a range of concentrations 1.5 - 0.5 mg / mL. Stock solutions were filtered through membrane filters with a nominal pore size of 0.45 μm and transferred to dust-free vials. The angle of detection was 90 ° for all measurements.

Effective diffusion coefficients were determined from the first cumulant, which is the *z*-average relaxation rate, $\Gamma_z(s^{-1})$, of the autocorrelation function, $g_1(\tau)$. Values of the second cumulant, μ/Γ_z^2, indicated relatively low polydispersities of relaxation rates for all three samples. Effective diffusion coefficients did not vary significantly in this range of concentrations, and were therefore assumed to be equivalent to D_0, the diffusion coefficient at infinite dilution. R_h values were calculated from D_0 using the Stokes-Einstein relation for diffusing spheres.

8.3.5. Small-Angle Neutron Scattering

SANS experiments were performed on a small-angle neutron scattering spectrometer (beamline NG7) in the cold neutron research facility at the National Institute of Standards and Technology (NIST). Sample to detector distances of 200 and 1350 cm were used, with a neutron wavelength of $\lambda = 6$ Å, to obtain scattering profiles in the regions $q = 0.012 - 0.30$ Å^{-1} and $q = 0.0020 - 0.030$ Å^{-1}, respectively. In the intermediate region ($q = 0.012 - 0.30$ Å^{-1}), samples I, II, and III were investigated in toluene solutions at polymer concentrations of 1, 3, and 5 wt. %; the same solutions were investigated in the range of low q values ($q = 0.0020 - 0.030$ Å^{-1}), together with an additional dilute concentration (0.25 wt. % polymer) for each sample.

Small-angle scattering data were collected using a 2D detector, and normalized to a fixed number of incident neutrons corresponding to a monitor count of 10^8. The toluene background scattering was subtracted from the data, after which corrections for detector nonuniformity were performed through pixel-by-pixel division of the data by the measured scattering of water. A detector mask was applied to discard nonfunctional pixels, then the data was circularly averaged to obtain scattering profiles of the form I_{ave} vs. q.

Scattering profiles were placed on an absolute scale by calculating $I_{abs}(q)$ from $I_{ave}(q)$, where $I_{abs}(q)$ is the absolute scattering cross section per unit volume of sample. Scattered intensity from circular averaging is related to the absolute scattering cross section by the following expression:

$$\frac{I_{abs}(q)}{I_{ave}(q)} = \left(\phi A d T \Delta\Omega \varepsilon t\right)^{-1} \tag{1}$$

where ϕ is the flux on the sample, A is the sample area, d is the sample thickness, T is the measured sample transmission, $\Delta\Omega$ is the solid angle subtended by one pixel, ε is the detector efficiency, and t is the effective counting time (normalized to 10^8 counts). For a given sample and spectrometer configuration, $I_{abs}(q)$ was determined by dividing eq 1 over all scattering vectors by the equivalent expression for an appropriate standard when $q = 0$. Since ϕ, A, $\Delta\Omega$, and ε are identical for the sample and standard under the same spectrometer conditions, the following expression is obtained:

$$I_{abs}(q) = \frac{I_{ave}(q) d_s T_s I_{abs,s}(0)}{I_{ave,s}(0) dT} \qquad (2)$$

where d_s and T_s are the thickness and transmission of the standard, respectively. $I_{ave,s}(0)$, the circularly averaged intensity for the measured standard at $q = 0$, was determined by fitting $I_{ave,s}$ vs. q for the appropriate spectrometer configuration; $I_{abs,s}(0)$, the absolute scattering cross section for the standard at $q = 0$, is a tabulated quantity for all available standards. To reduce the present data, different standards were used for each of the two spectrometer configurations, based on minimum q-values for the data and scattering patterns of the standards. In the range $q = 0.012 - 0.30$ Å^{-1}, a water standard was used ($I_{abs,s}(0) = 0.96$ cm^{-1} at $\lambda = 6$ Å), while for low-q values, $q = 0.0020 - 0.030$ Å^{-1}, a polystyrene standard ($I_{abs,s}(0) = 220$ cm^{-1}) was considered to be optimal. For the remainder of this chapter, the subscript "abs" is omitted in references to scattered intensity profiles, such that $I(q)$ represents absolute scattering cross sections.

8.4. Results and Discussion

8.4.1. Static and Dynamic Light Scattering Results

Static light scattering data of samples I (240-**190**-390-*48*), II (370-**250**-180-*79*), and III (590-**270**-*60*) in toluene were used to construct Zimm plots, from which the radii of gyration, R_g, and molecular weights, M_w, of the micelles were determined. Since the weight fraction of single chains relative to total polymer was very low in all samples (≤ 4 %), M_w values from Zimm plot analysis were assumed to be equal to the molecular weights of reverse micelles; aggregation numbers, Z, for the three micelle samples were therefore calculated using values of M_w and the molecular weights of the component unimer chains. The radii of ionic cores, R_{core}, were calculated from aggregation numbers, assuming that the cores were spherical and free of solvent; in this calculation, the core density was equal to the measured bulk density of poly(cesium acrylate), 2 g/mL.[17] Considering strong ionic interactions in the core, and high surface tension at the core-solvent interface, exclusion of solvent from the ionic core is a reasonable assumption.

Values of Z, R_{core}, and R_g for the three samples are listed in Table 8.1. Aggregation numbers range from 82 to 110, with core radii of 0.6 nm for samples I (240-**190**-390-*48*) and III (590-**270**-*60*), and 0.7 nm for sample II (370-**250**-180-*79*). The radii of gyration for samples I and II are very similar, 30 and 33 nm, respectively, while R_g for sample III, 23 nm, is somewhat lower.

Table 8.1. Characteristics of block ionomer micelles and overlap concentrations from light scattering data.

PS-*b*-**dPS**-*b*-PS-*b*-*PACs*	N_{PS}	Z	R_{core} (nm)	R_g (nm)	R_h (nm)	R_g/R_h	corona ext. (%)	c^*, fcc (wt.%)	c^*, bcc (wt.%)
sample I (240-**190**-390-*48*)	820	96	0.60	30	44	0.68	21	3.6	3.2
sample II (370-**250**-180-*79*)	800	110	0.70	33	46	0.72	22	3.8	3.4
sample III (590-**270**-*60*)	860	82	0.60	23	36	0.64	17	5.9	5.3

In order to compare SANS profiles for deuterated labels at different positions within the micelle corona, all other micelle parameters should be held constant, especially those that influence the coronal structure. Values in Table 8.1 indicate that differences in aggregation numbers are not too significant, considering that the coronal brush height, H, is expected to scale only weakly with Z ($H \sim Z^{0.2}$ for starlike brushes);[13] however, a closer comparison of micelle structure in samples I, II, and III by light scattering techniques is worthwhile.

The hydrodynamic radius, R_h, provides useful information on the structure of micelles in solution. This quantity was determined from dynamic light scattering measurements in dilute solutions, and therefore represents the overall radius of individual, noninteracting micelles. A combination of static and dynamic light scattering results allows the ratio R_g/R_h to be determined (Table 8.1), and this quantity yields useful information on the geometry of colloidal particles.[18] These values are found to be slightly less than the ratio for hard spheres ($R_g/R_h = 0.775$). Since anisotropic geometry, resulting from rod or disclike structures, would result in ratios > 0.775, these results seem to suggest spherical geometry of micelles for all three samples. It is not fully understood why R_g/R_h values (0.64-0.72) are somewhat less than those of hard spheres, though this may be related to long-range interactions in solution, resulting in slight increases in the apparent R_h, or to the existence of a free-draining term in the hydrodynamic behaviour of the micelles.[18]

To determine the average extension of coronal chains in the micelle samples, the height of the spherical brush, H, was first calculated from:

$$H = R_h - R_{core} \tag{3}$$

The percentage coronal extension (Table 8.1) was then obtained by comparison of the brush height with the fully extended contour length of PS chains,[19] as described in the expression:

$$\%extension = \frac{100H}{aN_{PS}} \tag{4}$$

where a = 0.25 nm, which is the length of one PS repeat unit; N_{PS} is the total number of PS and dPS units in a single coronal chain, which is between 800 and 860 units for all three samples. The percentage of extension in samples I (240-**190**-390-*48*) and II (370-**250**-180-*79*) were found to be very similar (21 and 22 %) and these micelle populations were therefore assumed to have very similar coronal structure. The micelles in sample III (590-**270**-*60*), were found to have somewhat less extended coronae (17 %), which can be attributed both to a lower aggregation number (Z = 82) and longer coronal chains (N_{PS} = 860). Fortuitously, the deuterated labels in sample III are located closest to the ionic core, where coronal chains are expected to be most severely stretched; the overall "less extended" structure of the micelle corona in this sample should therefore not obscure the effect of label position.

Another parameter that can be determined from R_h is the micelle overlap concentration, c^*, which is simply the concentration at which the coronal regions of neighbouring micelles begin to overlap. Calculations of c^* in toluene were made for both face-centered cubic (fcc) and body-centered cubic (bcc) packing of spheres[6,7,9] (where R_h = the radius of the spheres) (Table 8.1). Although interparticle correlations are considered in a later section of this chapter, a detailed analysis of the structure factor is beyond the scope of the present work; therefore, the type of ordering at high polymer concentrations has not been confirmed and values of c^* presented in Table 8.1 should be regarded as rough estimates of actual overlap concentrations. With these considerations, it was determined that micelle overlap in toluene begins at a polymer concentration of ca. 3 wt. % for samples I (240-**190**-390-*48*) and II (370-**250**-180-*79*), and at ca. 5 wt. % for sample III (590-**270**-*60*). In the discussion of SANS results, these results are compared with interparticle distances at different concentrations, as calculated from the Bragg peak of the structure factor.

8.4.2. Small-Angle Neutron Scattering Results

Corrected scattering profiles of I vs. q for samples I (240-**190**-390-*48*), II (370-**250**-180-*79*), and III (590-**270**-*60*), in toluene can be attributed mainly to coherent scattering from the deuterated labels. This follows from relative scattering cross sections of dPS labels (6.5 x10^{-6} Å^{-2}), PS blocks (1.4 x 10^{-6} Å^{-2}), PACs cores (1.5 x 10^{-6} Å^{-2}), and toluene (0.9 x 10^{-6} Å^{-2}), which strongly suggest that the reverse micelles, with the exception of the deuterated labels, are "contrast-matched" with the surrounding solvent. Only the labels, therefore, are "seen" by the neutrons, although the labels themselves will "feel" the steric influence of both deuterated and undeuterated PS segments. It should be noted that the undeuterated material will contribute a considerable amount of incoherent scattering to the raw data, although this component is removed in the data reduction process, by subtraction of the solvent background.

The coherent scattered intensity consists of both interparticle and intraparticle contributions, known as the structure factor, $S(q)$, and form factor, $P(q)$, respectively:

$$I(q) \sim S(q)P(q) \qquad (5)$$

The interparticle structure factor is the Fourier transform of the pair correlation function, *g*(*r*):

$$S(q) = 1 + \frac{4\pi}{\rho}\int r[g(r) - 1]\sin(qr)dr \qquad (6)$$

where ρ is the particle number density of micelles. At high values of the scattering vector, the structure factor asymptotically approaches unity, and the form factor becomes the dominant contribution to coherent scattering. As well, the structure factor becomes insignificant at extremely low concentrations, where correlations between particles are negligible. At sufficient degrees of dilution, therefore, it is possible to relate the scattered intensity at low *q* values to intraparticle scattering; this is known as the Guinier region of the form factor, and yields the radius of gyration of individual particles.

The following section is divided into three parts. In section 8.4.2.1, scattered intensity profiles at intermediate *q* values are discussed, and the contribution of interparticle scattering in this region is considered. Analysis of $I(q)$ yields information on the structure and stiffness of deuterated labels within the micelle corona, and comparison of the samples allows these parameters to be determined as a function of distance from the ionic core. In section 8.4.2.2, the intensity $I(q)$ is considered at low values of the scattering vector, where the effect of interparticle scattering becomes significant. The structure factor is discussed as a function of polymer concentration. Finally, in section 8.4.2.3, the form factors at low *q* values are recovered, by sufficient dilution of the samples; radii of gyration are calculated from the Guinier region of the scattering profiles, and compared with values obtained from light scattering data.

8.4.2.1. Coronal Structure of Block Ionomer Micelles

In the intermediate region of the scattering vector, corrected profiles $I(q)$ obtained at 1, 3 and 5 wt .% polymer were normalized with concentration; most plots of I/c vs. *q* for identical samples at different concentrations show excellent superposition (Figure 8.1). This suggests that the scattered intensity in this region is dominated by the form factor,

$P(q)$, and is therefore not influenced by interparticle concentration effects. The one exception appears to be sample I (240-**190**-390-*48*) at the highest polymer concentration (5 wt. %), where negative deviations in the scattering profile are observed at vectors below $q \sim 0.05$ Å^{-1}, possibly due to structure factor contributions.

For a polymer concentration of 3 %, the scattering profiles for samples I (240-**190**-390-*48*), II (370-**250**-180-*79*), and III (590-**270**-*60*) were compared in the form of Kratky representations, $Iq^{5/3}$ vs. q (Figure 8.2); the exponent, 5/3, was chosen based on the expected intensity scaling for swollen chains in the intermediate region of the scattering vector ($I \sim q^{-5/3}$). It should be stressed that the most significant difference between samples I, II, and III is the position of the deuterated label, which is located at 390, 180 and 0 PS units, respectively, from the ionic core. For sample I (240-**190**-390-*48*), the Kratky plot approaches a horizontal asymptote, indicating $q^{-5/3}$ scaling above $q^* \sim 0.05$Å^{-1}. This is in agreement with the Daoud and Cotton model of starlike brushes, in which polymer chains are represented by a string of "blobs" of radially increasing size; within these blobs, scattered intensity scales as $I \sim q^{-5/3}$, in the manner of isolated swollen coils.[13] In the previous chapter, for dPS labels at 820 and 1080 units from the core, scattered intensity also showed local single chain behaviour at intermediate q, scaling as $q^{-5/3}$ in a good solvent.[11] However, from the Kratky plots of samples II (370-**250**-180-*79*) and III (590-**270**-*60*), it can be seen that scattering from the deuterated labels does not approach $q^{-5/3}$ scaling, as evinced by a steady increase of $Iq^{5/3}$ with increasing q.

Another distinct feature in Kratky plots of samples II (370-**250**-180-*79*) and III (590-**270**-*60*) is a maximum at $q \sim 0.02$ Å^{-1}, which is significantly more pronounced in the latter sample. This peak is an expected feature for fully-contrasted stars, and in Benoit's model of Gaussian stars occurs at $q \sim 1/R_g$.[20] The scattered intensity will increasingly resemble that of a polymer star as contributions from interchain scattering become more prominent; this will occur as the local segment densities of the contrasted labels increase. Thus the clear growth of the Kratky maximum suggests higher local segment densities for dPS probes situated closer to the core. In star polymer systems, Kratky maxima were also found to be more pronounced when the contrast of the inner brush was increased.[2] Gast and coworkers observed maxima in Kratky plots for symmetrical PS-*b*-PEO micelles in

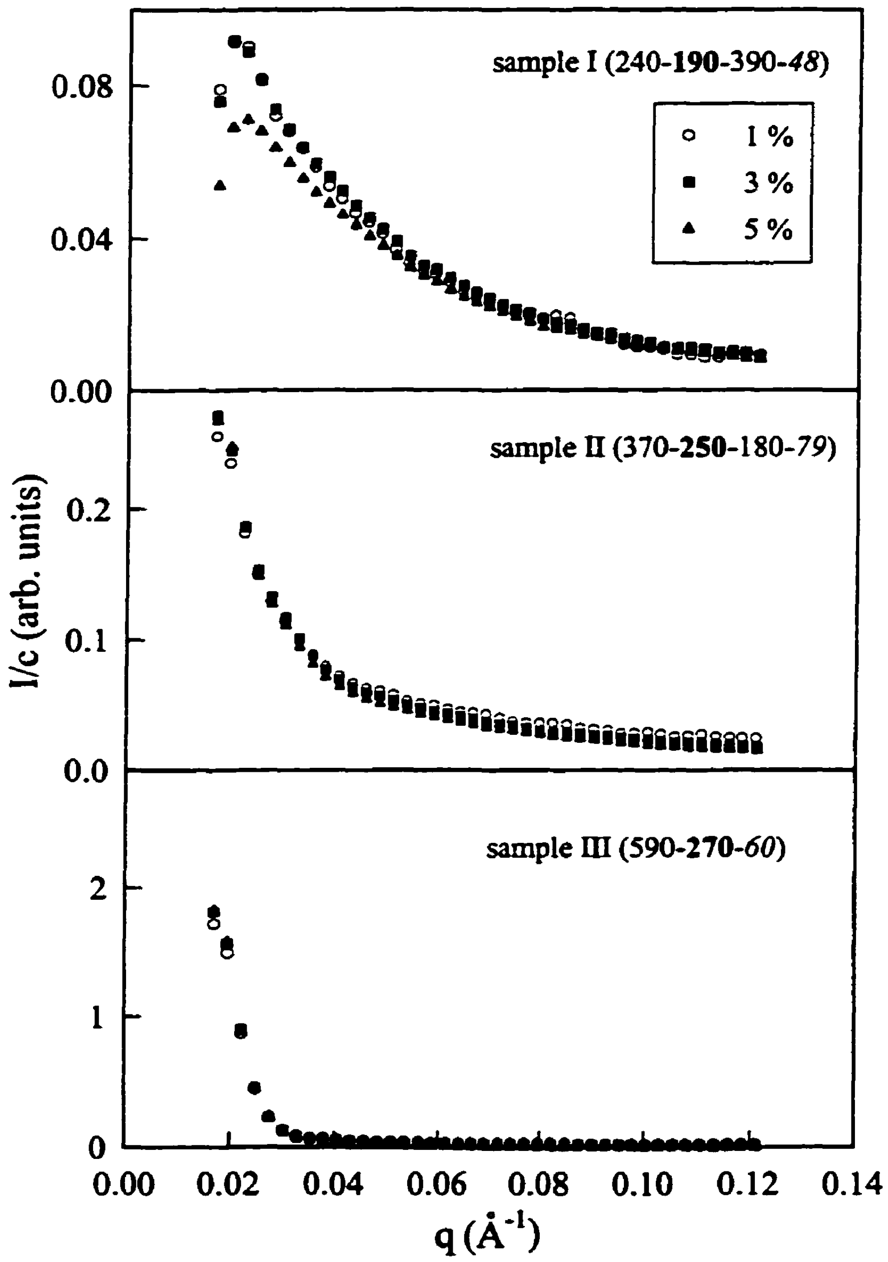

Figure 8.1. Scattered intensity normalized with concentration, *I*(*q*)/*c* (1, 3, and 5 wt. % polymer), versus scattering vector in the intermediate region.

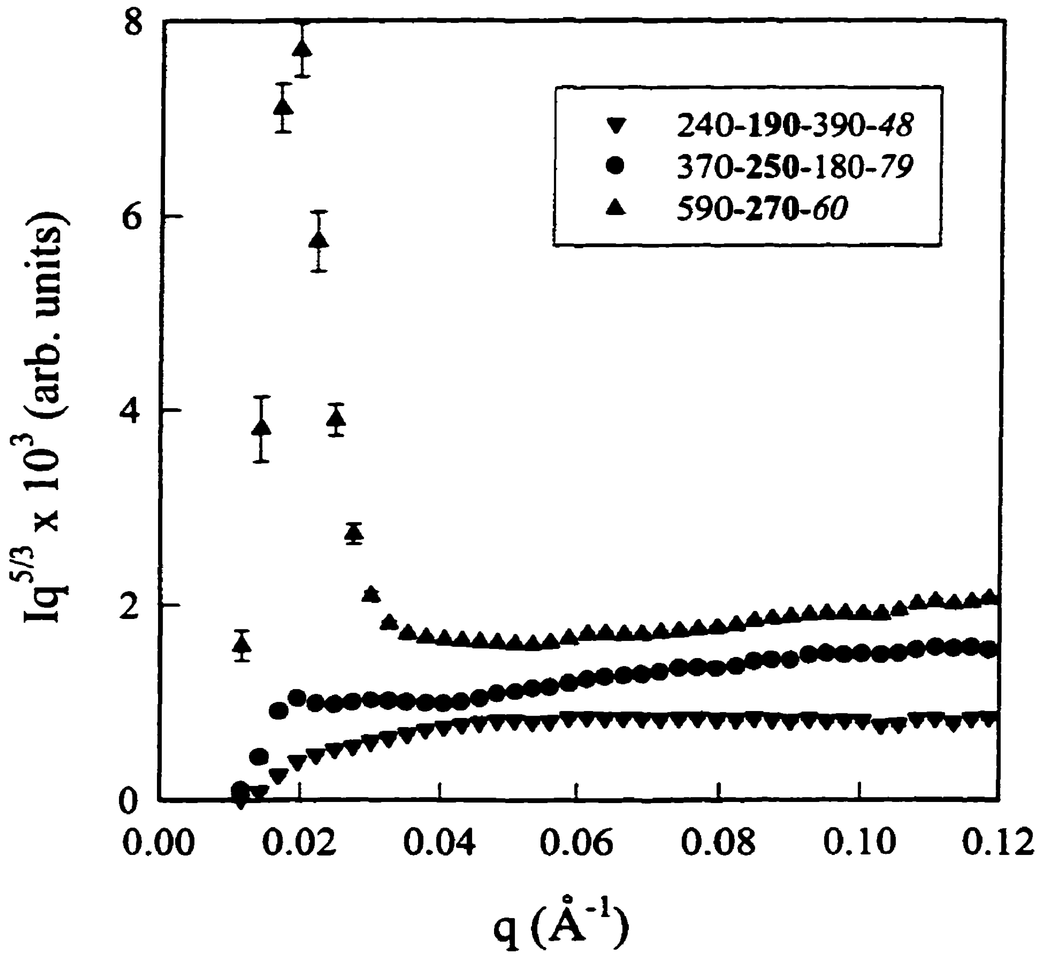

Figure 8.2. Kratky plots for samples I (240-190-390-*48*), II (370-250-180-*79*), and III (590-270-*60*), at a concentration of 3 wt. %. Only sample I (▼) approaches the $q^{-5/3}$ scattering of swollen coils.

cyclohexane/water; no contrast labeling was used in that study, although average densities of coronal regions were high enough to show evidence of significant scattering between chains.[5]

A quantitative comparison of I vs. q in the intermediate region of the scattering vector was obtained by plotting SANS profiles on a log-log scale. Such plots for micelles at 3 wt. % polymer are shown in Figure 8.3. For all three samples, the profiles exhibit linear behaviour above $q = 0.05$ Å^{-1} ($\approx e^{-3}$); slopes obtained from least squares regression of the linear regions yield scaling exponents for $I \sim q^{-\alpha}$, where α is termed the characteristic exponent, and these are listed in Table 8.2. As described earlier, a swollen coil is expected to show scattered intensity scaling as $I \sim q^{-5/3}$ ($\alpha = 5/3$ or 1.7) in the intermediate region of q; this is also true of semidilute solutions in good solvents, which show local swollen coil behaviour at length scales shorter than the blob size. In general, stiffer chains will show lower values of the characteristic exponent, with $\alpha = 1$ indicating rod-like scaling at certain length scales.

At 3 wt. %, a value of $\alpha = 1.7$ was determined for sample I (240-190-390-*48*), confirming the results of Kratky analysis and suggesting a semidilute environment for dPS labels 390 units from the core. At the same polymer concentration, scattering from dPS labels 180 units from the core (sample II) gave $\alpha = 1.3$, indicating $I \sim q^{-1.3}$ scaling for $q >$ 0.05 Å^{-1}; thus the stiffness of chains is markedly higher in this region of the corona, such that the labels no longer exhibit single chain behaviour at intermediate q. The environment of the labels is no longer semidilute, and steric perturbations to chain conformations are more severe. This trend is further demonstrated by scattered intensity for sample III (590-270-*60*) at the same concentration (3%), which shows rod-like scaling, $I \sim q^{-1.0}$, for scattering vectors greater than 0.05 Å^{-1}. From the minimum scattering vector for $q^{-1.0}$ scaling,[21] $q = 0.05$ Å^{-1}, it is determined that the dPS labels next to the core can be described in terms of statistical units of ca. 75 Å in length; this value can be compared with the fully-extended contour length of the dPS labels (270 units), which is 675 Å. Each label contains only 9 statistical units, and will therefore behave in a "worm-like", rather than a statistical, manner.

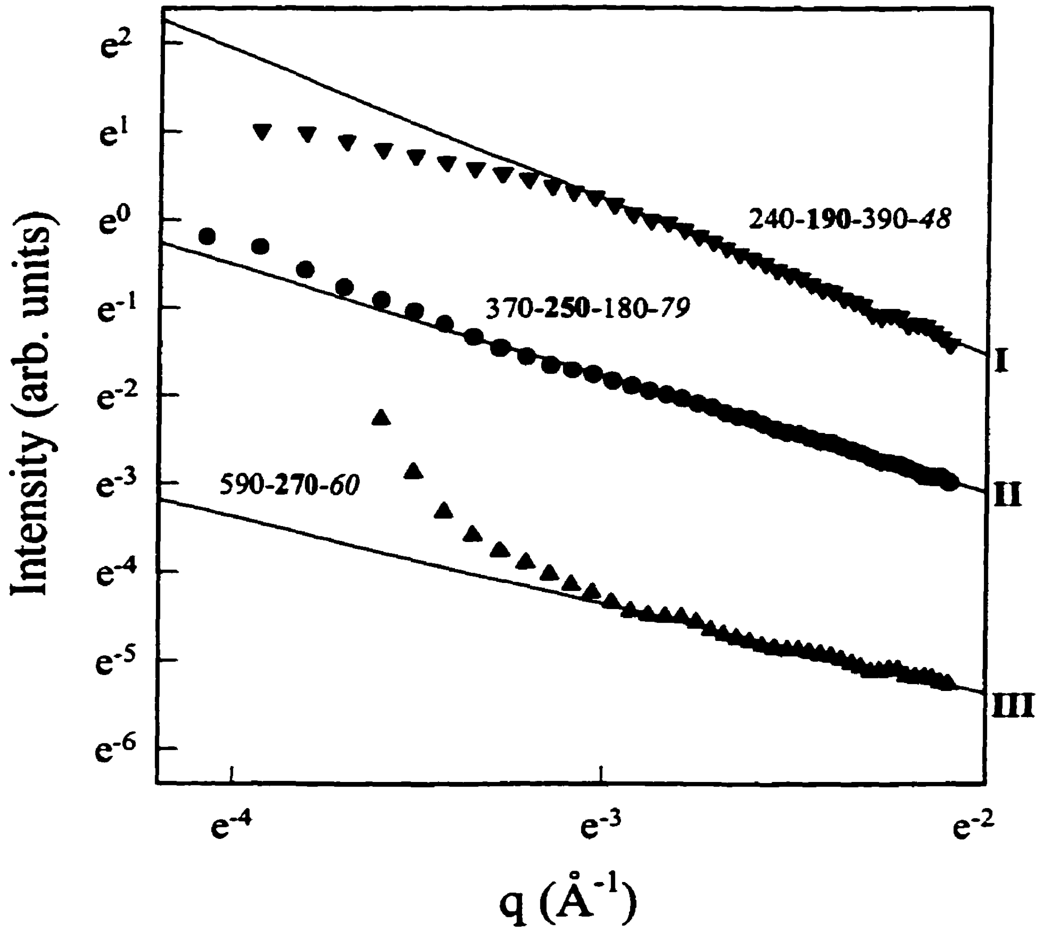

Figure 8.3. SANS profiles on a natural log scale for samples I (240-**190**-390-*48*), II (370-**250**-180-*79*), and III (590-**270**-*60*), at a concentration of 3 wt. %. Solid lines indicate linear regression in the region $q > 0.05$ $Å^{-1}$; the slopes of the lines yield characteristic exponents for the scaling relation $I \sim q^{-\alpha}$.

Table 8.2. $I(q)$ scaling exponents ($I \sim q^{-\alpha}$) at intermediate scattering vectors, for deuterated labels in block ionomer micelles.

PS-*b*-**dPS**-*b*-PS-*b*-*PACs*	poly. conc. (wt. %)	α, $q > 0.05$ Å^{-1}
sample I (240-**190**-390-*48*)	1	1.8
sample II (370-**250**-180-*79*)	1	1.0
sample III (590-**270**-*60*)	1	0.7
sample I (240-**190**-390-*48*)	3	1.7
sample II (370-**250**-180-*79*)	3	1.3
sample III (590-**270**-*60*)	3	1.0
sample I (240-**190**-390-*48*)	5	1.7
sample II (370-**250**-180-*79*)	5	1.4
sample III (590-**270**-*60*)	5	1.1

The observed increase in the stiffness of dPS labels with decreasing distance from the core can be attributed to higher local segment densities closer to the center of the polymer brush. This supports the results of Kratky analysis, and suggests a segment density profile which decreases with radial distance from the center, as predicted by Daoud and Cotton in their model of starlike polymer brushes. However, by labeling different parts of the corona in block copolymer micelles, it has also shown that the "blob" concept of that model can only be applied at distances sufficiently removed from the core, where coronal chains exist in a semidilute environment. Close to the core of starlike micelles, high segment densities result in large steric perturbations to swollen coil behaviour, such that $q^{-5/3}$ scaling of scattered intensity is not observed on any length scale. A breakdown of the blob model near the core of starlike block copolymer micelles has been predicted by Gast et al.;[5] to our knowledge, this work provides the first direct support of that prediction.

Values of characteristic exponents for the relation $I \sim q^{-\alpha}$, where $q > 0.05$ Å^{-1}, are listed in Table 8.2 for different polymer concentrations. For all samples, it is found that the values obtained for 5 % and 3% solutions are nearly identical. In the previous chapter, an increase in the stiffness of dPS labels was observed in some samples as the concentration was increased well above c^*; this was attributed to an increase in local segment densities of the probes, resulting from the overlap of coronal regions.[11] In the present case, it is thought that two important factors prevent a manifestation of the same effect. In the first place, the overlap concentrations are higher for these samples (3 - 5 wt. %) than those used in the previous study (ca. 2 wt. %). As well, the dPS labels in the present samples are located closer to the core, and are therefore screened from overlap effects by relatively high local segment densities.

We further note that samples II (370-**250**-180-*79*) and III (590-**270**-*60*) show somewhat depressed characteristic ratios ($\alpha = 1.0$ and 0.7, respectively) at polymer concentrations of 1 %. These effects are believed to be artifacts resulting from extremely low scattering intensities, in particular at high *q* values, from dPS probes in the 1% solutions. In the case of sample III, the measured exponent, $\alpha = 0.7$, is not physically meaningful, as the smallest possible exponent is $\alpha = 1.0$ for rod-like scaling.

8.4.2.2. Interparticle Scattering and Solution Structure

In the range of low *q* values ($q = 0.0020 - 0.030$ Å^{-1}), scattered intensity from dPS probes revealed clear interparticle correlations for most polymer concentrations. Plots of *I* vs. *q* in this region are shown for sample III (590-**270**-*60*) at polymer concentrations of 0.25, 1, 3, and 5 wt. % (Figure 8.4). Except for the lowest concentration, a maximum is observed in all SANS profiles; this is the first-order structure peak, or Bragg peak, and is related to the average distance between particles, d_{Bragg}, by:

$$d_{Bragg} = 2\pi \, / \, q_{\max} \qquad (7)$$

where $q_{\max}$ is the position of the first structure factor maximum. From Bragg peak positions, d_{Bragg} was calculated for the three samples at polymer concentrations of 1, 3, and 5 wt. % (Table 8.3); due to overlap with the form factor, the Bragg maximum for sample I at 5 wt. % was not clearly defined, and is therefore not reported in Table 8.3.

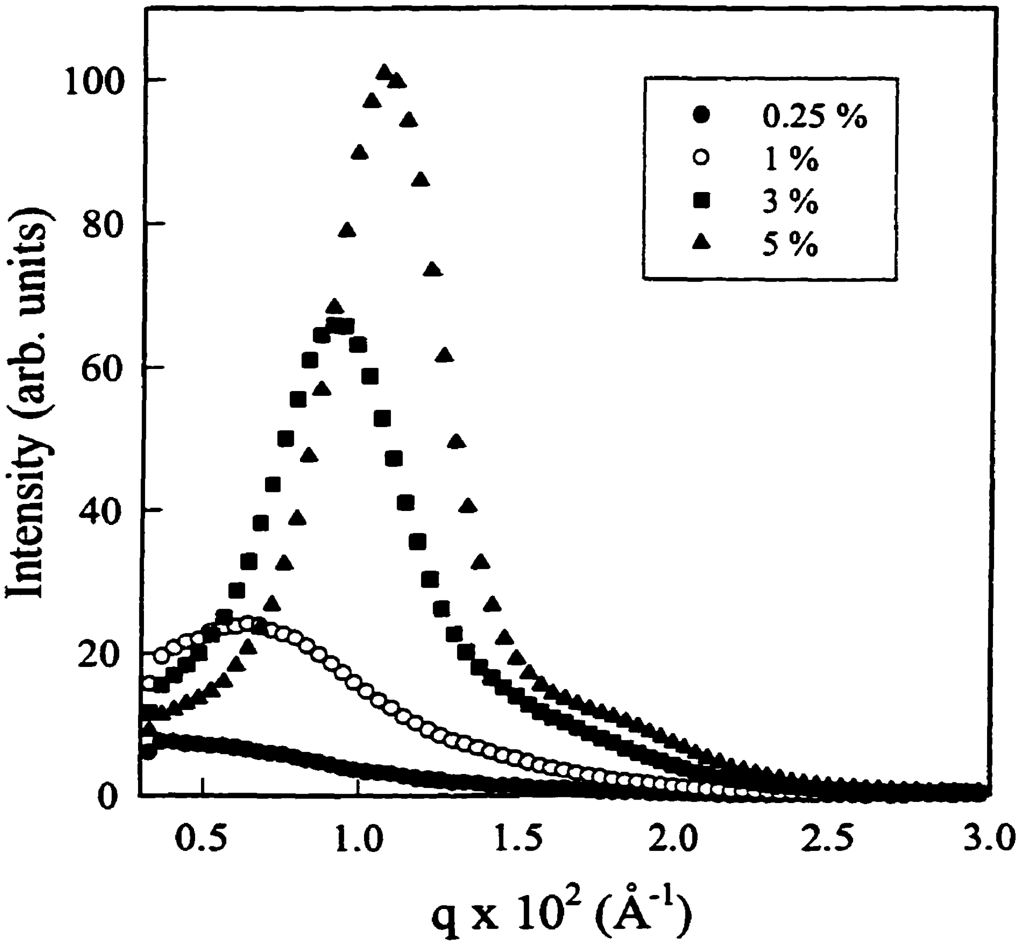

Figure 8.4. SANS profiles in low-*q* region, for sample III (590-270-60) at different polymer concentrations. The Bragg peak (observed for 1, 3, and 5 wt. % solutions) is found to shift to higher *q* with as the concentration is increased.

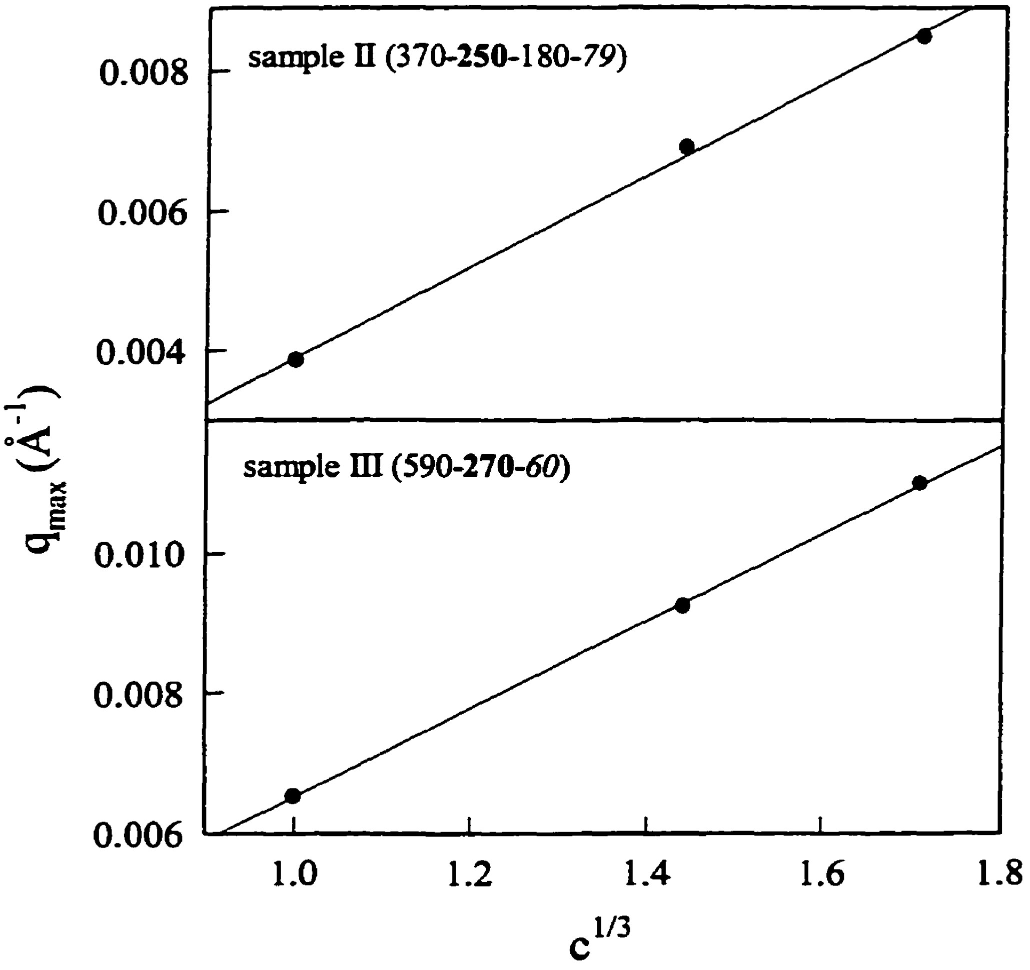

Figure 8.5. Plots of the Bragg peak position, q_{max}, vs. $c^{1/3}$ for samples I and II. The linear relation indicates liquid ordering in these solutions.

Table 8.3. Comparison of interparticle distances and micelle hydrodynamic diameters.

PS-*b*-dPS-*b*-PS-*b*-*PACs*	poly. conc. (wt. %)	$2R_h$ (nm)	q_{max} x 10^2 ($Å^{-1}$)	d_{Bragg} (nm)
sample I (240-**190**-390-*48*)	1	88	0.42	149
sample I (240-**190**-390-*48*)	3	88	0.77	82
sample I (240-**190**-390-*48*)	5	88		
sample II (370-**250**-180-*79*)	1	92	0.39	163
sample II (370-**250**-180-*79*)	3	92	0.69	91
sample II (370-**250**-180-*79*)	5	92	0.85	74
sample III (590-**270**-*60*)	1	72	0.65	96
sample III (590-**270**-*60*)	3	72	0.92	68
sample III (590-**270**-*60*)	5	72	1.10	57

In order for micelle overlap to occur, the average distance between particles, d_{Bragg}, must be equal to or less than twice the particle radius. Hydrodynamic diameters from dynamic light scattering results, $2R_h$, are therefore listed alongside d_{Bragg} values (Table 8.3). The hydrodynamic radii, R_h, are defined for dilute conditions, as they describe the overall size of isolated micelles in solution; as indicated in Table 8.3, these values do not vary with polymer concentration. Comparison of $2R_h$ and d_{Bragg} indicates that the condition of micelle overlap, $2R_h = d_{Bragg}$, is fulfilled for all three samples at a polymer concentration of ca. 3 %. For samples I (240-**190**-390-*48*) and II (370-**250**-180-*79*), this finding agrees well with c^* values in Table 8.1, which were calculated using the assumption of a cubic lattice for solution ordering. Using the same assumption, c^* for sample III (590-**270**-*60*) was determined to be ca. 5 %, which is higher than the value of ca. 3 % from Bragg spacings. A possible reason for this discrepancy is the lower percentage of extension for coronal chains in sample III (Table 8.1), which may allow the particles to pack into a somewhat less ordered lattice type.

For samples II and III, the position of the Bragg maximum, q_{max}, was plotted vs. $c^{1/3}$, where c is the weight percent polymer concentration; a linear relation was obtained in both cases (Figure 8.5). This supports the existence of liquid order in the system, for which q_{max} is expected to scale as $c^{1/3}$; sample I was not included in this analysis, since only two data points were available.

A more detailed description of solution structure would require fitting of the form factor, *P*(*q*), in the region of low *q*, such that *S*(*q*) could be mathematically extracted from the corrected scattering profile *I*(*q*), according to eq 5. In this case, higher-order structure peaks may be detected at high concentrations, which, in principle, would allow determination of the micelle packing lattice. In another study,[22] SAXS profiles of PS-*b*-PACs reverse micelles were obtained at various solution concentrations and in the bulk; isolated structure factors revealed up to three peaks related to interparticle correlations. The systems were found to exhibit liquid order, although the exact structure of the solutions could not be solved.

8.4.2.3. Guinier Analysis

Guinier plots were also constructed from SANS profiles in the region of low *q*, using data obtained at a polymer concentration of 0.25 wt. %. At this degree of dilution, *I*(*q*) did not show evidence of interparticle scattering for any of the samples; in Figure 8.4, the Bragg maximum has completely disappeared at 0.25 %, suggesting that the form factor, *P*(*q*), has been recovered at low *q*. When interparticle effects are negligible, the particle radius of gyration can be determined from the scattered intensity profile at small scattering vectors, according to the Guinier approximation:

$$I(q) = I(0)\exp\left[-q^2 R_g^2 / 3\right] \qquad (8)$$

Radii of gyration for the three samples were thus obtained from slopes of *I*(*q*) (on a natural log scale) vs. q^2 in selected linear regions at low *q*. These plots are shown in Figure 8.6 for samples I (240-**190**-390-*48*), II (370-**250**-180-*79*), and III (590-**270**-*60*), and yield R_g values of 32, 33, and 16 nm, respectively. The values for samples I and II agree well with those obtained from static light scattering measurements (30 and 33 nm), which suggests that neutron scattering in the Guinier regime reflects the size of the overall micelle, rather than individual deuterated labels; this follows from the mobility of the polymer chains, which should allow the labels to "explore" all parts of the micelle corona,

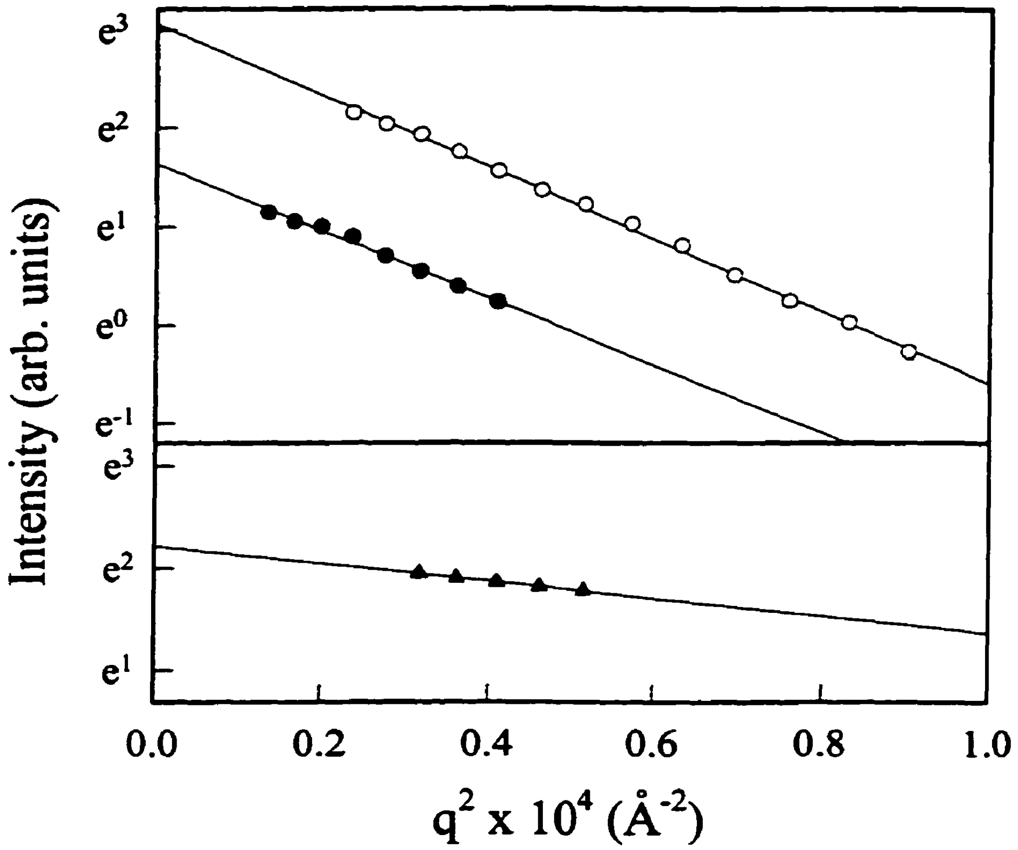

Figure 8.6. Guinier plots, I vs. q^2, for sample I (○), II (●), and III (▲) at a polymer concentration of 0.25 wt. %.

even though their average local densities are governed by their most probable position within the brush. In sample III, however, the dPS labels are linked directly to the ionic core, such that their mobility within the corona is restricted to the inner polymer brush. The radius of gyration from Guinier analysis of the SANS profile (16 nm) is therefore somewhat smaller than R_g of the whole micelle (23 nm), as determined by static light scattering.

Since the ionic core is very small ($R_{core} = 0.60$ nm) compared with the size of the brush, the contrast situation in sample III (590-**270**-*60*) allows the neutrons to "see" what resembles a dense star polymer, with 82 arms of 270 dPS units radiating out from a single point. From the radius of gyration of this star, $R_g = 16$ nm, the radius of gyration of each individual arm[23] was calculated using the expression:

$$\frac{R_{g,star}}{R_{g,arm}} = \left[\frac{(3Z-2)}{Z}\right]^{1/2} \qquad (9)$$

where the right-hand-side of eq 9 equals 2.98 when $Z = 82$. The radius of gyration of the deuterated arms in sample III was thus determined to be 9.3 nm. As expected, this value lies between the radius of gyration of a "free" dPS label of equivalent length in toluene (5 nm), and that of the fully-extended label (19 nm). It is also useful to compare the radius of gyration of the star from Guinier analysis, $R_g = 16$ nm, with the value determined from the Kratky peak in Figure 8.2, which should occur at $1/R_g$ for Gaussian stars.[20] The latter method yields $R_g = 5$ nm, more than three times smaller than the Guinier result. This suggests that the Gaussian model does not apply to the tightly-packed star in sample III (590-**270**-*60*).

8.5. Conclusions

Small-angle neutron scattering (SANS) experiments were used to study solutions of PS-*b*-**dPS**-*b*-PS-*b-PACs* starlike block ionomer micelles in toluene, in which contrast was provided by deuterated labels situated at different distances from the ionic core.

Characteristic exponents for the scaling relation $I \sim q^{-\alpha}$ were determined from corrected scattering profiles at intermediate scattering vectors. For deuterated labels situated at 390 PS units from the core, the scattered intensity scaled as $I \sim q^{-1.7}$ at intermediate q, suggesting a semidilute environment for the labels and local swollen coil behaviour. When the probes were 180 PS units from the core, however, they did not show single chain scaling at any length scale, and the relation $I \sim q^{-1.3}$ was found at intermediate q. The stiffness of dPS probes directly attached to the core was even greater; in this case, $I \sim q^{-1.0}$ scaling indicated worm-like chains with statistical units of ca. 75 Å. In Kratky representations of the three samples, a maximum characteristic of polymer stars was found to be more pronounced for dPS labels located closer to the core, indicating greater contributions from interchain scattering. The observed increases in chain stiffness and interchain scattering suggest a significant increase in local segment densities with decreasing distance from the ionic core, in agreement with the Daoud and Cotton model for star polymers. However, in the present case of starlike block ionomer micelles, it is found that the use of "blobs" of local single chain behaviour to describe the polymer brushes is applicable only at distances sufficiently removed from the core.

In the region of low q, interparticle scattering was investigated as a function of polymer concentration. From the position of the Bragg maximum, the average distance between particles was calculated, and the concentration at which $2R_h = d_{\mathrm{Bragg}}$ was estimated. For samples I (240-**190**-390-*48*) and II (370-**250**-180-*79*), overlap concentrations, c^*, determined in this manner agreed with values calculated for body and face-centered lattices of micelle packing. The position of the Bragg peak was found to scale with concentration as $c^{1/3}$, suggesting liquid ordering of the solution.

Radii of gyration determined from Guinier analysis agreed well with light scattering results for samples I (240-**190**-390-*48*) and II (370-**250**-180-*79*). In sample III (590-**270**-*60*), however, in which the labels were attached directly to the core, R_g from SANS (16 nm) was smaller than the value determined for micelles by static light scattering (23 nm). In this case, the neutrons "see" only the inner part of the spherical brush, which resembles a densely-packed star polymer. R_g for a single dPS arm of the star was determined to be 9.3 nm, which lies between “extreme” values for the equivalent free swollen coil (5 nm) and the fully extended chain (19 nm).

Acknowledgments

This work was supported by the Natural Sciences and Engineering Research Council of Canada (NSERC). M.M. is grateful for scholarship funding provided by NSERC and Le Fonds pour la Formation de Chercheurs et l’Aide à la Recherche (FCAR, Quebec).

References

(1) Lantman, C. W.; MacKnight, W. J.; Rennie, A. R.; Tassin, J. F.; Monnerie, L. Fetters, L. J. *Macromolecules* **1990**, *23*, 836.

(2) Richter, D.; Farago, B.; Fetters, L. J.; Huang, J. S.; Ewen, B. *Macromolecules* **1990**, *23*, 1845.

(3) Dozier, W. D.; Huang, J. S.; Fetters, L. J. *Macromolecules* **1991**, *24*, 2810.

(4) Willner, L.; Jucknischke; Richter, D.; Roovers, J.; Zhou, L.-L.; Toporowski, P. M.; Fetters, L. J.; Huang, J. S.; Lin M.Y.; Hadjichristidis, N. *Macromolecules* **1994**, *27*, 3821.

(5) Cogan, K. A.; Gast, A. P.; Capel, M. *Macromolecules* **1991**, *24*, 6512.

(6) McConnell, G. A.; Gast, A. P.; Huang, J. S.; Smith, S. D. *Phys. Rev. Lett.* **1993**, *71*, 2102.

(7) McConnell, G. A.; Lin, E. K.; Gast, A. P.; Huang, J. S.; Lin, M. Y.; Smith, S. D. *Faraday Discuss.* **1994**, *98*, 121.

(8) Förster, S.; Wenz, E.; Lindner, P. *Phys. Rev. Lett.* **1996**, *77*, 95.

(9) Gast, A. P. *Langmuir* **1996**, *12*, 4060.

(10) McConnell, G. A.; Gast, A. P. *Macromolecules* **1997**, *30*, 435.

(11) Moffitt, M.; Yu, Y.; Nguyen, D.; Graziano, V.; Schneider, D, K.; Eisenberg, A. Manuscript in Preparation.

(12) Desjardins, A.; Eisenberg, A. *Macromolecules* **1991**, *24*, 5779.

(13) Daoud, M.; Cotton, J. P. *J. Phys.* **1982**, *43*, 531.

(14) Long, T. E.; Allen, R. D.; McGrath, J. E. In *Chemical Reactions On Polymers*; Benham, J. L.; Kinstel, J. F., Eds.; ACS Symposium Series 364; American Chemical Society: Washington, DC, 1988; Chapter 19.

(15) Gauthier, S.; Duschesne, D.; Eisenberg, A. *Macromolecules* **1987**, *20*, 753.

(16) Zhong, X. F.; Varshney, S. K.; Eisenberg, A. *Macromolecules* **1992**, *25*, 7160.

(17) Nguyen, D.; Williams, C. E.; Eisenberg, A. *Macromolecules* **1994**, *27*, 5090.

(18) Burchard, W. *Adv. Polym. Sci.* **1983**, *48*, 1.

(19) Zhang, L.; Barlow, R. J.; Eisenberg, A. *Macromolecules* **1995**, *28*, 6055.

(20) Benoit, H. *J. Polym. Sci.* **1953**, *11*, 507.

(21) Kratky, O. *Pure Appl. Chem.* **1966**, *12*, 483.

(22) Nguyen, D.; Varshney, S. K.; Williams, C. E.; Eisenberg, A. *Macromolecules* **1994**, *27*, 5086.

(23) Burchard, W.; Kajiwara, K.; Nerger, D.; Stockmayer, W. H. *Macromolecules* **1984**, *17*, 222.

They intend to send a wire
To the moon;
And they'll set the Thames on fire
Very soon...
And weasels at their slumbers
They'll trepan;
To get sunbeams from cucumbers
They've a plan.
They've a firmly rooted notion
They can cross the Polar Ocean,
And they'll find Perpetual Motion,
If they can!

W. S. Gilbert

CHAPTER 9

Conclusions, Contributions to Original Knowledge, and Suggestions for Future Work

9.1. Conclusions and Contributions to Original Knowledge

This section provides a summary of the notable findings discussed in the thesis, with an emphasis on original aspects of these results. Reflecting the two main parts of the work, this section will be divided into two parts. Section 9.1.1 concerns block ionomers as inorganic microreactors of controllable size, and thus presents important results from chapters 3, 4, 5, and 6. In section 9.1.2, the study of coronal structure in block ionomers by SANS (chapters 7 and 8) is discussed.

9.1.1. Block Ionomer Microreactors

Chapter 3 of this thesis introduces a new and reliable method of size control for inorganic particle synthesis, in which the sizes of particles can be "tuned" at the nanoscale level via variations in the structure or composition of the ionomer host. The ability to control sizes is a practical application of a priori knowledge of ionomer aggregation numbers. In a system of PS-based random ionomers, aggregation numbers were controlled via the lengths of side chains connecting the polymer backbone with carboxylate functional groups. A series of ionomers with varying side-chain lengths was formed by neutralization of the carboxylic acid precursors with cadmium or lead ions; the ionomers were then reacted with H_2S to form CdS and PbS nanoparticles, respectively. UV-vis analysis showed that the semiconducting nanoparticles were quantum-confined, so the actual sizes could be determined from the absorption edge. The sizes of CdS nanoparticles ($2R_{CdS}$) were found to increase in a linear fashion with the length of the sidechains, with a slope of ca. 0.40. An identical slope has been found in plots of multiplet sizes versus side chain lengths, suggesting that nanoparticle growth is limited by the number of ions in the multiplet. This was supported by comparison of the number of ion pairs in CdS and PbS nanoparticles, which were remarkably similar for the same ionomer host. In the random ionomer series, the sizes of nanoparticles were controlled in the extremely narrow range of $2R = 18 - 23$ Å, and were shown to have a low polydispersity, with radii polydispersity indexes of ca. 1.03. For a representative sample, nanoparticle sizes were also calculated from small-angle x-ray scattering measurements, using a simple-cubic packing model to calculate the number of ion pairs from the Bragg peak; SAXS results were found to agree well with sizes determined from UV-vis data. Along with acting as a system of "microreactors" for nanoparticle synthesis, the ionomer matrix was also found to stabilize and protect the nanoparticles from agglomeration and other mechanisms of long-term particle growth. After 7 months storage under ambient conditions, the particle sizes were found to increase by only 1-3 Å.

The concept of inorganic microreactors was expanded to include a system of block ionomers (PS-*b*-PACd), in which ionic core sizes are dependent on ionic block lengths (chapter 4). In this study, the ionic cores were plasticized with water to effect a "cherry morphology". CdS particle sizes were controlled in the range of $2R = 20\text{-}50$ Å, using ionic block lengths of 4-32 repeat units. RPI values of 1.02-1.05 were determined, indicating a narrow distribution of sizes. The nanoparticle size was found to increase linearly with the size of ionic core, and scale with the ionic block length as $N_B^{3/5}$, in agreement with the Halperin model for starlike block copolymers. The relation $2R_{CdS} = 1.9N_B^{3/5} + 9.4$ Å was determined for this system, indicating that particle sizes can be "tuned" at the nanometer scale through variations in ionic block lengths. The "cherry" morphology (i.e., a single nanoparticle per core) was confirmed in most cases by comparison of the number of ion pairs in the nanoparticles with the aggregation numbers of the original ionomer host. In the largest ionic cores, however, ($2R_{core} > 100$ Å) it was found that the microreactors adopt a "raspberry" morphology, as indicated by a plateau region in the plot of $2R_{CdS}$ vs. $2R_{core}$.

CdS-block ionomer composites were suspended in organic solvents to form CdS-containing reverse micelles. It was found that these aggregates could be stabilized by reneutralization of the acrylic acid layers surrounding the nanoparticles. Following reneutralization (or "fixing") with NaOH or $Cd(Ac)_2$, the micelles were precipitated into methanol then redissolved in toluene. The sequence of dissolution and recovery of the composite was repeated several times, without loss of CdS or changes in nanoparticle sizes. As well, it was found possible to process the CdS-polymer composites by casting from toluene or compression molding at 130 °C, without affecting the nanoparticle sizes. A method of controlled continued growth was also demonstrated, by reloading CdS-containing microreactors with Cd^{2+} ions, followed by secondary treatment with H_2S. By this method, the nanoparticle sizes were increased from 37 Å to 56 Å in two steps.

Chapter 5 describes a detailed study of polystyrene-*b*-poly(metal acrylate) block ionomer micelles containing a variety of different metal ions. This work is the first study to explore the effect of the nature of the counterion on block ionomer aggregation, and expands the size control of block ionomer microreactors to include a wide range of inorganic precursors. Using static light scattering (SLS) and size-exclusion chromatography (SEC) to characterize the colloids, it was found that the aggregation numbers and ionic core radii scale with the ionic block length in a similar manner for all metal ions, $Z \sim N_B^{0.74\pm0.03}$ and $R_{core} \sim N_B^{0.58\pm0.03}$, in agreement with the insoluble block length dependence predicted by Halperin. The proportionality constants $K_{Z,av}$ and $K_{R,av}$ are dependent on the metal ion and decrease as $Ni^{2+} > Cs^{+} > Co^{2+} > Ba^{2+} > Cd^{2+} > Pb^{2+}$. Excellent linear correlation was obtained in plots of R_{core} vs. $N_B^{0.58}$ ($r^2 = 0.99$), indicating potential size control for different metal ions. In the case of block ionomers neutralized with metal acetates, it was also found that the proportionality constant for aggregation numbers, $K_{Z,av}$, decreases linearly with the crystal ionic radius (r_{ion}). The soluble block length dependencies of Z and R_{core} were determined: $Z \sim N_A^{-0.42\pm0.06}$ and $R_{core} \sim N_A^{-0.14\pm0.02}$

for Cs^+, Ba^{2+}, Cd^{2+} and Ni^{2+} ions; and $Z \sim N_A^{-0.10\pm0.05}$ and $R_{core} \sim N_A^{-0.04\pm0.02}$ for Pb^{2+} and Co^{2+} ions.

Block ionomer micelles containing different metal ions were also investigated by dynamic light scattering (DLS). A combination of SLS and DLS results yielded the ratio R_g/R_h, which, in most cases, was between the values for stars and compact spheres. The coronal brush height, H, was calculated from the hydrodynamic radius, R_h. Combining the data for all metal ions, the following scaling relation was determined, $H \sim Z^{0.3\pm0.1}N_A^{0.9\pm0.2}$, which agrees reasonably well with the Daoud and Cotton model for starlike systems.

Chapter 6 concerns the "secondary" self-assembly of CdS-containing microreactors in aqueous media to form novel spherical assemblies of quantum dots. Self-assembly was induced by the slow addition of water to solutions of CdS-containing reverse micelles in the presence of a PS-*b*-PAA stabilizing copolymer. The resulting aggregates were found to closely resemble large compound micelles, such as those observed in aqueous solutions of PS-*b*-PAA in the "crew-cut" composition regime. The internal structure of the aggregates was found to consist of ca. 60 quantum dots dispersed in a spherical PS matrix. These novel assemblies of nanoparticles in aqueous media may have several electro-optical or photocatalytic applications. Water-soluble, stabilized nanoparticles are quite rare, and it is recognized that such systems are extremely appealing in terms of their environmental compatability. It was found that the number of aggregate populations was dependent on the percentage of stabilizing copolymer that was added, with an excess of stabilizer resulting in the coexistence of LCMs and regular micelles of PS-*b*-PAA.

9.1.2. Coronal Structure of Block Ionomers

The work described in chapters 7 and 8 of this thesis represents the first detailed study of coronal structure in block ionomers. As well, this is the first small-angle neutron scattering (SANS) investigation of block copolymer micelles that employs deuterated labels to probe specific regions of the corona. In the first part of this study (chapter 7), the scattering from deuterated labels near the outside of the coronal brush was studied as a function of solvent conditions and polymer concentration. Two samples of similar micelles were investigated, with deuterated labels located at two different positions, 1080 and 820 PS units from the ionic core. In a good solvent at 3 wt. % polymer, the scattered intensity for both samples scaled as $I \sim q^{-1.7}$ in the intermediate region of the scattering vector, indicating a semidilute environment for the labels. The average "blob" size was found to be larger for the label that was further from the core (1080 units), as determined by the minimum vector of the intermediate region, q^*. This finding was in agreement with the blob model for starlike spherical brushes. When the polymer concentration in toluene was increased to 5 wt. %, a decrease in the characteristic exponent for intensity scaling, α, indicated an increase in the steric crowing of the labels; this concentration-induced chain stiffening within the corona was attributed to the overlap of neighbouring micelles at concentrations well above c^*. In cyclohexane at 40 °C (near-θ conditions) the labels were found to be "worm-like" at 3 wt. % polymer, and collapse to near-Gaussian behavior when the polymer concentration was increased to c^*. To our knowledge, these effects of solvent and concentration on spherical brush structure have not been observed in other systems of block copolymer micelles or star polymers.

In the second part of the study, the range of label positions was expanded to obtain a more detailed picture of coronal structure, especially in the crowded region near the center of the brush. Three samples were investigated, with labels situated at 390, 180 and 0 units from the core. Labels situated at 390 PS units from the core showed scattered intensity that scaled as $I \sim q^{-1.7}$ at intermediate q, suggesting a semidilute environment in which swollen coils exhibit local single chain behaviour. A semidilute coronal environment in starlike brushes is a fundamental assumption of the "blob" model. For labels 180 PS units from the core, intensity scaled as $I \sim q^{-1.3}$ at intermediate q, which indicated that local segment densities were higher than those in a semidilute solution. The stiffness of labels directly attached to the core was even greater, and showed $I \sim q^{-1.0}$ scaling typical of "worm-like" chains. Kratky representations showed a characteristic maximum for polymer stars, which was more pronounced for dPS labels located closer to the core; this indicated greater contributions from interchain scattering, and provided further evidence of increasing local segment densities with decreasing distance from the ionic core, as predicted in the Daoud and Cotton model of star polymers. It is found that the use of "blobs" of local single chain behaviour to describe the polymer brush is applicable only at distances sufficiently removed from the core. This is reflective of higher average densities in block ionomer coronae, compared with the more open star polymer systems.

In the low-q regime of the scattering vector, interparticle scattering was investigated as a function of polymer concentration. The position of the Bragg peak was found to scale with concentration as $c^{1/3}$, suggesting liquid ordering of block ionomer micelle solutions. At low concentrations, Guinier analysis was also performed at low-q. R_g values agreed well with light scattering results, for samples in which the labels were removed from the core by 390 or 180 PS unit "spacers". For the sample in which labels were attached directly to the core, R_g from SANS (16 nm) was smaller than the static light scattering value (23 nm). In this case, the form factor represented only the inner part of the spherical brush, which resembled a densely-packed star polymer; the radius of gyration from SANS was therefore quite different from that determined for the whole micelle. The radius of gyration for a single arm of the star was determined to be 9.3 nm. This value falls between the equivalent free swollen coil (5 nm) and the fully extended chain (19 nm), which further suggests that coronal chains experience significant steric crowding near the core.

9.2. Suggestions for Future Work

9.2.1. Suggested Research on Semiconductor-Polymer Composites and Block Ionomer Microreactors

The work described in chapters 3-6 focused on the synthesis of semiconductor nanoparticles in block ionomers, and especially on the size control that is possible in this medium. Although the resulting materials were studied in terms of their stability in micelle solutions and in the solid state, it is recognized that further characterization of the composites would be extremely useful, in order to determine the feasibility of electro-optical and photocatalytic applications.

One possible application of these materials is in the area of integrated optics, as they are good candidates for artificial dielectric waveguides; these are materials in which the effective dielectric properties are determined both by the optical properties of the polymer and the conductivity properties of the embedded semiconductors.[1] Waveguiding properties could be studied as a function of CdS particle sizes, which would be "tuned" via the composition of the host material. For block ionomer composites containing metallic particles, waveguiding techniques could be used to study surface-enhanced Raman spectra of the polymer host near the guest particles. This would allow nanoparticle-polymer interactions to be studied spectroscopically under a wide range of conditions.

Nonlinear optical properties of the CdS-polymer composites could also be studied using pump-probe experiments, which measure transient bleaching of the excitonic absorption.[2] For such experiments, the "pump" is a laser pulse which excites the semiconductor particles, creating both excitons and, in the presence of surface defects, longer-lived, "trapped" electron-hole pairs. For the duration of their lifetime (nano to picosecond time scale) these excitons and trapped e-h pairs will interact with the excitons of subsequent probe pulses, resulting in a transient red shift and decreased oscillator strength of the excitonic absorption. A nonlinear absorption coefficient can thus be studied, and this is defined as the change in the absorption coefficient divided by the intensity of the pump pulse. As quantum confinement effects will shift the energy of the exciton with changing particle size, it should also be possible to "tune" the nonlinearities using the accurate size control of the present system. Since "trapped" e-h pairs play an important role in this transient bleaching effect, especially following the decay of the original exciton, the modification of surface defects provides another means of influencing nonlinearities. The "reloadable" nature of the microreactors is very appealing in this respect, as it allows a variety of ions or (via simple chemistry) metal and semiconducting materials to be introduced near the surface of the original particles. In this manner, defect sites could be "healed" or created by subsequent treatment of the nanoparticle surface.

Another aspect of CdS-polymer composites that could be explored is the potential photoconductivity of these materials. For such applications, the PS matrix of the present system would not be optimal, as the polymer host should act as an effective medium for carrier transport. The carriers are induced by optical excitation of the semiconductor nanoparticles, such that conductivity of the composite is controlled by the sizes of particles and the wavelength of excitation.[3] A system of microreactors with comparable size control, in which the PS block is replaced by a conducting polymer (e.g. polyvinylcarbazole), therefore represents an interesting and worthwhile challenge.

Colloidal CdS particles coated with a thin platinum or palladium layer have been shown to be effective photocatalysts.[4] Electrons generated by photo-excitation are transported via the metallic layer to chemical reagents at the surface. In this manner, photocatalytic hydrogen production by the reduction of water has been demonstrated in colloids of surfactant-stabilized CdS. In the present system, preliminary work has involved the development of a block copolymer "battery", by reloading CdS-containing microreactors with Pd^{2+} ions, and reducing the ions onto the particle surface.[5] Continued work in this area should include the detailed study of the photocatalytic properties of these materials. This would require the use of analytic techniques, such as gas chromatography or a membrane polarographic detector (MPD), that are sensitive to micromolar quantities of hydrogen gas.

Another aspect of this system that remains to be explored is the wide range of simple chemistry that could be used to convert different metal ions into metallic or semiconducting particles. For most of this thesis, CdS and PbS nanoparticles have been chosen as "model products", as their sizes are easily characterized spectroscopically. However, it has also been shown that a variety of ions can be incorporated into the core; therefore the range of inorganic chemistry in the microreactors should be even more diverse. Now that a system has been developed in which reliable size control is possible, a creative and aggressive "nanoparticle synthesis spree" would undoubtedly produce some interesting materials.

In the production of aqueous semiconductor assemblies, such as those discussed in chapter 6, an interesting problem is the control of aggregate morphology. Although the combination of reverse micelles and stabilizing block copolymer used in this work gave exclusively large compound micelle (LCM) aggregates, a number of other morphologies, including rods, vesicles, and numerous bilayer structures have been observed in solutions of PS-*b*-PAA in the crewcut composition range. Further studies should include variations in the composition of both the stabilizing and reverse micelle copolymers, relative amounts of these two components, solvent conditions, solution ionic strengths, etc. Through systematic variations in these parameters, it is feasible that semiconducting nanoparticles could be incorporated into other interesting morphologies in aqueous solutions.

9.2.2. Suggested Research on Block Ionomer Coronal Structure

Further SANS studies of block ionomers could employ a greater number of label positions, such that the structure of coronal chains as a function of radial distance is determined in more detail. In semidilute regions of the corona, an average "blob" size could be calculated for each label position, from which average segmental densities could also be determined. If the number of different label positions is sufficiently high, then a fully empirical segmental density profile is conceivable. Of course, the synthetic difficulties surrounding such a project are not trivial, as a large number of tetrablock copolymers that give very similar aggregation numbers would have to be synthesized individually.

A more modest "next step" would be the continued investigation of samples discussed in chapters 7 and 8, for a greater range of polymer concentrations and solvent conditions. In particular, a study of coronal structure as a function of temperature, especially under near-θ conditions, may allow interesting transitions in chain conformations to be observed in situ. As well, the present work did not include an investigation of coronal structure for very dilute samples in the near-θ solvent. In this solvent (cyclohexane, 40 °C), dramatic concentrations effects were observed in the vicinity of c^*; it is possible that, under near-θ conditions, information on isolated coronal structure could only be obtained at extremely low concentrations.

A more detailed investigation of solution structure would also be possible for this system. As mentioned in the previous chapter, this would involve a careful fitting of the form factor in the region of low-q, such that form and structure factors could be mathematically separated. In the present system, form factors could be fitted to models for stars, spheres, or hollow spheres, depending on the position and length of the deuterated label. Analysis of the isolated structure factor as a function of concentration would then yield information on the lattice type for micelle packing.

As a final "check" of these results, the SANS experiments described in chapters 7 and 8 could be repeated using "mirror image" samples, i.e. deuterated micelles and hydrogenated labels. The main advantage of such a system would be the lower degree of incoherent scattering, which is mainly attributed to hydrogen nuclei; the use of largely deuterated micelles in deuterated solvent would therefore significantly increase the signal to noise ratio, allowing solutions of lower polymer concentrations to be investigated. From a synthetic point of view, it would be extremely difficult to produce exact "mirror image" replicas of samples used in this work, although similar samples could be used to validate general trends.

References

(1) Grebel, H.; Chen, P. *Op. Lett.* **1990**, *15*, 667.

(2) Wang, Y.; Suna, A.; McHugh, J.; Hilinski, E. F.; Lucas, P. A.; Johnson, R. D. *J. Chem. Phys.* **1990**, *92*, 6927.

(3) Wang, Y.; Herron, N. *Chem. Phys. Lett.* **1992**, *200*, 71.

(4) Meyer, M.; Wallberg, C.; Kurihara, K.; Fendler, J. H. *J. Chem. Soc., Chem. Commun.* **1984**, 90.

(5) Moffitt, M.; Corbierre, M.; Bartels, C.; Eisenberg, A. Unpublished results.